Human Pose Estimation During Physical Human-Robot Collaboration

by

Richardo Khonasty

A thesis submitted in partial fulfilment of the
requirements for the degree of Doctor of Philosophy

at the
Centre for Autonomous Systems
Faculty of Engineering and Information Technology
University of Technology Sydney

February 2020

Certificate of Original Authorship

I certify that the work in this thesis has not previously been submitted for a degree nor has it been submitted as part of requirements for a degree except as fully acknowledged within the text.

I also certify that the thesis has been written by me. Any help that I have received in my research work and the preparation of the thesis itself has been acknowledged. In addition, I certify that all information sources and literature used are indicated in the thesis.

This research is supported by the Australian Government Research Training Program.

Signed: Production Note: Signature removed prior to publication.

Date: 22/02/2020

Human Pose Estimation During Physical Human-Robot Collaboration

by

Richardo Khonasty

A thesis submitted in partial fulfilment of the requirements for the degree of Doctor of Philosophy

Abstract

Robotic systems designed for physical Human-Robot Collaboration (pHRC) are being increasingly used to augment the strength of a human co-worker by providing assistance during the collaboration. The pose of the human body greatly affects the physical strength of the human co-worker and is often difficult to measure in real pHRC applications due to factors such as poor illumination, air quality and the close proximity of the human co-worker to the robot. This thesis aims to address three research challenges in human pose estimation during pHRC in practical industry applications: (1) the effect of interaction between the human and the robot on the pose of the human; (2) whether the pose of the human can be estimated by exploiting the Human-Robot Interaction (HRI); and (3) if the estimated pose can be used to facilitate real-time appraisal of the human co-worker's physical strength.

The challenge in determining the pose of a human co-worker during pHRC was approached in two ways. Firstly, experiments were performed to observe the effect that the interaction between the human and the robot had on the adopted pose of the human upper limb. This study determined whether existing pose estimation methods can be used in real pHRC applications. The second approach was to exploit the HRI for estimating the pose of the human in applications where the hand poses of the human co-worker were able to be inferred from the interaction. Thus the nullPose method was developed to

estimate the pose of the human upper body in real-time. The nullPose method integrates sensor measurements and approximations to the pose of the upper body whilst ensuring the estimated poses are humanly possible. The nullPose method was then used to perform a real-time appraisal of the human co-worker's capability which was compared to a conventional batch-processed method of estimating the human strength.

Experiments were conducted in two different environments to verify the methods. The first environment was a motion capture lab which allowed the pose of the human to be recorded such that the effect of HRI on the upper limb pose was able to be studied. This environment also allowed the estimated pose from the nullPose method to be compared to the real pose of the human co-worker. The second environment was an abrasive blasting chamber where a real pHRC operation was performed. This environment was used to determine the suitability of the nullPose method for use in real challenging industrial environments where traditional methods of pose estimation were not able to be relied upon.

Acknowledgements

This work would not have been possible without the support from those around me.

Firstly, I would like to thank my supervisor Dist. Prof. Dikai Liu who have given me the opportunity to work on this topic and the advice you have provided throughout. Your direction and motivation allowed me to accomplish this significant milestone in my life.

I would also like to thank my co-supervisor Dr. Marc Carmichael who have provided advice, expertise and support throughout my candidature. Your assistance was very helpful and contributed greatly to the completion of this work.

I am grateful for all of the assistance provided by all of the professors, researchers, engineers and students at the Centre for Autonomous Systems in UTS, especially the ANBOT team. I am glad to have had the opportunity to work in such a supportive environment filled with wonderful people who ensured that everything will be alright.

Finally I would like to acknowledge the encouragement provided by my family and friends. Over the past four years, your support have helped me work through this endeavour.

Contents

Declaration of Authorship iii

Abstract v

Acknowledgements vii

List of Figures xiii

List of Tables xix

Glossary of Terms xxiii

1 Introduction 1
- 1.1 Background and Motivation . . . 3
- 1.2 Research Questions . . . 5
  - 1.2.1 Research Question 1: Effect of Interaction Between the Human and Robot on the Pose of the Human . . . 6
  - 1.2.2 Research Question 2: Exploiting the Interaction in physical Human-Robot Collaboration (pHRC) for Estimate the Pose of the Human . . . 6
  - 1.2.3 Research Question 3: Appraisal of the Human Co-worker's Physical Strength by using an Estimated Pose . . . 7
- 1.3 Scope . . . 7
- 1.4 Contribution . . . 9
- 1.5 Publications . . . 9
- 1.6 Thesis Outline . . . 10
  - 1.6.1 Chapter 2 . . . 10
  - 1.6.2 Chapter 3 . . . 10
  - 1.6.3 Chapter 4 . . . 11
  - 1.6.4 Chapter 5 . . . 11
  - 1.6.5 Chapter 6 . . . 11

2 Review of Related Work 13
- 2.1 Physical Human-Robot Collaboration . . . 14
  - 2.1.1 Traditional Robots . . . 14

2.1.2 Autonomous Robots . . . 15
2.1.3 Collaborative Robots . . . 16
2.1.3.1 Collaborative Robots for Strength Augmentation . . . 17
2.1.3.2 Collaborative Robots in Rehabilitation . . . 17
2.1.4 Types of Assistance . . . 19
2.1.5 Robots Providing Adaptive Assistance . . . 20
2.2 Adaptive Assistance . . . 21
2.2.1 Level of Assistance . . . 21
2.2.2 Performance Based Assistance-as-Needed . . . 22
2.2.3 Model Based Assistance-as-Needed . . . 23
2.2.4 Assistance-as-Needed in practical pHRC applications . . . 23
2.3 Human Pose Tracking . . . 25
2.3.1 Existing Pose Tracking Technologies . . . 25
2.3.2 Pose Tracking Through Models . . . 26
2.3.3 Limitations of Common Pose Tracking Technologies . . . 27
2.4 Human Physical Strength and pHRC . . . 29
2.4.1 Physical Strength of the Human . . . 29
2.4.2 Musculoskeletal Models of the Human Body . . . 30
2.4.3 Estimation of Human Physical Strength . . . 31
2.4.4 Muscle Fatigue . . . 32
2.4.5 Physical Strength Estimation in Practical pHRC Applications . . . 32
2.5 Summary . . . 33

3 Effect of External Force and Bimanual Operation on Upper Limb Pose 35
3.1 Background Information . . . 36
3.2 Overview . . . 37
3.2.1 Redundancy in the Human Upper Limb and Pose Definition . . . 37
3.2.2 Physical Interaction Between the Human and the Robot . . . 39
3.3 Design of Experiments . . . 41
3.3.1 Robotic Platform . . . 41
3.3.2 Experiments . . . 42
3.4 Results and Discussion . . . 47
3.4.1 Experiment 1 - Unimanual Operation with No Force Applied . . . 48
3.4.2 Experiment 2 - Bimanual Operation with No Force Applied . . . 52
3.4.3 Experiments 3 and 4 - Unimanual Operation with 20N or 40N Force in the +X Direction . . . 53
3.4.4 Experiments 5 and 6 - Unimanual Operation with 20N or 40N Force in the YZ Plane . . . 59
3.4.5 Summary of Each Individual . . . 64
3.4.6 Strength Comparison using a Musculoskeletal Model . . . 65
3.5 Conclusion . . . 67

4 nullPose: an Upper Body Pose Estimation Method 69
4.1 Overview of the Methodology . . . 70

4.2 The nullPose Method . . . 74
4.2.1 Upper Limb Kinematic Model . . . 77
4.2.2 Task Composition . . . 78
4.2.3 Task Prioritization . . . 81
4.2.4 Joint Step Calculation . . . 82
4.2.5 Mode 1 - Kinematic Chain Closed . . . 84
4.2.6 Mode 2 - Kinematic Chain Open . . . 86
4.2.7 Task Composition and Prioritization Example . . . 87
4.3 Experiment Setup . . . 89
4.4 Experiment 1 - Verifying the nullPose Method in an Ideal Environment . . . 91
4.4.1 Pose Estimation Scenarios . . . 93
4.4.2 Results and Discussion . . . 94
4.5 Experiment 2 - Determining the Accuracy of the nullPose Method in a Practical pHRC . . . 98
4.5.1 Pose Estimation Scenarios . . . 99
4.5.2 Results and Discussion . . . 102
4.6 Experiment 3 - Implementation of the nullPose Method in a real pHRC application . . . 105
4.6.1 Pose Estimation Scenarios . . . 106
4.6.2 Results and Discussion . . . 107
4.7 Conclusion . . . 110

5 Appraisal of Human Physical Strength Using the nullPose Method 113
5.1 Appraisal of Human Physical Strength . . . 114
5.1.1 Musculoskeletal Model . . . 116
5.2 Transforming the Upper Body Kinematic Model Pose to Musculoskeletal Model Joint Coordinates . . . 117
5.3 Estimating the Physical Strength of the Human Co-Worker . . . 122
5.4 Experiment 1: Comparison of Estimated Physical Strength Using the null-Pose Method to the Conventional Batch Processed Method . . . 124
5.4.1 Pose Estimation Scenario . . . 126
5.4.2 Results and Discussion . . . 127
5.5 Experiment 2: Estimating the Strength of a Human Co-Worker in a Real pHRC Application . . . 130
5.5.1 Pose Estimation Scenario . . . 131
5.5.2 Results and Discussion . . . 132
5.6 Conclusion . . . 134

6 Conclusion 137
6.1 Summary of Contributions . . . 139
6.1.1 Effect of the Physical Interaction Between the Human and the Robot on the Pose of the Human Co-Worker . . . 139
6.1.2 nullPose: an Upper Body Pose Estimation Method for pHRC . . . 140
6.1.3 Real-Time Appraisal of Human Strength Using the nullPose Method 141
6.2 Discussion and Limitations . . . 142

6.2.1 Inferring the Hand Poses in the nullPose Method 143
6.2.2 The Combination of Targets Used by the nullPose Method 144
6.2.3 Upper Limb Models Approximating the Human Body 145
6.2.4 Human Capability in pHRC 145
6.2.5 Benefit of Assistance-as-Needed Paradigm in pHRC 146
6.3 Future Work 147
6.3.1 Accommodating the Rotation of the Human Co-Worker's Hands Around a Cylindrical Handle 147
6.3.2 Dynamic Task Allocation Based on Available Sensor Measurements for the nullPose Method 148
6.3.3 Determining the Minimum Combination of Tasks for the nullPose Method 148
6.3.4 Extending the nullPose Method for a Full Body Pose Estimation . . 149
6.3.5 Implementing Assistance-as-Needed in pHRC 149

Appendices **151**

Appendix A Additional Results From Experiments in Chapter 3 **151**

Appendix B nullPose method: Combinations of Targets **162**

Appendix C Additional Simulation Results of the nullPose Method **165**

Appendix D Shoulder Rotational Matrix Conversion **168**
D.1 Rotational matrix between the scapula frame to the humerus frame of the right upper limb musculoskeletal model 168
D.2 Rotational matrix between the scapula frame to the humerus frame of the left upper limb musculoskeletal model 169

Appendix E Distribution of Muscle Activation of the Musculoskeletal Models **170**

Bibliography **174**

List of Figures

1.1 An example of a pHRC application where the human and the robot collaborate to complete an operation. 2
1.2 The three components that are required to adapt the assistance to be provided to the human by the robot in a model-based Assistance-as-Needed (AAN) paradigm. 5

2.1 Industrial robots being used in the automotive industry. Cages are setup around the robot to ensure human workers do not accidentally enter the workspace of the robot [1]. 15
2.2 Examples of human safe robots designed for collaborative applications: (A) Universal Robot UR10 [2] (B) Kuka LBR iiwa [3] (C) Rethink Robotics Sawyer [4]. 16
2.3 A human wearing the BLEEX [5] used to support the human carry a heavy load. 18
2.4 An upper body exoskeleton the JEXO designed based on the range of motion of the human shoulder to be used in upper limb rehabilitation [6]. 18
2.5 Motion capture suit worn to track a human using the OptiTrack system [7] 26
2.6 (A) The redundancy in the human upper limb. (B) An example of a model based upper limb redundancy resolution [8], based on the manipulability of the hand towards the head where poses of the shoulder and wrist are known. 27
2.7 A comparison of the point cloud data being observed by a Kinect for Xbox 360 camera (left) with the output of a skeleton tracking algorithm (right) showing that the upper limbs adopted a default pose due to self occlusion during collaboration with a robot. 28

3.1 A human co-worker working collaboratively with a robot in an abrasive blasting operation. 37
3.2 A) The human upper limb showing the positions of the shoulder $\boldsymbol{p}_S$, elbow $\boldsymbol{p}_E$ and wrist $\boldsymbol{p}_W$ and the lengths of the upper arm U and lower arm L (B) Location of the swivel coordinate frame $\boldsymbol{p}_C$ in relation to the subject's shoulder $\boldsymbol{p}_S$, elbow $\boldsymbol{p}_E$, wrist $\boldsymbol{p}_W$ and the angle α. (C) Swivel coordinate frame $\boldsymbol{u} \times \boldsymbol{v}$ showing the swivel angle ϕ and direction of gravity $\boldsymbol{g}$. 38
3.3 The end effector of a pHRC robot showing the left and right handle to be held onto by the human co-worker. 40
3.4 The Assistance-as-Needed roBOT (ANBOT) platform with a human co-worker performing a collaborative abrasive blasting operation. 41
3.5 The field of view of the four Kinect v1 cameras on the ANBOT. 42

3.6 (A) Path of the end effector to be followed during each experiment with the coordinate system of the force to be applied by the human subjects. (B) Experimental setup showing a subject with markers attached to their upper limb and the ANBOT platform used for the experiment [9]. 43
3.7 (A) Depiction of the force window applied by the human hand where the region in green satisfies the set constraint and the region in red will cause the robot to halt. (B) Visual aid used to display current Force/Torque sensor output alongside current experimental requirements such as the magnitude and direction of the force required from the subject and the current end effector motion. 44
3.8 The experimental setup showing the positions of the OptiTrack cameras as well as the seat placement. 48
3.9 Calculated swivel angles of Subjects (A) 5 and (B) 7 in Experiment 1. . . . 50
3.10 Mean swivel angles of all ten subjects in Experiment 1. 51
3.11 Calculated swivel angles of Subjects (A) 7 and (B) 9 in Experiment 2. . . . 52
3.12 Mean swivel angles of all ten subjects in Experiment 2. 53
3.13 Comparison of the mean and standard deviation of the swivel angles of Subjects (A) 4 and (B) 5 in Experiment 2 and Experiment 1. 54
3.14 Comparison of the mean and standard deviation of the swivel angles of Subjects (A) 8 and (B) 10 in Experiment 2 and Experiment 1. 55
3.15 Calculated swivel angles of Subject 4 in (A) Experiment 3 and (B) Experiment 4. 56
3.16 Mean swivel angles of all ten subjects in (A) Experiment 3 and (B) Experiment 4. 57
3.17 Comparison of the mean and standard deviation of the swivel angles of Subject 5 in (A) Experiment 3 and (B) Experiment 4 to Experiment 1. . . 58
3.18 Calculated swivel angles of Subject 5 in (A) Experiment 5 and (B) Experiment 6. 59
3.19 Mean swivel angles of all ten subjects in (A) Experiment 5 and (B) Experiment 6. 60
3.20 Comparison of the mean and standard deviation of the swivel angles of Subjects (A) 5 and (B) 10 in Experiment 5 and Experiment 1. 61
3.21 Comparison of the mean and standard deviation of the swivel angles of Subjects (A) 1 and (B) 9 in Experiment 5 and Experiment 1. 62
3.22 Comparison of the mean and standard deviation of the swivel angles of Subjects (A) 5 and (B) 9 in Experiment 6 and Experiment 1. 63
3.23 Comparison of the strength of Subject 5 during Experiment 1 and Experiment 4 66

4.1 Poses of the upper body estimated by the nullPose method. 71
4.2 Human-Robot interaction through a forearm cuff. 71
4.3 The right and left upper body halves. 72
4.4 A visualization of an elbow target and the corresponding task to move the elbow towards the target. 73
4.5 Flowchart of the nullPose method which updates the estimate to the upper body pose when new hand poses are received. 75

4.6 The nine DOF on each of the upper limb kinematic models. 78
4.7 Visualization of the shoulder girdle movement as the upper limb moves from (A) a downward elbow position to (B) an upward elbow position. 79
4.8 (A) The motion capture suit and handles used to track the human hands. (B) The collaboration between the human and the robot being simulated in Motion 3. 91
4.9 The poses being performed by the subjects in Motion 1. 92
4.10 The configuration of the two handles used in Motion 3. 93
4.11 Graphed result of the mean error with standard deviations of the upper body segments for Subject 1 in (A) Motion 1, (B) Motion 2 and (C) Motion 3. Errors are shown in meters for position and radians for rotation. 96
4.12 A snapshot of the recorded point cloud of the human subject (left) and the human pose obtained using skeleton tracking with the Kinect (right). 100
4.13 Box and whiskers plots of the error in the upper body pose from all subjects across the different scenarios in Experiment 2. 102
4.14 Box and whiskers plots of the torso position and orientation error compared against the two targets, the AR marker (AR) in Scenario 1 and the point cloud approximation (PCL) in Scenario 2. 107
4.15 A snapshot of estimated upper body pose with the two sets of torso targets used in Experiment 3 viewed from different angles. 108
4.16 Box and whiskers plot of the torso position and orientation error using the biomechanical limit vs no limit. 109

5.1 The real-time strength appraisal method using the nullPose method (left) and the conventional batch processed method (right). 115
5.2 Musculoskeletal model of the right upper limb [10] showing the different coordinates and their range of motion. (A) Elevation angle. (B) Shoulder Elevation. (C) Shoulder Rotation. (D) Elbow Flexion. (E) Pronation/-Supination. (F) Wrist Deviation. (G) Wrist Flexion/Extension 118
5.3 The musculoskeletal model of the right upper limb showing the thorax frame which grounds the musculoskeletal model as well as the scapula frame and the humerus frame. 119
5.4 Order of rotation for the right upper limb musculoskeletal model. 120
5.5 Visualization of the musculoskeletal model of the left and right upper limbs within the biomechanical model used by the nullPose method. 121
5.6 End effector of the ANBOT used in the experiments, showing the orientation and position of the handles and the direction of the force to be opposed by the human operator. 126
5.7 Estimated physical strength of the right (R) and left (L) upper limbs using the nullPose method (nP) and the batch processed method (BP). 128
5.8 Estimated strength of the right (R) and left (L) upper limbs using the nullPose method (nP) and the batch processed method (BP) of a subject with a large difference in estimated strength of left upper limb. 129
5.9 A human co-worker wearing a standard protective equipment for an abrasive blasting operation with the ANBOT. 131

5.10 The abrasive blasting chamber where the experiment was performed for Experiment 2. 132
5.11 Estimated strength of the left and right upper limbs in the abrasive blasting operation (Experiment 2). 133

6.1 Defined right and left hand poses on the end effector of the ANBOT. 143
6.2 The actual hand orientation in comparison to the cylindrical handle orientation. 148

A.1 Comparison of the mean and standard deviation of the swivel angles of subject 1 in (A) Experiment 2, (B) Experiment 3, (C) Experiment 4, (D) Experiment 5 and (E) Experiment 6 to Experiment 1. 152
A.2 Comparison of the mean and standard deviation of the swivel angles of subject 2 in (A) Experiment 2, (B) Experiment 3, (C) Experiment 4, (D) Experiment 5 and (E) Experiment 6 to Experiment 1. 153
A.3 Comparison of the mean and standard deviation of the swivel angles of subject 3 in (A) Experiment 2, (B) Experiment 3, (C) Experiment 4, (D) Experiment 5 and (E) Experiment 6 to Experiment 1. 154
A.4 Comparison of the mean and standard deviation of the swivel angles of subject 4 in (A) Experiment 2, (B) Experiment 3, (C) Experiment 4, (D) Experiment 5 and (E) Experiment 6 to Experiment 1. 155
A.5 Comparison of the mean and standard deviation of the swivel angles of subject 5 in (A) Experiment 2, (B) Experiment 3, (C) Experiment 4, (D) Experiment 5 and (E) Experiment 6 to Experiment 1. 156
A.6 Comparison of the mean and standard deviation of the swivel angles of subject 6 in (A) Experiment 2, (B) Experiment 3, (C) Experiment 4, (D) Experiment 5 and (E) Experiment 6 to Experiment 1. 157
A.7 Comparison of the mean and standard deviation of the swivel angles of subject 7 in (A) Experiment 2, (B) Experiment 3, (C) Experiment 4, (D) Experiment 5 and (E) Experiment 6 to Experiment 1. 158
A.8 Comparison of the mean and standard deviation of the swivel angles of subject 8 in (A) Experiment 2, (B) Experiment 3, (C) Experiment 4, (D) Experiment 5 and (E) Experiment 6 to Experiment 1. 159
A.9 Comparison of the mean and standard deviation of the swivel angles of subject 9 in (A) Experiment 2, (B) Experiment 3, (C) Experiment 4, (D) Experiment 5 and (E) Experiment 6 to Experiment 1. 160
A.10 Comparison of the mean and standard deviation of the swivel angles of subject 10 in (A) Experiment 2, (B) Experiment 3, (C) Experiment 4, (D) Experiment 5 and (E) Experiment 6 to Experiment 1. 161

B.1 The Hilbert-Schmidt Norm of the null space based on the different combination of tasks that can be implemented. 163

C.1 Graphed result of the mean error with standard deviations of the upper body segments for Subject 2 in (A) Motion 1, (B) Motion 2 and (C) Motion 3. Errors are shown in meters for position and radians for rotation. 166

C.2 Graphed result of the mean error with standard deviations of the upper body segments for Subject 3 in (A) Motion 1, (B) Motion 2 and (C) Motion 3. Errors are shown in meters for position and radians for rotation. 167

E.1 Estimated muscle activation of the right and left musculoskeletal model in Experiment 2. 171

List of Tables

3.1 Root mean square deviation of a subject's mean swivel angle against the raw swivel angles of all subjects calculated for Experiment 1. 51
3.2 root mean square deviation (RMSD) of the swivel angles in different experiments, measured against the mean swivel angle of the same subject in Experiment 1. 65

4.1 Joints limits of the upper limb model used by the nullPose method. 78
4.2 Range of motion of each joint of the upper limb model 79
4.3 Scenario list with targets used by the nullPose method for Experiment 1 . . 93
4.4 Results showing the mean and standard deviation of error in the upper body pose estimates using different scenarios for each recorded data in Experiment 1. 95
4.5 The different combinations of targets used in Experiment 2. 99
4.6 Mean and standard deviation of the error of upper body poses for all subject in Experiment 2. 103
4.7 The two scenarios used in Experiment 3. 106

5.1 Table of the upper limb musculoskeletal model joint coordinates along with the conversion from the biomechanical model of the upper limb used by the nullPose method for both the right and left upper limbs of the human. . . . 121
5.2 The combination of targets used by the nullPose method for Experiment 1 set in the motion capture environment. 126
5.3 Estimated physical strength with the mean error and standard deviation using the nullPose method (nP) and the conventional batch processing method (BP) 128
5.4 Scenario list with targets used by the nullPose method for Experiment 2: Abrasive Blasting Chamber 131

B.1 A list of potential targets being used to resolve the redundancy of the upper body pose. 164
B.2 The combination of seven sets of information being used to obtain a fully constrained upper body pose where a 1 symbolize a target being used and a 0 symbolizes an information that is not used. Target # corresponds to the information shown in Table B.1 164

E.1 List of muscles in the musculoskeletal model and their abbreviations [10] pt.1.172
E.2 List of muscles in the musculoskeletal model and their abbreviations [10] pt.2.173

Acronyms & Abbreviations

1D	One-Dimensional
2D	Two-Dimensional
3D	Three-Dimensional
AAN	Assistance-as-Needed
ANBOT	Assistance-as-Needed roBOT
AR	Augmented Reality
CAS	Centre for Autonomous Systems
DOF	Degrees of Freedom
EMG	Electromyography
GH	Glenohumeral
HRI	Human-Robot Interaction
IAD	Intelligent Assist Device
IK	Inverse Kinematic
IMU	Inertial Measurement Unit
UTS	University of Technology Sydney
MoCap	Motion Capture
MRI	Magnetic Resonance Imaging

MTU	Musculo-Tendon Units
pHRC	physical Human-Robot Collaboration
pHRI	physical Human-Robot Interaction
RMSD	root mean square deviation
RMSE	root mean square error
ROM	range of motion
sEMG	surface electromyography
SE(3)	special Eucledian group representing a rigid transformation in a 3-dimensional Euclidean Space
SO(3)	special orthogonal group in 3 dimensions representing a rotation
SG	shoulder girdle
SNS	Saturation into the Null Space
WMSD	Workplace Musculoskeletal Disorder

Glossary of Terms

Assistance	The act of helping someone by sharing the work or load.
Bimanual	Requiring two hands.
Capability	The power or ability to perform a certain operation.
Collaboration	The action of working with another human or robot to complete an operation.
Fatigue	The decline in the capability of a human.
Human co-worker	The human collaborating with the robot to complete an operation.
Inverse kinematics	Calculation performed to determine the joint values given a pose in Cartesian co-ordinates.
Kinematic chain	An assembly of rigid bodies connected by joints.
Musculoskeletal	Relating to the musculature and skeletal structure of a body.
Operation	Work to be completed by the human and robot.
Real-time	Able to respond to input immediately.
Physical strength	The amount of force able to be generated or opposed at the hand of the human co-worker.
Pose	The position and orientation of an object such as the end effector of a robot or the hand of the human co-worker.
Redundancy	The ability to adopt a different configuration without affecting the end-effector pose.
Swivel angle	The angle between the vertical plane passing through the shoulder and the wrist and the plane containing the whole upper limb.

Task	Motion to be accommodated by the joints of the upper limb kinematic models.
Target	A kinematic constraint obtained through sensors or approximations, used by the nullPose method to generate a better upper body pose estimate.
Torso half	The upper body of the human divided vertically in half.
Unimanual	Using a single hand.
Upper body	The human human from the waist up including the upper limbs, torso and head.
Upper body half	The human upper body from the waist up divided vertically in half. Each upper body half consists of a torso half and an upper limb.
Upper limb	The human upper limb starting from the shoulder down to the hand.

Chapter 1

Introduction

Fully autonomous robotic systems have been developed in order to eliminate the requirement of a human in operations which have high potential risks. An example of such a robot is the Alpha 1 by Sabre Autonomous Solutions [11] which was used to clean metallic surfaces in tight, confined spaces such as within the steel structure of a bridge. An operation which would have required a human worker to perform an abrasive blasting operation in an enclosed space could be completed using a robot, eliminating the risk of injury and other health issues to the human worker. These robots are designed to operate in confined spaces, isolated from human workers and do not take them into account.

Through the development of sensing and actuation technologies and advancement in robotics, the boundary between the human and the robot has been broken down [12]. A field of robotics that studies the physical interaction between a human and a robot is physical Human-Robot Interaction (pHRI) [13]. pHRI considers physical interaction between human and robot, with an emphasis on maintaining human safety [14]. A subset of pHRI, physical Human-Robot Collaboration (pHRC) refers to a type of human-robot interaction in which the human controls the robot through direct physical contact, applying forces onto the robot (Figure 1.1). In pHRC systems, the robot is often controlled through well-defined interaction points such as handles for the human co-worker to hold on to.

Unlike fully automated robotic systems, by having the human in the loop in a pHRC system, operations which were difficult for the robot or the human to complete individually

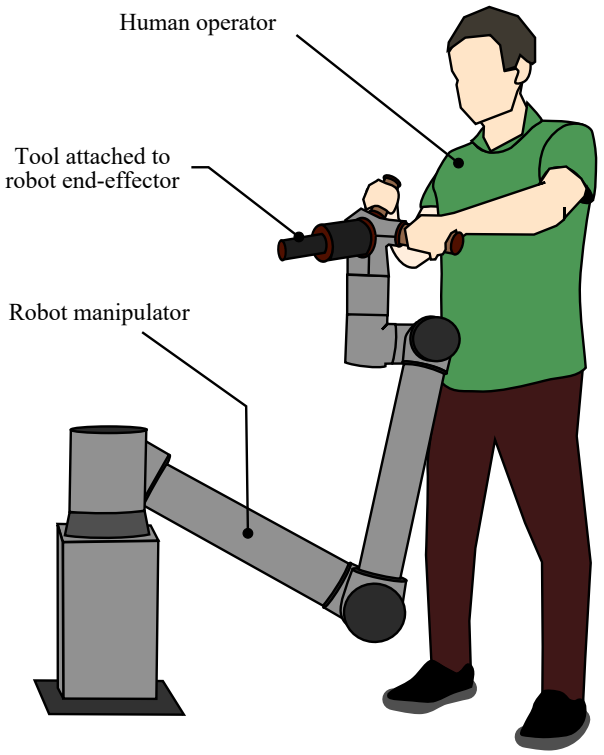

FIGURE 1.1: An example of a pHRC application where the human and the robot collaborate to complete an operation.

could be performed with less effort. The expertise of a skilled human co-worker in their specialized profession could be leveraged to achieve a better outcome whilst reducing the required physical strain on the human co-worker. This allows the task to be completed by the human co-worker with a reduced risk of injury [15].

A common form of assistance that is provided by a pHRC robotic system is the removal of unwanted vibrations [16] or the reduction of reaction loads. This allows the operation to be completed by the human co-worker with a reduced human effort. One form of assistance that has gained interest in rehabilitative application is Assistance-as-Needed (AAN) paradigms. In these paradigms, the level of assistance to be provided to the human co-worker is adapted based on the need of the human co-worker. One way in which the need of the human can be estimated is through appraisal of the human capability, such as the physical strength of the human co-worker.

If the physical strength of the human co-worker is able to be appraised, it is envisaged that the interaction between the human and the robot is able to be improved through

the adaptation of the assistance to be provided to the human. For a collaborative robot to appraise the physical strength of a human co-worker in real-time, an estimate of the human co-worker's pose is required. Estimating the pose of the human co-worker can be challenging, especially in practical industrial applications where factors such as poor illumination and suspended particulates in the air may be prominent. Unlike other types of Human-Robot Interaction (HRI), in pHRC the human co-worker and the robot work in close proximity to one another, resulting in additional challenges when determining the pose of the human co-worker. Non-ideal environments in which the collaboration takes place can also increase the difficulty in estimating the pose of the human co-worker.

1.1 Background and Motivation

In the past, due to the limitation in technologies, humans and robots could not work in the same environment. Risk of injury to the human is high when a human is in close proximity with robots which are conventionally used in industrial applications. These industrial robots are designed to perform repetitive or physically intensive and well defined operations. Not all applications are able to be completed solely by a robot and may require human input. Due to this, solutions such as commercial collaborative robots have been developed to allow a human co-worker to collaborate with robots to achieve a common goal.

Whereas conventional industrial robots often require an enclosed environment devoid of human presence, in pHRI or pHRC applications the human input is necessary for the robotic system. With the human in the loop, an operation which traditionally would be required to be well defined could be perceived and interpreted by the human, allowing for greater flexibility in the type of operations being performed. The adaptability to react to an unexpected situation, as well as decision making capability of a human co-worker complements the strength, endurance and precision of the robot such that a wide variety of operations could be performed.

A human co-worker collaborating with a robot may receive various types of assistance from the robot, such as increased precision [17] or motivation [18]. A common type of assistance

to be provided by a robot is the reduction of large reaction loads from the operation to reduce the fatigue of the human co-worker. Tasks which are often found to be difficult or impossible for a human to complete alone are able to be performed with a reduced effort through assistance provided by a collaborative robot.

As a human observing another human co-worker, a decision is made to determine whether a co-worker is in need of assistance through various implicit cues such as the amount of time spent on an operation, the co-worker's posture or their performance with regards to the operation. Robots do not have this innate ability to empathize with a struggling co-worker during a human-robot collaboration and often require an explicit cue or command in order to provide assistance to the human co-worker. A similar assistance behaviour in pHRC is expected to be achieved if the robot can perceive and determine the appropriate amount of support required by the human co-worker.

AAN paradigms have been developed to adapt the assistance provided by the robot based on the current need of the human to assist patients to complete rehabilitation exercises with a robot [19, 20]. The need of the human co-worker is commonly defined by a perception of the human co-worker's performance (performance based AAN) or appraisal of the human co-worker's capability (model based AAN). An advantage of model based AAN in industrial applications is that an appropriate level of assistance can be provided to the human co-worker without requiring a measure of the performance in the operation, allowing for a larger variety of operations to be performed by the human co-worker and the robot.

Figure 1.2 shows a framework that could be used to provide adaptive assistance in a model-based AAN paradigm. To determine how much assistance that is to be provided to a human co-worker, three key components are present. The first is the capability of the human which in this thesis is represented by physical strength. The second component is the requirement from the application which relates to the forces required in order to achieve a goal. The last component is the capability of the robot to ensure that the required assistance is able to be supplied by the robot during the pHRC.

In Figure 1.2 the physical strength of the human has been simplified to two factors, the current pose of the human body and a corresponding musculoskeletal model. Using these two factors an estimate to the human physical strength is able to be obtained [21, 22].

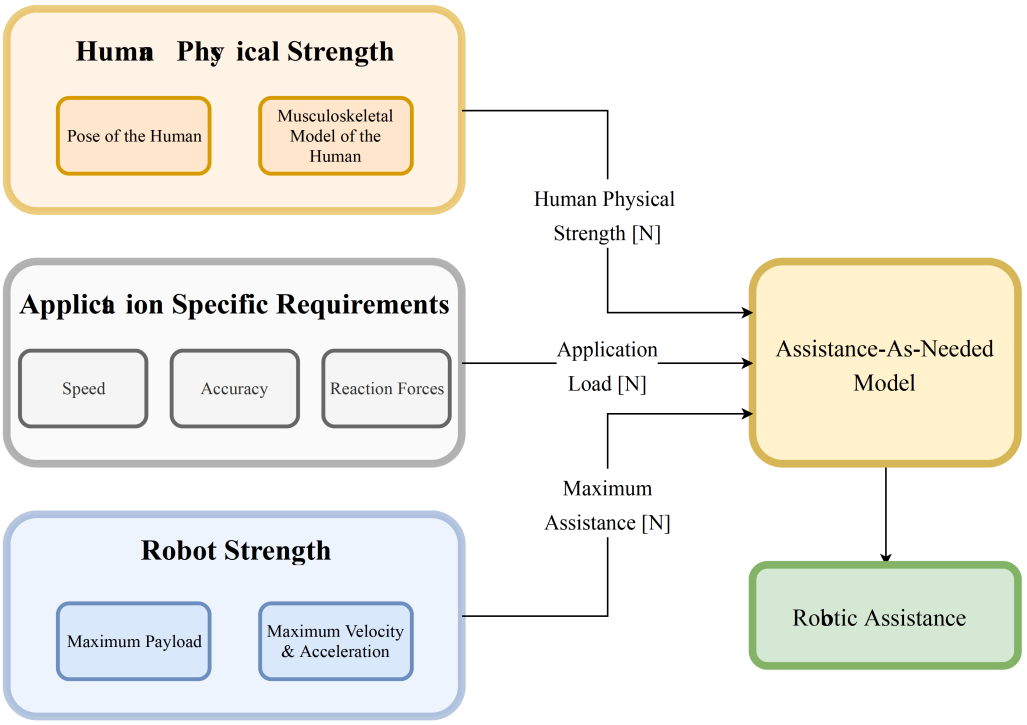

FIGURE 1.2: The three components that are required to adapt the assistance to be provided to the human by the robot in a model-based AAN paradigm.

Unlike the robot strength and the application requirements, the human physical strength is more challenging to appraise due to the redundancy in the human body allowing for a wide variety of poses to be adopted to achieve the same outcome and the physical fitness of the individual. To appraise the physical strength of the human co-worker in a framework such as the one shown in Figure 1.2, the human co-worker's pose is required. The environment in which the collaboration is to take place increases the difficulty in measuring the pose of the human co-worker. In a practical industrial environment, factors such as poor illumination, suspended particulates in the air as well as occlusions from the close proximity of the human and the robot affect the sensors and methods that are able to be used to measure the pose of the human.

1.2 Research Questions

This thesis aims to answer the research questions surrounding the estimation of the human co-worker's pose during pHRC to facilitate the real-time appraisal of the human physical

strength. It is envisaged that if the robot is able to appraise the physical strength of the human co-worker, more intuitive assistance is able to be provided. The pose of the human body, especially the upper body, greatly affects the physical strength of the human co-worker [21, 23] and is often challenging to measure in real pHRC applications due to factors such as poor illumination, suspended particulates in the air and the close proximity of the human co-worker to the robot. The first research question explores the effect of the interaction between the human and robot on the pose of the human. The second research question explores whether the interaction in pHRC can be exploited to provide an estimate to the pose of the human. The final research question explores the real-time appraisal of the human co-worker's physical strength in real pHRC applications using the estimated pose of the human co-worker.

1.2.1 Research Question 1: Effect of Interaction Between the Human and Robot on the Pose of the Human

Due to the redundancy in the upper body, a wide variety of poses are able to be adopted by the human. Humans will generally adopt a pose that is deemed most natural to the individual. Pose estimation models have been used in applications where it is difficult or impractical to directly measure the pose of the human [8, 24]. For a human collaborating with a robot, inherent constraints are placed onto the human which may result in a different pose being adopted by the human [25]. An investigation was performed to determine whether the pose of the human upper limb is affected by the interaction during pHRC. Two main factors were investigated. The first factor is the direction and magnitude of the force to be exerted in pHRC. The second factor is the effect of restricting the relative pose between the two hands in a bimanual pHRC operation.

1.2.2 Research Question 2: Exploiting the Interaction in pHRC for Estimate the Pose of the Human

In a real pHRC application, it is often difficult to directly measure the pose of the human co-worker. Tracking methods requiring specialized suits to be worn by the human worker are unlikely to be used in practical industrial applications. In an outdoor environment

or in environments where lighting is poor the feasibility of human tracking using sensors such as a motion capture system is reduced. The close proximity of the robot to the human increases the likelihood of occlusion of the human due to the robot, limiting the capability of skeleton tracking algorithms. On the other hand, some pHRC applications are able to provide information that can be exploited for estimation of the human pose, for example, the pose of the human co-worker's hands during the collaboration with the robot. Alongside sensor measurements and approximations, the pose of the hands may be able to be used to estimate the upper body pose.

1.2.3 Research Question 3: Appraisal of the Human Co-worker's Physical Strength by using an Estimated Pose

Estimating the physical strength of a human co-worker is difficult due to the complexity of the human body. In order to estimate the physical strength of the human, musculoskeletal models can be used to estimate muscle path and activation given a specific pose or motion. These models are conventionally used with a motion capture recording for batch processed analysis of the motion. These analyses had to be performed as a batch process as real-time Inverse Kinematic (IK) of the model using existing software packages are computationally expensive. To estimate the physical strength of the human co-worker the real time pose of the human co-worker is required. In practical pHRC applications, it is often not feasible to measure the current pose of the human and thus an estimate is used. Errors in the estimated pose will likely introduce error in the appraisal of the human physical strength. Therefore an investigation needs to be performed to determine whether the error from the estimated pose of the human results in an acceptable appraisal of the human physical strength.

1.3 Scope

This thesis investigates real-time estimation of the human co-worker's pose during pHRC to improve the interaction between the human and the robot, addressing the three research questions listed in Section 1.2. The work presented in this thesis focuses on pHRC where

the human co-worker controls the robot by exerting forces on to the handles attached to the end effector of the robot as shown in Figure 1.1. Although the methods and algorithms detailed in this work are applied under an abrasive blasting environment with a pHRC robot, it can be extended to other pHRC applications where sensory information is limited. Sensory information may be limited in different robotic applications due to factors such as occlusion of the necessary information or failure of sensors during the operation.

Unlike the free motion assumed by existing pose estimation models, constraints are placed on the human co-worker during pHRC. To explore the effect of the interaction between the human and the robot on the naturally adopted pose of the human co-worker, experiments were performed with ten human subjects where the poses of the right upper limbs were compared under different constraints. The constraints implemented in this thesis were the direction and magnitude of the force as well as bimanual operation, where the human subjects were required to place both hands on the end effector of the robot.

The nullPose method presented in this thesis is a method of estimating the pose of the human upper body in pHRC applications where the hands of the human co-worker are able to be inferred from the interaction between the human and the robot. In this thesis the nullPose method was tested in pHRC applications where the hands of the human co-worker are inferred from poses of the handles attached to the end effector of the robot. In reality as long as the human co-worker's hand poses are known, the nullPose method is able to be used to provide the pose of the human upper body. Only the upper body of the human co-worker is estimated by the nullPose method as the most common form of interaction between the human and the robot is through the hand of the human co-worker. Factors relating to the extension of the nullPose method to estimate the pose of the full human body and directions for future works was discussed in Chapter 6.

The capability of the human co-worker was also appraised in real time by implementing the nullPose method. The scope of the human capability that is addressed in this work is the physical strength. Although the capability of a human to complete an operation is not only limited to the physical strength of the human, the other factors are not considered and may be addressed in future works. The aim of obtaining the physical strength of the human is to allow the robot to adapt the assistance provided to the human through AAN

paradigms. How the physical strength of the human may be used to adapt the assistance was considered but was not discussed in details in this thesis.

To estimate the upper body pose of the human, a biomechanical model of the human upper limb was used. This model provided a set of limits for each of the joints of the upper limb. These joint limits were generic and not individualized. Work towards individualization of such models was not included in this thesis. Similarly to practically appraise the physical strength of the human co-worker in a pHRC operation, musculoskeletal models of the upper limb were used. Generic upper body musculoskeletal models were used that reflect the population rather than the individual. Work towards individualized musculoskeletal models was not conducted in this thesis.

1.4 Contribution

The following are the main contributions from the work in this thesis:

- Effect of the interaction between a human and robot in a pHRC application on the naturally adopted pose of the human upper limb. (Chapter 3)
- nullPose, a method of estimating the upper body pose of a human co-worker working collaboratively with a robot, capable of being used in practical unstructured environments. (Chapter 4)
- Real-time appraisal of the human physical strength using the nullPose method during a pHRC operation. (Chapter 5)
- Development towards the Assistance-as-Needed roBOT (ANBOT) prototype, a pHRC robot designed to assist human workers in abrasive blasting operations.

1.5 Publications

- Khonasty, R., Carmichael, M. G., Liu, D. & Aldini S., Effect of External Force and Bimanual Operation on Upper Limb Pose during Human-Robot Collaboration.

Australasian Conference on Robotics and Automation (ACRA), 2017, ISBN: 978-0-9807404-8-6 ISSN: 1448-2053

- Khonasty, R., Carmichael, M. G., Liu, D. & Waldron K., Upper Body Pose Estimation Utilizing Kinematic Constraints from Physical Human-Robot Interaction. Australasian Conference on Robotics and Automation (ACRA), 2017, ISBN: 978-0-9807404-8-6 ISSN: 1448-2053

- Khonasty, R., Carmichael, M. G. & Liu, D., nullPose: An Upper Body Pose Estimation Method for physical Human-Robot Collaboration. (to be submitted to IEEE Transactions on Robotics)

- Carmichael M. G., Khonasty R. & Liu D., A multi-stage design framework for the development of task-specific robotic exoskeletons, 2015 37th Annual International Conference of the IEEE Engineering in Medicine and Biology Society (EMBC), Milan, 2015, pp. 1176-1180. doi: 10.1109/EMBC.2015.7318576

1.6 Thesis Outline

This thesis is organized as follows:

1.6.1 Chapter 2

In Chapter 2, a review of works related to this thesis is presented. In this chapter a variety of pHRC systems are presented, highlighting the trend of humans and robots working together to complete tasks. The notion of human strength and how it is beneficial for a human-robot collaborative scenario is also explored. Lastly the concept of human tracking with an emphasis on a pHRC setting is reviewed.

1.6.2 Chapter 3

In Chapter 3, an investigation was performed to determine the effect of interaction between the human and the robot on the adopted pose of the human upper limb. The two

main factors tested were the effect of force exertion by the human as well as bimanual operation with a pHRC robot. The experiments were conducted with human subjects in a motion capture lab to determine whether existing pose estimation methods are able to be implemented to provide the pose of the human upper body during pHRC.

1.6.3 Chapter 4

Chapter 4 presents the nullPose method, an upper body pose estimation method where the poses of the human co-worker's hands are known or able to be inferred from the interaction between the human and the robot. A biomechanical model of the human upper limbs was used to ensure that the estimated upper body pose is humanly feasible. The nullPose method controls the upper limb models through differential kinematics to estimate the pose of the full upper body. Redundancy in the upper body was resolved by incorporating sensor measurements and approximations as tasks to be achieved by the upper body.

1.6.4 Chapter 5

Chapter 5 presents an implementation of the nullPose method to facilitate a real-time appraisal of the human physical strength during a pHRC operation with a collaborative robot. Experiments were conducted in two environments to assess the estimated physical strength of the human co-worker. In the first environment, the estimated strength using the nullPose method was compared to a commonly used batch processed method of estimating strength. The second environment highlighted the advantage of the nullStrength method in being able to estimate the strength of the human co-worker in difficult environments.

1.6.5 Chapter 6

In Chapter 6, a summary of the thesis and the conclusion is outlined. A discussion of the limitations in the presented methods, as well as future works, are included in this chapter.

Chapter 2

Review of Related Work

This chapter presents the background information and research related to the estimation of the human co-worker's pose to facilitate appraisal of human capabilities in physical Human-Robot Collaboration (pHRC). Section 2.1 introduces the field of pHRC and various robotic systems used to assist humans performs a wide variety of operations. Robotic systems presented in this section are often used to augment the strength of a human co-worker or assist the human performing certain operations such that less effort is required from the human.

Section 2.2 provides a review of Assistance-as-Needed (AAN) paradigms commonly used by robotic systems to provide adaptive assistance to a human subject or patient. Two main categories of AAN paradigms are discussed along with the benefits and disadvantages of the different methods.

Section 2.3 explores the different methods that are commonly used to determine the pose of the human co-worker and their applicability in a pHRC application. The pose of the human co-worker is important in a pHRC application as the physical strength of the human co-worker is able to be estimated from the pose. Methods of measuring or estimating the pose of the human reviewed in this section have an emphasis on human-robot collaborative applications set in an industrial environment where visibility is often not ideal.

Section 2.4 reviews the methodologies for determining the physical strength of the human. The different applications that have utilized these methods are also reviewed. The physical

strength of the human is important in pHRC as it provides a method of determining the safety of the human and will also allow for the robot to provide a more intuitive form of assistance.

2.1 Physical Human-Robot Collaboration

Whereas industrial robots used in the past have been separated from humans, improving technologies have seen humans and robot interact with one another to complete an operation. Human-Robot Interaction (HRI) is a field of robotics that studies the interaction between a human and a robot. A subset of this field is physical Human-Robot Collaboration (pHRC) in which a human and a robot collaborate with sustained physical contact between the human and the robot. This section presents works related to the assistance being provided by these robots in various forms of HRI with a larger emphasis on pHRC.

2.1.1 Traditional Robots

Traditionally robots were developed to perform a variety of operations that are too difficult for humans to perform [26]. Robots have also been implemented in operations which are deemed too dangerous for humans, such as in military applications [27] and ordinance disposal [28]. The precision and repeatability of the robot can be utilized to ensure a standard quality of the outcome of the operation but are unable to adapt to unexpected changes in the operation [29]. These robots require the operation to be well defined [30] or for the robot to be controlled through teleoperation by a human operator [31].

In operations involving these types of robots, humans are not able to work in the surrounding workspace whether it be due to the hazardous environment or the risk of injury to the human due to collision or other risks. Industrial robots often have limited sensing capabilities, requiring the robot to be enclosed in a cage to ensure that a human does not wander into the workspace of the robot (Figure 2.1). Accidents that involve industrial robots commonly occur when a human enters the workspace of the robot whether due to the human negligence or during maintenance of the robot [32].

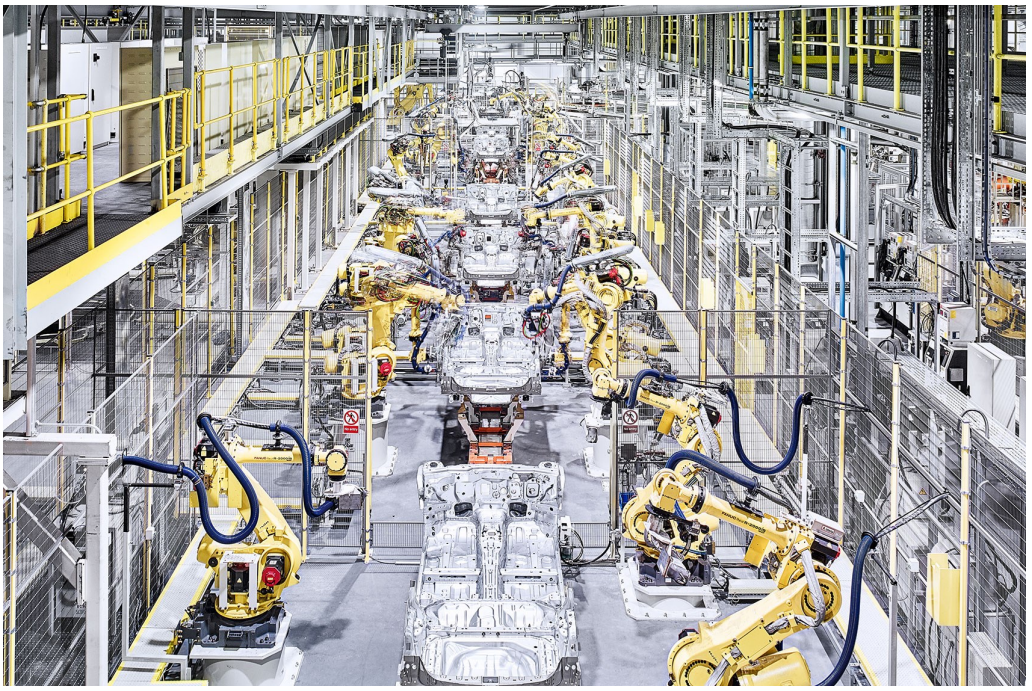

FIGURE 2.1: Industrial robots being used in the automotive industry. Cages are setup around the robot to ensure human workers do not accidentally enter the workspace of the robot [1].

2.1.2 Autonomous Robots

Autonomous robots have been developed in tasks where it is difficult or impossible to predefine the problem to be completed by the robot. An example of an autonomous robot is the inchworm inspired robot designed for inspection of a steel bridge where it is difficult for a human to fit within the steel structure [33, 34] and the autonomous abrasive blasting robot [35, 36] which is deployed in an enclosed environment full of suspended particle unsuitable for human workers.

Similarly to traditional robots, these robots have little to no contact with the human operators and are often deployed in environments that are deemed to be too hazardous for humans. The advantage of the autonomous robot is that the robots are able to adapt to the current environment and recognize the current situation to complete the operation [37].

2.1.3 Collaborative Robots

Advancements in technology have seen human and machine work together, leading to the development of human safe robots designed for collaborative operations such as ones shown in Figure 2.2. These type of robots are designed to share their workspace with human co-workers to achieve a common goal [38, 39]. Sensing and control algorithms have been developed to ensure the safety of a human working in close proximity to robots [40, 41]. Compliant joints also increases the safety of the human in the event that a collision is to occur between the human and the robot [42–44].

(A) (B) (C)

FIGURE 2.2: Examples of human safe robots designed for collaborative applications: (A) Universal Robot UR10 [2] (B) Kuka LBR iiwa [3] (C) Rethink Robotics Sawyer [4].

In physical Human-Robot Interaction (pHRI) applications the main imperative is the safety of the human [45]. Factors such as the amount of forces and torques produced by the robot and the velocity of the end effector of the robot are some of the aspects that have to be considered when a human is sharing the workspace with a robot [46, 47]. These factors are often defined by standards such as [48–51].

In applications where the operation to be completed is well defined and structured, autonomous robotic systems can be used to a high degree of accuracy and repeatability [52]. In applications where it is difficult to define the required operation or in applications set in dynamic unstructured environments, the adaptability and expertise of the human is beneficial. In this manner the complementary skills of the human and robot can be combined to perform difficult operations [13].

A common form of assistance that a robot often provides is to increase the physical strength of the human. These robots are designed as a device that provides humans with mechanical

advantage [53], reducing the effort required by the human to complete the operation. Unlike traditional industrial robots, collaborative robots are able to perform operations with a human in the loop [54, 55]. The robot can be used to lighten the workload of the human or to comply with the needs of the human co-worker [15], reducing the risk of Workplace Musculoskeletal Disorder (WMSD). From a report by Safe Work Australia, WMSDs accounted for 60 % of all serious work compensation claims over the five year period between 2009-2014 [56].

2.1.3.1 Collaborative Robots for Strength Augmentation

A common type of robot designed to augment the physical strength of a human are exoskeletons. These robots are designed to be worn by the human mimicking the movement of the human body while providing assistance to the human. An example of an exoskeleton is the Berkeley Lower Limb Exoskeleton (BLEEX) [5]. This robot is designed to be worn by a human, attached to their lower body. The main purpose of BLEEX is to provide the wearer with additional carrying capacity while reducing the strain placed on the human body. Another example is the ABLE exoskeleton [57] which has been used to assist workers in a car manufacturing factory performing an overhead operation in an awkward posture.

2.1.3.2 Collaborative Robots in Rehabilitation

Collaborative robots have been of interest in the field of rehabilitation [58–60]. Rehabilitation therapy to treat diseases such as stroke are often labour intensive and can be costly [61]. Physically collaborative robots have been used to assist physiotherapists performing rehabilitation exercises with the patient [62, 63]. These robots reduce the physical strain on the physiotherapist as no physical assistance is required from the therapist [64]. Another advantage of robot assisted therapy is the frequency in which the rehabilitation exercise could be performed correctly [65]. Movements of the patient can be accommodated by the robot, such as the one shown in Figure 2.4, to ensure the correct movements are performed by the human subject. A robotic system can be brought to the patient's

FIGURE 2.3: A human wearing the BLEEX [5] used to support the human carry a heavy load.

home to be used on a daily basis which will allow a correct exercise to be performed, promoting the recovery of the patient.

FIGURE 2.4: An upper body exoskeleton the JEXO designed based on the range of motion of the human shoulder to be used in upper limb rehabilitation [6].

2.1.4 Types of Assistance

Assistance has been provided to humans from different robotic systems with varying effect. In the case of the surgery devices such as the da Vinci robotic system [17], the assistance provided increased the dexterity of the surgeons [66]. The study done in [67] shows that for an operation being measured, the time required for an operation was largely improved where robotic assistance was provided. Assistance could also be implemented to help in training novice workers. In the study conducted in [68] the effect of assistance was beneficial to novice surgeons training for a laparoscopic procedure. The assistance enabled the novice operator to conduct the operation with increased speed and consistency over several repetitions. In another study conducted on a manufacturing application, the use of an assistive robot resulted in reduced performance in the operation [15]. The reduced risk of injury to the human workers was deemed to outweigh the negative of the reduced performance.

Although robotic assistance is able to positively influence the capabilities of human operators by extending their normal capabilities [66] or helping patients regain their previous capability [59] there could be unwanted side effects. In [69] an orthosis for walking assistance was developed. One of the positive outcomes that the authors discovered was that the size of the step of the human wearing the orthosis was increased. A side effect to the increase in performance which was observed in the patient is a higher muscle activation. Although an increased step size meant that the performance of the patient is theoretically increased, more muscles of the human were activated to stop the human from overbalancing which results in an increased strain on the human body.

Effect of assistance has also been investigated in [70] where an Intelligent Assist Device (IAD) was designed in operations requiring heavy loads to be moved up and down hills. The IAD in [70] was designed to assist workers in log winching operations by slack pulling. The IAD shows positive effects when the load is moved downhill as the work could be completed with a single worker rather than requiring two workers. Although there was a benefit to the slack puller IAD, it did not result in any reduction in the physiological workload of the single human worker. The workload of the human worker was unable to be reduced as the main cause of stress in the work was not being assisted by the IAD.

2.1.5 Robots Providing Adaptive Assistance

From these studies, it can be seen that robotic assistance can be beneficial in improving the performance of an operation being completed. Without eliminating or reducing the primary stressors in the operation, the assistance may result in an increased effort from the human in keeping up with the increased performance [69]. This may result in an increased risk of injury when performing the operation for a prolonged period of time. Therefore it can be argued that the assistance should be adapted based on the current operation being performed.

An example of robots which adapt the assistance to be provided to the human are robots which have been designed for rehabilitative applications [71]. These robots are often used to assist patients undergoing therapy for diseases such as stroke, motor-neuron disease and spinal cord injury. In the study conducted in [72], robot-assisted movement training was found to have a better outcome than manual training. Another advantage of robot-assisted therapy is in the engagement of the patient as well as the ability to provide high intensity therapy with less effort required from the therapist reviewing the progress of the patient [73].

Although adaptive assistance paradigms such as Assistance-as-Needed (AAN) have seen some success in rehabilitative applications, adaptive assistance is difficult to implement in real pHRC applications. Assistance being provided to humans in real pHRC applications is usually designed to reduce the effort being contributed by the human [74] such as reducing the load experienced by the human [75]. Another form of assistance is to provide the human with the necessary tools during a manufacturing or assembly operation [76, 77]. A difficult aspect in adapting the assistance to be provided by the robot is appraising the capability of the human. In real applications, appraising the capability of the human is difficult especially due to sensor limitations and the inherent non-deterministic nature of the human.

2.2 Adaptive Assistance

A paradigm which has found interest in rehabilitative application is AAN. AAN can be viewed as a form of the *challenge point theory*. The challenge point theory states that learning is related to the outcome of the operation and that the difficulty of the operation should be catered to the skill level of the person performing the operation for a better learning experience [78]. If an operation is considered too easy or too difficult for the learner to accomplish, it is likely that the performance of the learner would be reduced [79–81]. This theory has been used in applications ranging from novice surgeons performing a new operation [82] to stroke sufferers performing rehabilitative upper limb motions [83, 84] where it was found that novice learners were found to have a lower learning rate when a constant amount of assistance was provided. AAN paradigms can often be divided into two main categories. The first alters the amount of assistance to be provided to the human based on the perceived performance of the human [82]. The second category adapts the amount of assistance by estimating the current capability of the human [85].

2.2.1 Level of Assistance

Although collaborative robots are designed to assist the human perform certain difficult operations, providing the full assistance to the human may not always be beneficial. An intrinsic property of the human motor system is "slacking", a method of minimizing the amount of work required by the human [86, 87]. Therefore providing too much assistance to accommodate the full operation requirement may detract from the outcome of the operation. For example, in rehabilitative applications, providing the full amount of effort required for a patient to complete the exercise could promote slacking by the patient, leading to reduced engagement and impairing the therapy [88] and the progress of the patient's recovery.

Performing an operation which is too difficult for a worker or a patient will likely demoralize the worker or patient, leading to a decrease in participation or effort in the operation being attempted. In rehabilitative applications simple motion of the upper limb may be too difficult for a patient to complete causing the patient to rely on the assistance from

the rehabilitation specialist or robot. To reduce the reliance on assistance in rehabilitative applications, AAN paradigms have been developed to adapt the amount of assistance provided by the collaborative robot [19, 89, 90]. In [91] a normal assistance model was compared to the AAN paradigm where it was shown that the AAN paradigm led to an increased effort from the human. By minimally assisting the human to complete operations which they would not have been able to complete individually, patients were shown to have gained more from robotic assistance rehabilitation in comparison to traditional methods [64].

2.2.2 Performance Based Assistance-as-Needed

Performance based AAN paradigms have been developed for various rehabilitative applications [92]. This type of AAN paradigm was used to assist patients perform rehabilitative exercises based on the minimum amount of work required to assist the human complete the operation [93, 94]. By creating successes in the rehabilitation exercise, engagement is increased and the subject feels encouraged to continue the exercise [95]. Performance based AAN has been used in robot assisted movement training following neurological injuries to reduce the physical workload of rehabilitation physicians and to increase the reproducibility of the exercises.

The amount of assistance to be provided by the robot is often altered based on the assessment of the therapist [95, 96] or through the assessment of the human performance by the robot. In [97, 98], the force applied by the robot in the rehabilitation exercise is dependent on the trajectory of the limb being exercised. If the trajectory is outside of a desired band a higher force is applied to the human to reintroduce the motion to the patient.

Although this type of AAN is theoretically sound, it does not solve the slacking that occurs with rehabilitation patients. An issue with this type of AAN is that the user may become reliant on the assistance provided by the robot [90]. As the user becomes more and more reliant, the amount of participation by the user reduces, leading to a poorer perceived performance and an increase in assistance. This may lead to the assistance being provided to gradually increase rather than decrease as intended.

2.2.3 Model Based Assistance-as-Needed

To limit the reliance of a patient on the assistance provided by a robot, model based AAN paradigms were developed [99–101]. In a similar fashion to the performance based AAN paradigms, the assistance to be provided to the human is altered throughout the interaction. A musculoskeletal model of the human body can be used as a method of estimating the capability of the human [102]. The estimated capability is then used to determine the amount of assistance to be provided to the human collaborating with the robot [103].

Using musculoskeletal models allows the disability of the human to be accounted for [20] when determining the capability of the human. The musculoskeletal models have also been used alongside an Electromyography (EMG) to map muscle activation to the amount of force produced by the human [104]. Other methods determine the maximum strength based on the force to be opposed through an optimization procedure [21]. Impairment of certain muscles of the human is able to be replicated in the musculoskeletal model to obtain the estimated impaired strength of a patient [105]

An advantage of the model based approach to the performance based counterpart is that the robot will provide assistance to the human without requiring a previous attempt from the human. The model based AAN would be beneficial in an industrial application such as abrasive blasting where failure in the operation could be dangerous to the human. The model based AAN paradigm also reduces the reliance of the human on the assistance provided by the robot which in turn should promote engagement in the operation and increase awareness.

2.2.4 Assistance-as-Needed in practical pHRC applications

Various AAN paradigms have been developed for rehabilitation applications with varying degrees of success. In industrial applications, assistance is often provided as a mean of removing unwanted vibration to increase the precision of humans performing operations such as welding [106] or calligraphy [107]. This type of assistance requires a means of determining what constitutes a good performance in the specific operation. In certain

operations the performance may be easily quantified but this is not always the case. For example, when painting a wall with a collaborative robot, a simple performance measure may be the amount of time taken to paint the wall whereas a more appropriate measure may take into account factors such as the amount of overlap, the paint coverage as well as the time taken.

Another way in which assistance has been implemented is to alter the control parameters of a robot for novice workers such that the outcome of the operation is comparable to the operation being performed by a more experienced worker. In [108] it was suggested that in a welding operation involving untrained welders, the impedance should be increased in the direction perpendicular to the direction of travel. It can be argued that maintaining a constant level of assistance results in a reduced rate of learning by the novice user.

Collaborative robots such as the UR10 [2], Kuka LWR [3] and Sawyer [4] are designed to be human safe but have reduced capabilities in comparison to traditional industrial robots. For example the UR10 has a limited payload of 10 kg when close to the full extent of its reach. In some industrial applications the limited payload of human safe robots may not be able to account for the entire operation load and thus parts of the operation load would need to be accounted for by a human co-worker.

The limitation in the robot's capability in pHRI or pHRC applications may be beneficial for the collaboration. By requiring the human to undertake some of the operation load, the engagement and awareness of the human co-worker would be higher than when the operation is fully accounted for by the robot. In a full assistance scenario, although the human may not be physically fatigued, mental fatigue has also been shown to reduce performance in physical activities [109–111]. With some of the physical load of the operation being provided by the human, the human co-worker may be prompted to take rests which will reduce mental fatigue [112, 113]. An AAN paradigm can be used in the assistance to a human co-worker in industrial applications. The assistance to be provided to the human could be altered depending on the needs of the human co-worker.

Performance based AAN requires a measure of how well the operation is going. This means that the operation requires a criterion to define what constitutes a good performance versus a poor performance. The operations performed in practical pHRC applications are often

varied and requires flexibility. Therefore model based AAN, which provides assistance based on an estimate of the human capability, may be better suited to practical pHRC applications.

2.3 Human Pose Tracking

In order to adapt the assistance being provided by a robot to a human co-worker in pHRC an estimate of the human capability is required. A factor that affects the amount of force a human is able to exert or oppose in any given direction is the pose of the human body [23, 114]. The physical strength of the human can be estimated using a musculoskeletal model of the human alongside the current pose of the human [21, 22, 103]. Another benefit in the robot being able to ascertain the pose of the human is that collision between the human and the robot could be avoided [115, 116]. In this section various systems and models are reviewed with an emphasis on tracking the human upper limbs such that the strength of the human is able to be estimated for a force to be opposed at the hand.

2.3.1 Existing Pose Tracking Technologies

There are various methods of determining the pose of a human during a certain operation. A common example of a human tracking technology is Motion Capture (MoCap). MoCap allows for highly precise motion to be recorded, often involving markers to be tracked with a special suit to be worn by the human [7]. There are also marker-less based tracking using Inertial Measurement Unit (IMU) to be worn by the human on key parts of the body [117]. If high positional precision is required, marker based tracking is often preferable over IMU based systems, but if acceleration values are more important, IMU based tracking provide less noisy data without occlusion problems [118]. This technology often requires a well calibrated set of sensors to track the object from multiple views to obtain a high accuracy in the tracking [119]. Both IMU and marker based tracking are invasive, requiring the human being tracked to wear the corresponding technology which may be inconvenient to implement in practical applications.

FIGURE 2.5: Motion capture suit worn to track a human using the OptiTrack system [7]

Another option which has been used to track the pose of a human is through the use of RGB-D sensors. Low cost depth sensing cameras such as the Microsoft Kinect [120] and Intel RealSense [121] provides a cheaper alternative to MoCap systems. These cameras provide traditional RGB images as well as depth information which have been used to track the skeleton of a human to varying levels of accuracy [122, 123].

Machine learning algorithms have also been implemented to classify the pose of the human in various Two-Dimensional (2D) RGB images [124, 125]. These algorithms utilize a variety of training images used to segment out the human from the 2D images, classifying parts of the human body.

2.3.2 Pose Tracking Through Models

In applications where sensors are unavailable or unable to be used, models have been used to approximate the pose of certain parts of the human body, such as the upper limb, to the whole body based on limited information [126]. In [8] the redundancy in the human upper limb was resolved by estimating the position of the elbow such that the manipulability of the hand towards the head is maximized where the wrist pose relative to the shoulder is known. This concept was then further extended by taking into account the effect of the orientation of the wrist on the adopted upper limb pose [25]. In another work [127], the

notion of an equilibrium upper limb posture was used to estimate the pose of upper limbs for use with an exoskeleton robot.

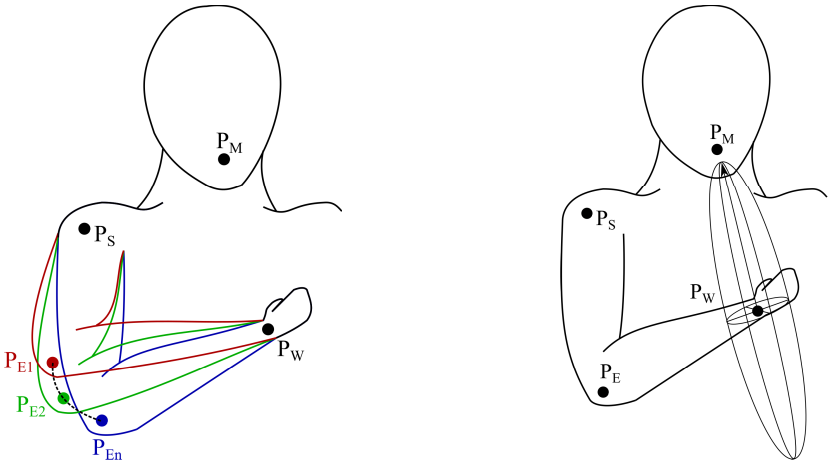

FIGURE 2.6: (A) The redundancy in the human upper limb. (B) An example of a model based upper limb redundancy resolution [8], based on the manipulability of the hand towards the head where poses of the shoulder and wrist are known.

In [24, 128] the concept of minimization of work was used to determine the pose of the upper limb. This concept is also supported by the work conducted in [129] where it was concluded that the predicted upper limb pose is affected by the previous upper limb pose and that the pose of the upper limb is affected by both the kinematics and dynamics of the upper limb. Another method utilized a musculoskeletal model of the upper limb was used to predict the natural reaching postures of the upper limb by estimating the muscle effort necessary for the motion [130].

2.3.3 Limitations of Common Pose Tracking Technologies

In a real pHRC application existing pose tracking technologies are often difficult to implement or may become inaccurate. Marker based motion tracking systems require multiple cameras to be placed in the environment. These cameras are required to be well calibrated and are often situated such that an object being tracked is able to be seen by multiple cameras. In real industrial applications, there are limitation to the placement and number of cameras that could be used in a given environment. The environment in which the collaboration will take place may not always be consistent which limits the use of motion capture systems in real pHRC applications.

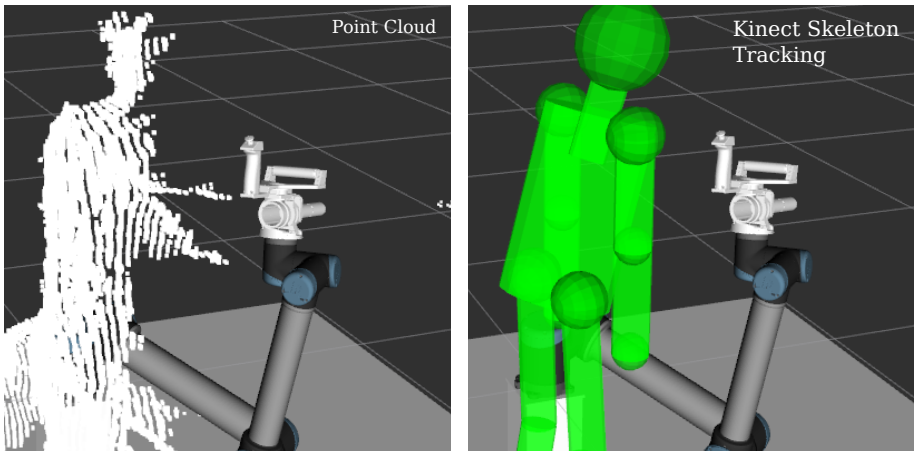

FIGURE 2.7: A comparison of the point cloud data being observed by a Kinect for Xbox 360 camera (left) with the output of a skeleton tracking algorithm (right) showing that the upper limbs adopted a default pose due to self occlusion during collaboration with a robot.

Skeleton tracking algorithms using RGB-D cameras are also limited in their capability to be used in real pHRC applications. Skeleton tracking algorithms often require the human to be facing the camera as the algorithms do not take into account which way the human is facing. When parts of the human body are unable to be seen, the algorithm will either return no pose estimate or will assume a default pose (Figure. 2.7). In applications such as pHRC there is a high probability that parts of the human body will be occluded by the robot which will reduce the accuracy of the skeleton tracking algorithms [131].

Models that have been developed to estimate the pose of the upper limb often assume that the upper limb is able to take any configuration and is free from any constraints. This is not always the case as the close proximity between the human and the robot may restrict the pose that could be adopted by the human. Interaction points such as handles on the end effector of the robot will affect the adopted pose of the hand and wrist, which was shown to alter the adopted pose of the upper limb [25].

In pHRC existing pose estimation methods are difficult to implement or have reduced effectiveness. The environments in which the pHRC is to take place may limit the sensing options able to be used. Models used to estimate the pose of the upper limb are often based on free unconstrained motion which may not be applicable in certain pHRC operations due to constraints placed onto the human from the interaction between the human and the robot.

Due to the invasive nature of and impracticality of human tracking methods such as MoCap a practical method of estimating the pose of the human co-worker pose is needed for pHRC applications. A factor that needs to be addressed if the pose of the human co-worker is to be estimated is the effect of the interaction between the human and the robot. The interaction between the human and the robot will likely restrict some of the poses that are able to be adopted by the human co-worker which may reduce the accuracy of the estimated pose using existing pose estimation models. Although some restrictions are placed on the human co-worker, the interaction may be able to be used to aid in the estimation of the human co-worker's pose.

2.4 Human Physical Strength and pHRC

To determine the amount of assistance to be provided to the human, an estimate of the human capability is required. Capability of a human may range from the skill level of the human worker to the amount of physical load able to be resisted by the human. The capability is dependent on factors such as the health of the human, the current pose of the human body, the experience of the human as well as the type of operation being performed. In this thesis, the capability of the human being explored is the physical strength of the human during collaboration with a robot.

2.4.1 Physical Strength of the Human

Unlike the robot, the physical strength of the human is difficult to quantify. To exert forces or perform certain motions, the central nervous system determines the required amount of muscle activation [132]. Along with the muscle activation, the amount of force that each muscle can exert is dependent on other factors such as fatigue, the distribution of muscle fibre types and cross sectional area of the muscle [133].

Measurements of the human strength come in a variety of manners. EMG sensors are one method of estimating the amount of work being conducted by the human[134]. These sensors provide a measure of the activation of muscles which need to be normalized. EMG sensors have also been used to control robotic systems based on the activation of targeted

muscle groups [135, 136]. Although EMG is able to provide a measure of the muscle activation, it does not measure the muscle force output.

Other methods of estimating the strength include performing a Magnetic Resonance Imaging (MRI) scan of the human body to measure the volume of certain muscles in order to estimate the force generation capability of the human [137]. Another method of estimating strength which is less accurate is through visual judgement of the human [138]. Direct measurement of exerted force has also been performed which targets specific area of the human body, performed using load cells to measure the amount of force exerted [139, 140].

Most studies are conducted by targeting a specific area of the human body such as the grip strength [141]. Tests are often performed offline to determine the maximum isometric strength of the human. However maximum isometric strength does not always correlate to an increase in performance. In [142], it was shown that athletes who had a higher isometric strength relative to their weight performed similar vertical jump distance to athletes who had a lower isometric strength relative to their weight. Therefore studies performed to determine the maximum strength are unlikely to reflect the capability of a human in performing a certain operation.

2.4.2 Musculoskeletal Models of the Human Body

Musculoskeletal models of the human body have been developed as a method of estimating various information regarding the human body. Software such as OpenSim [143] can analyze and simulate the human body. These musculoskeletal models facilitate studies on the inner workings of various biomechanical systems, ranging from an ankle [144] to a full human body [145]. Musculoskeletal models have also been used to provide the activation of certain muscles to determine the stability of the glenohumeral joint in a lifting operation [146].

Musculoskeletal models such as the upper extremity model [10] have been developed to estimate the physicality of a human. These models often represent a statistical representation of a human, such as the physicality of a 50th percentile male, which may be scaled to fit the specific person of interest. Musculoskeletal models have been used in a wide

variety of applications ranging from movement studies [147] to adaptive control of robots [144].

Using musculoskeletal models the capability of the human can be estimated in real-time. In [148] a real-time motion capture system was used to provide the pose of a human to be used alongside the musculoskeletal model. Similar works utilized a specialized suit with embedded IMUs [149] in order to provide a real-time pose of the human. In these works the real-time pose of the human is able to be used alongside software packages such as OpenSim to perform rapid clinical evaluations.

2.4.3 Estimation of Human Physical Strength

The physical strength of a human considered in this thesis is the magnitude of the force that a human is able to withstand at a given force direction. Determining the amount of force that is able to be generated by a given individual is difficult without using direct measurement through devices such as force/torque sensors [150]. One method of appraising the physical strength of a human is through the use of models such as the musculoskeletal model [103].

A common method of estimating the strength of a human limb or part of the human body is through EMG. EMG is able to be used to provide a measure the muscle activity of the human to be used alongside a musculoskeletal model to estimate the physical strength of the human [151]. In [152] the forces applied by the human finger were estimated through EMG electrodes placed on the forearm of the human subject. A linear regression model was generated to estimate the finger force levels from normalized EMG signals. Others used artificial neural networks to convert raw EMG signals to estimate the output force of the human upper limb muscle [153]. Factors such as the stiffness of the human arms may also affect the amount of force that a human can withstand [154]. Muscle forces have also been estimated using the inverse dynamic using a lower limb musculoskeletal model based on specific motions such as walking and known reaction force at the foot [155].

The forces that are experienced during certain operations or motion could also be used to predict the amount of exertion that a human will experience. In [156] it was shown that

the amount of force that is required for an operation performed by the same person is quite repeatable. Measurements from force sensors attached to handles could be used to record the amount of force required to accomplish an operation [157] which can be used to estimate the required physical strength exertion of the human.

The operation or the motion being performed by the human greatly affect the amount of force being generated by the human. The pose of the human greatly affects the amount of force that a human is able to generate and therefore it is important for the robot to know the pose of the human if the human strength is to be quantified by the robot.

2.4.4 Muscle Fatigue

Muscle fatigue is one of the main reasons leading to musculoskeletal disorders [158]. Muscle fatigue is defined as a decrease in muscle force capacity often due to a mismatch between central motor drive magnitude and mechanical muscle response [159]. When fatigued it has been reported that humans matched the perceived effort to complete the operation rather than the perceived force exerted by an unfatigued arm [160]. Muscle fatigue that is localized in specific muscle groups may cause changes in the muscle coordination [161] and the timing in the resultant movement outcome [162]. The performance of a fatigued human has also been shown to have decreased in a path tracking operation [163].

Muscle fatigue can be monitored through sensors such as the one detailed in [164]. Models have also been developed to estimate the muscle fatigue based on the required movements of the joints as well as the forces experienced by the human body [165] which could be potentially used to detect the risk of musculoskeletal disorders in workers [166]. In [167] a muscle fatigue model was presented that considers the force production history of muscles in a musculoskeletal model to estimate the fitness level of each muscle during an upper limb motion[167].

2.4.5 Physical Strength Estimation in Practical pHRC Applications

In pHRC applications, the strength of the human co-worker could be used to adapt the amount of assistance to be provided by the robot. Certain operations could be halted in

order to maintain the safety of the human co-worker. Currently the strength of the human is commonly measured through the use of direct force sensing. By directly measuring the force applied by the human co-worker, the true capability of the co-worker is unable to be known and thus the wrong assistance may be applied instead. EMG based strength estimation is impractical for use in real operations due to the invasive nature of the sensor which requires careful placement of electrodes on the skin or within the muscle of the human.

For the human physical strength to be estimated in a practical pHRC application set in an unstructured industrial environment, invasive sensors such as EMG and MoCap are unlikely to be used due to the impracticality of the sensors. Therefore a non-invasive method of estimating the physical strength of the human is required if a collaborative robot is to take into account the physical strength of the human co-worker for adaptive assistance paradigms such as AAN to be implemented on the robot. Using an estimated pose of the human co-worker with a musculoskeletal model of the human is one method of estimating physical strength. Errors in the estimated pose will likely introduce error in the appraisal of the human physical strength and this needs to be addressed.

2.5 Summary

Robots for pHRC have been designed to assist humans perform a variety of operations. These robots are utilized to provide various forms of assistance such as suppressing unwanted vibrations or reducing the load experienced by the human in strenuous operations. Although providing assistance is able to reduce the physical strain experienced by the human co-worker, providing too much assistance may result in a reduced growth of the human co-worker's capability, increasing the reliance of the human co-worker on the robot. Model based AAN paradigms have been developed to adapt the level of assistance provided to the human based on the estimated capability of the human such as the current physical strength of the human co-worker. For such AAN paradigms to be implemented by pHRC robotic systems, an estimate of the human co-worker's physical strength is required.

A factor that is important in appraising the physical strength of a human co-worker is the pose of the human co-worker. Existing pose tracking methods are impractical to implement in real pHRC applications whereas models estimating the pose of the human co-worker assume free unconstrained motion of the human co-worker, which is not the case. In pHRC the interaction between the human co-worker and the robot may place constraints on the pose that is able to be adopted by the human co-worker. Therefore the effect of the interaction on the pose of the human co-worker needs to be addressed when considering the estimation of the human pose in pHRC applications. The constraints placed onto the human from the interaction between the human and the robot may also be beneficial when attempting to resolve the redundancy in the human body such that a more accurate pose of the human body is able to be estimated. With the pose of the human being estimated, the capability of the human is able to be appraised. Due to the estimation of the pose, errors in the pose will likely result in error in the appraisal of the physical strength. Thus the accuracy of the appraised physical strength will also need to be addressed.

Chapter 3

Effect of External Force and Bimanual Operation on Upper Limb Pose

The redundancy in the human upper body allows for a wide variety of poses to be adopted to perform an operation. In this chapter, the effect of the interaction between a human and a robot in physical Human-Robot Collaboration (pHRC) on the pose of the human upper limb is investigated. Existing estimation models of the human upper limb were developed under the assumption that the human is able to move freely. In pHRC applications, the interaction between the human and the robot restricts some of the poses that are able to be adopted by the human. This chapter presents an investigation that was performed to observe the effect of the interaction between the human and the robot on the pose of the human upper limb. Experiments were conducted with human subjects collaborating with a robot to perform a path-following operation. In Section 3.1 background information is presented. Section 3.2 provides an overview of this study. Section 3.3 presents the design of the experiments as well as the robotic platform used to conduct the experiments. The obtained results are presented and discussed in Section 3.4. The findings are then concluded in Section 3.5.

3.1 Background Information

In physical Human-Robot Cooperation (pHRC), it is advantageous for the collaborative robot to ascertain as much information as possible regarding the state of the human co-worker. One of the important pieces of information to obtain is the pose of the human co-worker. Knowing the pose of the human co-worker increases the situational awareness of the robot, allowing for collision between the human [40] and the robot to be avoided. The information of the co-worker pose could also be used to estimate the physical strength of the human [21] and alter the assistance that the robot provides to the human co-worker [90, 168].

Determining the pose of the human co-worker in a practical application is often challenging due to several factors. In a pHRC operation, the human and the robot share a workspace resulting in frequent occlusion of the human which reduces the effectiveness of sensors such as RGB-D cameras to measure the pose of the human. One way in which occlusions of the human could be minimized is by increasing the sensors in the environment. Increasing the number of sensors may not always be practically feasible. For higher accuracy, sensors require careful calibration and in a pHRC application where the workspace of the robot and the human is dynamic it may be difficult to maintain the correct calibration for each sensor. In outdoor or dusty environments, the effectiveness of vision based sensing is also reduced, limiting the reliability of the measurements obtained from these sensors. Models have been developed to predict the pose of the upper limb as an alternative to direct sensor measurements of the upper limb pose [24, 25], such as estimating the position of the elbow given the pose of the wrist relative to the shoulder [8].

In pHRC applications such as the one shown in Figure 3.1 the protective clothing to be worn by the human worker increases the difficulty of measuring the pose of the human using sensors. Hence models that estimate the worker's pose are appealing for pHRC applications. Models that predict the pose of the human co-worker performing a collaborative operation with a robot may not be able to provide an accurate pose estimate. These pose estimation models are often developed with an assumption that the human co-worker is performing a free unconstrained motion, which is not the case in pHRC applications. By having the robot in physical contact with the human co-worker, several constraints are

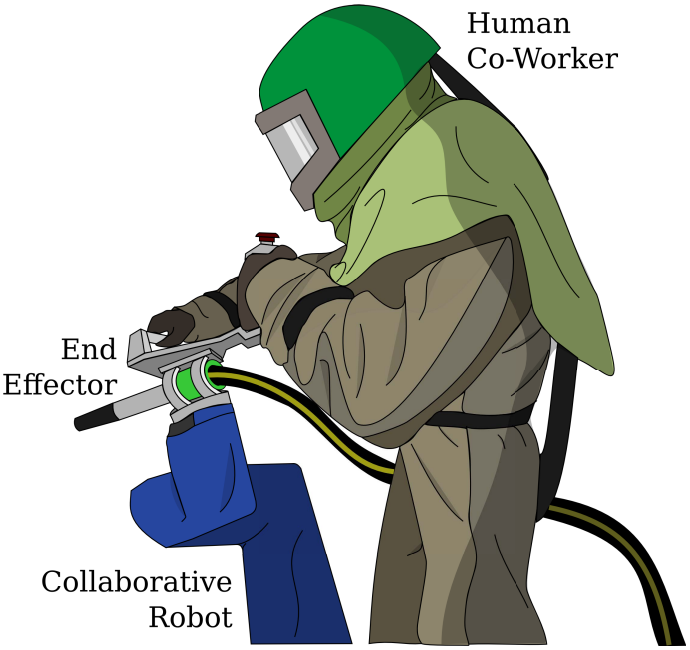

FIGURE 3.1: A human co-worker working collaboratively with a robot in an abrasive blasting operation.

placed on the poses that the human is able to undertake. Therefore an investigation was performed on the effect that interaction between the human and the robot would have on the pose of the human subject.

3.2 Overview

3.2.1 Redundancy in the Human Upper Limb and Pose Definition

The human body has a large number of Degrees of Freedom (DOF). This results in the human body being able to adopt a pose that is deemed most natural to the individual. As an example, for a given position and orientation of the hand relative to the shoulder, the human is able to position their elbow in a wide variety of positions. Due to this redundancy, there are a large variety of poses that are able to be adopted by the upper limb.

The human upper limb is often simplified to a seven DOF system. The spherical joint of the shoulder can be represented as three rotational DOF. One rotational DOF represents

the hinge joint of the elbow and three rotational DOF represents the spherical joint at the wrist. With the simplification of the upper limb into a seven DOF system and with the hand position and orientation fixed, there is still one degree of redundancy in the pose of the upper limb.

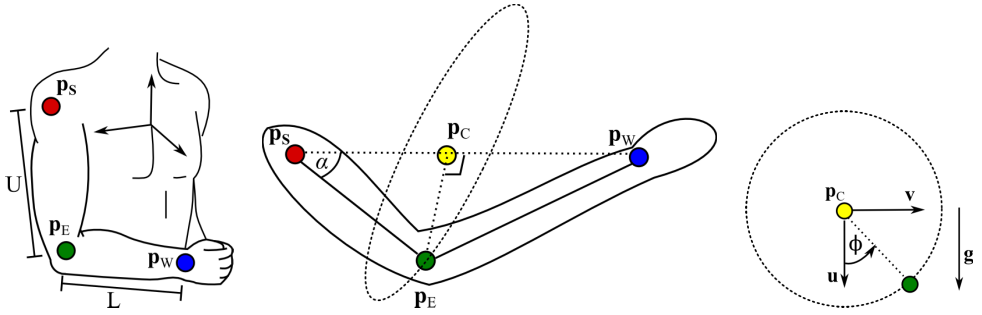

FIGURE 3.2: A) The human upper limb showing the positions of the shoulder $\boldsymbol{p}_S$, elbow $\boldsymbol{p}_E$ and wrist $\boldsymbol{p}_W$ and the lengths of the upper arm U and lower arm L (B) Location of the swivel coordinate frame $\boldsymbol{p}_C$ in relation to the subject's shoulder $\boldsymbol{p}_S$, elbow $\boldsymbol{p}_E$, wrist $\boldsymbol{p}_W$ and the angle α. (C) Swivel coordinate frame $\boldsymbol{u} \times \boldsymbol{v}$ showing the swivel angle ϕ and direction of gravity $\boldsymbol{g}$.

This redundancy means that even if the pose of the wrist is defined the current pose of the upper limb is not. For a given position of the wrist with respect to the shoulder $\boldsymbol{p}_W$, consisting of $[p_{W,x}, p_{W,y}, p_{W,z}]$, the redundancy of the upper limb can be parameterized as the swivel angle (ϕ) [169].

$$\boldsymbol{p}_C = \boldsymbol{p}_S + U\cos(\alpha) \tag{3.1}$$
$$\cos(\alpha) = \frac{L^2 - U^2 - ||\boldsymbol{p}_W - \boldsymbol{p}_S||}{2U||\boldsymbol{p}_W - \boldsymbol{p}_S||}$$

The swivel angle, ϕ, refers to the angle relative to an imaginary coordinate frame positioned along a vector between the wrist and the shoulder on the point $\boldsymbol{p}_C$. $\boldsymbol{p}_C$ is located along a vector between $\boldsymbol{p}_S$ and $\boldsymbol{p}_W$, calculated using the position of the shoulder $\boldsymbol{p}_S$, the position of the wrist $\boldsymbol{p}_W$, and the lengths of the upper and lower arm, U and L respectively as shown in Equation 3.1.

$$\begin{aligned} \boldsymbol{p}_E &= r[cos(\phi)\boldsymbol{u} + sin(\phi)\boldsymbol{v}] + \boldsymbol{p}_C \\ r &= U\sin(\alpha) \end{aligned} \tag{3.2}$$

$$\boldsymbol{n} = \frac{(U\sin(\alpha)_W - U\sin(\alpha)_S)}{||U\sin(\alpha)_W - \boldsymbol{p}_S||}, \quad \boldsymbol{u} = \frac{\boldsymbol{g} - (\boldsymbol{g}\cdot\boldsymbol{n})\boldsymbol{n}}{\boldsymbol{g} - (\boldsymbol{g}\cdot\boldsymbol{n})\boldsymbol{n}}, \quad \boldsymbol{v} = \boldsymbol{n}\times\boldsymbol{u} \tag{3.3}$$

The coordinate frame is arranged in such a way that the position of the elbow, $\boldsymbol{p}_E$ (Equation 3.2), lies on the $\boldsymbol{uv}$ plane. The vector $\boldsymbol{u}$ is suggested to be aligned to the direction of gravity $\boldsymbol{g}$ as shown in Figure 3.2 (Equation 3.3). The swivel angle ϕ of a given upper limb pose can be calculated by determining the angle between $\boldsymbol{u}$ and $\overrightarrow{\boldsymbol{p}_C\boldsymbol{p}_E}$.

Utilizing the swivel angle, the pose of the upper limb can be defined alongside the position $\boldsymbol{p}_S$ and orientation of the wrist $\boldsymbol{R}_W$ (Equation 3.4). In this thesis, $\boldsymbol{R}_W$ is represented as a quaternion.

$$pose = [\boldsymbol{p}_W, \boldsymbol{R}_W, \phi] \tag{3.4}$$

3.2.2 Physical Interaction Between the Human and the Robot

Previous works have shown that a prescribed wrist orientation can affect the pose of the upper limb [25]. Due to the interaction between the human and the robot in pHRC the configuration of interaction points such as the handle may also affect the pose of the upper limb. To determine the effect of the interaction between the human and the robot, two variables were investigated on its effect on the adopted pose of the upper limb. The two variables were:

- The effect of bimanual operation (two handed vs single handed operation)
- The effect of force exertion (direction and magnitude)

The first variable to be tested is whether operations involving both hands of the human co-worker (bimanual operation) in pHRC affects the pose of the human upper limb. In a practical pHRC, bimanual operations may be enforced by safety standards such as [170]. By enforcing the pHRC robot to be operated with both of the human co-worker's hands, risks of the hands being trapped by the robot can be reduced. Handles such as ones shown in Figure 3.3 restricts the relative position and orientation of the left hand to the right hand. A side effect of bimanual operation is a restriction in the pose that is able to be adopted by the left and right hand of the human co-worker as the worker is restricted to form a closed kinematic loop with the handles. Due to the bimanual operation, the orientation of the wrist becomes restricted, which has been previously found to alter the adopted pose of the human upper limb [25].

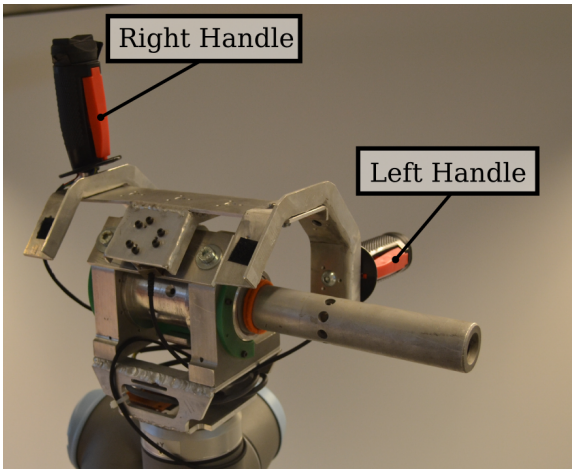

FIGURE 3.3: The end effector of a pHRC robot showing the left and right handle to be held onto by the human co-worker.

The second variable to be tested is whether requiring the human co-worker to exert forces in a pHRC operation causes the adopted upper limb pose to change. Forces are generally exerted by the hand of the human co-worker onto the end effector of a robot to contribute towards the operation or to control the robot. The magnitude and direction of the force being exerted by the human co-worker is dependent on the type of operation being attempted or the manner in which the robot is to be controlled. It has been previously shown that the pose of the upper limb alters the exerted force at the hand [23, 103]. Therefore an investigation was performed to determine whether the magnitude and direction of the force

to be exerted will cause the adopted upper limb to change such that a more advantageous pose is adopted by the human co-worker.

3.3 Design of Experiments

3.3.1 Robotic Platform

The Assistance-as-Needed roBOT (ANBOT) was used to facilitate experimentation in a pHRC application (Figure 3.4). This robotic platform was designed at the Centre for Autonomous Systems (CAS) in collaboration with Burwell Technologies to facilitate human-robot collaboration in an abrasive blasting application. Abrasive blasting is a physically intensive operation which is traditionally done manually with the human worker experiencing reaction forces which have been measured to be around 100 N [171]. A side effect of abrasive blasting is suspended particulate in the environment, which degrades the capability of vision based sensors.

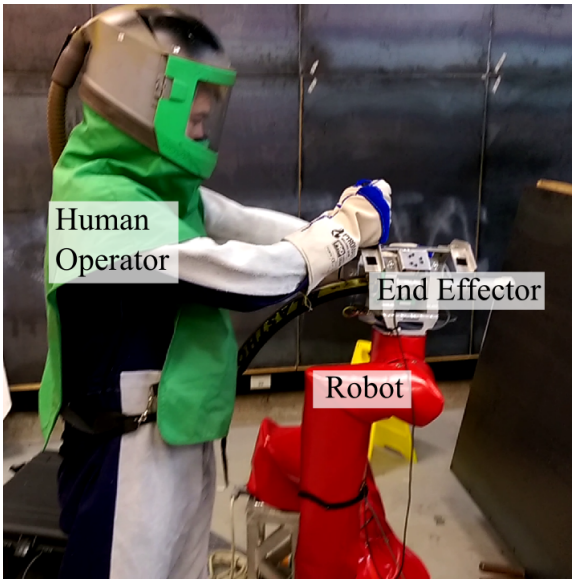

FIGURE 3.4: The ANBOT platform with a human co-worker performing a collaborative abrasive blasting operation.

At the core of the ANBOT robotic platform is a Universal Robot UR10, a collaborative robotic manipulator which was designed to be safe for use in close proximity to a human. Attached to the end effector of the robot are two handlebars to be held onto by the human

co-worker during the pHRC application. An ATI Mini45 force/torque sensor is fitted to the end effector of the robot to detect the force input from the human co-worker which is to be used to maneuver the end effector.

Mounted on a post extending upright from the base of the ANBOT are four Kinect v1 cameras, shown in Figure 3.5. These cameras are used to obtain a depth image of the surrounding environment to avoid collision between the robot and the environment. The Kinect cameras are also used to obtain point cloud of the human co-worker working with the ANBOT as a method of estimating the centroid of the human co-worker's torso. Although sensors are placed on the robotic platform, due to environmental factors as well as the non-deterministic nature of the human co-worker, sensors may not provide the necessary information. Therefore methods which are less reliant on sensory information are needed to provide feasible estimates of the human co-worker's pose.

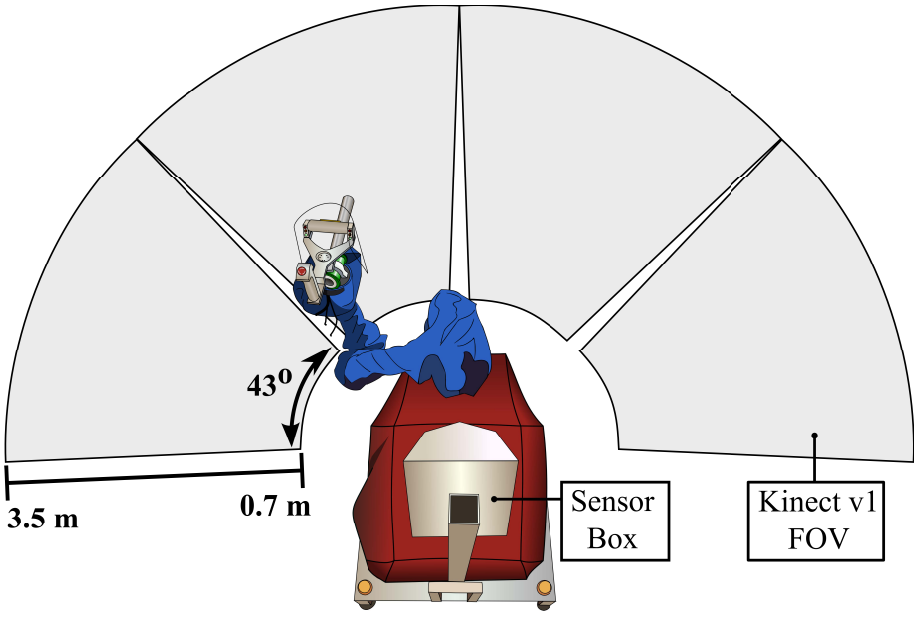

FIGURE 3.5: The field of view of the four Kinect v1 cameras on the ANBOT.

3.3.2 Experiments

The following experiments were performed to determine whether it would be feasible to estimate the pose of the human co-worker during the physical collaboration between the human and the robot. It was hypothesized that due to interaction forces being applied

by the human onto the robot, the pose adopted by the human will be affected. These experiments also serve to determine whether simple methods of estimating the upper limb configuration are appropriate in pHRC applications where forces are applied by the human. In these experiments, which was published in [9], the end effector of the ANBOT (Figure 3.6b) was set to move around a predefined path (Figure 3.6a) with the human subject holding onto the end effector of the ANBOT. The path was programmed as an end effector trajectory to be executed by the ANBOT to remove the human error in the motion being performed. This ensures the repeatability of the experiments such that comparison against other experiments or subjects were able to be made at set intervals along the path. In each experiment the end effector moved along the path six times in a counter-clockwise direction, starting and ending at Pt. 1 of the path. The orientation of the end effector was kept constant throughout the experiment to remove the effect of the wrist orientation on the pose of the upper limb as well as promoting movement of the whole upper limb rather than just the wrist.

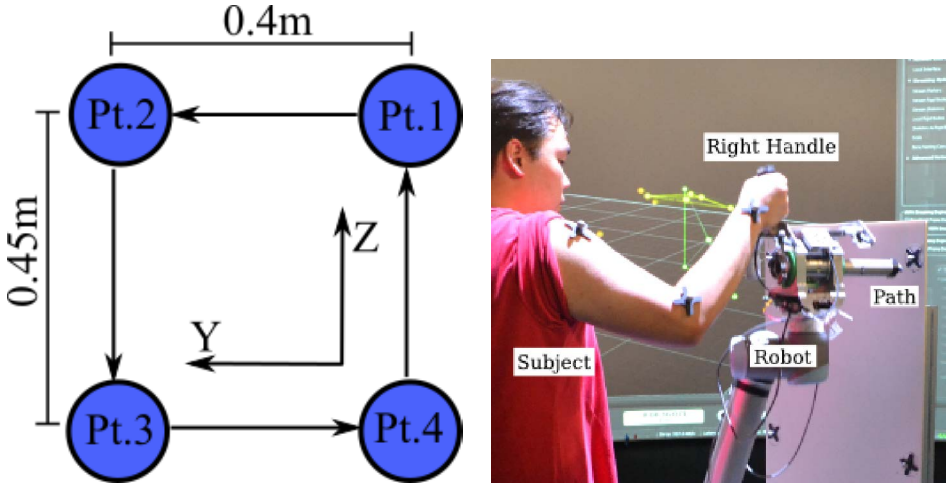

(A) (B)

FIGURE 3.6: (A) Path of the end effector to be followed during each experiment with the coordinate system of the force to be applied by the human subjects. (B) Experimental setup showing a subject with markers attached to their upper limb and the ANBOT platform used for the experiment [9].

Different experiments required the human subjects to apply a given force magnitude and direction onto the end effector of the ANBOT. In Experiments 1-2 the human subject is constrained to apply no force onto the end effector in order to progress through the preset trajectory of the path, whereas in Experiments 3-6 the human subject is required

to apply a specified magnitude of force at a specified direction. Human force input was measured and recorded using an ATI Mini45 sensor attached to the end effector of the robot. Maintaining a specific force output at the hand while the robot moves is difficult to achieve, therefore a ± 5N force window was set to ensure a smooth motion of the end effector. Without a suitable force window the robot would stutter as the force applied by the human varied in and out of range. The stuttering of the end effector had to be removed as it may cause the adopted upper limb pose to change. A visual aid, shown in Figure 3.7b, was used to display the forces being applied onto the end effector to aid the user in applying the correct magnitude and direction of force. Visual cues dictated the direction in which the force needed to be applied. The visual aid also served as a distraction to the subject, with the intention of reducing the subject's self-consciousness in the movement of their upper limb, to promote a more natural upper limb pose.

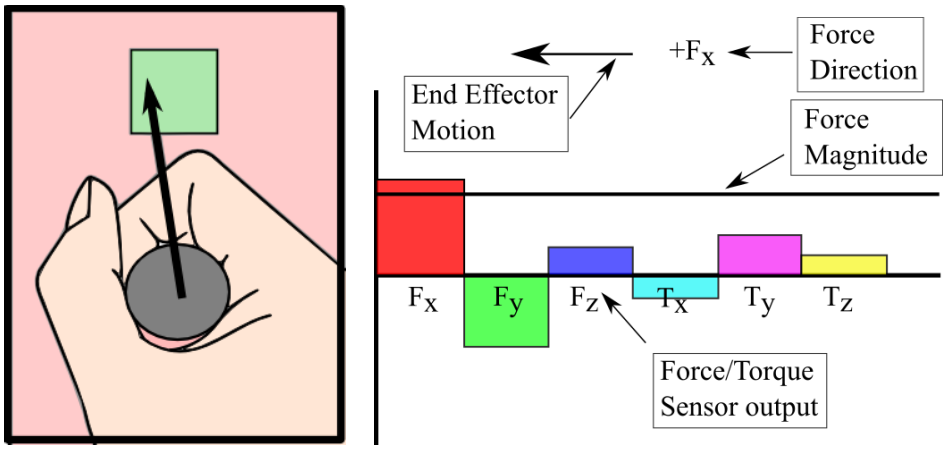

FIGURE 3.7: (A) Depiction of the force window applied by the human hand where the region in green satisfies the set constraint and the region in red will cause the robot to halt. (B) Visual aid used to display current Force/Torque sensor output alongside current experimental requirements such as the magnitude and direction of the force required from the subject and the current end effector motion.

Whilst the human subject satisfies the specified force constraints of each experiment, the end effector was programmed to travel along the predefined trajectory at of 0.1 m/s. The velocity of the end effector was chosen to minimize the effect of rapid movement of the hand on the adopted pose of the upper limb. The low velocity of the end effector also ensures a safe operation as the human subjects are required to be in close proximity to the robot and those unfamiliar with the robot may feel uncomfortable at a higher velocity of

the end effector. In the event that the human subject applied a force in the wrong direction or outside of the specified force magnitude threshold, movement of the end effector halted until the specified force constraints are satisfied. Figure 3.7a shows a representation of the force magnitude threshold. The region shown in green represents a region where the force applied by the subject's hand (black arrow) would allow movement of the robot whereas if the force was to be applied to the red region, the ANBOT will halt movement of the end effector.

Six experiments were performed by each human subject to observe the pose that is adopted by the human upper limb under different conditions or constraints. Experiments were chosen to test the effect of the two variables. The experiments conducted were:

- Experiment 1: 1 hand, with 0 ± 5 N force applied by the human subject (1 Hand, 0 N force)
- Experiment 2: 2 hands, with 0 ± 5 N force applied by the human subject (2 Hands, 0 N force)
- Experiment 3: 1 hand, with 20 ± 5 N force being applied along the direction of the operation (1 Hand, 20 N force, +X)
- Experiment 4: 1 hand, with 40 ± 5 N force being applied along the direction of the operation (1 Hand, 40 N force, +X)
- Experiment 5: 1 hand, with 20 ± 5 N force being applied along the direction of motion (1 Hand, 20 N force, YZ Plane)
- Experiment 6: 1 hand, with 40 ± 5 N force being applied along the direction of motion (1 Hand, 40 N force, YZ Plane)

In Experiment 1, the human subject operating the robot is required to press the enabling switch attached to the handle of the robot whilst the robot moves along the predefined path. The robot continues along the preset trajectory of the end effector as long as the human subject maintains a 0 ± 5 N of force being applied through the end effector. This experiment was chosen to be the baseline to which the other experiments were to be

compared against. This experiment represents a case where the human is required to apply no load with the only constraint placed on the human subject being the pose of the hand which is dependent on the pose of the end effector along the predefined trajectory. The 0 ± 5 N force enforced in this experiment and Experiment 2 ensures that the human subject does not rest their upper limb on the end effector, resulting in an unnatural pose of the upper limb being recorded. In these two experiments, the robot was only used to determine the trajectory of the human subject's hand.

In Experiment 2, each subject was asked to place both hands onto the end effector for a bimanual operation of the robot at specified handles for their right and left hand. In this experiment, the effect of bimanual operation on the adopted pose of the right upper limb was investigated. The motive behind this experiment is to test whether prescribing a relative position and orientation between the left and right hand instigates a significant change in the adopted pose of the upper limb.

Experiments 3 and 4 required the human subjects to place their right hand on the end effector and push in the forward (+X) direction relative to their torso and perpendicular to the end effector motion. These experiments are performed to simulate an abrasive blasting operation where forces are directed along the nozzle towards the human co-worker. In Experiment 3 the human subjects were required to push with 20 ± 5 N force. In Experiment 4 a 40 ± 5 N force constraint was enforced in order to move the end effector of the robot. The two experiments were designed to determine whether the requirement of pushing in the +X direction alters the adopted pose of the human. By comparing the adopted pose of the human upper limb in Experiments 3 and 4 the effect of the magnitude of the exerted force can be investigated.

In Experiments 5 and 6 the force to be exerted by the human subject is aligned in the direction of end effector motion represented by the arrows in (Figure 3.6a). For example, between Pt. 1 and Pt. 2 the human subject was required to apply a force in the +Y direction, whereas during the motion between Pt. 2 and Pt. 3 the force is to be applied in the -Z direction. Similarly to Experiments 3 and 4 the force to be exerted by the human subject is 20 ± 5 N and 40 ± 5 N for Experiments 5 and 6 respectively. Both of these

experiments were designed to simulate the human subject being required to move a heavy object or a slow responding end effector.

Ten healthy male subjects performed all six experiments with the ANBOT in the UTS Data Arena, a lab equipped with motion capture capabilities. All subjects volunteered to perform the experiments and are part of the Centre for Autonomous Systems. The heights of the subjects range from 165 cm to 185 cm where two subjects were left handed. The number of subjects was decided upon through literature review of similar works [8, 25]. In all experiments other than Experiment 2 the right hand of the subjects was used regardless of their dominant hand. A seat is placed to the right of robot base with the path plane set to a distance based on the arm length of the individual subject as shown in Figure 3.8. The seat placement was altered to ensure that the subject's arm was never completely straight as the swivel angle calculation becomes inaccurate, i.e. the straighter the arm, the closer $\boldsymbol{p}_E$ is to $\boldsymbol{p}_C$ and a small change in $\boldsymbol{p}_E$ results in a large change in the swivel angle ϕ. Each subject was asked to maintain contact between their back and the backrest of the seat as they perform the experiment. This ensures that the upper body of the subject does not shift during the experiment and minimizes the rotation of the upper body which would result in a different upper limb pose.

Reflective markers were attached to each subject's shoulder, elbow and wrist to record the adopted pose of the upper limb (Figure 3.6b). Markers were also attached to the end effector of the robot to track the subject's progress. The upper limb poses were recorded using an OptiTrack motion capture system which used 12 OptiTrack Prime 17 W cameras placed 3 m above the ground and evenly spaced around a 10 m diameter motion capture lab (Figure 3.8). The upper limb data of each subject was recorded at 120 frames per second.

3.4 Results and Discussion

The data obtained from the OptiTrack motion capture system were used to calculate the swivel angle, ϕ, of the right upper limb at each recorded time frame (Equation 3.2). In each experiment a mean and standard deviation of the swivel angle were calculated at

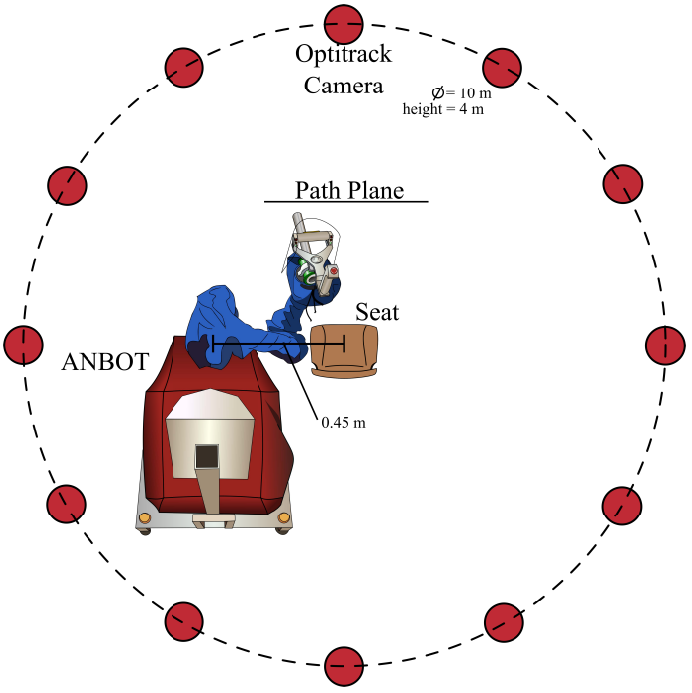

FIGURE 3.8: The experimental setup showing the positions of the OptiTrack cameras as well as the seat placement.

specific end effector points along the path. A comparison was then conducted using the mean swivel angle obtained in Experiment 1 against data obtained in the other experiments. The mean swivel angle from Experiment 1 was used as the baseline for comparison against other experiments as this experiment represents an operation where the subject is under no load other than gravity whilst still constrained by the robot on the position and orientation of their hands. The mean swivel angles for each subject in Experiment 1 were also compared to determine variability across the ten subjects tested. In the following figures, the horizontal axes correspond to the distance travelled by the end effector along the path in the experiment. The vertical axes represent the calculated swivel angle measured in degrees.

3.4.1 Experiment 1 - Unimanual Operation with No Force Applied

In Experiment 1, each subject was required to apply as little force as possible whilst holding onto the end effector with their right hand. A 0 ± 5 N force window was enforced

to ensure that the subject does not rest their upper limbs on the end effector during the experiment such that a natural upper limb pose could be recorded.

Figure 3.9 shows the mean and standard deviation of the calculated swivel angle (marked in red) in Experiment 1 for two subjects (Subjects 5 and 7). In Figure 3.9 it can be seen that both subjects had exhibited a consistent swivel angle profile. A consistent swivel angle indicates that the adopted pose of the upper limb on the specific point of the path is similar. This trend of consistency of the adopted upper limb was able to be seen across all ten subjects. In this experiment, it was observed that the swivel angle reaches a maximum value between Pt. 1 and Pt. 2 then decreases until a minimum is reached between Pt. 3 and Pt. 4. The results of each subject can be seen in Appendix A. The mean swivel angle values from Experiment 1 for each subject was also used as the baseline for comparison with the swivel angles calculated from other experiments and subjects.

Figure 3.10 shows the mean swivel angle values for all ten subjects. Even though it was shown that for a specific individual the calculated swivel angle is repeatable, this trend was not visible when comparing one subject to another. Although each subject seemed to exhibit a maximum swivel angle around Pt. 1 and Pt. 2 and a minimum swivel angle was calculated around Pt. 3 and Pt. 4, there is a significant difference between the magnitude of the swivel angles. Each subject was shown to adopt a different upper limb pose in order to perform a similar trajectory of the hand. This trend is caused by the redundancy in the human body allowing for a similar trajectory of the hand to be performed by adopting different poses. The natural difference in the human body between each subject likely resulted in a different upper limb pose to be preferred.

To calculate the dissimilarity in the adopted upper limb pose between different subjects, a root mean square deviation (RMSD) calculation was performed. The RMSD was calculated using one subject's mean swivel angle to the subject's own or another subject's raw swivel angles throughout Experiment 1. Table 3.1 shows the RMSD of the adopted swivel angle for each of the subjects in Experiment 1. A lower RMSD value represents a more similar adopted upper limb pose.

As expected, the lowest RMSD value was observed for each individual's recorded swivel angle. Subjects 1-3 was shown to have performed Experiment 1 using a similar upper limb

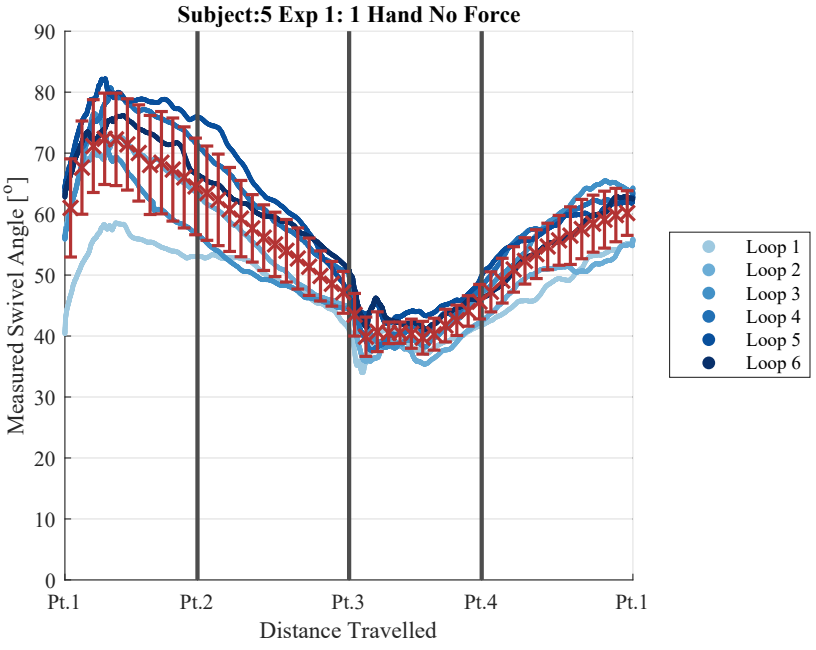

(A)

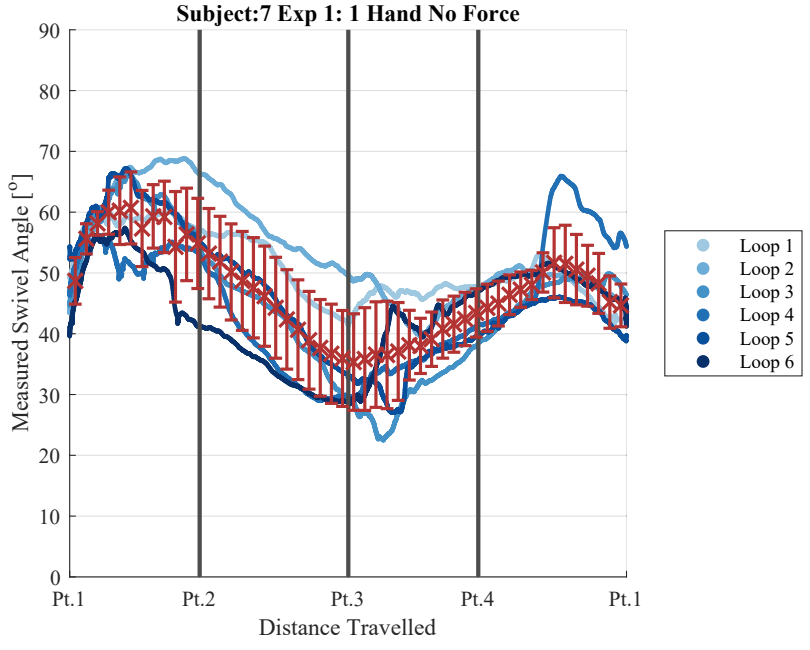

(B)

FIGURE 3.9: Calculated swivel angles of Subjects (A) 5 and (B) 7 in Experiment 1.

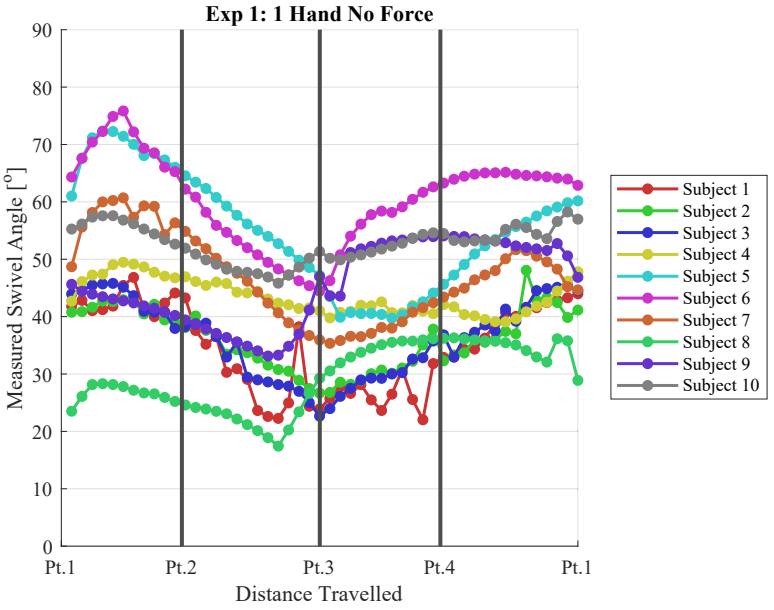

FIGURE 3.10: Mean swivel angles of all ten subjects in Experiment 1.

		Raw Swivel Angles [°]									
		Sub 1	**Sub 2**	**Sub 3**	**Sub 4**	**Sub 5**	**Sub 6**	**Sub 7**	**Sub 8**	**Sub 9**	**Sub 10**
Mean Swivel Angle [°]	**Sub 1**	4.97	6.08	5.69	9.93	21.08	26.19	13.98	10.04	12.87	18.34
	Sub 2	6.42	4.57	5.07	8.83	19.80	24.90	12.78	9.54	11.18	17.06
	Sub 3	6.07	5.34	4.34	8.79	19.62	24.71	12.58	10.02	11.33	16.87
	Sub 4	10.96	9.49	9.49	3.50	13.11	17.57	8.86	14.50	9.81	9.86
	Sub 5	21.43	19.91	19.52	13.14	5.00	9.41	10.48	25.90	16.20	9.11
	Sub 6	26.67	24.99	24.77	17.51	10.31	4.28	15.24	31.15	16.06	9.23
	Sub 7	13.80	12.15	11.85	7.17	9.71	14.28	5.96	18.01	11.61	8.04
	Sub 8	10.86	10.26	10.56	14.66	26.05	31.22	18.97	3.49	16.86	23.38
	Sub 9	13.94	11.82	11.92	9.45	15.81	15.58	12.27	16.61	4.35	8.40
	Sub 10	19.14	17.50	17.28	10.03	10.04	9.61	9.96	23.45	9.71	2.94

TABLE 3.1: Root mean square deviation of a subject's mean swivel angle against the raw swivel angles of all subjects calculated for Experiment 1.

pose but the trend was not shared with any other subjects. Results from Experiment 1 suggests that an individualized model for pose estimation will lead to a more accurate estimated pose as the natural variance between different individuals seemed to greatly affect the adopted pose of the upper limb.

3.4.2 Experiment 2 - Bimanual Operation with No Force Applied

In Experiment 2, each subject was required to apply as little force as possible whilst holding onto the end effector with both hands. In this experiment, the only difference is the addition of the left hand onto the end effector of the robot, so that the effect of bimanual operation can be tested. Similarly to results found in Experiment 1, the calculated swivel angles in Experiment 2 were repeatable (Figure 3.11). Figure 3.12 shows the mean swivel angles for all ten subjects where it can be seen that each subject performed Experiment 2 in a different manner.

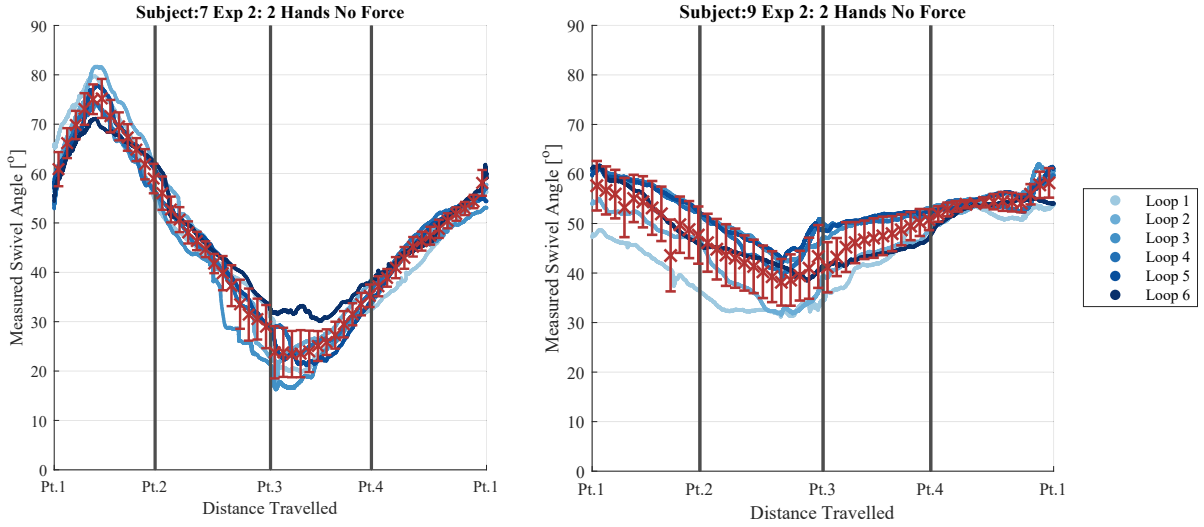

(A) (B)

FIGURE 3.11: Calculated swivel angles of Subjects (A) 7 and (B) 9 in Experiment 2.

To determine the effect that bimanual operation places on the adopted upper limb pose, the mean swivel angles in Experiments 1 and 2 were compared. Figure 3.13 shows the comparison of the mean swivel angles for two subjects in Experiments 1 and 2. The trend from these two subject shows that there is a slight change in the calculated swivel angle in Experiment 2.

However, the effect of bimanual operation had differing effects when observing different subjects. For Subject 8 (Figure 3.14a), bimanual operation resulted in a reduction of swivel angle throughout the experiment. For Subject 10 (Figure 3.14b), the swivel angle

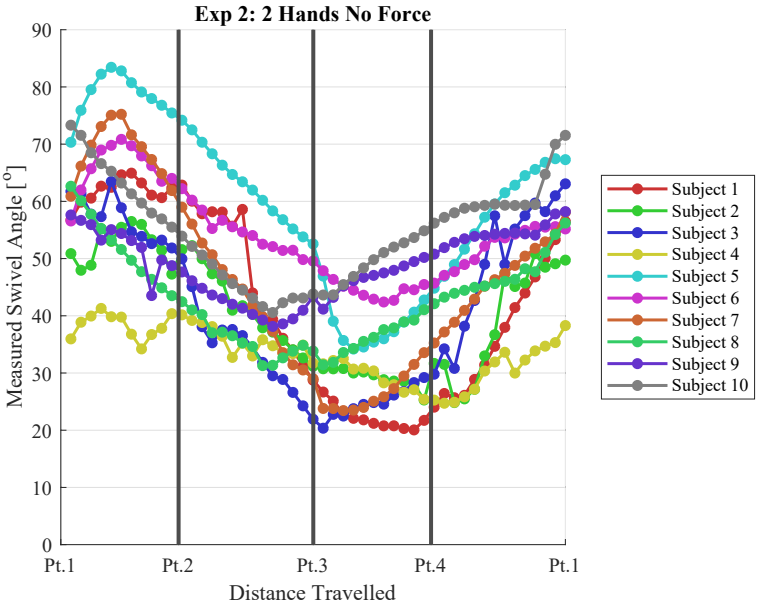

FIGURE 3.12: Mean swivel angles of all ten subjects in Experiment 2.

was similar to Experiment 1 for the majority of the experiment, except between Pt. 3 and Pt. 4.

The effect of bimanual operation on the swivel angle of the right upper limb is difficult to ascertain from the results obtained in Experiment 2 with the ten subjects. It is hypothesized that some subjects exhibited a change in the adopted swivel angle only around Pt. 1 of the path due to the left upper limb being close to its maximum reach surrounding this area. For some subjects, the adopted swivel angle surrounding points 3 and 4 of the path was also found to have less variation than in the rest of the experimental path. This is likely due to the right upper limb of the subjects being close to the full reach, limiting the variability in the adopted upper limb pose.

3.4.3 Experiments 3 and 4 - Unimanual Operation with 20N or 40N Force in the +X Direction

In Experiments 3 and 4, each subject was required to apply a 20 ±5 N (Experiment 3) or a 40 ±5 N (Experiment 4) force in a direction forward relative to their torso (+X direction). The direction of the force in this experiment was chosen to replicate physical operations

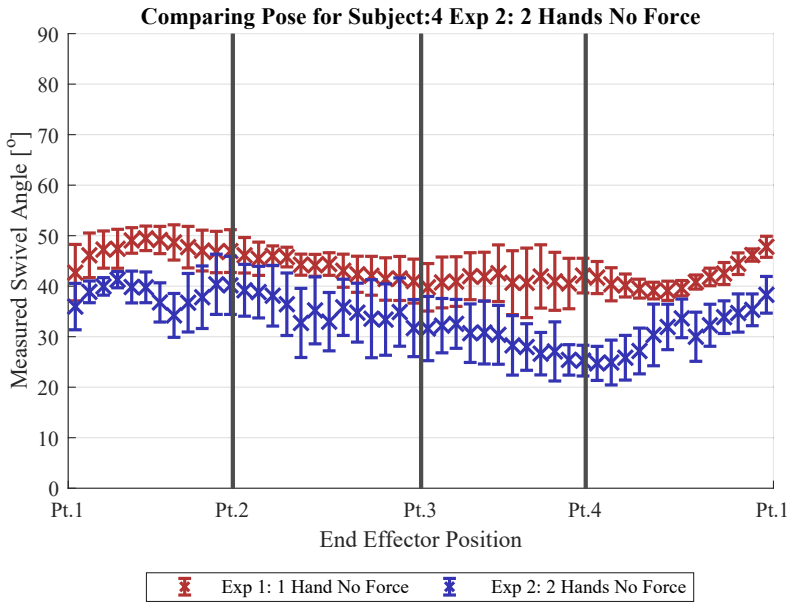

(A)

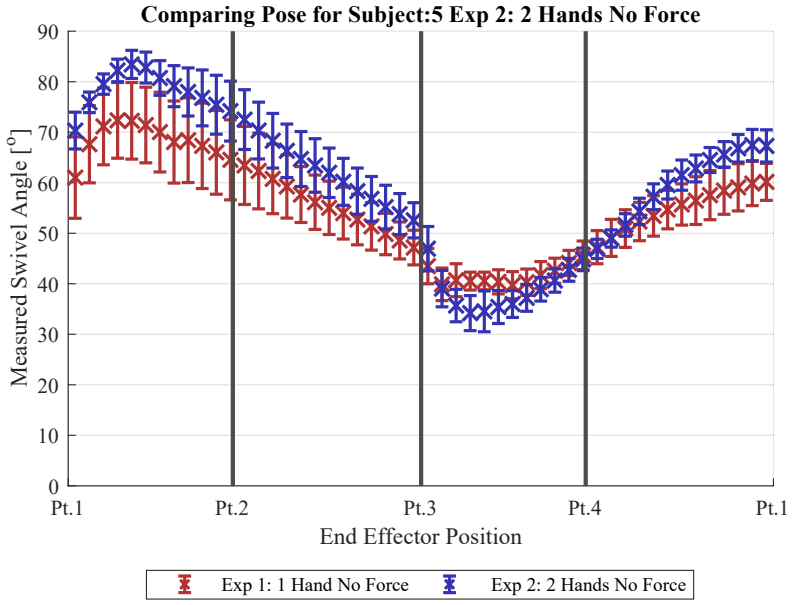

(B)

FIGURE 3.13: Comparison of the mean and standard deviation of the swivel angles of Subjects (A) 4 and (B) 5 in Experiment 2 and Experiment 1.

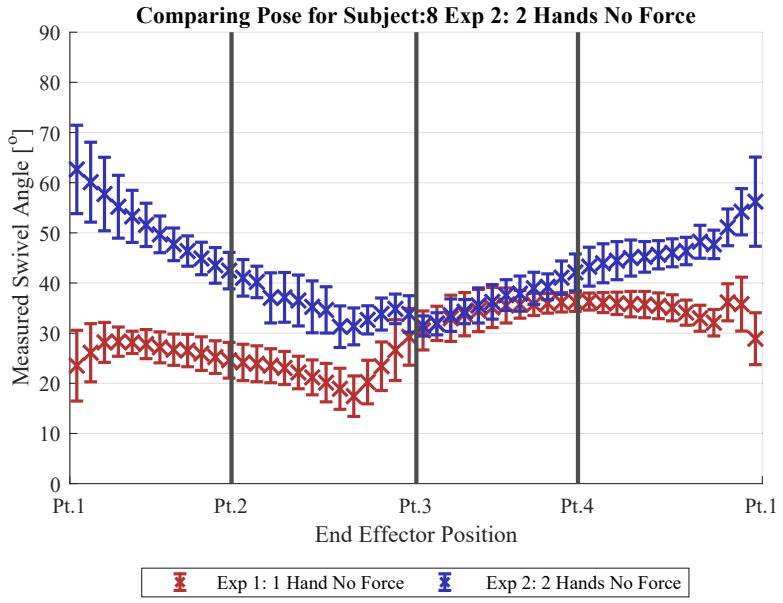

(A)

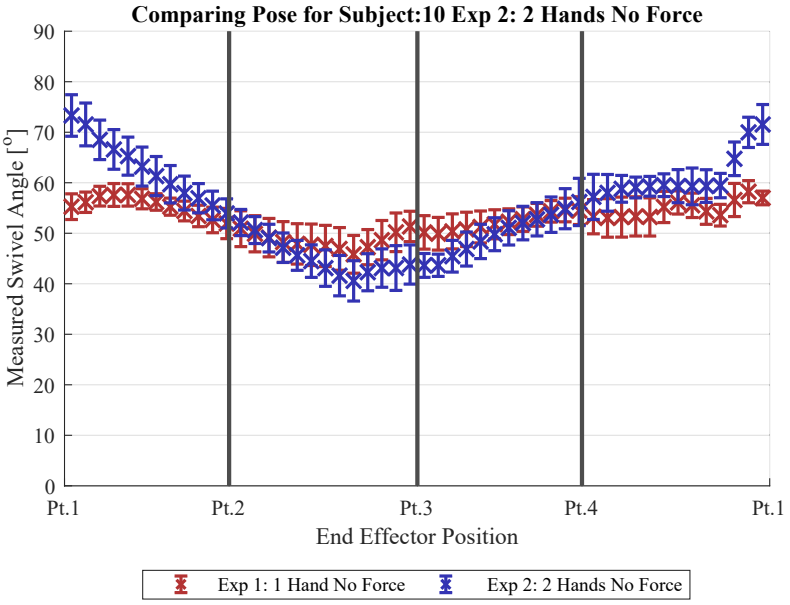

(B)

FIGURE 3.14: Comparison of the mean and standard deviation of the swivel angles of Subjects (A) 8 and (B) 10 in Experiment 2 and Experiment 1.

such as drilling or abrasive blasting, where the worker is required to push away from their body. Similarly to the other experiments, as shown in Figure 3.15, the calculated swivel angle for an individual in these two experiments were repeatable.

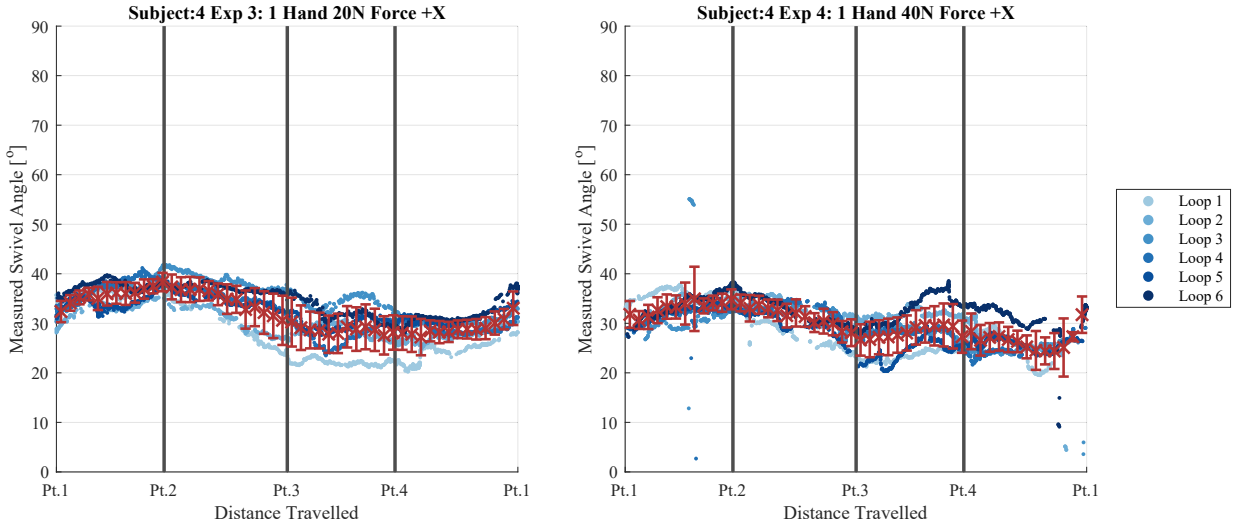

(A) (B)

FIGURE 3.15: Calculated swivel angles of Subject 4 in (A) Experiment 3 and (B) Experiment 4.

Figure 3.16 shows the mean swivel angle of all 10 subjects in Experiments 3 and 4. By Comparing the two figures, it can be clearly seen that as a whole, the 10 subjects adopted a much lower swivel angle in Experiments 3 and 4. A lower swivel angle correlates with the elbow being brought closer to the torso of the human subject. Figure 3.17 highlights the trend that was exhibited across all ten subjects. In Experiment 3, the adopted swivel angle was lower in value when compared to Experiment 1 (Figure 3.17a). Additionally, seven out of ten subjects adopted swivel angle values which were on average lower in Experiment 4 compared to Experiment 3. The other three subject adopted similar swivel angle values to Experiment 3.

The trend from these two experiments seems to suggest that in order to accommodate for a larger pushing force a lower swivel angle is adopted. The lower swivel angle means that the elbow is brought closer to the torso of the human which allows for the forearm to be aligned in the direction of the force which may allow the human body to exert a larger

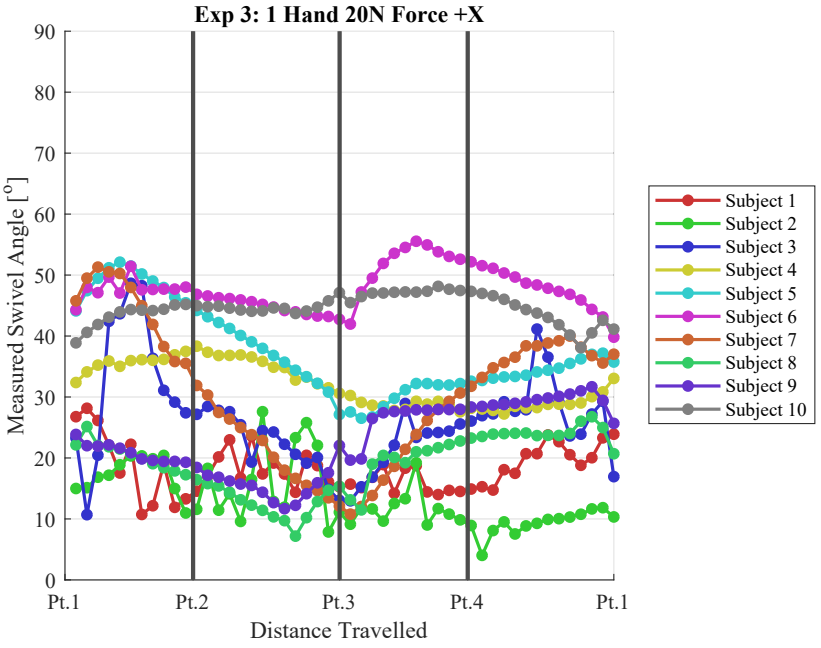

(A)

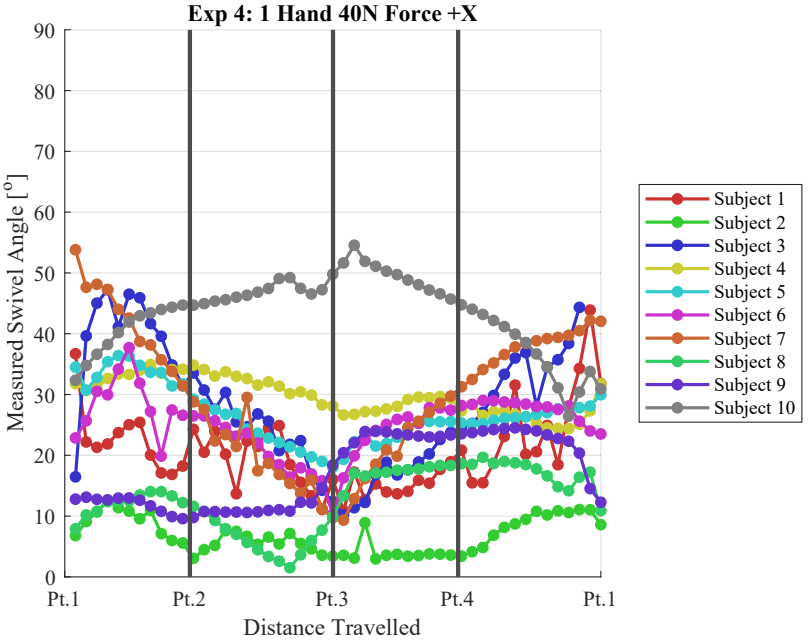

(B)

FIGURE 3.16: Mean swivel angles of all ten subjects in (A) Experiment 3 and (B) Experiment 4.

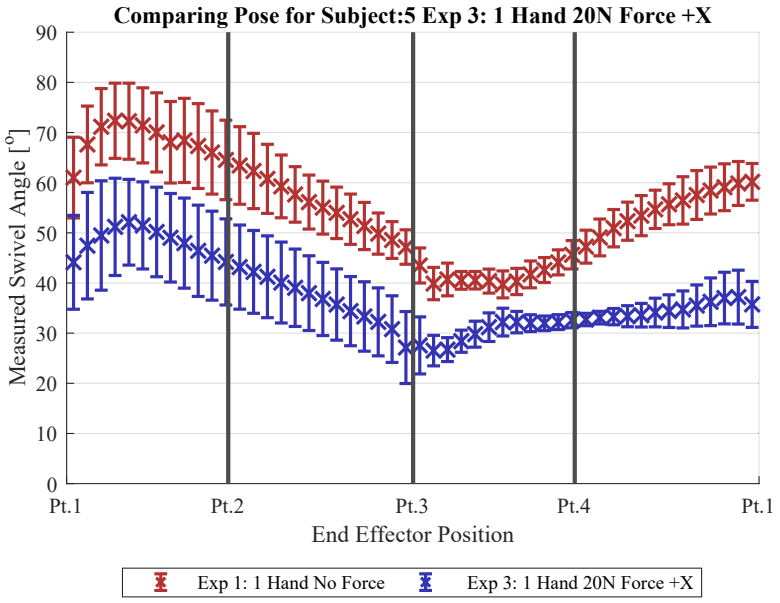

(A)

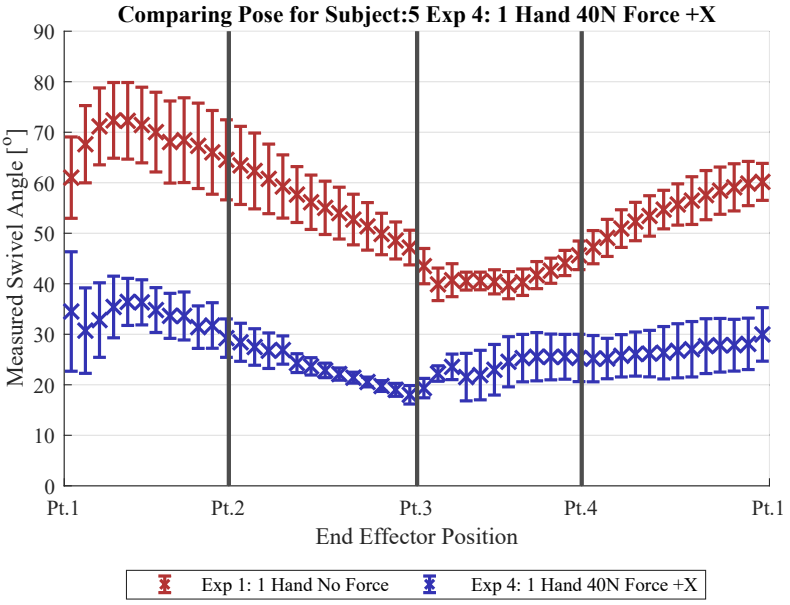

(B)

FIGURE 3.17: Comparison of the mean and standard deviation of the swivel angles of Subject 5 in (A) Experiment 3 and (B) Experiment 4 to Experiment 1.

force in the forward direction, in a similar manner to [23] where it was found that handle orientation affected the maximum force that a human was able to exert.

3.4.4 Experiments 5 and 6 - Unimanual Operation with 20N or 40N Force in the YZ Plane

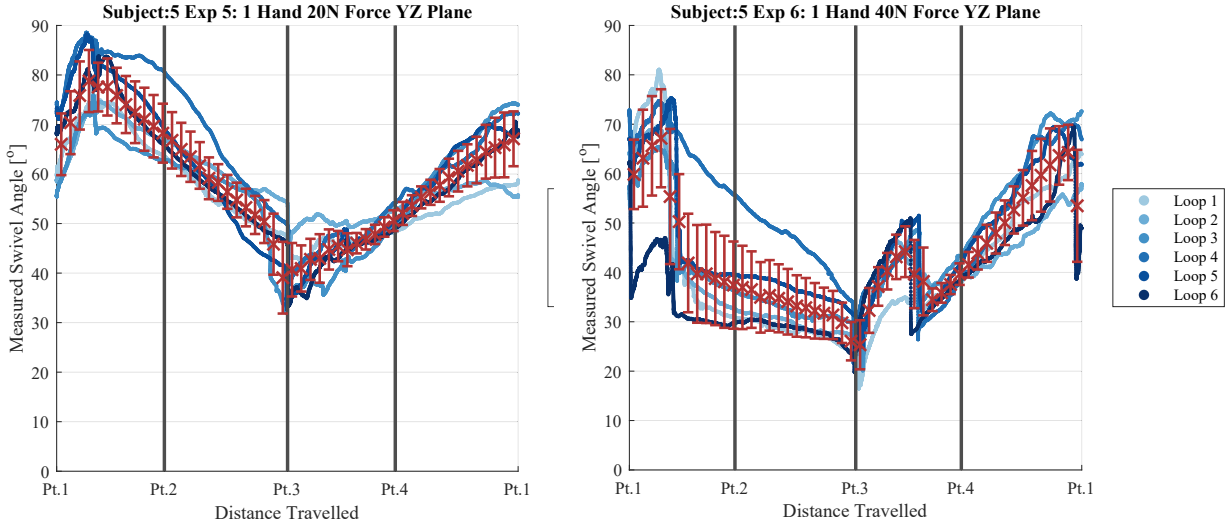

(A) (B)

FIGURE 3.18: Calculated swivel angles of Subject 5 in (A) Experiment 5 and (B) Experiment 6.

In Experiments 5 and 6 each subject was tasked with applying a 20 ±5 N or a 40 ±5 N force in the direction of travel of the end effector. These experiments were used to simulate movement of a heavy load around the path. Figure 3.18 shows that for an individual, the adopted upper limb pose is still repeatable when the subject was required to apply forces in the YZ plane. The mean swivel angle of all ten subjects in Experiments 5 and 6 are shown in Figure 3.19.

Unlike the trend visible in Experiments 3 and 4, in Experiment 5 there are different effects visible across the ten subjects. Figure 3.20 shows a comparison of the adopted swivel angle in Experiment 5 for two subjects. In Figure 3.20, it can be seen that the effect of applying forces in the YZ plane did not seem to affect the adopted pose greatly for these two subjects.

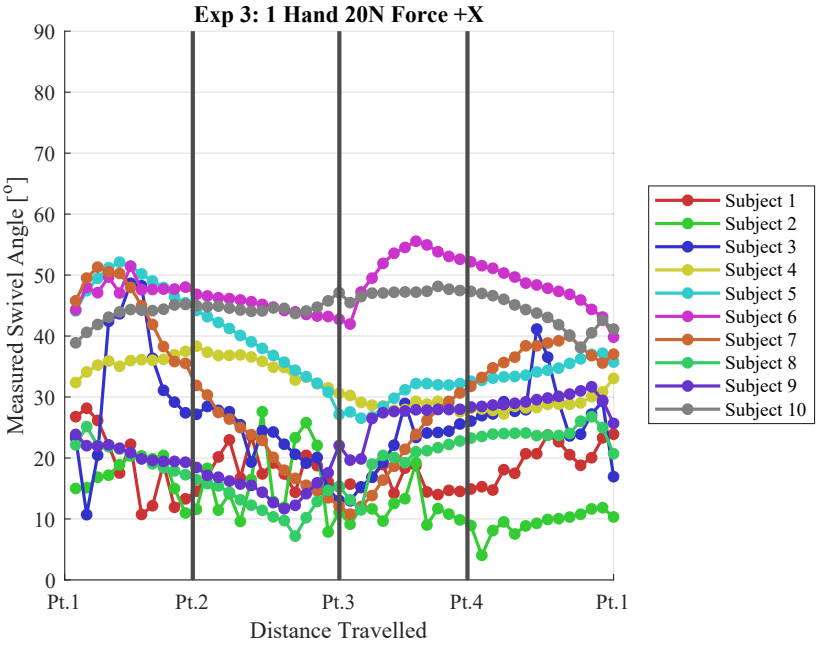

(A)

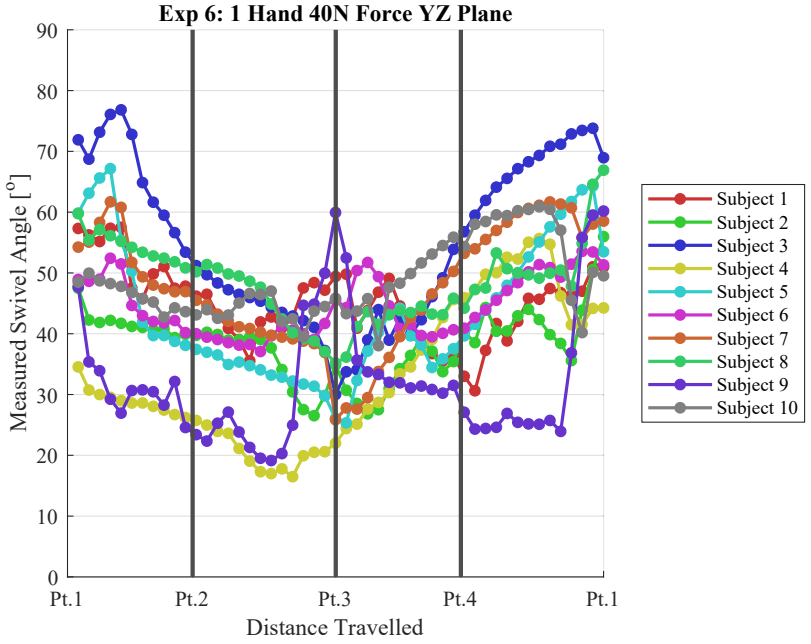

(B)

FIGURE 3.19: Mean swivel angles of all ten subjects in (A) Experiment 5 and (B) Experiment 6.

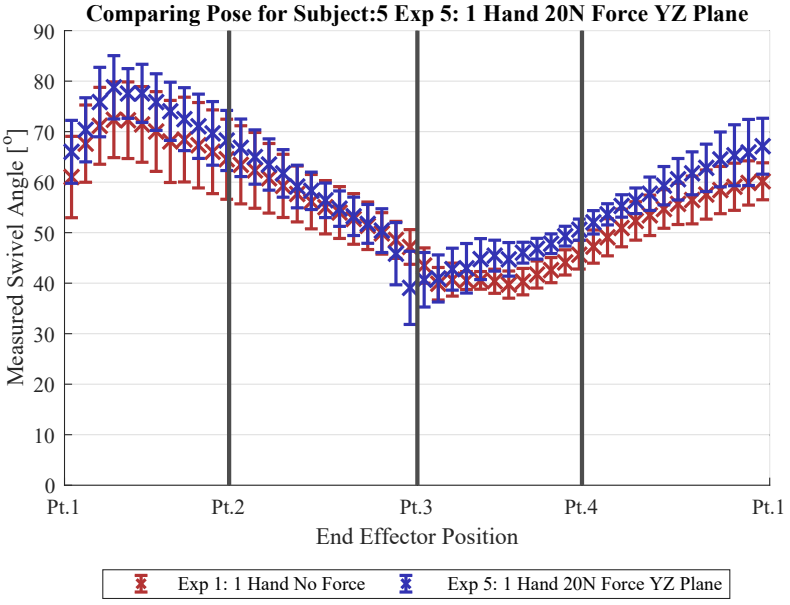

(A)

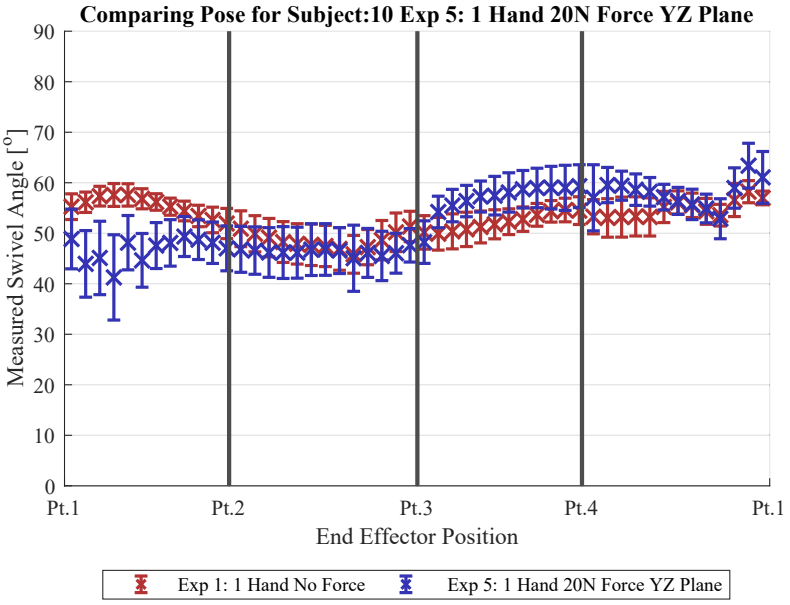

(B)

FIGURE 3.20: Comparison of the mean and standard deviation of the swivel angles of Subjects (A) 5 and (B) 10 in Experiment 5 and Experiment 1.

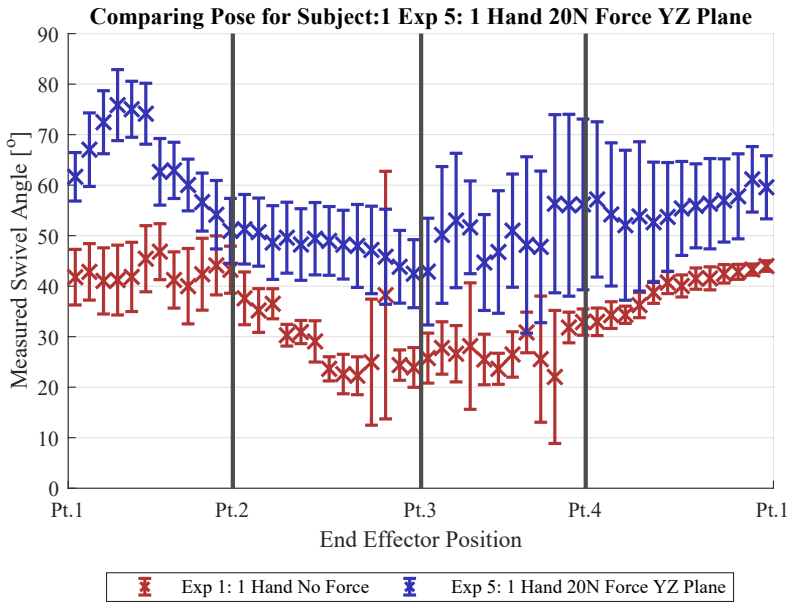

(A)

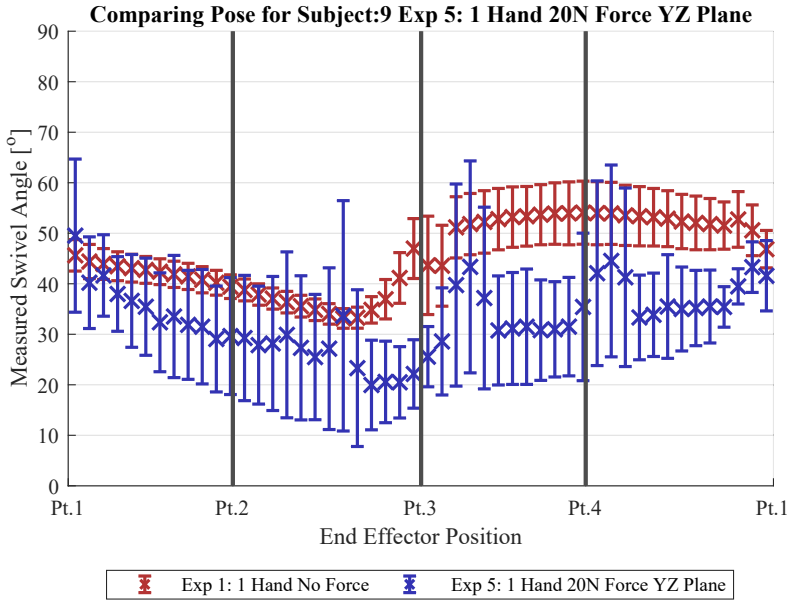

(B)

FIGURE 3.21: Comparison of the mean and standard deviation of the swivel angles of Subjects (A) 1 and (B) 9 in Experiment 5 and Experiment 1.

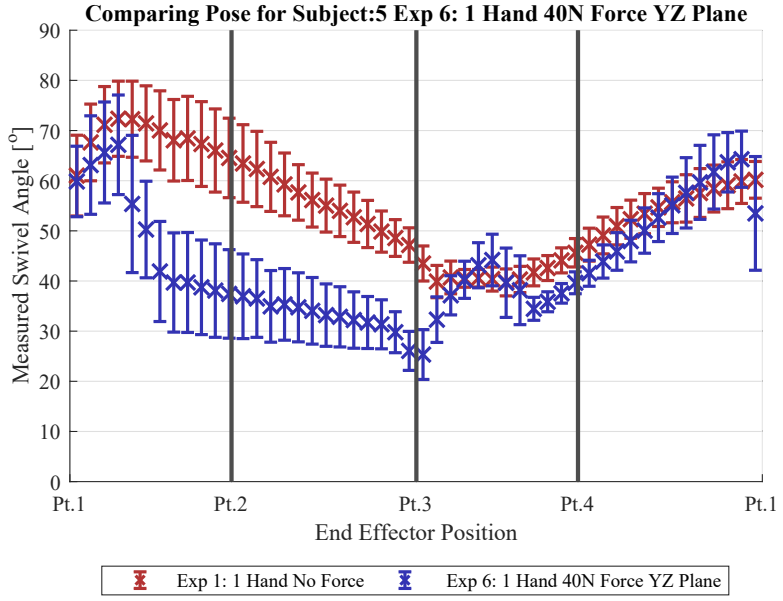

(A)

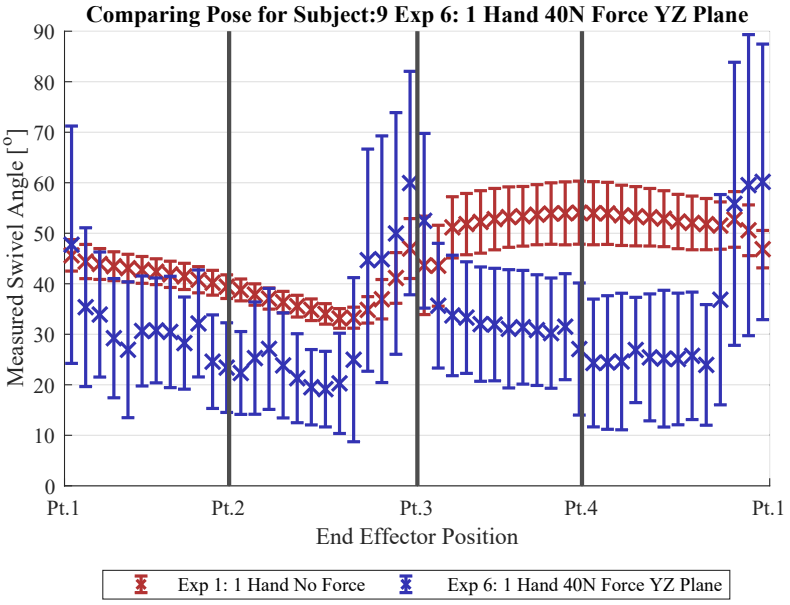

(B)

FIGURE 3.22: Comparison of the mean and standard deviation of the swivel angles of Subjects (A) 5 and (B) 9 in Experiment 6 and Experiment 1.

Figure 3.21 shows the comparison of the adopted swivel angle in Experiment 5 for another set of two subjects. As shown in these figures, the adopted swivel angle in the same experiment varied depending on the subject. In Figure 3.21a the adopted swivel angle for Subject 1 is shown to be overall higher whereas in Figure 3.21b the adopted swivel angle is overall lower.

In Experiment 6 a different effect was shown when compared to Experiment 5. For example whereas previously Subject 5 exhibited very little change in the adopted swivel angle, in Experiment 6 a considerable change in the adopted swivel angle is visible between point 1 and 3 of the path (Figure 3.22a). For another subject (Subject 9) the variability in the adopted swivel angle was increased in Experiment 6 (Figure 3.22b) in comparison to Experiment 5 (Figure 3.21b).

The large change in adopted swivel angle in Experiment 6 is likely caused by the difficulty experienced by the subjects in isolating the force that they applied in the different directions. There was visible readjustment of the upper limb in order to exert forces in the required direction. Although no visible trend across all of the subjects was seen, this phenomenon of readjusting the upper limb pose supports the trend visible in Experiments 3 and 4 where each user adopted a more advantageous upper limb pose in order to exert the required forces.

3.4.5 Summary of Each Individual

Table 3.2 highlights the difference between the swivel angles from each experiment with respect to each subject. Each column in the table shows the calculated RMSD of the subject's swivel angle when compared against the mean swivel angle calculated in Experiment 1. RMSD values obtained for the same experiment were not consistent between subjects. This further highlights that each individual had a different observed reaction to the factors being considered in this paper.

Shown in Table 3.2, the difference in Experiment 3 to Experiment 1 shows that even though the trend of lowering the swivel angle is visible across all subjects, the magnitude in which the swivel angle is lowered differs between different subjects. In Experiment 4,

	Exp 2	**Exp 3**	**Exp 4**	**Exp 5**	**Exp 6**
Sub 1	13.37	17.83	17.41	22.34	14.14
Sub 2	7.96	25.81	29.43	9.27	8.75
Sub 3	9.22	14.08	9.32	14.51	19.67
Sub 4	11.31	11.86	14.00	14.36	16.28
Sub 5	7.25	18.72	28.75	6.31	14.91
Sub 6	10.26	15.60	35.66	17.84	17.00
Sub 7	8.25	16.95	18.87	8.88	8.70
Sub 8	13.98	11.83	16.87	17.53	21.48
Sub 9	7.11	24.45	28.80	18.03	22.68
Sub 10	6.38	8.52	11.15	6.74	9.34

TABLE 3.2: RMSD of the swivel angles in different experiments, measured against the mean swivel angle of the same subject in Experiment 1.

eight out of ten subjects exhibited a greater difference in the swivel angle when compared to Experiment 3. Subject 1 exhibited almost no difference from Experiment 3 to Experiment 4, whereas Subject 3 exhibited a smaller magnitude of change in Experiment 4 to Experiment 3 when compared to the natural motion in Experiment 1. Unlike Experiments 3 and 4, in Experiment 5 and 6 there was no visible trend that was shared by all of the subjects.

3.4.6 Strength Comparison using a Musculoskeletal Model

It was speculated that in Experiments 3 and 4, subjects adopted an upper limb pose with the elbow closer to the torso in order to exert a larger forward force. To investigate the trend of a lower swivel angle observed in Experiments 3 and 4, a musculoskeletal model of the upper limb [10] was used to estimate the physical strength of Subject 5. Whereas [130] minimized the muscle activation required to maintain a certain joint configuration, this analysis attempts to estimate the maximum physical strength of the human for a given pose of the upper limb. It was hypothesized that there was some form of biomechanical advantage with a lower swivel angle and hence a lower swivel angle would be adopted when each subject was required to exert a larger forward force at the hand. The upper limb musculoskeletal model was used with the OpenSim software [143] to estimate the maximum opposable strength at the hand. Experiments 1 and 4 were chosen as the two scenario to be compared. Experiment 1 represents a case where the subject performed the operation with minimal force interaction. Experiment 4 represented a case where the subject was

required to apply a large force in the forward direction. These two experiments resulted in a different pose being adopted by the user and it was expected that the maximum strength of the subject would be different in these two experiments.

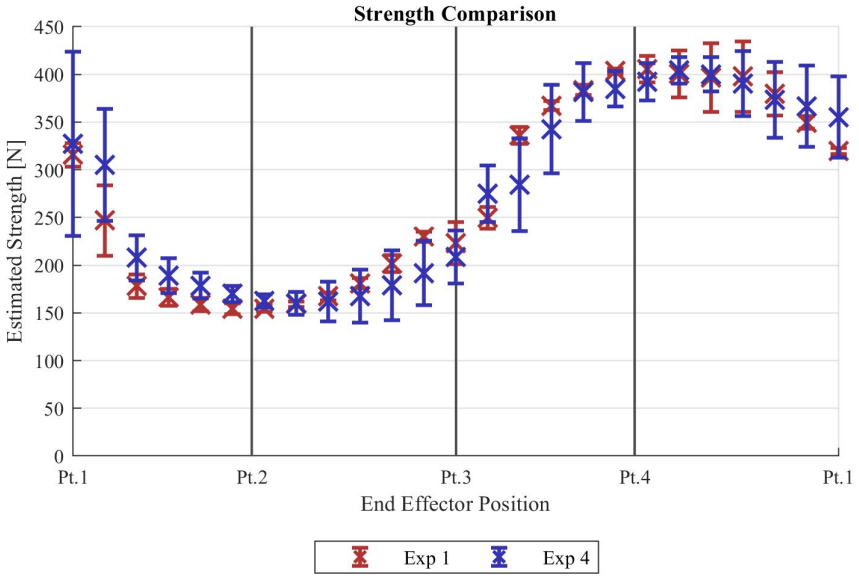

FIGURE 3.23: Comparison of the strength of Subject 5 during Experiment 1 and Experiment 4

The standard procedure for performing a musculoskeletal modelling analysis was followed. The positions of the reflective markers used to record the motion of the upper limb were added to the musculoskeletal model. Using the recorded upper limb motion, the upper limb musculoskeletal model was scaled using an inbuilt function of OpenSim.

Figure 3.23 shows the mean and standard deviation of the maximum opposable force at the hand in the +X direction of subject 5 for upper limb poses adopted in Experiments 1 and 4. The mean values of the maximum opposable force were shown to have little variation and all values were greater than the 40 N specified in Experiment 4. The difference in the adopted poses from Experiments 1 and 4 did not result in a large difference in the maximum strength of the human to change, as the directions of the forces being opposed by the human subject are similar in their workspace. The change in the upper limb pose in Experiment 4 may have reduced the joint loading in the elbow similar to the findings in [172]. In Experiment 1 the calculated standard deviations of the maximum opposable force is on average smaller than those in Experiment 4. It is hypothesized that the increase

in the standard deviation is likely due to the subject's pose altering due to fatigue whereas in Experiment 1 the maximum opposable forces were consistent due to the low strength requirement of the operation.

3.5 Conclusion

From the experimental results collected on the upper limb poses adopted by the ten subjects, it was found that for each subject the swivel angle was observed to be repeatable with some variation. The difference in the adopted upper limb pose was significantly larger when comparing poses across subjects for the same experiment. The calculated swivel angle does not remain consistent when comparing two different subjects. This implies that for a model designed to estimate the pose of the human upper limb, it is advantageous to individualize the model rather than developing a general model that is designed to fit a generic human. The natural variation in the body of different people was found to affect the adopted pose of the upper limb even when a similar trajectory at the hand was enforced.

The effect of bimanual operation on the upper limb pose differs between individuals. Although no trend was visible in the adopted right upper limb pose across the ten subjects, some subjects exhibited an alteration in the adopted pose surrounding the full reach of the right upper limb. With the left hand being placed onto another handle on the same end effector (Figure 3.3), some restrictions were likely placed on the right upper limb pose.

When the user was required to apply a force to push forward, it was found that this force constraint resulted in an overall lower swivel angle. The magnitude of the force to be applied further lowered the swivel angle adopted by eight out of ten subjects. The lowering of the swivel angle correlates to the elbow being brought closer to the upper body, aligning the forearm of the user to the required direction of force generation.

In experiments where the force is to be applied in the direction of motion, the magnitude of the force had a larger impact in the adopted pose. Some subjects had difficulty in producing the 40 N force in the specified direction, resulting in a large change to the swivel angle which supports the findings in [173]. This suggests that the direction of the

force in human-robot collaboration and the magnitude of force are important factors that are likely to change the adopted pose of the user. Subjects were found to alter their pose significantly to apply a force in certain directions.

The maximum opposable strength for Experiments 1 and 4 has shown that the musculoskeletal model exhibited a similar strength profile even with the change in the swivel angle. It is hypothesized that although the change in the swivel angle did not greatly alter the maximum opposable force, the effect of bringing the elbow closer to the body allowed a more comfortable pose to be adopted in order to generate the required force. Aligning the forearm to the direction of force to be applied reduces the moment required to be generated.

The results obtained have several implications for the development of robotic systems to cooperate with humans. The experiments were able to show that each individual will adopt a different upper limb pose given a similar hand pose. In order to achieve a good estimate to the upper limb pose, where applicable, sensors should be used to provide information regarding the current pose of the human co-worker. This is especially true in pHRC scenarios where the current pose of the human co-worker may affect the performance of the operation and the safety of the human co-worker.

The interaction between the human and the robot in pHRC operations was shown to affect the pose of the human subjects in a different manner. The requirement of producing a forward pushing force resulted in a lower adopted swivel angle for all ten subjects. This suggests that for a pHRC operation where the human co-worker is required to exert forces either to control the robot or to counteract the reaction forces from the operation, models that assumes a free unconstrained motion may not be able to accurately estimate the true pose of the human. Therefore in pHRC applications where the human pose is needed, a different method of estimating the pose of the human operator is required.

Chapter 4

nullPose: an Upper Body Pose Estimation Method

In Chapter 3 the effect of the interaction between a human and robot on the pose of the human upper limb were investigated. From the investigation it was found that subjects adopted different upper limb poses in order to perform a similar trajectory of the hand. It was also found that the interaction between the human and robot resulted in a different upper limb pose to be adopted. This suggests that existing human pose prediction models are unlikely to provide an accurate estimate of the human pose in a physical Human-Robot Collaboration (pHRC) operation, as these models are often developed based on free unconstrained motions. Therefore in pHRC applications where the human pose is needed, a different method of estimating the pose is required.

This chapter presents nullPose, a method of estimating the pose of the human upper body designed for pHRC applications where the poses of the human co-worker's hands are known or able to be inferred from the interaction. This method utilizes the information that exists during a pHRC operation where the robot is controlled through a direct contact force exchange. Although the interaction between the human and the robot may lead to uncertainty in the overall human pose, any known information regarding the human state is valuable, especially in a difficult environment. The physical contact between the human and the robot allows pose information of the human co-worker to be inferred, such as the

pose of their hands. This information can then be used as the basis for the upper body pose estimate.

Section 4.1 provides an overview of the nullPose method with the definitions and assumptions. In Section 4.2 the algorithms used by the nullPose method are presented. Section 4.3 outlines the experiments which were performed to verify and validate the nullPose method. In Section 4.4 the nullPose method was tested in an ideal situation where a Motion Capture (MoCap) system was used as targets for the nullPose method to achieve. The experiment performed in Section 4.5 compared the output of the nullPose method against a MoCap system during a pHRC operation. The nullPose method was also tested in a real world and highly challenging pHRC operation set in an abrasive blasting environment (Section 4.6). The conclusions are presented in Section 4.7.

4.1 Overview of the Methodology

In pHRC applications, the presence of the robot is often a source of occlusion which makes tracking the pose of the human co-worker challenging. When trying to estimate the pose of a human co-worker, the number of possible solutions is huge. However the number of possible solutions can be reduced by limiting the estimated poses to biomechanically feasible poses. The number of possible solutions can be further reduced by exploiting the kinematic constraints imparted by the physical interaction between the human and the robot. The nullPose method exploits the kinematic constraints from the physical interaction with the robot alongside a biomechanical model of the human body to provide an estimate to the human co-worker's upper body pose.

The upper body poses estimated by the nullPose method consists of the poses of the wrists, elbows, shoulders and torso (Figure 4.1). The nullPose method can be used in applications where the hand poses are known or able to be inferred. This makes the nullPose method well suited for applications such as pHRC where the interaction points between the human and the robot are specifically defined. Due to standards such as [170] such interactions are likely required to ensure the safety of the human. The interaction between the human and the robot usually occurs through handles to be held onto by the human or through

attachments such as a forearm cuff to be worn by the human (Figure 4.2). From the interaction points the poses of the hand are able to be inferred during a collaboration between the human and the robot.

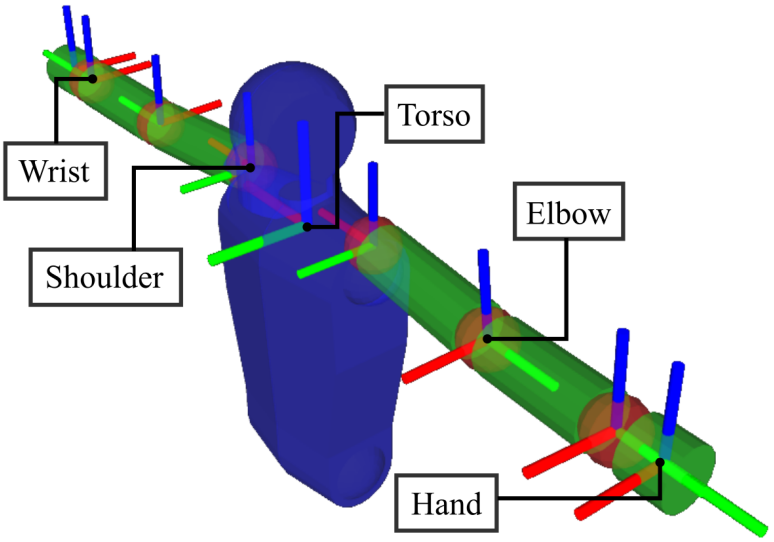

FIGURE 4.1: Poses of the upper body estimated by the nullPose method.

FIGURE 4.2: Human-Robot interaction through a forearm cuff.

The hand poses are used by the nullPose method as the basis to the upper body pose solution. Since the human hand poses are assumed to be known, it is proposed that the upper body is to be divided vertically in half as shown in Fig. 4.3. In this manner the hand poses of the estimated upper body pose are ensured to always be equal to the known hand poses. Each upper body half consists of a nine Degrees of Freedom (DOF) upper limb as well as a torso half. The upper limbs are treated as kinematic chains, analogous

to redundant robotic manipulators, which are controlled through differential kinematics. The hand of each upper limb kinematic chain are treated as the base of the kinematic chain as the poses of the hands are known (or able to be inferred) from the interaction points of the collaborative robot.

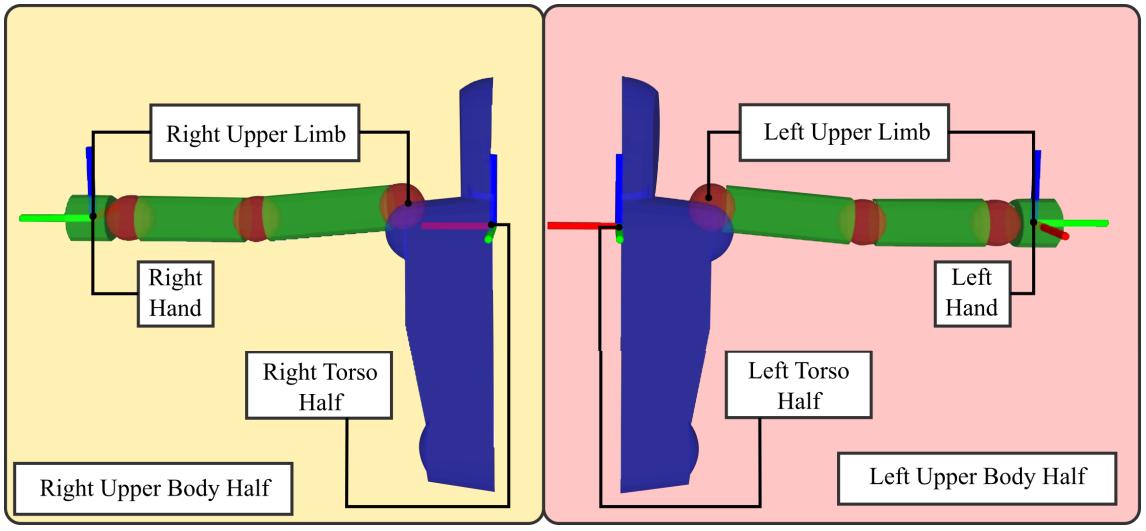

FIGURE 4.3: The right and left upper body halves.

From the poses of the hands, one possible solution for the human co-worker's pose can be found by aligning the two torso halves to close the kinematic chain from the left hand to the right. However this solution is unlikely to resemble the actual pose of the human co-worker. To obtain a better estimate to the human co-worker's upper body pose additional kinematic constraints are used. These additional constraints are referred to as "targets".

A target is implemented to obtain a more accurate estimate of the upper body pose. In an ideal situation, sensor measurements are used to define targets that resolve the redundancy in the human upper body to obtain an accurate pose of the human co-worker. In a practical pHRC application it is not likely that sensor measurements are able to fully constrain the pose of the human co-worker. Therefore, when sensor measurements of the human co-worker's pose are not able to be obtained, targets can be generated from approximations of the human body based on heuristics or existing pose estimation models. Targets are converted into "tasks" for the upper limbs to satisfy such that the estimated upper body pose reflects the targets used as the input to the nullPose method. For example, the model in [8] provides an elbow position approximation that could be used as a target

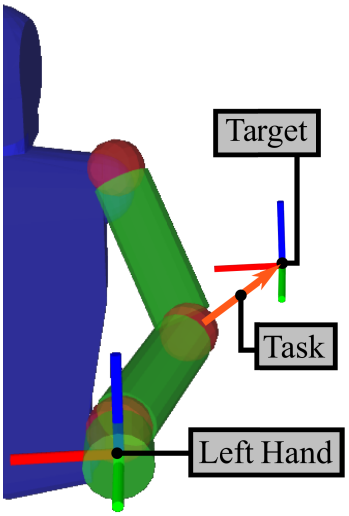

FIGURE 4.4: A visualization of an elbow target and the corresponding task to move the elbow towards the target.

such as shown in Figure 4.4. Another target could be point cloud data obtained from a Kinect camera that provides measurements regarding the position and orientation of the co-worker's torso. Using the elbow target and the torso pose target, the nullPose method is expected to generate an upper body pose estimate which is the same as the provided targets.

A task represents the motion to be performed by the upper models. Tasks can be motions that are defined by targets, such as shown in Figure 4.4, or motions used to ensure that the estimated upper body poses are humanly feasible, such as avoiding collision between the torso and the upper limbs. Each task is used alongside the respective task Jacobian which converts the motion from the task space, such as Cartesian space, to the required joint motions of the upper limb kinematic models while satisfying the biomechanical limit of human upper limbs.

A key feature of the nullPose method is the prioritisation of different tasks that are incorporated into the upper body pose solution. The redundancy in the upper body means that multiple tasks can be incorporated to define the pose of the upper body. Targets obtained from different sources may also provide conflicting information. For example a task obtained from a target that defines the pose of the human from a highly accurate sensor would be given a higher priority compared to a task from a target which approximates the torso pose based on heuristic. The priority ensures that the joint values for the upper limbs

calculated using a task of a lower priority do not affect the outcome of the task of a higher priority. Generally, tasks from sensor based targets are given a higher priority whereas tasks from approximations are given a low priority as approximations may not reflect the true pose of the human co-worker. In certain applications, these approximations may be appropriate such as when limited sensor measurements are available as a more realistic upper body pose is likely to be estimated using the approximations.

4.2 The nullPose Method

The nullPose method provides an upper body pose estimate by using two inputs as shown in Figure 4.5. The first input consists of the poses of the hands. When a new hand pose is received, the upper body halves are updated such that the pose of the hands of the upper limb kinematic models matches that of the inputs. The pose of the left hand in the global frame is denoted by ${}^{G}\mathbf{T}_{LH} \in SE(3)$ with ${}^{G}\mathbf{R}_{LH} \in SO(3)$ defining the orientation and ${}^{G}\mathbf{p}_{LH} \in \mathbb{R}^{3\times1}$ the position. Likewise the right hand in the global frame is denoted by ${}^{G}\mathbf{T}_{RH} \in SE(3)$ with ${}^{G}\mathbf{R}_{RH} \in SO(3)$ defining the orientation and ${}^{G}\mathbf{p}_{RH} \in \mathbb{R}^{3\times1}$ the position. The second input to the nullPose method consists of targets for the estimated upper body pose to achieve.

During a bimanual operation of a pHRC robot the human upper body forms a closed loop kinematic chain. The nullPose method operates in two distinct modes which are dependent on whether the two upper body halves form a closed kinematic chain. The kinematic chain is considered closed when the pose of the left torso half is ${}^{G}\mathbf{T}_{LT}$ is approximately equal to the pose of the right torso half ${}^{G}\mathbf{T}_{RT}$ (Equation 4.1). When the kinematic chain is closed, the normal operating mode (Mode 1) is selected to resolve the redundancy in the human upper body using the provided targets such that a good estimate of the upper body can be obtained. In the event that the kinematic chain is open, such as during the initialization of the two upper limb models, Mode 2 is selected to close the kinematic chain. In this research the threshold used was a maximum relative rotation θ_{Tr} of 0.01 radians and a maximum separation distance Δp_T of 1 cm. This threshold can be relaxed to increase the computational efficiency of the nullPose method whilst being strict enough such that the two torso halves are adequately aligned.

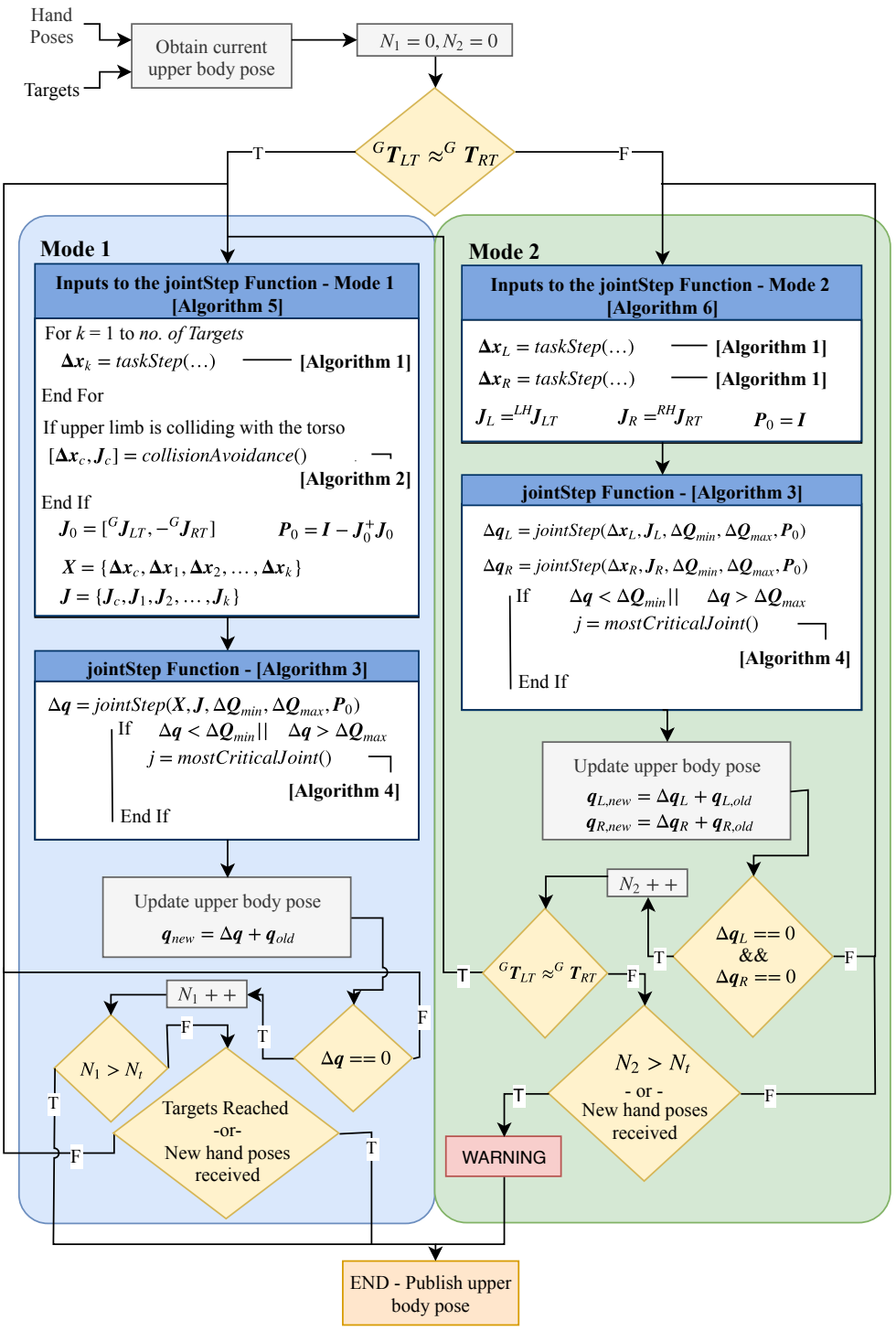

FIGURE 4.5: Flowchart of the nullPose method which updates the estimate to the upper body pose when new hand poses are received.

$$
\begin{aligned}
\Delta \boldsymbol{p}_T &= \boldsymbol{p}_{LT} - \boldsymbol{p}_{RT} \\
\Delta \boldsymbol{R}_T &= \boldsymbol{R}'_{LT} \times \boldsymbol{R}_{RT} \\
\|\theta\| &= \arccos\left(\frac{Tr(\Delta \boldsymbol{R}) - 1}{2}\right) \\
{}^{G}\mathbf{T}_{LT} &\approx {}^{G}\mathbf{T}_{RT} \quad \text{when} \quad \|\theta\| < \theta_{Tr} \quad \&\& \quad \|\Delta \boldsymbol{p}_T\| < \Delta p_{Tr}
\end{aligned} \tag{4.1}
$$

The pose of the upper body is dictated by the joint configuration of the closed kinematic chain from the left hand to the right, $\boldsymbol{q} \in \mathbb{R}^{18\times 1}$. $\boldsymbol{q}$ combines the joint configurations of the left and right upper limb kinematic model, $\boldsymbol{q}_L \in \mathbb{R}^{9\times 1}$ and $\boldsymbol{q}_R \in \mathbb{R}^{9\times 1}$ respectively, as shown in Equation 4.2.

$$
\boldsymbol{q} = \begin{bmatrix} \boldsymbol{q}_L \\ \boldsymbol{q}_R \end{bmatrix} \tag{4.2}
$$

The *taskStep* function (Algorithm 1) is used to calculate $\Delta \boldsymbol{x}$ which encompasses the motion required to move the upper body such that the current pose ${}^{G}\mathbf{T}_{C}$ is moved towards the desired pose ${}^{G}\mathbf{T}_{D}$. In Mode 1 the *taskStep* function is used to convert the targets into tasks for the upper body model to achieve. In Mode 2 the *taskStep* function calculates the motion to bring the two torso halves towards one another.

The *jointStep* function (Algorithm 3) is used to calculate the necessary joint step, $\Delta \boldsymbol{q}$, for the left and right upper limbs based on the task steps, $\Delta \boldsymbol{x}$. Through the calculation of $\Delta \boldsymbol{q}$ the upper body pose can be moved to reach targets or to ensure a humanly feasible upper body pose. Each $\Delta \boldsymbol{q}$ is calculated iteratively using the null space to ensure that the $\Delta \boldsymbol{q}$ calculated for a lower priority task does not detract from the outcome of a higher priority task. Joint limit constraints, $\Delta \boldsymbol{Q}_{min}$ and $\Delta \boldsymbol{Q}_{max}$ calculated using the biomechanical model of the upper limbs are used to ensure that the calculated $\Delta \boldsymbol{q}$ is able to be performed by human upper limbs.

The calculations performed in the two modes will continue repeatedly until certain end conditions are met. In Mode 1 the nullPose method will end by outputting the estimated

upper body pose once the targets are reached, new hand poses are received or when a maximum number of iterations have been reached ($N_1 > N_t$). N_1 and N_2 represent counters which are initialised to start at 0 and are used in Mode 1 and Mode 2 respectively. N_t represents the number of allowable iterations. Since Mode 2 is used to close the kinematic chain, the nullPose method will not proceed to resolve the redundancy in the upper body (Mode 1) until the two torso halves are brought together. In the unlikely event that the two torso halves are unable to be brought together whether it be due to the calculation limit being reached ($N_2 > N_t$) or new hand poses being received, the upper body poses are published alongside a warning to note the failure in closing the kinematic chain.

4.2.1 Upper Limb Kinematic Model

To ensure that the estimated upper body pose results in a biomechanically feasible pose, the Klopčar-Lenarčič model [174] was used. This model incorporates limits on the range of motion (ROM) of each joint to match the movement of a human upper limb. To model the whole upper body of a human, a left and right upper limb kinematic model was used. The two upper limb models are visualized in Figure 4.6. The upper limb model used consisted of nine DOF. Two DOF represent the inner shoulder which articulates the shoulder girdle (SG). Three DOF represent the Glenohumeral (GH) joint which orientates the humerus. Two DOF at the elbow control the elbow flexion/extension as well as the forearm pronation/supination. The last two DOF at the hand represent the wrist deviation and wrist flexion/extension. The maximum and minimum values of each joint used in the upper limb model are listed in Table 4.1.

In the Klopčar-Lenarčič model, the motion of the SG is represented as two rotational and one translational joint. The motion of the translational joint is prescribed by the two rotational joints q_1 and q_2 to articulate the SG. This model also includes a series of coupled equations which represent the joint limit of the shoulder. These equations represent a more realistic limit to the shoulder rotational joints which ensures a biomechanically feasible pose of the humerus relative to the torso. The range of motion of each joint is presented in Table 4.2 along with the equations limiting the minimum and maximum value of the

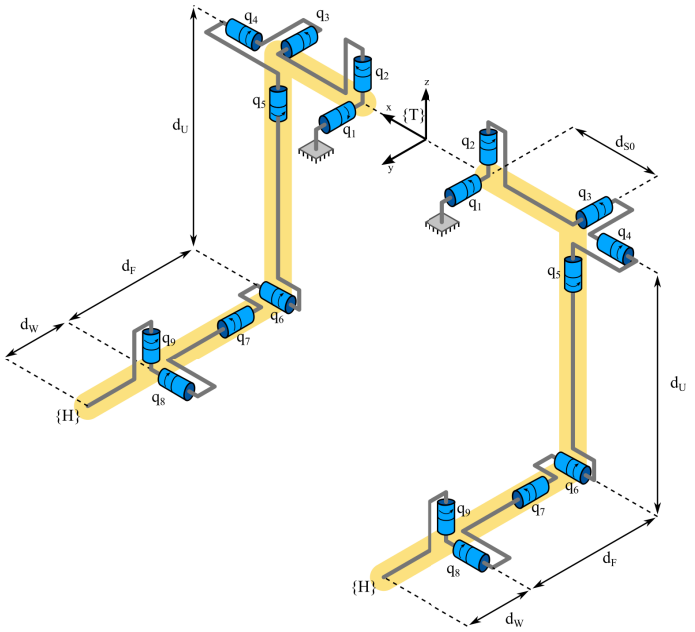

FIGURE 4.6: The nine DOF on each of the upper limb kinematic models.

TABLE 4.1: Joints limits of the upper limb model used by the nullPose method.

Joint Name	***Joint Number***	***Min Parameter***	***Max Parameter***
SG elevation	q_1	$\phi_{1m} = -14°$	$\phi_{1M} = 30°$
SG retraction	q_2	$\phi_{2m} = -26°$	$\phi_{2M} = 30°$
GH abduction	q_3	$\phi_{3m} = -10°$	$\phi_{3M} = 170°$
GH flexion	q_4	$\phi_{4m} = -60°$	$\phi_{4M} = 170°$
GH rotation	q_5	$\phi_{5m} = -90°$	$\phi_{5M} = 60°$
Elbow flexion/extension	q_6	$\phi_{6m} = -90°$	$\phi_{6M} = 60°$
Forearm pronation/supination	q_7	$\phi_{7m} = -90°$	$\phi_{7M} = 90°$
Wrist deviation	q_8	$\phi_{8m} = -25°$	$\phi_{8M} = 10°$
Wrist flexion/extension	q_9	$\phi_{9m} = -70°$	$\phi_{9M} = 70°$

GH joints. Figure 4.7 shows a visualization of the movement the shoulder girdle using the prescribed motion as the upper limbs are moved from a position where the elbow points directly downward to an upward elbow position.

4.2.2 Task Composition

The *taskStep* function calculates a task step $\Delta\boldsymbol{x}$ that represents a motion for a given current pose ${}^{G}\mathbf{T}_{C}$ and desired pose ${}^{G}\mathbf{T}_{D}$ that satisfies the maximum position and angular change, $\Delta p_{max}, \Delta\theta_{max}$ respectively. $\Delta\boldsymbol{x}$ consists of a desired position $\Delta\boldsymbol{p}$ and angular step $\boldsymbol{w}$ in Cartesian space and is used by both modes to define how each upper limb should

TABLE 4.2: Range of motion of each joint of the upper limb model

Joint	***Range***
SG elevation	$q_1 = [\phi_{1m}\ ,\ \phi_{1M}]$
SG retraction	$q_2 = [\phi_{2m}\ ,\ \phi_{2M}]$
GH abduction	$q_3 = [\phi_{3m}\ ,\ \phi_{3M}]$
GH flexion	$q_4 = [\phi_{4m} + \frac{1}{3}q_3\ ,\ \phi_{4M} - \frac{1}{6}q_3]$
GH rotation	$q_5 = [\phi_{5m} + \frac{7}{9}q_3 + \frac{1}{9}q_4 + \frac{4}{9\pi}q_3q_4\ ,\ \phi_{5M} + \frac{4}{9}q_3 - \frac{5}{9}q_4 + \frac{10}{p\pi}q_3q_4]$
Elbow flexion/extension	$q_6 = [\phi_{6m}\ ,\ \phi_{6M}]$
Forearm pronation/supination	$q_7 = [\phi_{7m}\ ,\ \phi_{7M}]$
Wrist deviation	$q_8 = [\phi_{8m}\ ,\ \phi_{8M}]$
Wrist flexion/extension	$q_9 = [\phi_{9m}\ ,\ \phi_{9M}]$

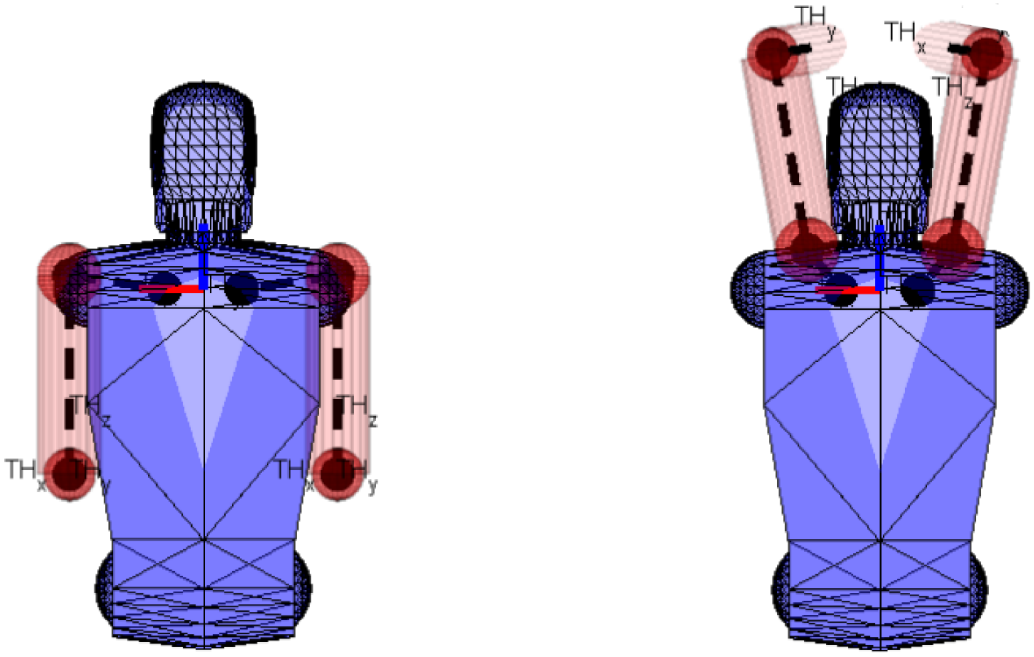

(A) (B)

FIGURE 4.7: Visualization of the shoulder girdle movement as the upper limb moves from (A) a downward elbow position to (B) an upward elbow position.

be moved. ${}^{G}\mathbf{T}_{C}$ and ${}^{G}\mathbf{T}_{D}$ may range from poses that define the poses of parts of the upper limb, such as the elbow or the shoulder, to poses of the torso halves. In Mode 1 this function is used to calculate the task steps that convert the targets, obtained through sensor based information or approximations, to a desired upper body pose. The amount and combination of targets to be used in this mode are determined by the implementer based on the availability and accuracy of sensory measurements. In Mode 2 this function is used to calculate the required transformation to align the two torso halves.

Algorithm 1 taskStep Function

Function $\boldsymbol{\Delta x} = \text{taskStep}({}^{G}\mathbf{T}_{C}, {}^{G}\mathbf{T}_{D}, \Delta p_{max}, \Delta\theta_{max})$
$\boldsymbol{\Delta p} = \boldsymbol{p}_D - \boldsymbol{p}_C$
if $\|\boldsymbol{\Delta p}\| > \Delta p_{max}$ **then**
  $\boldsymbol{\Delta p} = \Delta p_{max} \times \frac{\boldsymbol{\Delta p}}{\|\boldsymbol{\Delta p}\|}$
end if
$\boldsymbol{\Delta R} = \boldsymbol{R}'_C \times \boldsymbol{R}_D$
Let θ = magnitude of the axis angle representation of $\boldsymbol{\Delta R}$
$\|\theta\| = \arccos\left(\frac{Tr(\boldsymbol{\Delta R}) - 1}{2}\right)$
$\boldsymbol{e} = \frac{1}{2\sin\theta}\begin{bmatrix}\boldsymbol{\Delta R}_{3,2} - \boldsymbol{\Delta R}_{2,3} \\ \boldsymbol{\Delta R}_{1,3} - \boldsymbol{\Delta R}_{3,1} \\ \boldsymbol{\Delta R}_{2,1} - \boldsymbol{\Delta R}_{1,2}\end{bmatrix}$
$\boldsymbol{w} = \boldsymbol{e} \cdot \theta$
if $\|\boldsymbol{w}\| > \Delta\theta_{max}$ **then**
  $\boldsymbol{w} = \Delta\theta_{max} \times \frac{\boldsymbol{w}}{\|\boldsymbol{w}\|}$
end if
$\boldsymbol{\Delta x} = \begin{bmatrix}\boldsymbol{\Delta p} \\ \boldsymbol{w}\end{bmatrix}$

The position vectors of ${}^{G}\mathbf{T}_{C}$ and ${}^{G}\mathbf{T}_{D}$ are represented by $\boldsymbol{p}_C$ and $\boldsymbol{p}_D$ respectively. Rotational aspect of the pose is denoted with $\boldsymbol{R}$. Using this function the position step $\boldsymbol{\Delta p}$ and angular step $\boldsymbol{w}$ can be calculated within the distance Δp_{max} threshold and the angular threshold $\Delta\theta_{max}$.

In the event that a certain task k does not constrain all of the dimensions, only the constrained row is kept in the corresponding task Jacobian $\boldsymbol{J}_k$. For example, setting the torso of the co-worker to a certain height restricts only the z component of the torso position, therefore only the component of $\boldsymbol{J}_k$ corresponding to the z axis is kept. For example, the elbow task shown in Figure 4.4 shows a task of moving the elbow towards an elbow target. This target only constrains the position of the elbow (i.e. $\boldsymbol{\Delta x} = \boldsymbol{\Delta p}$) so only the rows of the Jacobian which corresponds to the position are used.

Certain tasks may be necessary in order to achieve a realistic pose of the upper body. For example, although the biomechanical model of the upper limbs provides limits reflecting the biomechanical model of the joint ROM it does not account for collision between the upper limb and the torso. If a high priority task was to be implemented to move the torso to a pose such that the colliding part is outside of the torso, a lower priority task from a target regarding the torso position will be unlikely to contribute towards the final upper

body pose estimate. Lowering the priority of the task to move the torso to avoid collision with the upper limb will likely result in the upper limb to remain colliding with the torso.

Algorithm 2 Collision Avoidance for the Wrist

Function $[\Delta \boldsymbol{x}_c, \boldsymbol{J}_c] = collisionAvoidance()$
if $((p_{w,x} - p_{t,x})^2 - (p_{w,y} - p_{t,y})^2) < t_r^2$ **then**
  $\Delta \boldsymbol{x}_c = t_r^2 - ((p_{w,x} - p_{t,x})^2 - (p_{w,y} - p_{t,y})^2)$
  $\Delta dir = 2 \times [p_{w,x} - p_{t,x}, p_{w,y} - p_{t,y}]$
  $\boldsymbol{J}_c = \Delta dir \times J_{w,xy}$
end if

Algorithm 2 shows a task $\boldsymbol{X}_c$ and the corresponding Jacobian $\boldsymbol{J}_c$ that is implemented as a high priority task in the event that the wrist of the upper limb is found to collide with the torso. In this function the horizontal cross section of the torso is defined as a circle with a radius t_r centered on the torso position $\boldsymbol{p}_t$. In the event that the position of the wrist $\boldsymbol{p}_w$ in the xy plane is found to be within the torso boundary, a one dimensional repulsion force is calculated for Δx_{col}. A corresponding one dimensional Jacobian $\boldsymbol{J}_c$ is calculated by incorporating the direction that the force is to be applied Δdir alongside the corresponding Jacobian that moves the wrist in the xy plane $\boldsymbol{J}_{w,xy}$. Setting up the task in this manner shifts the wrist outside of the torso whilst not specifying the exact location of the wrist, allowing for a lower priority task to alter the pose of the upper limb with minimal restrictions.

4.2.3 Task Prioritization

Different targets may result in conflicting tasks being considered in the redundancy resolution. The accuracy and reliability of the targets used to resolve the redundancy will affect the estimated upper body pose. Tasks created from sensor based targets are generally placed at a higher priority to tasks created from approximation based targets as measured data should better reflect the current situation. Targets from approximations are used by the nullPose method in order to provide partial upper body pose information in the event that sensory measurements are unreliable or unavailable.

Multiple $\Delta \boldsymbol{x}$ can be incorporated in order to resolve the redundancy in the upper body pose in Mode 1. In the task priority array, $\boldsymbol{X}$, $\Delta \boldsymbol{x}$ of higher priority precede those of lower

priority. For example, if $\Delta \boldsymbol{x}_1$ is to specify the desired pose of the torso, solutions found by a lower priority $\Delta \boldsymbol{x}_k$ will be restricted as the torso position should not change. For the kth task vector $\boldsymbol{\Delta x}_k$, an accompanying Jacobian $\boldsymbol{J}_k$ is required to calculate the new joint angles of the upper limb models. Similarly, each task Jacobian is placed in the same order to the corresponding task in the array $\boldsymbol{J}$ (Equation 4.3).

$$\begin{aligned} \boldsymbol{X} &= \{\boldsymbol{\Delta x}_1, \boldsymbol{\Delta x}_2, \ldots, \boldsymbol{\Delta x}_k\} \\ \boldsymbol{J} &= \{\boldsymbol{J}_1, \boldsymbol{J}_2, \ldots, \boldsymbol{J}_k\} \end{aligned} \tag{4.3}$$

Currently the prioritization of the tasks is not dynamic and is determined manually. The priority is determined based on what the implementer deems to be the reliable or accurate source of information and is kept constant throughout the entire time the pose is to be estimated. The task priority structure is useful as it allows for certain restrictions to be placed to eliminate unlikely upper body poses. For example setting a task of keeping the torso upright will remove the likelihood that the estimated pose results in the body being parallel to the ground.

4.2.4 Joint Step Calculation

A variation of the velocity level saturation in the null space method [175] was implemented to move the upper limbs to reflect the implemented tasks in $\boldsymbol{X}$. A joint step $\Delta \boldsymbol{q}$ is iteratively calculated, accommodating tasks until all tasks within $\boldsymbol{X}$ are satisfied or all of the joints in the upper limb model have reached the joint limits set by the biomechanical model. By projecting through the null space, a joint step calculated using a lower priority task $\Delta \boldsymbol{q}_k$ will not negatively affect the previously calculated joint step from a higher priority task $\Delta \boldsymbol{q}_{k-1}$.

In Algorithm 3 the symbol $^+$ denotes a Moore-Penrose pseudo-inversion of the matrix. The limits to each joint are represented by the vectors, $\Delta \mathbf{Q}_{min}, \Delta \mathbf{Q}_{max}$. For each task $\boldsymbol{\Delta x}_i$ for $i = 1 \rightarrow k$, the current joint step $\Delta \boldsymbol{q}_k$ is calculated. The symbol $\boldsymbol{P}_0$ represents the initial projection matrix and $\boldsymbol{P}_{k-1}$ represents the subsequent projection matrices which

Algorithm 3 jointStep Function

Function $\Delta \boldsymbol{q}$ = jointStep($\mathbf{X}, \mathbf{J}, \Delta\mathbf{Q}_{min}, \Delta\mathbf{Q}_{max}, P_0$)
for k = 1 to m **do**
  $\boldsymbol{W}_k = I, \Delta\boldsymbol{q}_{N,k} = 0, \bar{\boldsymbol{P}}_k = \boldsymbol{P}_{k-1}$
  while solution_found == false **do**
    $\tilde{\boldsymbol{P}}_k = (\boldsymbol{I} - (\boldsymbol{J}_k\bar{\boldsymbol{P}}_k)^+\boldsymbol{J}_k)((\boldsymbol{I} - \boldsymbol{W}_k)\boldsymbol{P}_{k-1})^+$
    $\Delta\boldsymbol{q}_k = \Delta\boldsymbol{q}_{k-1} + (\boldsymbol{J}_k\bar{\boldsymbol{P}}_k)^+(\boldsymbol{\Delta x}_k - \boldsymbol{J}_k\Delta\boldsymbol{q}_{k-1}) + \tilde{\boldsymbol{P}}_k\Delta\boldsymbol{q}_{N,k}$
    if $any(\Delta\boldsymbol{q}_k < \Delta\mathbf{Q}_{min} \| \Delta q_k > \Delta\mathbf{Q}_{max})$ **then**
      $j = mostCriticalJoint(\Delta\boldsymbol{q}_k, \Delta\mathbf{Q}_{min}, \Delta\mathbf{Q}_{max})$
      $\boldsymbol{W}_k(j, j) = 0$
      $\Delta\boldsymbol{q}_{N,k}(j) = \begin{cases} \Delta\mathbf{Q}_{min,j} & \Delta q_k(j) < \Delta\mathbf{Q}_{min,j} \\ \Delta\mathbf{Q}_{max,j} & \Delta\boldsymbol{q}_k(j) > \Delta\mathbf{Q}_{max,j} \end{cases}$
      $\bar{\boldsymbol{P}}_k = (\boldsymbol{I} - ((\boldsymbol{I} - \boldsymbol{W}_k)\boldsymbol{P}_{k-1}^+)\boldsymbol{P}_{k-1}$
      if $\boldsymbol{W}_k$ == *zero* **then**
        $\tilde{\boldsymbol{P}}_k = (\boldsymbol{I} - (\boldsymbol{J}_k\bar{\boldsymbol{P}}_k)^+((\boldsymbol{I} - \boldsymbol{W}_k)\boldsymbol{P}_{k-1})^+$
        $\Delta\boldsymbol{q}_k = \Delta\boldsymbol{q}_{k-1} + (\boldsymbol{J}_k\bar{\boldsymbol{P}}_k)^+(\boldsymbol{\Delta x}_k - \boldsymbol{J}_k\Delta\boldsymbol{q}_{k-1}) + \tilde{\boldsymbol{P}}_k\Delta\boldsymbol{q}_{N,k}$
        solution_found = true
      end if
    else
      solution_found = true
    end if
  end while
  $\boldsymbol{P}_k = \boldsymbol{P}_{k-1} - (\boldsymbol{J}_k\boldsymbol{P}_{k-1})^+(\boldsymbol{J}_k\boldsymbol{P}_{k-1})$
end for
$\Delta\boldsymbol{q} = \Delta\boldsymbol{q}_k$
End Function

ensures that the solution found by incorporating the kth task does not interfere with the outcome of any previous tasks.

Each time a new joint step for the kth task is calculated, a check is performed to ensure that the current joint step $\Delta\boldsymbol{q}_k$ is within the set joint limits before proceeding to the next task. If any of the joints are found to be outside of the limits, the *mostCriticalJoint* function (Algorithm 4) is used to determine which joint exceeded the limit by the largest margin. When joint j is found to exceed the set limits, the joint value is then set to the limit and this joint is considered saturated.

A matrix $\boldsymbol{W}$ is used to represent an index of the joints of the upper limb which are within set joint limits. Initially $\boldsymbol{W}$ is an identity matrix with a dimension $m \times m$ where m equals the number of joints in the upper limb model. When a joint is saturated and is set to the joint limit, the corresponding value of $\boldsymbol{W}$ is set to zero and $\Delta\boldsymbol{q}_k$ is recalculated with

the saturated joint disabled. The calculation for $\Delta \boldsymbol{q}_k$ is repeated until all joints satisfy the limit or until all joints become saturated. For each new task k, W is reset to an identity matrix as the calculated $\Delta \boldsymbol{q}_k$ may result in previously saturated joints becoming unsaturated whilst maintaining the same outcome of the previous task.

Algorithm 4 mostCriticalJoint Function

Function $j = \text{mostCriticalJoint}(\Delta \boldsymbol{q}, \Delta \mathbf{Q}_{min}, \Delta \mathbf{Q}_{max})$
$\boldsymbol{a} = \Delta \boldsymbol{q} - \Delta \mathbf{Q}_{max}$
$\boldsymbol{b} = \Delta \boldsymbol{q} - \Delta \mathbf{Q}_{min}$
$\boldsymbol{a}(\boldsymbol{a} \leq 0) = 0$
$\boldsymbol{b}(\boldsymbol{b} \geq 0) = 0$
$\boldsymbol{c} = \boldsymbol{a} + \boldsymbol{b}$
Let j be such that $c_j = max(|\boldsymbol{c}|)$

4.2.5 Mode 1 - Kinematic Chain Closed

The redundancy in the human upper body allows for different poses of the upper body to be naturally adopted. To obtain a good estimate of the true upper body pose, additional information are normally required to resolve the redundancy. In Mode 1, targets with information regarding the human upper body pose are integrated into the upper body pose estimate.

Targets that are able to be used by the nullPose method are dependent on the setup of the robot and sensors. A camera placed behind the human co-worker could be used to detect the position of the head [176] or a laser scanner could determine the position of the co-worker's legs or torso. These targets can be used to provide known position of parts of the upper body, reducing the solution space for the upper body pose. The more reduced the solution space, the more accurate the estimate of the upper body pose.

To avoid requiring sensor measurement of the complete upper body to resolve the upper body pose, the nullPose method can make use of modeled approximations. One target that is often difficult to obtain through sensors and can be approximated is the orientation of the human co-worker's torso. In certain pHRC applications, it may be appropriate to assume that the co-worker is standing in a relatively upright position. This approximation can be useful in determining the pose of the upper body when the measurements from the

sensor is not useful or when the approximation is reasonable. Estimation models such as the elbow position estimation in [8] could also be implemented as an approximation target to aid in the redundancy resolution.

Integrating various targets in the redundancy resolution may result in the two torso halves becoming separated. To ensure that the kinematic chain from the left hand to the right hand is kept closed, a self motion projection P_0 is used (Equation 4.4). The projection P_0 ensures that motion of the left upper limb could be accommodated by motion of the right and vice versa. The velocities of the left and right torso halves, ${}^{G}\boldsymbol{\Delta x}_{LT}$ and ${}^{G}\boldsymbol{\Delta x}_{RT}$, need to be equated in order to maintain the two torso halves being closed.

In Equation 4.4, ${}^{G}\boldsymbol{J}_{LT}$ and ${}^{G}\boldsymbol{J}_{RT}$ represent the Jacobian of the left and right torso halves in the global frame with $\boldsymbol{q}_L$ and $\boldsymbol{q}_R$ being the current joint values for the left and right upper limb model. Equating the velocities of the two torso halves allows the Jacobian J_0 to be calculated. Using $\boldsymbol{P}_0$ in the *jointStep* function, calculated $\Delta\boldsymbol{q}$ will ensure that the two torso halves are kept together.

$$\boldsymbol{P}_0 = \boldsymbol{I} - \boldsymbol{J}_0^{+}\boldsymbol{J}_0 \tag{4.4}$$

where:

$$\begin{aligned}
{}^{G}\boldsymbol{\Delta x}_{LT} &= {}^{G}\boldsymbol{J}_{LT}(\boldsymbol{q}_L)\cdot\Delta\boldsymbol{q}_L \\
{}^{G}\boldsymbol{\Delta x}_{RT} &= {}^{G}\boldsymbol{J}_{RT}(\boldsymbol{q}_R)\cdot\Delta\boldsymbol{q}_R \\
{}^{G}\boldsymbol{J}_{LT}\cdot\Delta\boldsymbol{q}_L &= {}^{G}\boldsymbol{J}_{RT}\cdot\Delta\boldsymbol{q}_R \\
\underbrace{\left[{}^{G}\boldsymbol{J}_{LT}(\boldsymbol{q}_L) - {}^{G}\boldsymbol{J}_{RT}(\boldsymbol{q}_R)\right]}_{\boldsymbol{J}_0}
&\begin{bmatrix}\Delta\boldsymbol{q}_L \\ \Delta\boldsymbol{q}_R\end{bmatrix} = 0
\end{aligned}$$

Equation 4.5 shows the Jacobian $\boldsymbol{J}_k$ for a given task k. In order to accommodate velocity of the upper body, $\boldsymbol{\Delta x}_k$, the Jacobian of the left and right upper limb, $\boldsymbol{J}_{k,L}\&\boldsymbol{J}_{k,R}$, are placed along the diagonal to create the Jacobian for the upper body $\boldsymbol{J}_k$.

$$\boldsymbol{\Delta x}_k = \underbrace{\begin{bmatrix} \boldsymbol{J}_{k,L} & 0 \\ 0 & \boldsymbol{J}_{k,R} \end{bmatrix}}_{\boldsymbol{J}_k} \begin{bmatrix} \Delta \boldsymbol{q}_L \\ \Delta \boldsymbol{q}_R \end{bmatrix} \tag{4.5}$$

Algorithm 5 Inputs to the jointStep Function - Mode 1

for $k = 1$ *to no. of Targets* **do**
  $\boldsymbol{\Delta x}_k = taskStep({}^{G}\mathbf{T}_C, {}^{G}\mathbf{T}_D, \ldots)$ – [**Algorithm 1**]
end for
if upper limb is colliding with the torso **then**
  $[\boldsymbol{\Delta x}_c, \boldsymbol{J}_c] = collisionAvoidance()$ – [**Algorithm 2**]
end if
$\boldsymbol{J}_0 = [\boldsymbol{J}_{LT}, -\boldsymbol{J}_{RT}]$
$\boldsymbol{P}_0 = \boldsymbol{I} - \boldsymbol{J}_0^{+}\boldsymbol{J}_0$
$\boldsymbol{X} = \{\boldsymbol{\Delta x}_c, \boldsymbol{\Delta x}_1, \boldsymbol{\Delta x}_2, \ldots, \boldsymbol{\Delta x}_k\}$
$\boldsymbol{J} = \{\boldsymbol{\Delta J}_c, \boldsymbol{J}_1, \boldsymbol{J}_2, \ldots, \boldsymbol{J}_k\}$

4.2.6 Mode 2 - Kinematic Chain Open

Mode 2 is used in the event when the kinematic chain is open i.e. the torso halves are separated. During initialization of the pose estimation, depending on the orientation and position of the two hands, it is likely that the two torso halves are separated. When the upper limb models are close to singularity, i.e. $det(\boldsymbol{J}_{LT}) \rightarrow 0$ *or* $det(\boldsymbol{J}_{RT}) \rightarrow 0$, calculated joint steps may result in the two torso halves separating.

In this mode a single task is implemented for the left and right upper limbs, which is to align the two torso halves and close the kinematic chain. The two upper body halves are treated as separate kinematic chains with their own task and task Jacobian. The kinematic chains are treated separately as the pose of the left and right limb may originate from different hand poses thus it is unlikely that the left and right upper limbs will adopt a symmetrical configuration. From the current joint values of the left and right upper limb models, $\boldsymbol{q}_L$ and $\boldsymbol{q}_R$, the poses of the two torso halves, ${}^{LH}\mathbf{T}_{LT}$ and ${}^{RH}\mathbf{T}_{RT}$, are calculated. Using ${}^{LH}\mathbf{T}_{LT}$ and ${}^{RH}\mathbf{T}_{RT}$, the pose of the torso in the global frame ${}^{G}\mathbf{T}_{LT}$ and ${}^{G}\mathbf{T}_{RT}$ is able to be calculated using Equation 4.6.

$$
\begin{aligned}
{}^{G}\mathbf{T}_{LT} &= {}^{G}\mathbf{T}_{LH} \cdot {}^{LH}\mathbf{T}_{LT} \\
{}^{G}\mathbf{T}_{RT} &= {}^{G}\mathbf{T}_{RH} \cdot {}^{RH}\mathbf{T}_{RT}
\end{aligned} \tag{4.6}
$$

Where:

$$
{}^{LH}\mathbf{T}_{LT} = \begin{bmatrix} ({}^{LT}\mathbf{R}_{LH})^{T} & -({}^{LT}\mathbf{R}_{LH})^{T} \cdot {}^{LT}\mathbf{p}_{LH}) \\ 0 \quad 0 \quad 0 & 1 \end{bmatrix}
$$

$$
{}^{RH}\mathbf{T}_{RT} = \begin{bmatrix} ({}^{RT}\mathbf{R}_{RH})^{T} & -({}^{RT}\mathbf{R}_{RH})^{T} \cdot {}^{RT}\mathbf{p}_{RH}) \\ 0 \quad 0 \quad 0 & 1 \end{bmatrix}
$$

The *taskStep* function (Algorithm 1) is used to calculate the task step to iteratively calculate the joint steps of the upper limb models to align the two torso halves. In this mode, $\boldsymbol{\Delta x}_L$ is calculated to move the left torso half towards the right. A Jacobian that moves the torso frame relative to the hand frame ${}^{LH}\boldsymbol{J}_{LT}$, a vector of the minimum and maximum joint step, $\Delta\mathbf{Q}_{L,min}$ and $\Delta\mathbf{Q}_{L,max}$, and the task step $\boldsymbol{\Delta x}_L$ are used to calculate the new joint step $\Delta\boldsymbol{q}_l$. The projection $\boldsymbol{P}$ is set to an identity matrix $\boldsymbol{I}$ as the two torso halves are not yet aligned. A similar calculation is performed for the right upper limb until the two torso halves are sufficiently aligned within a set threshold, at which point the kinematic chain is considered closed.

Algorithm 6 Mode 2 - Closing the Kinematic Chain

$\boldsymbol{P}_0 = \boldsymbol{I}$
$\boldsymbol{\Delta x}_L = taskStep({}^{G}\mathbf{T}_{LT}, {}^{G}\mathbf{T}_{RT}, \ldots)$ – [**Algorithm 1**]
$\boldsymbol{\Delta x}_R = taskStep({}^{G}\mathbf{T}_{RT}, {}^{G}\mathbf{T}_{LT}, \ldots)$ – [**Algorithm 1**]
$\boldsymbol{J}_L = {}^{LH}\,\boldsymbol{J}_{LT}$
$\boldsymbol{J}_R = {}^{RH}\,\boldsymbol{J}_{RT}$

4.2.7 Task Composition and Prioritization Example

In this example, there are two sources of information available to be used by the nullPose method to estimate the pose of the human. The first is the torso pose obtained through

a Kinect RGB-D sensor and the second is the position of the left elbow through a model approximation [8]. The torso and elbow information can be provided to the nullPose method as 4 by 4 transformation matrices. Since the elbow information does not have a rotational component, the rotational aspect of the matrix is kept as identity.

$$\boldsymbol{torso_d} = \begin{bmatrix} cos(30^o) & -sin(30^o) & 0 & 0.1 \\ sin(30^o) & cos(30^o) & 0 & 0 \\ 0 & 0 & 1 & -0.2 \\ 0 & 0 & 0 & 1 \end{bmatrix}$$
$$\boldsymbol{elbow_{d,l}} = \begin{bmatrix} 1 & 0 & 0 & -0.4 \\ 0 & 1 & 0 & -0.3 \\ 0 & 0 & 1 & 0 \\ 0 & 0 & 0 & 1 \end{bmatrix} \tag{4.7}$$

Equation 4.7 show the two poses, the torso pose and the left elbow pose, received by the nullPose method as targets for the upper body model. Assuming that the current torso pose and left elbow pose are shown by Equation 4.8, to reach the desired torso pose a translation and rotation is required.

$$\boldsymbol{torso_c} = \begin{bmatrix} 1 & 0 & 0 & 0 \\ 0 & 1 & 0 & 0 \\ 0 & 0 & 1 & 0 \\ 0 & 0 & 0 & 1 \end{bmatrix}$$
$$\boldsymbol{elbow_{c,l}} = \begin{bmatrix} 1 & 0 & 0 & -0.3 \\ 0 & 1 & 0 & -0.4 \\ 0 & 0 & 1 & 0.2 \\ 0 & 0 & 0 & 1 \end{bmatrix} \tag{4.8}$$

By inserting the current and the desired poses into Algorithm 1, $\Delta \boldsymbol{x}$ can be obtained. With Δp_{max} set to 0.1 and $\Delta \theta_{max}$ set to 0.1, the calculations to obtain the task step for

the torso, $\Delta \boldsymbol{x}_{torso}$, using Algorithm 1 are shown in Equation 4.9.

$$\begin{aligned}
\Delta \boldsymbol{p} &= \begin{bmatrix} 0.1 & 0 & -0.2 \end{bmatrix}' \\
Since\ ||\Delta \boldsymbol{p}|| &= 0.2236 > \Delta p_{max} = 0.1 \\
\Delta \boldsymbol{p} &= 0.1 \times \frac{\Delta \boldsymbol{p}}{0.2236} = \begin{bmatrix} 0.0447 & 0 & -0.0894 \end{bmatrix}' \\
Since\ \theta &= \frac{\pi}{6} > \Delta \theta_{max} = 0.1 \\
\boldsymbol{w} &= 0.1 \times \frac{\Delta \boldsymbol{w}}{\frac{\pi}{6}} = \begin{bmatrix} 0 & 0 & \frac{0.1\pi}{6} \end{bmatrix}' \\
\Delta \boldsymbol{x}_{torso} &= \begin{bmatrix} 0.0447 & 0 & -0.0894 & 0 & 0 & \frac{0.1\pi}{6} \end{bmatrix}'
\end{aligned} \tag{4.9}$$

Similarly to the calculations in Equation 4.9 the task step for the elbow, $\Delta \boldsymbol{x}_{elbow}$, can be found to be $[-0.0408,\ 0.0408,\ -0.0817,\ 0,\ 0,\ 0]$. Since there are no rotational constraint for the elbow, the last three term of $\Delta \boldsymbol{x}_{elbow}$ can be removed which results in Equation 4.10. The rows of the Jacobian for the elbow motion corresponding to the rotational component, in this case the bottom three rows are also removed.

$$\Delta \boldsymbol{x}_{torso} = \begin{bmatrix} -0.0408 & 0.0408 & -0.0817 \end{bmatrix}' \tag{4.10}$$

Equation 4.11 show the task array $\boldsymbol{X}$ and the Jacobian array $\boldsymbol{J}$ for the two task steps calculated in this example. The torso task step was prioritized higher than the elbow task, therefore the torso task step was placed before the elbow task step. In this manner, the nullPose method will attempt to move the torso prior to moving the elbow.

$$\begin{aligned}
\boldsymbol{X} &= \{\boldsymbol{\Delta x}_{torso}, \boldsymbol{\Delta x}_{elbow}\} \\
\boldsymbol{J} &= \{\boldsymbol{J}_{torso}, \boldsymbol{J}_{elbow}\}
\end{aligned} \tag{4.11}$$

4.3 Experiment Setup

Three experiments were performed to validate and verify the nullPose method. Experiments 1 and 2 were conducted in a motion capture lab to evaluate the nullPose by determining the accuracy of the estimated upper body pose. An OptiTrack MoCap system

was used to accurately track the upper body pose of the human co-worker during a pHRC operation. The recorded upper body poses were used as the ground truth to validate the estimated upper body poses from the nullPose method. The third experiment was performed in an industrial abrasive blasting chamber to verify that the nullPose method is able to be used in real pHRC applications. The abrasive blasting chamber represent an environment where it is difficult to ascertain the pose of the human co-worker due to factors such as suspended particulates in the air and protective equipment worn by the worker.

Experiment 1 was performed to verify the capability of the nullPose method in estimating the upper body pose of a human co-worker when the poses of the left and right hand are known. In this experiment the poses of the hands as well as targets used to estimate the upper body pose were obtained from the OptiTrack MoCap system. Experiments 2 and 3 were conducted to test the real application viability of the nullPose method with the poses of the hand being provided from a pHRC robot with targets being provided from additional sensors and approximations. In Experiments 2 and 3 the Assistance-as-Needed roBOT (ANBOT), which was introduced in Chapter 3, was used as the robotic platform for collaboration between the human and the robot. The interaction between the human and the ANBOT occurs through two handles attached to the end effector of the robot. During the collaboration the human co-worker is expected to firmly hold onto both handles of the ANBOT, allowing for the poses of the co-worker's hands to be inferred throughout the experiments.

The pHRC operation being performed in all experiments is a collaborative abrasive blasting operation. Abrasive blasting is a physically intensive task where grit is propelled through highly pressurized air, often used in cleaning and maintenance operations. The abrasive blasting environment represents a practical field application where visibility is often poor due to abrasive media and fine dust suspended in the air. High speed rebound particulates limit the placement of sensors such as cameras in the environment. Due to these factors, no ground truth was able to be obtained in Experiment 3. Although no ground truth was able to be obtained, this experiment was conducted as a proof of concept which shows the capability of the nullPose method to be used in real environments.

4.4 Experiment 1 - Verifying the nullPose Method in an Ideal Environment

To verify the methodology behind nullPose method, several experiments were conducted using a motion capture system. The experiments were performed by three subjects wearing a motion capture suit for marker based tracking such that the position and orientation of key body segments of the upper body can be recorded. The suit worn utilized reflective markers (Figure 4.8) processed with the MoCap system software. The motions were recorded using twelve OptiTrack cameras. During each experiment handles were held by the subject to provide the position and orientation of the subject's hands. A set of reflective markers with a unique configuration were attached to each handle to distinguish between the left and right hand of the human co-worker. For each time frame recorded by the Optitrack MoCap system, the position and orientation of both hands of the human from the tracked handles were used as an input to the nullPose method to estimate the pose of the upper body.

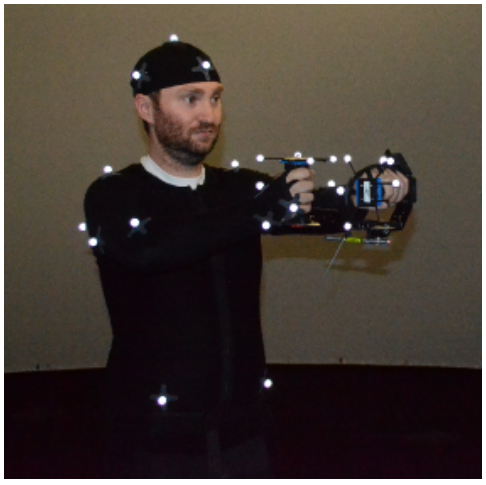

(A)

(B)

FIGURE 4.8: (A) The motion capture suit and handles used to track the human hands. (B) The collaboration between the human and the robot being simulated in Motion 3.

In this experiment three sets of motion were performed by each individual, which are:

1. Motion 1: Subject moving to match set poses (Figure 4.9)

2. Motion 2: Subject moving freely for a period of one minute

FIGURE 4.9: The poses being performed by the subjects in Motion 1.

3. Motion 3: Simulated pHRC abrasive blasting operation (Figure 4.8)

Motion 1 was used to test the capability of the nullPose method in estimating the pose of the human co-worker as they perform various movements. During this motion, the handles are firmly held by the human subject but the hands of the human are not constrained in any manner. The experiment was conducted in this manner to highlight the potential of the nullPose method to be used in various applications as long as the hand poses of the human are known.

Motion 2 had each subject perform various motions of their own volition. The motions performed for these experiments were used to show the capability of the nullPose method to estimate the upper body pose in a wide variety of operations other than operations involving robots.

Motion 3 represents a simulated pHRC abrasive blasting operation with a robot (Figure 4.8b). In this motion the position and orientation of the human hands are restricted relative to each other due to the way the handles are configured (Figure 4.10). Each subject was asked to trace the outline of a box placed two meters in front of the subject using a laser pointer attached to an end effector.

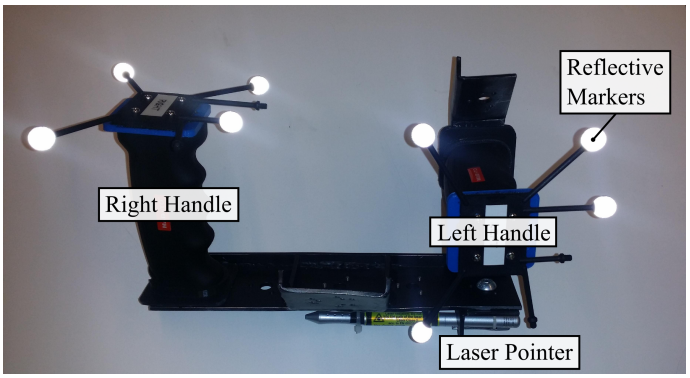

FIGURE 4.10: The configuration of the two handles used in Motion 3.

4.4.1 Pose Estimation Scenarios

To test the capability of the nullPose method in estimating the upper body pose of the human co-worker in different conditions, several scenarios were used based on the combination of targets to be used by the nullPose method. In this experiment, the targets were generated from the recorded MoCap data. At each time interval the estimated position of the elbow, shoulder and torso as well as the torso orientation were compared against the recorded upper body pose.

Table 4.3 shows the different sets of targets that are being used in the different scenarios. In this table, the number 1 represents the highest priority target to be completed whereas the number 2 represents the second priority target. The columns of the table represents the different targets able to be used by the nullPose method. T.Pos represents the torso position, T.Ori represents the torso orientation and E.Pos represents the elbow position which were obtained from the MoCap system. Approximations to the upper body are also used as targets which were E.H2m, an approximation of the elbow position which is also known as the *hand to mouth approximation* [8], and keeping the torso upright relative to the ground plane to approximate the human co-worker standing upright (T.Lvl).

TABLE 4.3: Scenario list with targets used by the nullPose method for Experiment 1

	Target -MoCap			**Target - Approximation**	
Scenario #	**T.Pos**	**T.Ori**	**E.Pos**	**E.H2m**	**T. Lvl**
1	1	1	-	-	-
2	1	1	2	-	-
3	1	1	-	2	-
4	1	-	-	-	2
5	1	-	-	-	-

In all of the different scenarios, motion capture data was used as the input to the nullPose. This experiment was performed to verify that the nullPose method is capable of performing as expected in an ideal scenario where the targets being received are highly accurate. Only the subset of the motion capture data as specified for each scenario was used as the input. The output of the nullPose method is the full upper body pose which is then compared to the recorded pose of the human upper body.

4.4.2 Results and Discussion

The result of Experiment 1 is shown in Table 4.4. Each column in the table represent the mean and standard deviation of euclidean distance error of the upper body pose estimated using the nullPose against the recorded upper body pose. Elbow, shoulder and torso position error were calculated in millimetres whereas the torso orientation error was calculated in radians. The position errors E_{pos} were calculated as the Euclidean distance between two points whereas the orientation errors E_{ori} were calculated as the scalar component of an axis angle representation of the difference between the orientation of the two poses (Equation 4.12). On average the model was able to solve for the pose of the torso quite well, with a low mean error in the torso position.

$$\begin{aligned} E_{pos} &= \|\boldsymbol{p}_{est} - \boldsymbol{p}_{rec}\| \\ E_{ori} &= \arccos\left(\frac{Tr(\boldsymbol{R}'_{est}\boldsymbol{R}_{rec}) - 1}{2}\right) \end{aligned} \tag{4.12}$$

Across all of the scenarios, the largest mean error in the torso position of 42.37 mm was found in Subject 2 performing Motion 2 for Scenario 1 with the second largest torso position error being 38.41 mm for Subject 1 performing Motion 1 for Scenario 5. In both of these cases, there were no elbow targets being used by the nullPose method. Upon examination of the recorded data, the poor results from the two cases can be attributed to the joints of the upper limb kinematic models reaching the biomechanically feasible limits during the closure of the kinematic chain. The addition of extra targets resulted in a much more stable and accurate estimated upper body pose.

TABLE 4.4: Results showing the mean and standard deviation of error in the upper body pose estimates using different scenarios for each recorded data in Experiment 1.

Scenario #	L. Elbow [mm]	L. Shoulder [mm]	Torso [mm]	Torso [Rad]	R. Elbow [mm]	R. Shoulder [mm]
Subject: 1 Motion: 1						
1	77.65 ± 47.00	52.99 ± 34.99	21.53 ± 35.75	0.0249 ± 0.0277	80.16 ± 48.96	45.92 ± 34.69
2	45.50 ± 25.03	43.65 ± 14.41	2.22 ± 10.69	0.0231 ± 0.0504	64.66 ± 35.30	39.63 ± 15.31
3	64.80 ± 26.44	44.53 ± 15.73	2.33 ± 11.14	0.0221 ± 0.0445	87.96 ± 32.71	42.82 ± 18.21
4	64.82 ± 29.65	56.65 ± 43.14	4.98 ± 15.74	0.1919 ± 0.3997	92.86 ± 35.22	58.87 ± 46.39
5	101.93 ± 75.67	82.04 ± 53.48	0.00 ± 0.08	0.8933 ± 0.4245	114.34 ± 69.65	102.11 ± 60.70
Subject: 1 Motion: 2						
1	62.37 ± 40.01	49.73 ± 32.53	18.13 ± 37.75	0.0496 ± 0.1156	73.46 ± 48.98	39.73 ± 26.39
2	28.96 ± 14.37	34.92 ± 6.46	0.00 ± 0.00	0.0235 ± 0.0228	43.74 ± 12.23	31.14 ± 7.28
3	72.70 ± 26.24	41.76 ± 16.52	3.45 ± 16.07	0.0248 ± 0.0274	77.54 ± 30.03	38.02 ± 17.72
4	75.53 ± 47.80	50.37 ± 48.53	2.78 ± 22.02	0.1562 ± 0.3630	87.44 ± 54.10	42.02 ± 41.81
5	147.82 ± 69.04	164.11 ± 69.21	38.41 ± 100.41	1.1432 ± 0.4585	161.48 ± 89.41	147.62 ± 102.44
Subject: 1 Motion: 3						
1	46.16 ± 15.77	43.27 ± 4.58	2.19 ± 4.87	0.0143 ± 0.0059	65.68 ± 24.47	36.54 ± 9.78
2	41.29 ± 10.10	38.35 ± 4.70	0.00 ± 0.00	0.0142 ± 0.0059	40.77 ± 9.47	35.55 ± 8.35
3	90.50 ± 20.11	56.32 ± 19.75	23.01 ± 25.21	0.0159 ± 0.0059	78.31 ± 25.67	53.86 ± 18.74
4	77.70 ± 11.23	43.12 ± 4.93	0.00 ± 0.00	0.0359 ± 0.0676	94.98 ± 25.93	37.79 ± 13.73
5	77.82 ± 19.82	107.54 ± 17.72	0.07 ± 0.51	0.7590 ± 0.2854	188.47 ± 36.02	70.98 ± 16.78
Subject: 2 Motion: 1						
1	88.20 ± 62.53	77.51 ± 53.83	37.05 ± 56.02	0.0291 ± 0.0417	77.38 ± 44.09	67.32 ± 51.38
2	43.66 ± 27.75	47.18 ± 20.17	4.94 ± 17.51	0.0189 ± 0.0519	59.38 ± 32.37	43.95 ± 17.00
3	113.21 ± 81.32	56.26 ± 24.89	5.80 ± 20.42	0.0183 ± 0.0526	107.01 ± 60.56	51.29 ± 21.06
4	80.03 ± 43.15	51.65 ± 28.10	6.10 ± 20.27	0.0648 ± 0.1623	95.52 ± 35.99	50.96 ± 26.30
5	151.56 ± 85.82	125.14 ± 61.38	7.85 ± 23.80	0.9466 ± 0.4203	143.17 ± 59.35	104.55 ± 53.19
Subject: 2 Motion: 2						
1	93.41 ± 69.02	65.79 ± 105.57	42.37 ± 112.37	0.0571 ± 0.1405	80.43 ± 58.23	63.98 ± 98.03
2	44.08 ± 48.73	61.70 ± 98.38	29.44 ± 109.06	0.0665 ± 0.2126	58.16 ± 52.50	58.02 ± 93.83
3	63.34 ± 48.37	64.42 ± 97.50	33.74 ± 111.87	0.0786 ± 0.2399	83.23 ± 52.14	65.62 ± 99.49
4	69.16 ± 45.04	48.23 ± 41.14	7.74 ± 45.59	0.1152 ± 0.2570	84.46 ± 35.80	50.66 ± 43.43
5	104.57 ± 65.32	93.65 ± 48.81	1.82 ± 13.33	1.0213 ± 0.4564	106.77 ± 71.56	72.97 ± 35.51
Subject: 2 Motion: 3						
1	76.28 ± 21.14	42.01 ± 8.29	5.14 ± 10.58	0.0120 ± 0.0087	86.64 ± 28.65	33.46 ± 10.03
2	14.38 ± 10.69	36.51 ± 7.27	0.42 ± 1.60	0.0113 ± 0.0091	45.98 ± 24.72	31.97 ± 5.64
3	105.48 ± 22.18	44.60 ± 7.33	0.66 ± 2.60	0.0118 ± 0.0107	81.78 ± 19.70	30.65 ± 5.74
4	99.81 ± 25.57	44.13 ± 7.48	0.09 ± 2.90	0.0185 ± 0.0231	107.88 ± 29.11	29.99 ± 6.23
5	102.86 ± 26.42	98.77 ± 32.75	0.00 ± 0.09	0.7986 ± 0.4288	210.89 ± 20.39	63.06 ± 22.66
Subject: 3 Motion: 1						
1	66.94 ± 31.03	48.55 ± 17.16	13.35 ± 19.37	0.0167 ± 0.0112	61.07 ± 28.02	45.66 ± 16.96
2	41.47 ± 33.92	40.58 ± 11.21	0.72 ± 3.45	0.0148 ± 0.0178	46.77 ± 29.78	38.60 ± 9.67
3	77.70 ± 41.51	38.58 ± 12.88	0.76 ± 3.69	0.0149 ± 0.0180	80.61 ± 40.55	38.93 ± 12.59
4	83.79 ± 32.46	40.55 ± 12.16	0.26 ± 1.06	0.0322 ± 0.0339	80.79 ± 28.81	41.82 ± 11.23
5	159.06 ± 67.70	155.60 ± 82.00	0.14 ± 0.63	1.2381 ± 0.4636	100.78 ± 36.49	202.73 ± 84.13
Subject: 3 Motion: 2						
1	65.66 ± 46.92	38.15 ± 26.48	8.86 ± 30.20	0.0233 ± 0.0258	91.99 ± 57.80	36.16 ± 28.17
2	22.54 ± 18.12	30.88 ± 4.75	0.00 ± 0.00	0.0211 ± 0.0200	28.50 ± 13.97	30.79 ± 5.88
3	61.90 ± 44.48	40.23 ± 27.24	9.16 ± 31.16	0.0246 ± 0.0293	79.68 ± 59.30	38.07 ± 27.67
4	103.65 ± 45.60	35.29 ± 20.86	0.09 ± 0.89	0.0785 ± 0.1633	115.96 ± 70.61	33.78 ± 26.72
5	180.82 ± 68.41	152.03 ± 57.43	0.16 ± 2.49	1.3830 ± 0.4884	204.50 ± 86.88	203.80 ± 78.26
Subject: 3 Motion: 3						
1	50.59 ± 10.22	35.64 ± 1.80	0.00 ± 0.00	0.0057 ± 0.0022	135.13 ± 4.90	23.79 ± 3.51
2	29.34 ± 1.80	31.42 ± 1.99	0.00 ± 0.00	0.0057 ± 0.0022	25.91 ± 0.73	27.90 ± 3.61
3	53.37 ± 10.70	34.36 ± 1.66	0.00 ± 0.00	0.0057 ± 0.0022	73.31 ± 4.18	25.08 ± 3.46
4	74.37 ± 11.39	36.59 ± 1.78	0.00 ± 0.00	0.0093 ± 0.0049	149.15 ± 5.06	23.69 ± 2.37
5	76.87 ± 9.32	92.33 ± 9.46	0.00 ± 0.00	0.3602 ± 0.0721	190.11 ± 10.92	43.61 ± 11.13

Overall, the nullPose method was able to estimate the pose of the torso reliably, with some scenarios closely matching the recorded motion capture data such as Subject 3 performing Motion 3. The low error in the torso poses were due to the torso position target being placed as the highest priority in all of the scenarios that were tested. It is hypothesized that

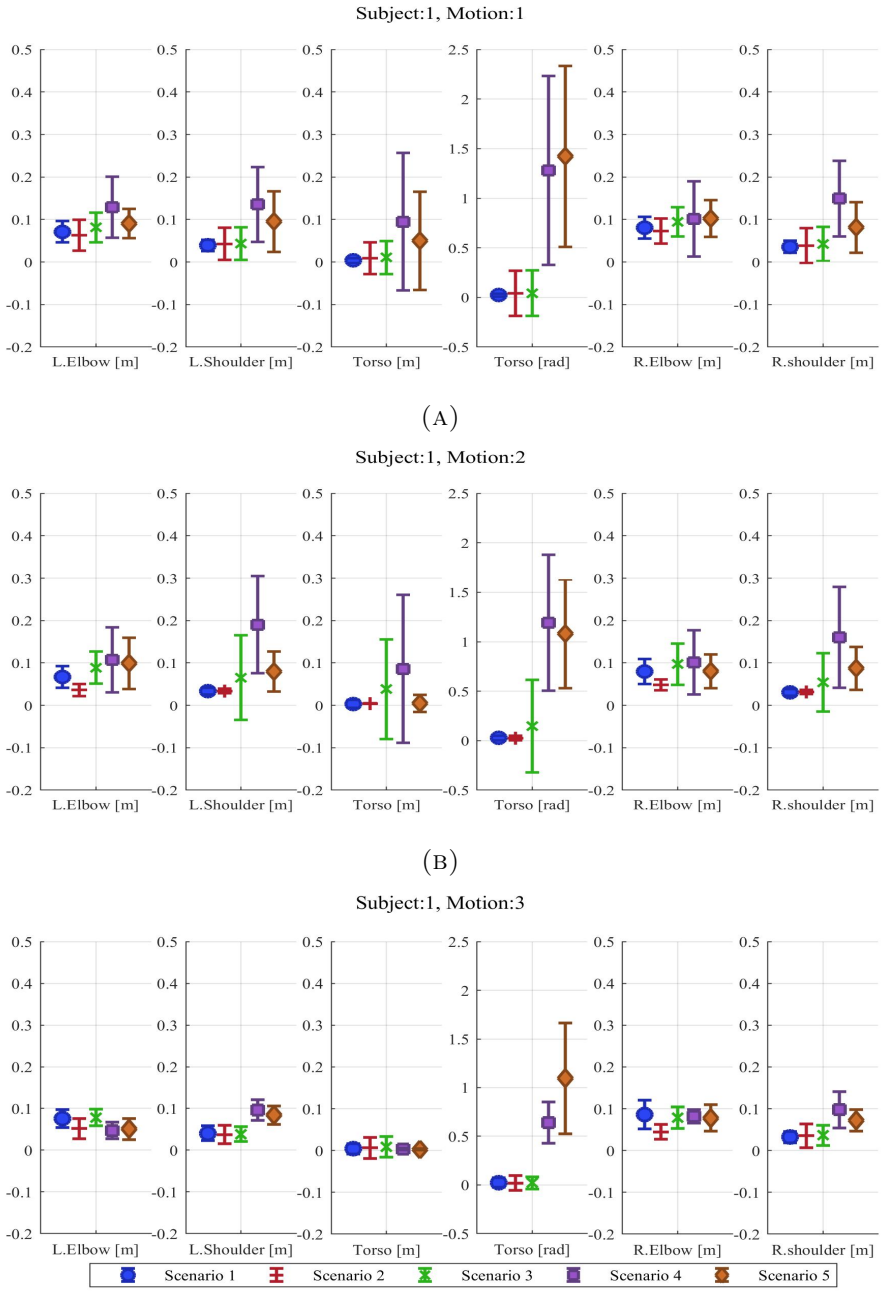

FIGURE 4.11: Graphed result of the mean error with standard deviations of the upper body segments for Subject 1 in (A) Motion 1, (B) Motion 2 and (C) Motion 3. Errors are shown in meters for position and radians for rotation.

in Motion 3 the accuracy in the torso estimate were on average higher because the motion being performed in Motion 3 were more restrictive in comparison the other two motions. In Motion 3 each subject was focused on performing the task of tracing the outline of a

box using a laser pointer. The focus on the task as well as the prescribed hand poses likely resulted in subjects having smaller upper limb motions which likely led to reduced changes in the torso pose. The small change in the pose is beneficial for the nullPose method due to the way that the pose is estimated. To be able to estimate an upper body pose in real time, multiple calculations are performed until either an optimal result is found or until the time limit between each pose estimation has been reached. Larger displacements in the upper body pose targets may require more estimation iterations before they are reached and may not be reached in time. This lead to sub-optimal estimates to be produced, which may increase the error in the estimated upper body pose.

A summary of the effect the different scenarios had on the output of the pose estimation is visualized in Figure 4.11. In this figure Elb represents the elbow, Shl represents the shoulder and Trs represents the torso with the prefix L or R corresponding to the left or right upper limb. Due to the elbow target from the recorded motion capture data being used by the nullPose method in Scenario 2, this scenario resulted in a more accurate estimation of the pose. The addition of the *hand to mouth* approximation in Scenario 3 resulted in a mixed result. For Subject 1 performing Motion 1 (Figure 4.11a) the addition of the *hand to mouth* target in Scenario 3 resulted in a lower elbow position errors when comparing against Scenario 1 where no elbow targets were used. Contrastingly for the same subject performing Motion 3 the error from Scenario 3 was higher in comparison to Scenario 1. From the results collected from the three subjects, the torso pose were overall lower in Scenario 2 and 3 in comparison to Scenario 1. This is likely due to the elbow constraint being placed may have reduced the likelihood of the joints in the upper limb kinematic model reaching the biomechanical limits. Additional figures for Subjects 2 and 3 are included in Appendix C.

The mean and standard deviation error in the torso orientation were larger in Scenarios 4 and 5. This was expected as the only targets used in relation to torso orientation were to keep the torso upright relative to the ground in Scenario 4. Scenario 5 made no use of targets which constrained the torso orientation. Although an approximation to the torso orientation was used in Scenario 4 the estimated torso pose in Scenario 4 were better in comparison to the torso pose estimated in Scenario 5. When no torso orientation were used in Scenario 5, the estimated upper body pose may result in the torso becoming parallel to

the ground as long as the torso position constraint is met. Additionally this resulted in a poorer estimate of the elbow and shoulder position.

As shown from the results obtained in Experiment 1, where the nullPose method was provided with highly accurate upper body pose information, the level of accuracy obtained by the nullPose method does not always match that of the OptiTrack motion capture system. The main advantages of the nullPose method over motion capture systems or skeleton tracking algorithms are the robustness of the method and the capability of it to be used in real practical applications.

4.5 Experiment 2 - Determining the Accuracy of the nullPose Method in a Practical pHRC

Similarly to Experiment 1, Experiment 2 was performed in a motion capture lab. This experiment was performed to determine the accuracy of the nullPose method in a practical pHRC application. In this experiment, the MoCap system was only used to provide the ground truth against which the estimated upper body pose was to be compared. In this experiment, no recorded MoCap data was used in the pose estimation using the nullPose method.

Five human subjects were asked to perform the simulated abrasive blasting operation alongside the ANBOT. The subjects were all male and ranged in height from 165 cm to 185 cm. The operation being performed by each subject was to move the end effector of the ANBOT to simulate abrasive blasting the three visible surfaces of a box placed 3 m in front of the robot. A laser pointer was attached to the end effector of the ANBOT to provide the human subjects with a relative measure of the nozzle orientation on the surface being cleaned. Each subject was also restricted in the position of their body to within a square with 40 cm width next to the robot standing with a relatively upright posture. No other restriction or instructions were given to the subjects, allowing the task to be completed in a manner that each subject naturally preferred.

To assist in the redundancy resolution, a Kinect v1 camera was used to provide some upper body targets to the nullPose method. To ensure that the whole body of the subject

was able to be seen, the Kinect camera was placed 2 m behind the subject. The whole body needed to be captured to allow for skeleton tracking of the human subject to occur using the OpenNI NITE library. At the start of every experiment, the human subject was asked to face the camera and perform a calibration pose required for the skeleton tracking procedure. Both the raw point cloud data from the Kinect as well as the output of the skeleton tracking data of the human subject obtained by the Kinect v1 was used to estimate the upper body pose of the human. All of the required data, such as the point cloud data and the state of the robot, were recorded in the motion capture lab and were played back in real-time for pose estimation with the nullPose method. The estimated upper body pose was published at a rate of 30 Hz using a desktop computer with an intel i7 7700K processor.

4.5.1 Pose Estimation Scenarios

To test the nullPose method, eight scenarios were used in Experiment 2 to represent different combinations of targets used to resolve the redundancy in the upper body. Each scenario assumes that only certain targets are available to be used by the nullPose method. Although only eight scenarios were used, in reality a wide variety of different combinations of targets could be implemented depending on the sensors available during the pHRC.

TABLE 4.5: The different combinations of targets used in Experiment 2.

	Targets - Kinect Camera				**Targets - Approximation**		
	Skeleton Tracking		Point Cloud		Model	Heuristics	
Scenario	T.Pos	T.Ori	T.Pos	T.Ori	E.H2m	T.Hgt	T.Lvl
1	1	1	-	-	2	-	-
2	1	1	-	-	-	-	-
3	1	-	-	-	3		2
4	-	-	1	1	2	-	-
5	-	-	1	1	-	-	-
6	-	-	1	-	3	-	2
7	-	-	-	-	-	1	1
8	-	-	-	-	2	1	1

Table 4.5 shows the different combinations of targets in the eight scenarios for Experiment 2. In this table, the different targets are divided into two groups. The first is the targets obtained using the Kinect camera. This group is further divided into the skeleton tracking based targets obtained using the OpenNI NITE library and the point cloud

data. The second group is the approximations used which was divided into model based approximations and heuristic based approximations.

The abbreviations T.Pos and T.Ori in Table 4.5 refer to the torso position and orientation targets obtained using the Kinect skeleton tracking or point cloud data. E.H2m refers to the approximated elbow position by maximizing the velocity of the hand towards the mouth using the model presented in [8]. T.Hgt represent an approximation of maintaining the torso height based on the measured standing height of the subjects. T.Lvl refers to an approximation of the torso orientation such that the subject's torso is kept upright relative to the ground.

The position of the elbow is difficult to obtain reliably in a practical pHRC scenario. Although skeleton tracking through the NITE library is capable of determining the position of the elbow, it is often not reliable when the human is not facing the Kinect. In Fig. 4.12 it can be seen that the upper limb pose from the skeleton tracking was set to be the default configuration when the upper limbs were obstructed from the view of the camera. Increasing the number of sensors in the environment is an option but this option may not be feasible in practical industry or field environments. Rather than increasing the number of sensors, the model presented in [8] was used to provide an estimate of the elbow positions (E.H2m in Scenarios 1,3,4,6 & 8).

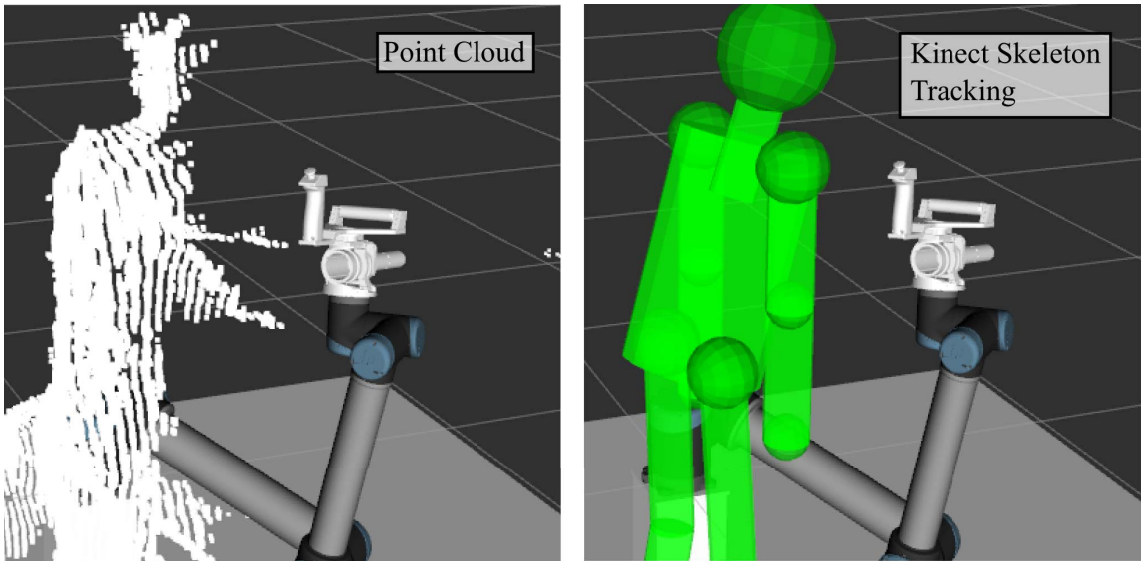

FIGURE 4.12: A snapshot of the recorded point cloud of the human subject (left) and the human pose obtained using skeleton tracking with the Kinect (right).

In Scenarios 1 to 3 the task of moving the torso to match the torso pose from the Kinect skeleton tracking was given the highest priority as it was the only sensor based target used in these scenarios. The torso pose was obtained through the NITE library with a Kinect camera. In Scenario 3 only the position obtained from the skeleton tracking was used. The torso orientation target in Scenario 3 was replaced with an approximation of keeping the torso upright.

In Scenarios 4 to 6, rather than using the torso pose from the Kinect skeleton tracking, a torso pose was estimated from the point cloud data of the human subject. The point cloud data was converted into a torso pose estimate by determining the centroid and the principle components of the human subject's point cloud. The axis of greatest variance was assumed to be the torso Z axis representing the direction from torso centroid to the top of the head. The second largest axis of variance was used as the torso X axis to represent the direction from the torso centroid to the right shoulder. The final axis is obtained by taking the cross product of the X and Z axes.

When no sensor measurements are available certain heuristics may be able to be used. In Scenarios 7 and 8 it is assumed that the torso pose was not able to be obtained using the Kinect skeleton tracking or the point cloud estimate. Therefore the heuristics of keeping the torso at a certain height based on the human co-worker's height and keeping the torso upright were used as targets for the nullPose method. Keeping the torso at a certain height poses a restriction to the torso position along the Z axis but pose no restrictions in the X or Y positions and no orientation restrictions. Keeping the torso level or standing upright pose restrictions on the X and Y orientation of the torso and no other restrictions. These approximation based targets were used in the redundancy resolution to ensure that estimated upper body pose is realistic when no sensor based targets are available i.e. the estimated upper body pose does not result in the torso at an unreasonable height or orientation such as the torso being parallel to the ground.

If the elbow or wrist was found to be colliding with the torso, a collision avoidance task (Algorithm 2) was implemented. When implemented, these tasks are placed at the highest priority, lowering the priority of the other tasks implemented in the scenario. Once the upper limb was not colliding with the torso, these tasks were disabled.

4.5.2 Results and Discussion

To determine the accuracy of the nullPose method, each estimated upper body pose using the nullPose method throughout the experiment is compared to the upper body pose captured by the motion capture system. In total 6400 estimated upper body poses from all five subjects were collected and compared to the motion capture recording in each scenario. Fig. 4.13 shows the distribution of the error between the upper body poses captured in the motion capture lab and the upper body poses estimated by the nullPose method in the eight scenarios. In Fig. 4.13 the horizontal axes of each plot represent the scenarios (Table 4.5) used by the nullPose method. The vertical axes represent the errors of the upper body poses.

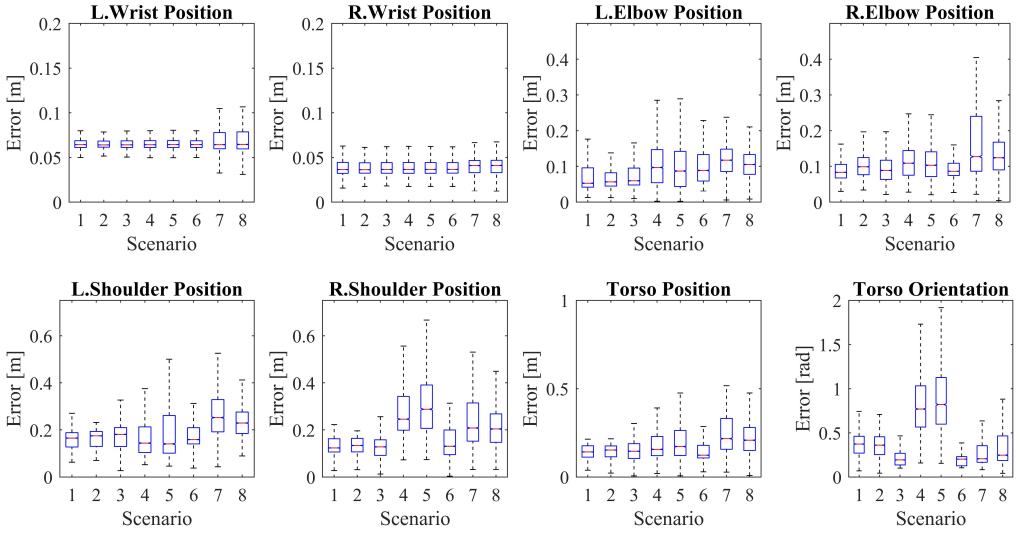

FIGURE 4.13: Box and whiskers plots of the error in the upper body pose from all subjects across the different scenarios in Experiment 2.

Table 4.6 shows the mean and standard deviation of the error in the upper body pose in the different scenarios. Scenario 1 resulted in the lowest mean torso position error at 145.7 ± 37.6 mm. Overall Scenarios 1-3 which utilized the torso position and orientation from the Kinect skeleton tracking obtained the lowest mean error with the smallest standard deviation in terms of torso position.

The mean and standard deviation of the torso orientation error was found to be the lowest in Scenario 6 at 0.2086 ± 0.1049 radians. The next lowest torso orientation error was

TABLE 4.6: Mean and standard deviation of the error of upper body poses for all subject in Experiment 2.

	Wrist Position		**Elbow Position**	
Scenario	Left [mm]	Right [mm]	Left [mm]	Right [mm]
1	68.8 ± 18.9	40.8 ± 19.9	68.7 ± 36.7	89.1 ± 29.4
2	68.9 ± 18.8	40.6 ± 19.8	64.2 ± 25.2	103.5 ± 34.1
3	68.8 ± 18.8	40.7 ± 19.7	71.8 ± 33.4	95.6 ± 40.3
4	68.8 ± 18.7	40.7 ± 19.7	106.1 ± 57.6	116.7 ± 58.0
5	68.9 ± 18.8	40.8 ± 19.7	108.4 ± 87.0	118.5 ± 71.1
6	69.0 ± 21.9	41.0 ± 22.8	100.0 ± 48.7	98.5 ± 40.9
7	71.6 ± 37.7	43.8 ± 37.4	120.4 ± 51.6	159.0 ± 92.6
8	71.7 ± 37.7	43.9 ± 37.4	106.1 ± 45.7	135.8 ± 71.8

	Shoulder Position		**Torso Pose**	
Scenario	Left [mm]	Right [mm]	Position [mm]	Orientation [Rad]
1	158.5 ± 34.3	130.7 ± 33.8	140.8 ± 37.6	0.365 ± 0.122
2	163.6 ± 36.1	132.8 ± 34.2	142.7 ± 39.6	0.351 ± 0.120
3	172.1 ± 50.2	128.2 ± 45.1	144.0 ± 51.0	0.250 ± 0.183
4	171.5 ± 88.8	271.3 ± 92.6	176.1 ± 66.3	0.796 ± 0.307
5	203.6 ± 153.0	311.0 ± 126.7	213.0 ± 122.4	0.881 ± 0.369
6	181.1 ± 61.4	145.4 ± 66.7	144.6 ± 55.0	0.200 ± 0.105
7	259.9 ± 94.5	233.2 ± 102.8	241.4 ± 105.7	0.363 ± 0.331
8	237.6 ± 74.8	220.2 ± 103.9	222.2 ± 107.9	0.336 ± 0.214

found in Scenario 3 at 0.2498 ± 0.1831 radians. The torso position target used were the Kinect skeleton tracking output and the point cloud approximation in Scenario 3 and 6 respectively. In both of these scenarios, upper body pose was resolved using an approximation based target which is to keep the torso in an upright orientation. This approximation resulted in a marginally better result than Scenarios 1 and 2 where torso orientation target was obtained using the Kinect skeleton tracking. When compared to Scenarios 4 and 5 where the torso orientation target is determined by the point cloud approximation, the error using the upright torso orientation approximation in Scenario 6 is on average 0.59 radians lower. It was observed that the torso orientation from the Kinect skeleton tracking and the point cloud estimation often results in a noisy and fluctuating orientation of the torso which may have resulted in the error when compared to the motion capture readings. Therefore it may be argued that an approximation could replace poor sensor readings, potentially resulting in a better estimate to the upper body pose.

The largest mean torso position was found in Scenario 7 in which no sensor based targets

were used. Scenarios 7 and 8 represent a case where no sensor measurements are available or the sensor measurements are poor, due to factors such as occlusion. The difference between Scenario 7 and Scenario 8 is the inclusion of the elbow position approximation (E.H2m in Table 4.5). The inclusion of the elbow approximation resulted in a lower upper body pose error, likely due to the inclusion of the elbow approximation reducing the solution space of the upper body pose which increased the accuracy of the overall upper body pose.

When comparing the shoulder position error, it can be seen that the larger mean error was observed in Scenarios 4, 5, 7 and 8. The high error in these scenarios is likely due to a combination of a poor torso position and torso orientation target used by the nullPose method. Scenario 6 utilized similar targets to Scenarios 4 and 5 but resulted in a better shoulder position estimate due to a difference in the torso orientation target being used. In Scenarios 7 and 8 the less restrictive torso position target resulted in a higher shoulder position error.

The lowest elbow position error obtained was 68.9 $\pm$ 25.1 mm for the left elbow in Scenario 2 and 93.8 $\pm$ 29.4 mm for the right elbow in Scenario 1. Scenario 1 utilized the elbow position approximation whereas Scenario 2 had no elbow position target. When comparing the elbow position error in Scenarios 1-3 to Scenarios 4-6, the elbow position error in Scenarios 4-6 was found to be on average 36 mm higher. This change in error is higher than comparing the effect of the elbow position approximation target on the resulting pose of the elbow. This suggests that by obtaining a more accurate torso pose estimate will result in a lower error even when no target is provided to the nullPose method regarding the position of the elbow. Overall the errors from the estimated wrist position across all scenarios were found to be low. The low error in the estimated wrist position is likely due to the wrist frame being situated close to the hand frame.

Even with targets that should define the full upper body being provided to the nullPose method, such as in Scenarios 1 and 4, the resulting upper body pose does not precisely match the recorded motion capture system. This is likely caused by several factors. Firstly the sensor measurements from the Kinect being used is less accurate when compared to a motion capture system. Another factor that affected the estimated upper body pose

of the nullPose method is the calibration that had to be performed to obtain a common reference frame between the Kinect camera, the robot and the motion capture system which likely introduced errors. The biomechanical upper limb models of the human used by the nullPose method may also be kinematically different to the actual human co-worker for which the upper body pose is to be estimated, which may also lead to errors in the pose estimation.

It can be argued that a tracking algorithm such as the Kinect skeleton tracking using the NITE library would perform similarly to the nullPose method if both methods were provided with similar levels of information. A benefit of the nullPose method is the potential of it being used in a real pHRC application with less dependence on the whole human body within view of sensors. Unlike the skeleton tracking with NITE which adopts a neutral pose of the upper limb when the upper limb is not able to be seen by the sensor, the nullPose method can provide a better estimate of the upper body pose.

From the results obtained in Experiment 2 it can be seen that the nullPose method is able to estimate the upper body pose of a human co-worker. Even when sensors are not able to be used or provide poor upper body pose data, the nullPose method is able to provide a realistic estimate of the full upper body pose. If a sensor is able to reliably track the torso pose of the human to be used as a target for the nullPose method, a more accurate pose of the rest of the upper body can be estimated, otherwise reasonable approximations could be used as substitute targets.

4.6 Experiment 3 - Implementation of the nullPose Method in a real pHRC application

In this experiment, a real abrasive blasting operation to clean a metallic plate was performed by a human co-worker with the ANBOT. Due to the nature of the abrasive blasting operation, this environment is often very dusty due to the suspended particulates in the air. This experiment was performed to verify that the nullPose method is able to be used in environments where sensing options are limited.

For a human-robot collaboration set in a real industrial environment, which is often unstructured, the number and types of sensors that can be used is limited. Experiment 3 was performed in such an environment, an enclosed abrasive blasting chamber. Due to the space limitation in the blasting chamber, skeleton tracking with the Kinect and the NITE library was not able to be implemented as the whole body of the human co-worker was not able to be seen. An Intel RealSense r200 camera was mounted on a 2 m tall post attached to the base of the ANBOT 1 m behind the human co-worker. The lower minimum range of the r200 camera allowed the point cloud data of the human co-worker's upper body to be reliably recorded. An AR marker was also attached to the back of the protective suit of the human co-worker as a means of obtaining an additional target for the torso pose.

4.6.1 Pose Estimation Scenarios

In Experiment 3, the AR marker attached to the human co-worker's protective suit was used to provide the torso pose target. Similarly to Scenarios 4-6 in Experiment 2, the point cloud of the human co-worker was used to provide an alternative target of the human co-worker's torso.

TABLE 4.7: The two scenarios used in Experiment 3.

	Targets - RealSense r200				**Targets - Approximation**
	AR Marker		Point Cloud		Model
Scenario	T.Pos	T.Ori	T.Pos	T.Ori	E.H2m
1	1	1	-	-	2
2	-	-	1	1	2

Two scenarios were implemented based on the torso targets from the two different sensing options (Table 4.7). These two scenarios utilize the torso pose target, using the AR marker or the point cloud estimate, in combination with the elbow position approximation in order to resolve the redundancy in the upper body pose. Similarly to Experiment 2, in the event that a section of the upper limb is found to collide with the torso, a task was included to shift the colliding part out of the torso (Algorithm 2).

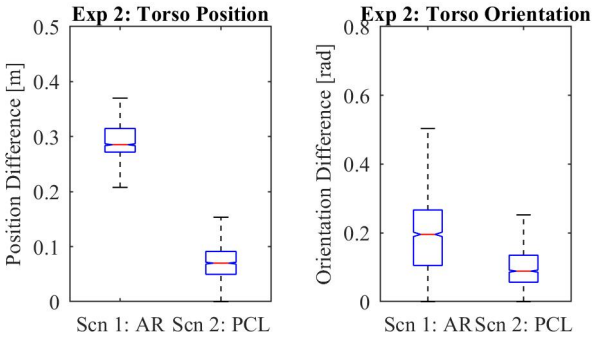

FIGURE 4.14: Box and whiskers plots of the torso position and orientation error compared against the two targets, the AR marker (AR) in Scenario 1 and the point cloud approximation (PCL) in Scenario 2.

4.6.2 Results and Discussion

The nullPose method was tested with two pose targets collected during the abrasive blasting operation in the abrasive blasting environment. Torso pose targets from the AR marker or from the point cloud, collected by a RealSense r200 camera, were used to estimate the upper body pose of the human co-worker. In this environment the full upper body pose of the human co-worker was not able to be measured and only the torso pose targets were able to be used for comparison against the estimated upper body pose.

In Scenario 1 the torso pose target from the AR marker was used as the highest priority task whereas in Scenario 2 the point cloud estimate of the torso pose from the r200 camera was used as the highest priority target (Table 4.7). Fig. 4.14 shows the distribution of the error in torso position and orientation in the two scenarios. The distributions of error in torso poses were calculated by comparing the estimated torso pose from the nullPose method against the target that is being used in the scenario, i.e. the torso pose from the AR marker in Scenario 1 and the point cloud estimate of the torso pose (PCL) in Scenario 2.

The estimated torso position using the point cloud estimate of the torso pose resulted in an average difference of 74.6 $\pm$ 33.5 mm. The difference in torso position obtained using the AR marker as the torso pose target was much larger (289.0 $\pm$ 35.3 mm). The larger error in the estimated torso pose may be caused by the AR marker being attached to the

protective suit of the human co-worker which may have resulted in a shift in the marker relative to the torso of the co-worker.

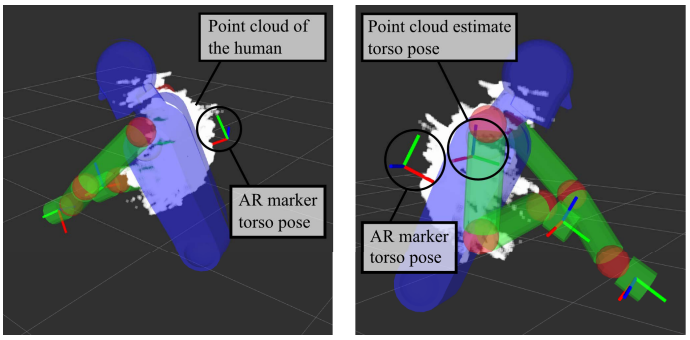

FIGURE 4.15: A snapshot of estimated upper body pose with the two sets of torso targets used in Experiment 3 viewed from different angles.

In this experiment, it was initially thought that the torso pose target from the AR marker would be able to provide a more accurate torso pose when compared to the point cloud estimate as the torso pose from the point cloud used a simple method of determining the centroid of the human point cloud. Due to the harsh environment and low visibility in the blasting chamber, the AR marker was not able to be detected reliably. Fig. 4.15 shows visualization of the detected AR marker position. As shown in Fig. 4.15 the AR marker was measured to be outside of the point cloud of the human co-worker with a considerable margin. A mean distance to the point cloud was calculated and an offset was added to the AR marker target to shift the AR marker position along the AR marker x-axis, towards the centre of the co-worker's torso. Even with the offset implemented, the error in the estimated torso position was still larger than the error in the estimated torso position using the point cloud estimate of the torso pose.

Another potential cause of the large torso position error in Scenario 1 is the torso position and orientation task being given the same priority. As seen in Figure 4.14 the difference in torso orientation was found to be on average 0.2137 ± 0.1506 radians. Since the position and orientation targets are given the same priority, the torso position and orientation errors have equal weightings. The pose of upper body being estimated is restricted due to factors considered by the nullPose method such as the biomechanically set joint limits and singularity. Certain poses may not be able to be reached without compromising these factors. In this case, obtaining a more accurate torso position estimate may result in an

increase in the torso orientation error. Achieving the low error in the torso orientation may have resulted in the torso position being unable to be reached due to restrictions placed by the biomechanical upper limb models. In the event that a certain aspect of the target, such as the torso position, is known to be critical to the application, a higher priority could be given to the torso position task and a lower priority given to the torso orientation task. This will force the nullPose method to minimize the error in torso position before minimizing the torso orientation error.

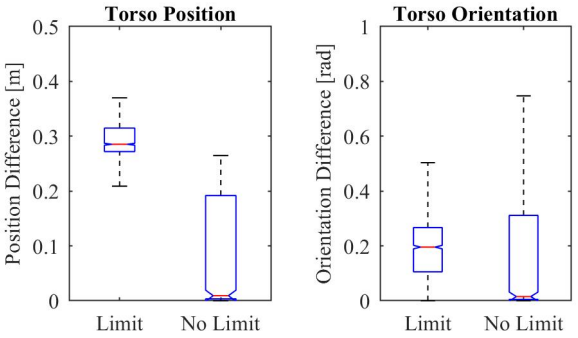

FIGURE 4.16: Box and whiskers plot of the torso position and orientation error using the biomechanical limit vs no limit.

Figure 4.16 shows the distribution of the torso pose error when the biomechanical limits of the upper limb were used against when the limits were removed in Scenario 1. Removing the biomechanical limits resulted in a lower mean error to the torso pose, from 289.0 ± 35.3 mm to 70.1 ± 87.9 mm and from 0.2137 ± 0.1506 radians to 0.1733 ± 0.1681 radians. Although the difference in the torso pose was lower, the resultant pose is likely to require the upper limb to adopt a pose that is not feasible for a human body to achieve.

The error from using the AR marker target highlights one of the benefits of the nullPose method, which is humanly feasible poses of the upper body are estimated. Other methods may result in the torso pose being equal to the torso pose obtained using the AR marker but in doing so likely extends the length of the upper limb or results in the estimated hand poses not being equal to the known hand poses. The biomechanical limits used in the nullPose method along with the hands of the upper limb being placed on the handles of the robot ensures that erroneous targets do not result in an unfeasible upper body pose. Another advantage of the nullPose method is the capability of obtaining the full upper body pose from limited sensor based targets as shown in Experiment 3.

4.7 Conclusion

This chapter presented the nullPose method, an upper body pose estimation method in applications where the hands of the human are known. The nullPose method was tested in both a motion capture environment and in a real abrasive blasting physical Human-Robot Collaboration (pHRC) operation. By comparing the estimated upper body pose to recorded motion capture data obtained through a commercial motion capture system, the error in torso position, torso orientation and both the left and right elbow position were able to be quantified. Different scenarios were implemented based on the combination of available targets used to resolve the redundancy in the upper body. The targets used ranged from measured sensor measurements to heuristic based approximations such as keeping the torso upright. The nullPose method was also tested in an abrasive blasting chamber during a human-robot collaborative abrasive blasting operation. The method was shown to be able to function robustly in an environment where vision is limited due to suspended particulates in the air. This work has demonstrated that the nullPose method is suitable for use in pHRC applications set in environments where it is difficult to directly measure the full pose of the upper body.

Three experiments were performed to verify the capability of the nullPose method as well as validate the potential of the nullPose to be used in pHRC. The first experiment showed that under ideal conditions the nullPose method was able to perform reasonably well when compared to a motion capture system. The second experiment shows the capability of the nullPose method for use in a pHRC application to track the human upper body pose without the need of a Motion Capture (MoCap) system. The third experiment highlight the potential of the nullPose method to be used in a practical application. The nullPose method was able to provide the pose of the full upper body where packages such as the NITE skeleton tracking library fails due to occlusion as it incorporates both the human upper limb biomechanical models as well as targets obtained from sensors and approximations.

Utilizing the nullPose method, the upper body pose of the human co-worker is able to be estimated, even where occlusions are prominent, allowing the collaboration between the human and the robot to be improved. By being able to estimate the pose of the human

co-worker during the collaboration between a human and a robot, the physical strength of the human is able to be estimated which allows for the assistance provided to the human to be altered. Adapting the assistance to suit the needs of the human could in turn provide a more natural interaction between the human and the robot.

Chapter 5

Appraisal of Human Physical Strength Using the nullPose Method

In Chapter 4 the pose of the human upper body was able to be estimated during a collaboration between a human and a robot using the nullPose method. With the hand of the human co-worker known, sensor measurements and approximations were integrated into the estimated upper body pose. This chapter presents of one of the ways that the nullPose method could be used in physical Human-Robot Collaboration (pHRC). In this chapter the physical strength of a human co-worker is appraised in real-time by using the estimated pose of the human upper body from the nullPose. If the physical strength of the human co-worker is able to be obtained, the assistance being provided to the human can be adapted without an explicit cue from the human co-worker, allowing for a more intuitive form of assistance to be provided.

This chapter is divided as follows. Section 5.1 presents a conventional method in which the physical strength of the human is able to be estimated and a method of estimating the physical strength of the human co-worker in real time using the nullPose. Section 5.2 presents a method of converting the estimated upper body pose from the nullPose method to the musculoskeletal model coordinates. Section 5.3 presents the optimization method

used to obtain the maximum strength of the human upper limb for a given pose and force direction. An experiment was then performed to compare the estimated strength of the human co-worker using the nullPose method to a conventional method (Section 5.4) and verify that the strength of the human co-worker is able to be performed in a practical application (Section 5.5). A summary is then presented in Section 5.6.

5.1 Appraisal of Human Physical Strength

In this thesis, the human capability being appraised is physical strength. Physical Strength of the human co-worker is defined as the maximum force that a human co-worker could withstand for a given pose and force direction. Factors that are important for appraisal of the human co-worker's capability includes the current pose of the human body [23] and the direction of the force to be opposed [173]. Whereas the direction of the force to be opposed may be simple to determine, often being dictated by the type of operation being performed, in a practical application, the pose of the human body is difficult to measure.

Using musculoskeletal models of the human body, physical capabilities are able to be estimated. Software packages such as OpenSim [143] can be used to perform various analyses to obtain information pertaining to the inner workings of the human body. For example, the activation of each muscles in the human upper limbs could be estimated to determine the effort being exerted by a human performing a certain motion.

In rehabilitative applications, the capability of a patient is appraised by a therapist as the patient performs rehabilitation exercises. Another common method of appraising the capability of a human employed systems such as Electromyography (EMG) to provide a measure of human effort [160, 177] or by modeling of the human body. These methods of appraising the capability are often conducted as a post-recording batch procedure. An Inverse Kinematic (IK) analysis is performed in order to transform recorded human pose into musculoskeletal model co-ordinates such that a variety of analyses could be performed such as inverse dynamics. Due to complexity of musculoskeletal models representing the human body, the IK is computationally expensive, limiting the viability of an IK analysis to be performed for real-time applications.

For practical applications, especially in pHRC, it would be beneficial to be able to appraise the capability of the human in real-time. In [149], to reduce the computation time of IK procedures, strategically placed Inertial Measurement Unit (IMU) markers are placed on the human upper limb in order to obtain a real-time coordinate of an upper limb musculoskeletal model so that additional studies can be performed within the OpenSim framework. Another approach estimated the fatigue of a human co-worker through measurements of muscle activities using a wireless EMG system in order to adapt the behavior of the robot [178]. These methods are difficult or not feasible to implement in practical applications due to the additional sensors to be worn by the human.

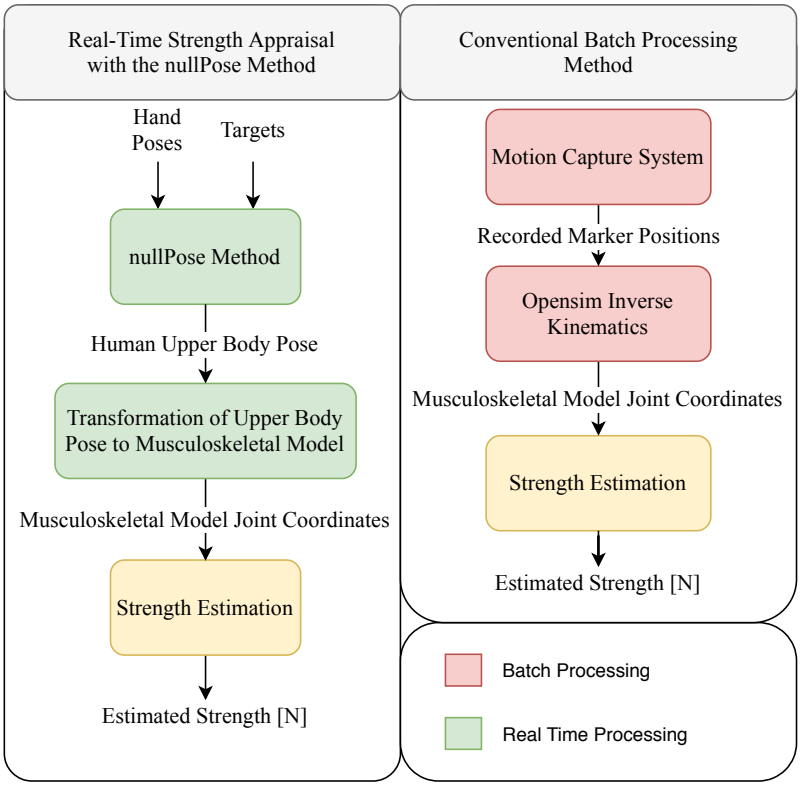

FIGURE 5.1: The real-time strength appraisal method using the nullPose method (left) and the conventional batch processed method (right).

Figure 5.1 shows a real-time strength appraisal method which utilizes the nullPose method, shown on the left side of the figure. On the right side of Figure 5.1 is a conventional batch processed method. The green blocks represent calculations that are able to be performed in real-time whereas the red blocks represent processes which are commonly performed as a batch process.

The estimation performed by the batch processing is widely used and accepted as the standard of musculoskeletal modelling. This method utilizes a musculoskeletal model along with a motion capture system to perform further complex analyses such as inverse dynamics. Due to difficulty in directly measuring human physical strength, methods such as this one became widely used.

The pose of the upper body estimated by the nullPose method is then transformed to the coordinates of the musculoskeletal model of the upper limb. The upper limb pose is converted into joint coordinates such that the musculoskeletal model is moved to reflect the estimated upper body pose. In this manner the computationally expensive IK analysis can be skipped allowing for analyses using the musculoskeletal model of the human body to be conducted in real time without the use of sensors such as IMU or EMG to be worn by the human co-worker. Although the physical strength can be estimated in real-time it may be less accurate when compared to the conventional batch processing method, due to the pose of the human being estimated, but allows for the human strength to be accounted for by the robot in real-time. Inaccuracy in estimating the physical strength of the human co-worker may result in an unsuitable amount of assistance to be provided to the human which would have to be taken into consideration when developing an AAN paradigm.

5.1.1 Musculoskeletal Model

The musculoskeletal model used to estimate the physical strength of the human co-worker is the Upper Extremity Kinematic Model [10] shown in Figure 5.2. This upper limb model consists of 15 Degrees of Freedom (DOF) with 50 Musculo-Tendon Units (MTU). MTU refers to a system of muscle and tendon that function to move the skeleton through contraction of the muscle. Each MTU in the musculoskeletal model is used to represent a particular muscle group. This musculoskeletal model has been previously used to estimate the maximum force able to be exerted at the hand of the model by estimating the activation of each muscles in the model [21].

Although 15 DOF were able to be used to determine the pose of the musculoskeletal model, only seven DOF (shown in Figure 5.2) were considered in the estimation of the human strength. The additional DOF, corresponding to DOF of the hand and fingers,

were kept constant at a neutral state as it was assumed that grip strength would not affect the amount of force able to be opposed at the hand.

Since the strength of the whole upper body needs to be considered, a left musculoskeletal model was created that mirrored the right upper limb model about the sagittal plane. For the left musculoskeletal model to have a similar convention to the right counterpart in terms of the range of motion (ROM), each DOF that rotates the limb inwards or outwards relative to the body (rotations around the Y-axes of the model) was rotated by 180^o.

The left and right musculoskeletal models were treated separately when determining the strength of the upper limbs. Each musculoskeletal model was grounded at the thorax frame (Figure 5.3) which was positioned to match the pose of the torso from the nullPose method. An assumption is made such that the force exerted by the upper limbs is able to be compensated by the human co-worker's lower body and would not destabilize human co-worker. This assumption is further discussed in Section 5.4.

5.2 Transforming the Upper Body Kinematic Model Pose to Musculoskeletal Model Joint Coordinates

In order to estimate the physical strength of the human upper body, a left and right musculoskeletal model of the upper limb was used to calculate the theoretical maximum strength of the human co-worker given a pose of the upper limb. The upper limb biomechanical model which was used by the nullPose method to estimate the pose of the human co-worker is kinematically different to the musculoskeletal model. The main difference is the way that the shoulder joint is defined, with the musculoskeletal model using generalized coordinates that are related to anatomical motions.

The estimated upper body pose of the nullPose method needed to be transformed to the musculoskeletal model coordinates. This transformation ensures that the pose of the musculoskeletal model corresponds to the estimated upper body pose from the nullPose method. To obtain the coordinate values of the musculoskeletal model, a rotational matrix that represents the transformation of the upper limb relative to the shoulder of the biomechanical model was used. Certain elements of the rotational matrix, which can be found

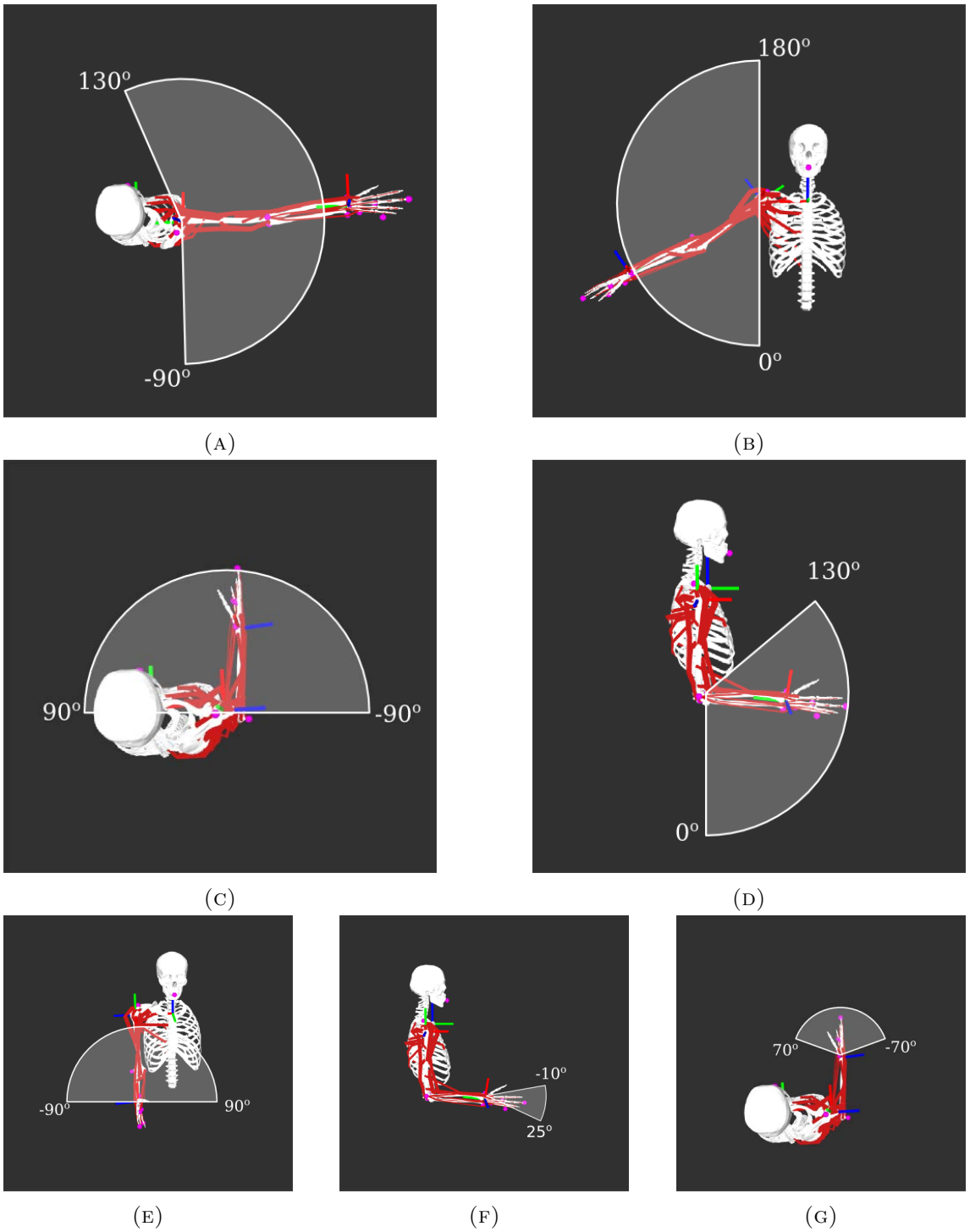

FIGURE 5.2: Musculoskeletal model of the right upper limb [10] showing the different coordinates and their range of motion. (A) Elevation angle. (B) Shoulder Elevation. (C) Shoulder Rotation. (D) Elbow Flexion. (E) Pronation/Supination. (F) Wrist Deviation. (G) Wrist Flexion/Extension

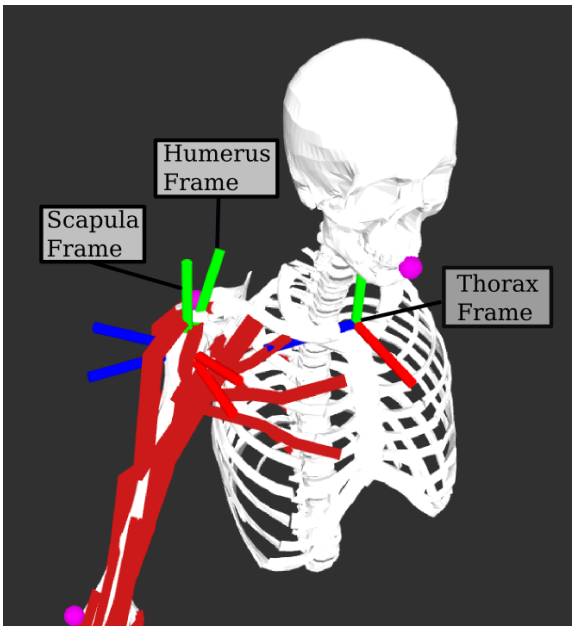

FIGURE 5.3: The musculoskeletal model of the right upper limb showing the thorax frame which grounds the musculoskeletal model as well as the scapula frame and the humerus frame.

in Appendix D, were then used to calculate the corresponding musculoskeletal model joint coordinates in a similar manner to [149].

The order of the rotation with reference to the scapula frame to the humerus frame for the musculoskeletal model of the right upper limb is shown in Equation 5.1. In this equation ${}^{scap}\boldsymbol{R}_{hum}$ refers to the rotation matrix between the humerus frame to the scapula frame (shown in Figure 5.3). The coordinates of the musculoskeletal model which rotates the humerus relative to the shoulder are represented as *shl_elv*, *elv_ang* and *shl_rot* as shown in Figure 5.4. *shl_elv* represents the shoulder elevation coordinate of the musculoskeletal model, *elv_ang* represents the elevation angle and *shl_rot* represents the shoulder rotation.

$$ {}^{scap}\boldsymbol{R}_{hum} = \boldsymbol{R}_y(elv\_ang) \times \boldsymbol{R}_x(shl\_elv) \times \boldsymbol{R}_y(-elv\_ang) \times \boldsymbol{R}_y(shl\_rot) \tag{5.1} $$

Equations 5.2-5.4 shows corresponding values of the musculoskeletal model shoulder joint coordinates relative to the rotation between the scapula frame to the humerus frame. These equations are derived from the rotation matrix obtained in Equation 5.1, detailed in Appendix D. $[l]$ and $[r]$ denotes the left and right musculoskeletal model as the rotations

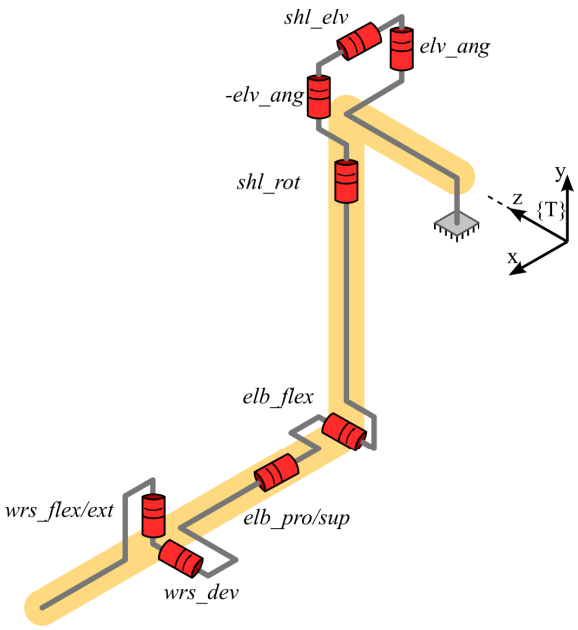

FIGURE 5.4: Order of rotation for the right upper limb musculoskeletal model.

between the two models are slightly different. In this notation $\boldsymbol{R}_{[i,j]}$ refers to the element of $\boldsymbol{R}$ in the ith row and the jth column.

$$shl\_elv = \arccos {}^{scap}\boldsymbol{R}_{hum[3,3]} \tag{5.2}$$

$$elv\_ang = \begin{cases} \arctan \frac{{}^{scap}\boldsymbol{R}_{hum[1,3]}}{{}^{scap}\boldsymbol{R}_{hum[2,3]}} ...[l] \\ \arctan \frac{{}^{scap}\boldsymbol{R}_{hum[2,3]}}{{}^{scap}\boldsymbol{R}_{hum[1,3]}} ...[r] \end{cases} \tag{5.3}$$

$$shl\_rot = \begin{cases} \arccos \frac{A\,{}^{scap}\boldsymbol{R}_{hum[3,1]} + B\,{}^{scap}\boldsymbol{R}_{hum[3,2]}}{A^2+B^2} ...[l] \\ \arccos \frac{A\,{}^{scap}\boldsymbol{R}_{hum[3,1]} + B\,{}^{scap}\boldsymbol{R}_{hum[3,2]}}{A^2+B^2} ...[r] \end{cases} \tag{5.4}$$

$$A = sin(elv\_ang)sin(shl\_elv)$$

$$B = cos(elv\_ang)sin(shl\_elv)$$

Table 5.1 shows the seven musculoskeletal coordinates alongside the conversion for the rest of the musculoskeletal model joint coordinates used.

Figure 5.5 shows the visualization of the conversion between the biomechanical model of the upper body used by the nullPose method (visualized as the red, green and blue mesh)

	Biomechanical Conversion	
Musculoskeletal Model Joint Coordinate	**Right Upper Limb**	**Left Upper Limb**
Elevation Angle	Equation 5.3	Equation 5.3
Shoulder Elevation	Equation 5.2	Equation 5.2
Shoulder Rotation	Equation 5.4	Equation 5.4
Elbow Flexion	$q_{6r} + \frac{\Pi}{2}$	$q_{6l} + \frac{\Pi}{2}$
Elbow Pronation/Supination	q_{7r}	q_{7l}
Wrist Deviation	$-q_{8r}$	$-q_{8l}$
Wrist Flexion/Extension	$-q_{9r}$	$-q_{9l}$

TABLE 5.1: Table of the upper limb musculoskeletal model joint coordinates along with the conversion from the biomechanical model of the upper limb used by the nullPose method for both the right and left upper limbs of the human.

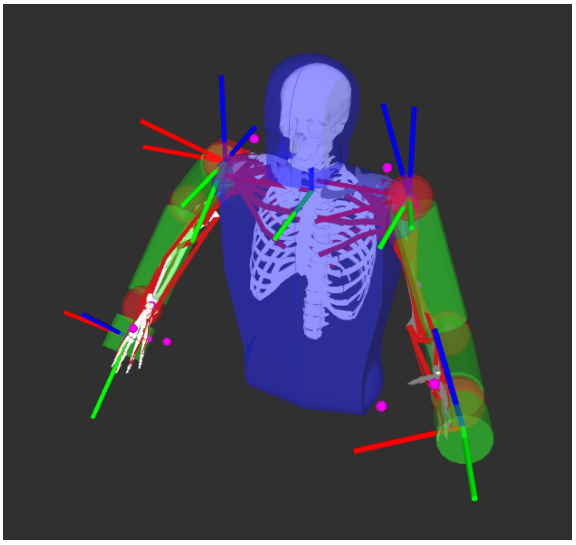

FIGURE 5.5: Visualization of the musculoskeletal model of the left and right upper limbs within the biomechanical model used by the nullPose method.

to the musculoskeletal model of the right and left upper limb. The two different models are positioned in such a way that the torso frame of the upper body model coincides directly to the thorax frame of the two upper limb musculoskeletal model.

5.3 Estimating the Physical Strength of the Human Co-Worker

With the pose of the upper body obtained, the physical strength of the human operator is able to be estimated. To estimate the physical strength of a human, the OpenSim API was used alongside the Upper Extremity Kinematic model [10]. Depending on the pose of the upper limb the amount of force that is able to be generated by a certain muscle in a given direction varies. The method of calculating the physical strength through an optimization procedure for a given upper body pose is detailed in [21, 103]. The strength estimation process is summarized in this section for completeness, additional details regarding the method can be found in [21, 103].

$$\boldsymbol{H}(\boldsymbol{q})\ddot{\boldsymbol{q}} + \boldsymbol{C}(\boldsymbol{q}, \dot{\boldsymbol{q}}) + \boldsymbol{\tau_g} = \boldsymbol{\tau} + \boldsymbol{J_v}^T \mathrm{f}_E \tag{5.5}$$

Equation 5.5 represents a dynamic equation which equates the mass matrix $\boldsymbol{H(q)}$, centrifugal and Coriolis effects $\boldsymbol{C(q, \dot{q})}$, and the joint torques due to gravity $\boldsymbol{\tau}_g$ to $\boldsymbol{\tau}$, a vector of generalized joint torques from muscle forces and the resultant torque of the external force f_e through the Jacobian $\boldsymbol{J_v}$. The Jacobian matrix $\boldsymbol{J_v}$ relates the joint-space generalized coordinate velocities to the Cartesian linear velocity of a rigid body point where the force generation capability of the musculoskeletal model is to be calculated.

$$\boldsymbol{\tau} = \underbrace{\left[-\boldsymbol{L^T K_A a}\right]}_{\boldsymbol{\tau}_A} + \underbrace{\left[-\boldsymbol{L^T} \mathrm{f}_{\boldsymbol{p}}\right]}_{\boldsymbol{\tau}_P} \tag{5.6}$$

The MTU force produces torque about the musculoskeletal joints which can be decomposed into active and passive components, $\boldsymbol{\tau}_P$ and $\boldsymbol{\tau}_A$ respectively. In Equation 5.6, $\boldsymbol{L}$ represents a muscle Jacobian that relates the velocities of the muscles to the velocities of the joint coordinates of the musculoskeletal model. The matrix $\boldsymbol{K_A}$ represents the active muscle force gain matrix which defines the amount of force that a muscle provides for a certain activation $\boldsymbol{a}$, $\mathrm{f}_{\boldsymbol{p}}$ denotes the passive force of the MTU.

The optimization procedure is conducted for a given model state, where the musculoskeletal model coordinates, velocities and acceleration are defined. The inertial, velocity and gravitational components of Equation 5.5 can be combined into a single torque vector which will be denoted as $\boldsymbol{\tau}_b$, which results in Equation 5.7.

$$\boldsymbol{\tau}_b = \boldsymbol{\tau}_A + \boldsymbol{\tau}_P + \boldsymbol{r}F_0 \tag{5.7}$$

In Equation 5.7 $\boldsymbol{r}$ refers to the moment arms of the external force about the generalized coordinates of the model and can be calculated as $\boldsymbol{r} = \boldsymbol{J}_{\boldsymbol{v}}^T \boldsymbol{u}$ where $\boldsymbol{u}$ represents the direction of the force in Cartesian space.

$$F_0 = \left[\frac{\boldsymbol{\tau_{bi}} - \boldsymbol{\tau_{Pi}}}{r_i}\right] + \left[\frac{[\boldsymbol{K}_A \boldsymbol{L}_i]^T}{r_i}\right] \boldsymbol{a} \tag{5.8}$$

To maximize the scalar value of F_0, it is isolated by selecting a row in Equation 5.7 and rearranging it to form Equation 5.8. To ensure integrity of the equation, the ith row corresponding to the largest absolute value of r_i is chosen.

$$\boldsymbol{A} = [\frac{\boldsymbol{r}}{r_i}\boldsymbol{L}_i^T - \boldsymbol{L}^T]\boldsymbol{K}_a \tag{5.9}$$

$$\boldsymbol{b} = \boldsymbol{\tau}_b - \boldsymbol{\tau}_P + \frac{\boldsymbol{r}}{r_i}(\tau_{Pi} - \tau_{bi}) \tag{5.10}$$

The objective function (Equation 5.8) does not take into account the intercoupling of joints that satisfy Equation 5.7. In order to satisfy this the equality constraint is formulated in the form of $\boldsymbol{Ax} = \boldsymbol{b}$ where $\boldsymbol{x} = \boldsymbol{a}$ and $\boldsymbol{A}$ and $\boldsymbol{b}$ are defined in Equation 5.9 and 5.10 respectively.

5.4 Experiment 1: Comparison of Estimated Physical Strength Using the nullPose Method to the Conventional Batch Processed Method

The aim of Experiment 1 was to determine whether a real-time appraisal of the human strength is able to perform similarly in comparison to the conventional batch processed method in the estimation of the human co-worker's physical strength. This experiment was set in a motion capture lab such that the pose of the human subjects' upper bodies are able to be recorded using a motion capture system. In this manner the physical strength of the human co-worker is able to be appraised with the conventional batch processed method.

Five human subjects were asked to perform a simulated abrasive blasting operation with the Assistance-as-Needed roBOT (ANBOT) in this experiment. Each subject wore a motion capture suit fitted with reflective markers such that the upper body poses of the human subjects were able to be recorded. No external force was applied to the human subjects during the experiment so that a more natural upper body pose of the human subjects are able to be recorded. Each subject's feet were restricted to a 40 cm square bounding box next to the ANBOT to promote movement of the upper limbs rather than movement of the whole body. Attached to the end effector of the ANBOT are reflective markers such that the motion of the end effector is able to be recorded. This allows the recorded motion from the motion capture system to be synchronized to the recorded data from the robot and the RGB-D camera.

As each subject performed the experiment the pose of the end effector and the point cloud from the Kinect camera was recorded. The recorded motion capture data of each subject was then batch processed through the IK analysis of the OpenSim desktop application.Virtual markers were added to the upper limb musculoskeletal model to match the placement of markers from the Motion Capture (MoCap) systems. This method of pose analysis represents the most commonly used method of utilizing a musculoskeletal model along with a MoCap system and forms the basis for more complex analyses such as inverse dynamics. Markers of the hand were given a higher weighting to reduce the error

in the orientation of the hand. From each IK analysis a set of joint coordinates for the right and left upper limb musculoskeletal coordinates was outputted which was then used to estimate the physical strength of each human subject (Equation 5.8).

In this experiment poses of the RGB-D images collected by a Kinect v1 camera were also recorded alongside the joint states of the robot and the poses of the two handles attached to the end effector. The Kinect v1 camera was placed 2 m behind the human subject. The collected data from the robot, Kinect v1 camera and the OptiTrack MoCap system allows for the physical strength of the human co-worker to be estimated using two different methods. The recorded RGB-D data and the robot were used to estimate the physical strength using the nullPose method whereas the MoCap data were used in the batch processed method.

The physical strength of each human subject is to be estimated for a force to be opposed at the left and right wrist of the musculoskeletal models. It is very difficult to measure the maximum physical strength that a human is able to exert. Generation of strength by a human muscle is a complex process and is often impractical to directly measure. A method of estimating the strength of the human is to measure the activation of the muscles using sensors such as surface electromyography (sEMG) but does not provide the maximum strength of the human. Therefore musculoskeletal models are used to simulate the human capabilities.

Parameters to the musculoskeletal model were kept consistent when comparing between the real-time strength estimation with the nullPose method to the conventional batch processed strength estimation. The blasting nozzle, as shown in Figure 5.6, dictates the direction of the force that the human co-worker would be required to oppose in a real abrasive blasting application. All of the recorded data were played back in real-time to be processed in real time using the nullPose method. All of the computation required for the real-time strength appraisal including the nullPose method was performed using a desktop computer with an Intel i7-7700K processor.

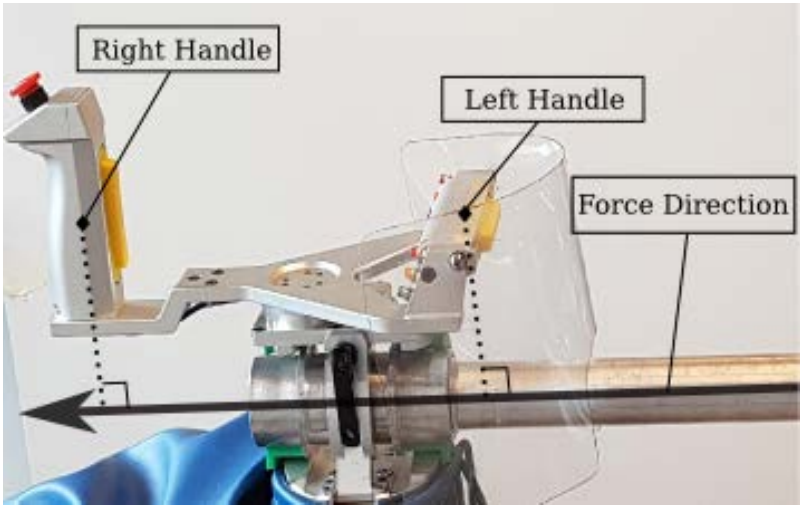

FIGURE 5.6: End effector of the ANBOT used in the experiments, showing the orientation and position of the handles and the direction of the force to be opposed by the human operator.

5.4.1 Pose Estimation Scenario

Experiment 1 was performed to determine the accuracy of the real-time appraisal to determine whether it would be able to be used in practical pHRC applications. Only a single combination of information was implemented to estimate the strength of the human operator. The information used to estimate the pose of the human subject is shown in Table 5.2.

TABLE 5.2: The combination of targets used by the nullPose method for Experiment 1 set in the motion capture environment.

	Targets - Kinect Camera Skeleton Tracking		**Targets - Approximation Model**
Scenario	**T.Pos**	**T.Ori**	**E.H2m**
1	1	1	2

The targets that were used in this experiment are the torso position (T.Pos) and orientation (T.Ori) which is obtained from the Kinect v1 camera alongside the skeleton tracking algorithm from the NITE library. To assist in the redundancy resolution an elbow position approximation (E.H2m) was used. E.H2m is an approximation based on aligning the elbow such that the velocity of the hand is highest towards the mouth of the human subject [8]. An additional target was implemented as the highest priority task, which was to shift any parts of the upper limb colliding with the torso out of the torso region when applicable. In

this experiment only a single combination was used as the main focus of the experiment was to determine the physical strength of the human subjects rather than the accuracy of the pose estimation using the nullPose method.

5.4.2 Results and Discussion

In Experiment 1 both methods were able to estimate the strength of the human subject throughout the experiment. In both methods the musculoskeletal models were kept the same. The musculoskeletal models of the left and right upper limbs were scaled to match the body lengths of the human through the inbuilt scaling function of OpenSim. The main difference between the performance of the two is the processing time of each method. With the nullPose method, the strength of the human was able to be calculated consistently at 30 Hz in real-time, albeit a lower frame rate than the data from the MoCap system. The advantage of the conventional batch processing method is that the true pose of the human subjects is able to be obtained though the motion capture system. In the batch processed method, the IK analysis was able to be performed at roughly 6 Hz but required the whole recorded motion to be used as an input. The OptiTrack system was able to record the pose of the human subjects at 120 Hz therefore the physical strength of the human subjects was able to be calculated at the same frame rate when using the batch processed method. The downfall of the batch processed method was that the physical strength of the human is not able to be estimated in real-time, hence it cannot be incorporated into the control paradigm of the robot.

A comparison was conducted on the estimated strength of the human operator using the poses of the upper body being obtained from the conventional batch processed method and the real-time strength appraisal when the nullPose method was used. Figure 5.7 shows the estimated strength of a human subject using the poses from the two different methods. As shown in Figure5.7 the real time strength appraisal method (nP) was able to obtain a similar physical strength estimate to the conventional batch processed method (BP).

Although certain strength estimates were found to be similar between the nullPose method and the conventional batch processing method, there are some differences among the five subjects that performed the experiment. Table 5.3 shows the estimated physical strengths

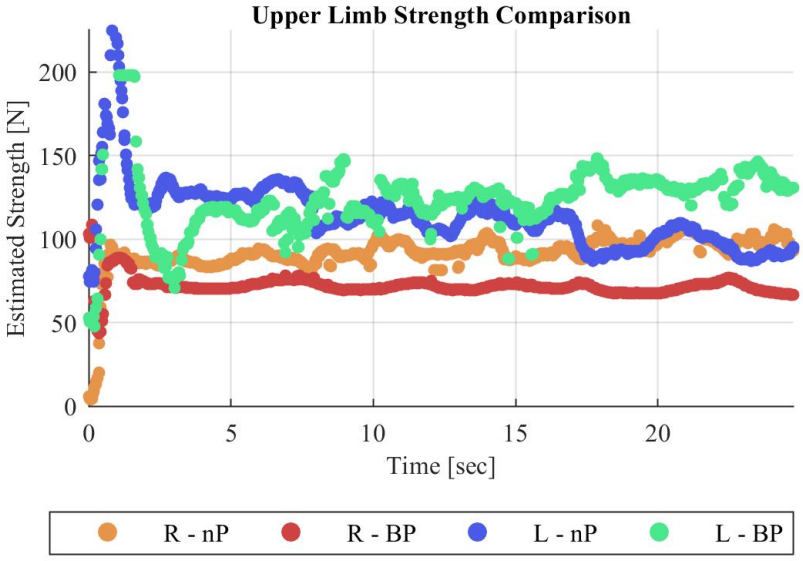

FIGURE 5.7: Estimated physical strength of the right (R) and left (L) upper limbs using the nullPose method (nP) and the batch processed method (BP).

TABLE 5.3: Estimated physical strength with the mean error and standard deviation using the nullPose method (nP) and the conventional batch processing method (BP)

	Left Upper Limb					Right Upper Limb				
	Mean Strength		Difference			Mean Strength		Difference		
Sub#	BP [N]	nP [N]	Mean [N]	St.Dev [N]	Mean [%]	BP [N]	nP [N]	Mean [N]	St.Dev [N]	Mean [%]
1	117.86	138.65	-21.29	27.75	-18.1	63.61	102.46	-36.68	25.84	-57.6
2	94.54	90.17	4.37	12.59	4.6	60.49	127.45	-67.05	42.54	-110.8
3	123.48	113.96	11.46	26.52	9.3	71.96	91.47	-19.50	13.11	-27.1
4	97.17	86.33	9.15	45.063	9.4	71.85	105.59	-33.73	39.15	-46.8
5	78.42	171.37	-98.18	34.91	-125.0	79.74	84.14	-4.40	7.22	-5.5

from the two methods as well as the mean error and standard deviation obtained for the five subjects performing the same experiment. The error is calculated to be the difference between the estimated strength from the two methods at the same time instance. Overall the estimated strength of Subject 3 was found to have the lowest overall error for both the left and right upper limbs. The lowest mean error was observed on the left upper limb of Subject 2 at 4.4 N whereas the highest was found in Subject 5 at -98.2 N. The difference in the estimated strength for Subject 5 can be seen in Fig. 5.8.

For the estimated strength of the left upper limb of Subject 5, it can be seen in Fig. 5.8 that the estimated physical strength of the left upper limb differs greatly with instances where the strength was not able to be estimated using the conventional batch processing method. One of the reasons that the strength was unable to be estimated in the batch processing

method was due to the motion capture system being unable to track the positions of the human subject's hands reliably. This was caused by several factors. The first was the reflectiveness of the metallic end effector resulting in poor tracking of the operator's hands as the markers being tracked rely on their reflective property. The second factor was the close proximity of the two hands, which meant that reflective markers used to obtain the poses of the hands are close to each other, causing issues determining the true pose of the hands.

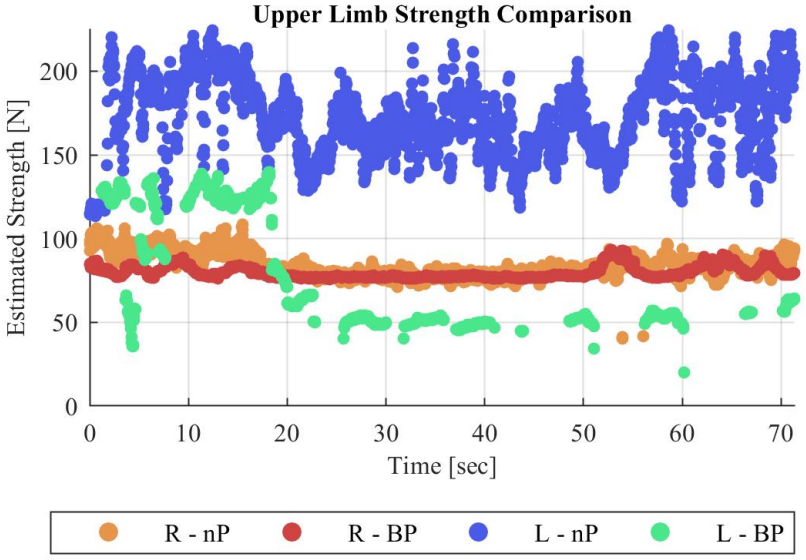

FIGURE 5.8: Estimated strength of the right (R) and left (L) upper limbs using the nullPose method (nP) and the batch processed method (BP) of a subject with a large difference in estimated strength of left upper limb.

It was also found that the real-time appraisal of the human strength using the nullPose often results in a more fluctuating strength estimate when compared to the conventional batch processing method. The batch processing method used more accurate upper body poses to perform the strength calculations. These poses were obtained by the motion capture system at 120 Hz. Using the nullPose method, the pose of the upper body was able to be processed such that the strength was able to be estimated in real-time at 30 Hz. Due to the restrictions of being real-time, the nullPose method may not be able to perform the necessary calculations fast enough to reach the targeted upper body pose. The accuracy of the upper body pose being estimated by the nullPose method was also unable to match the capability of the motion capture system, potentially leading to a

more fluctuating estimate of the upper body pose. This leads to a greater change in the coordinate values of the musculoskeletal model from one time frame to the next. One advantage of using the nullPose method is that the strength of the human operator can be consistently estimated. This is likely due to the limits set by the biomechanical model. This reduces the likelihood of an awkward upper body pose to be estimated especially with the pose of the hands being defined from the pose of the handles of the robot.

5.5 Experiment 2: Estimating the Strength of a Human Co-Worker in a Real pHRC Application

In this experiment, a real abrasive blasting operation to clean a metallic plate was performed by a worker with the ANBOT in an industrial abrasive blasting chamber. Due to the nature of the operation, abrasive blasting particulates are suspended in the air, lowering the effectiveness of vision based sensing. This experiment was conducted in order to highlight that the strength of the human co-worker is able to be estimated even in a difficult environment where sensing options can be quite limited.

Due to the space limitation in the abrasive blasting chamber, skeleton tracking with the Kinect v1 sensor was not able to be implemented as the whole body of the human operator was not able to be seen from a camera placed behind the human operator. An Intel RealSense r200 was used in the absence of the Kinect sensor, placed 1 m behind the human operator. The RealSense camera was used to provide point cloud data of the human operator's upper body as it had a lower minimum range when compared to the Kinect v1 camera. An AR marker was also attached to the back of the clothes of the human worker to obtain a different source of information of the upper body.

This experiment was performed by an experienced abrasive blasting worker. Only a single person performed the experiment as there was limited time available on site and the experiment was only able to be performed by an actual worker due to the dangerousness of the task. Figure 5.9 shows an example of the protective equipment to be worn by the human worker during an abrasive blasting operation. Due to the loose fitting protective clothes, the helmet and abrasive particulates in the air, equipment such as MoCap or

EMG are unable to be used during the operation. Therefore, in this application, both the physical strength and the pose of the human were not able to be directly measured. The reaction load experienced by the human worker during an unassisted operation amounts to forces of around 100 N [171] along the direction of the nozzle in the opposite direction to the expelled particulates. Similarly to Experiment 1, the human operator did not experience any reaction load from the task. No restrictions were placed on the human co-worker in terms of how to perform the task such that a natural motion can be observed.

FIGURE 5.9: A human co-worker wearing a standard protective equipment for an abrasive blasting operation with the ANBOT.

5.5.1 Pose Estimation Scenario

Similarly to Experiment 1, only a single combination of targets were used Experiment 2. The targets used to estimate the pose of the human used are shown in Table 5.4.

TABLE 5.4: Scenario list with targets used by the nullPose method for Experiment 2: Abrasive Blasting Chamber

	Targets - RealSense r200		**Targets - Approximation**
	Point Cloud		**Approximation**
Scenario	**T.Pos**	**T.Ori**	**E.H2m**
1	1	1	2

In this experiment, the targets used for the nullPose method were similar to the targets used in Experiment 1. The only difference in the targets between the two experiments

was the source of the targets (T.Pos & T.Ori) being obtained using a RealSense r200. In the event that a section of the upper limb is found to collide with the torso, an additional task was included to shift the colliding part out of the torso.

5.5.2 Results and Discussion

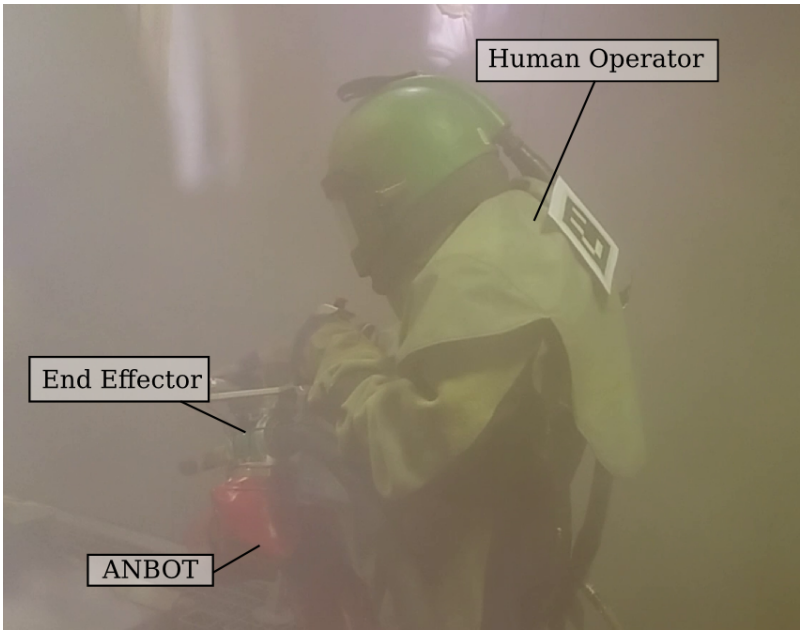

FIGURE 5.10: The abrasive blasting chamber where the experiment was performed for Experiment 2.

In Experiment 2, the strength of the human operator was estimated in a real application with the human performing an abrasive blasting task with the ANBOT. Figure 5.10 shows the environment in which the collaboration between the human co-worker and the ANBOT occurred. The strength of the human was estimated at 30 Hz throughout the experiment, shown in Figure 5.11. In this experiment the pose of the human was estimated since there was no ground truth for the pose of the human operator. This result shows that the human strength was able to be estimated in a practical environment without a motion capture system to provide the upper body pose of the human co-worker, as the nullPose method was able to perform robustly, even in the poor condition of the blasting chamber.

Although the musculoskeletal model being used in this experiment is the same model used in Experiment 1, the estimated strength of the experienced worker was several magnitudes

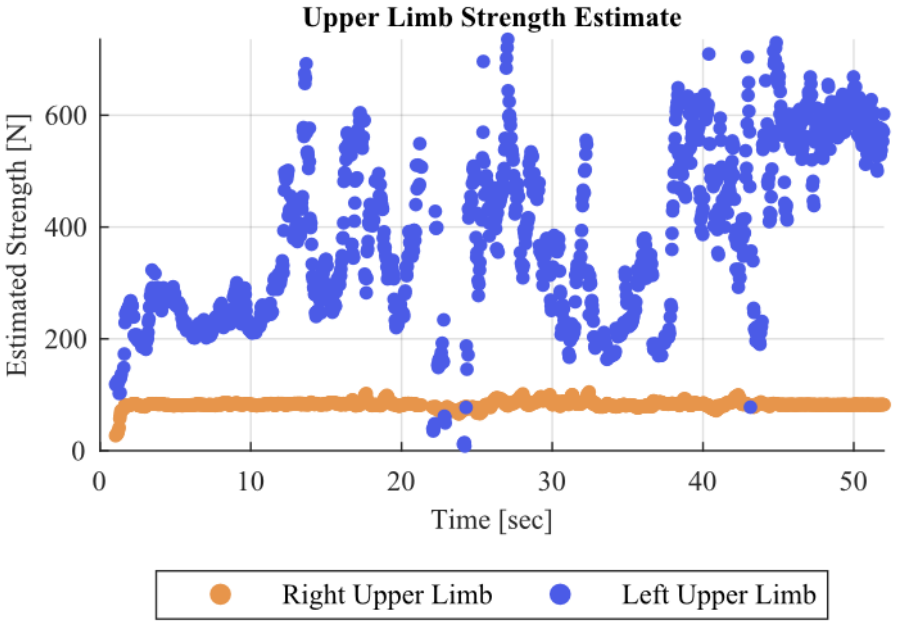

FIGURE 5.11: Estimated strength of the left and right upper limbs in the abrasive blasting operation (Experiment 2).

higher for the left upper limb compared to the results in Experiment 1. This is likely caused by the experienced abrasive blasting worker adopting a pose such that their upper limb is in a stronger pose. In this case the left upper limb of the human co-worker was found to be consistently close to singular. With the left handle placed in front of the right handle (Figure 5.6), the adopted pose of the left upper limb is likely to be close to singularity (Figure 5.9). Adopting a singular configuration allows the operator to perform the task with less effort but also causes the calculation of strength to become erroneous.

When the upper limb is straight and the direction of the force to be opposed is pointed towards the torso along the upper limb, the moment-arm distance between the force and the joints r (Equation 5.7) becomes small, leading to a large calculated physical strength. The strength estimation method does not take into account other physiological limitations to strength such as joint compression and stability. The estimated strength of the operator's right upper limb is lower than the left but the estimated strength is more consistent. Since the estimated strength of the left upper limb is higher than the right, it may represent a case where the left upper limb was used to provide support for the motion whereas the right upper limb was used to manipulate the end effector.

Due to the difficulty in measuring the actual maximum strength able to be exerted by the human co-worker, AAN paradigms may instead utilise the change in strength rather than the actual strength value itself. Certain regions in the workspace may result in the maximum strength able to be exerted by the human co-worker to be significantly larger than the forces required to do the task, therefore the amount of assistance to be provided to the human could be reduced. If the estimated physical strength is lower or if the physical strength could not be estimated then more assistance could be provided to the human co-worker. Strategies could also be used to limit the estimated strength in singular configurations, reducing the effect that singularity would have on the estimated physical strength of the human co-worker.

During the experiment conducted with the human, different groups of muscles were activated to achieve the strength output at the hand. Appendix E shows the distribution of the muscle activations of the musculoskeletal model Experiment 2 from the human co-worker. It was found that for the right hand the Deltoid muscles were observed to have a larger contribution to the strength when compared to the muscle usage of the left upper limb. This is likely due to the different pose being adopted by the left and right upper limb based on the orientation of the handles of the ANBOT.

5.6 Conclusion

This chapter presents one of the ways in which the nullPose method could be used in a pHRC application. By using the nullPose method a real-time appraisal of the human co-worker's capability was able to be performed. Using the nullPose method with an existing method of strength estimation, the physical strength of a human performing a pHRC operation was able to be estimated. In this manner the physical strength of the human co-worker could potentially be used to augment the assistance provided to the human co-worker.

Physical Strength of the human co-worker was estimated using two methods; the first utilized the nullPose method such that the physical strength can be appraised in real time. The second method was a conventional batch processed method. The conventional

batch processing method utilized poses of the upper limb obtained through an OpenSim IK procedure. The estimated strength obtained using both methods were compared where it was found that the strength outputs were comparable. An advantage of using the nullPose method was that the computationally expensive IK procedure could be avoided.

Using the nullPose method, the strength of the human was able to be robustly estimated in two different environments. The first environment represented an environment where the physical strength of the human is able to be estimated by the real-time strength appraisal method as well as the conventional batch processed method. The second environment is a harsh environment where the strength was not able to be estimated using the conventional batch processed method as it is difficult to implement a MoCap system in the environment.

The two experiments performed demonstrated that the nullPose method was able to be used as a substitute for computationally expensive IK procedures. The nullPose method was used to estimate the upper body pose of a human co-worker in real pHRC applications which was then used to obtain the musculoskeletal model joint coordinates. By allowing a robotic platform to appraise the physical strength of a human co-worker in real-time, the strength of the co-worker can be integrated into the control paradigm of the robot such that the need of the human co-worker is able to be accounted for by the robot.

Chapter 6

Conclusion

This thesis investigated the challenges surrounding the estimation of the human co-worker's pose during physical Human-Robot Collaboration (pHRC) to facilitate the real-time appraisal of the human co-worker's physical strength. It is envisaged that by a robot being able to appraise the physical strength of the human co-worker, a more intuitive form of assistance is able to be provided to the human. Firstly the effect of the interaction between the human and the robot on the adopted upper limb pose was investigated. The interaction between the human and the robot was then used to develop the nullPose method to estimate the pose of the human co-worker during pHRC. The nullPose method was then utilized to appraise the physical strength of a human co-worker in real-time during a pHRC operation set in a challenging industrial environment.

In practical pHRC applications, the pose of the human co-worker is not easy to ascertain. In the experiments performed with a collaborative robot platform, for a similar trajectory of the hand, the human subjects were found to adopt a different pose of the upper limb. During the interaction between the human and the robot, factors such as prescribed poses of the handles and the forces exerted by the human affected the naturally adopted pose of the human. The findings from the experiments conducted suggests that a generalized model will likely result in a less accurate estimated pose, which motivated the development of a pose estimation method that is suitable for pHRC.

Although interaction between the human and the robot altered the natural pose of the human upper body, there are information within the interaction that could be exploited to solve the upper body pose of the human co-worker. Due to the specified interaction points between the human and the robot in pHRC, the poses of the hands are able to be inferred at all times during the collaboration. The nullPose method was developed for applications where the hands of the human are known such as pHRC to estimate the pose of the human upper body in real-time. The nullPose method utilizes a biomechanical model of the human upper limbs to ensure the estimated upper body poses are humanly feasible. Targets from sensor measurements or approximations were incorporated into the upper body pose solution to provide a better estimate of the human co-worker's upper body pose.

The nullPose method was implemented to facilitate a real-time appraisal of the physical strength of a human co-worker. The upper body pose obtained through the nullPose method was used to obtain the musculoskeletal model co-ordinates such that a musculoskeletal model of the left and right upper limbs reflected the current pose of the human co-worker. The two musculoskeletal models were then used to calculate the maximum strength of the human co-worker in real-time. The strength of the human co-worker estimated in real-time was compared to the strength calculated in a conventional batch processing method. Through the use of the nullPose method, the physical strength of the human co-worker is able to be estimated by the robot which would allow for the assistance to be provided to the human to be adapted. By appraising the physical strength of the human co-worker, the interaction between the human and the robot could be improved. Future development could see the appraised human co-worker's strength to be used to alter the behavior of the robot.

6.1 Summary of Contributions

6.1.1 Effect of the Physical Interaction Between the Human and the Robot on the Pose of the Human Co-Worker

To observe the effect of physical interaction between the human and the robot on the pose of the human upper limb, experiments were performed such that the pose of the human upper limbs were able to be recorded with a Motion Capture (MoCap) system. The adopted poses of the upper limb were compared at specific points as the right hand of each subject moved along the specified path. Individually, the adopted pose of the upper limb of each subject, which was parameterized through the swivel angle, was observed to be consistent. This trend was observed across the six experiments when comparing the adopted upper limb poses within each experiment.

When comparing the adopted pose of different subjects, the variations in the upper limb were larger. From the ten subjects being recorded, each subject appeared to adopt a different pose to perform the same motion. The natural variation in each individual seemed to have a large effect in the adopted pose of the upper limb. This suggests that when estimating the pose of the human it is advantageous to individualize a model rather than developing a generic model that is designed to fit the population.

Due to the interaction between the human and the robot happening through specified interaction points such as handles attached onto the end effector of the robot, the adopted pose of the upper limb was found to change. In a bimanual operation where both hands of the human co-worker are used to maneuver the end effector of the robot, each individual was observed to alter their adopted pose in a different manner. By requiring both hands on the end effector of the robot, restrictions were likely placed on the poses that the right upper limb could adopt.

Another experiment was performed to compare the effect of applying a forward pushing force on the adopted pose of the upper limb to the natural motion where no forces were applied by the human. Even though each subject was found to adopt a different upper limb pose to perform the same trajectory, when asked to push forward, the calculated swivel

angle was overall lower. A lower swivel angle corresponds to the elbow being brought closer to the body. A calculation was performed to find the maximum opposable strength to determine whether the elbow being brought closer to the body provided an advantage in applying the pushing force. It was found that the two sets of poses resulted in a similar maximum strength which suggests that bringing the elbow closer to the body may have made exerting the force easier but did not affect the maximum strength.

Another set of experiments had each subject apply forces in the direction of motion. Whereas applying forces in the forward direction was found to be straightforward, applying forces horizontally and vertically in the torso plane was found to be quite difficult for some subjects. In these experiments, certain subjects were found to alter their upper limb pose significantly in order to apply the required force.

The experiments conducted with ten subjects suggests that each individual will adopt the pose that is most comfortable to them. In a pHRC application where the current pose of the human co-worker is essential to the performance of the operation and safety of the human co-worker, sensors should be used to obtain a good measure or estimate of the current human pose as it is likely that models that predict the human pose are based on free unconstrained motion where no force is applied by the human.

6.1.2 nullPose: an Upper Body Pose Estimation Method for pHRC

The pose of the human upper body in a real pHRC application can be difficult to obtain especially in a challenging environment where available sensors are limited. Determining the pose of the human would allow for a wide variety of additional things to be incorporated into the control of the robot system. The close proximity between the human and the robot during the collaboration increases the difficulty in determining the pose of the human co-worker.

To estimate the current upper body pose of the human co-worker in pHRC, the nullPose method was developed. The nullPose method exploits the kinematic constraint that occurs between the human and the robot during the interaction as the basis for the upper body pose estimate. The poses of the human co-worker's hands are able to be inferred through

the interaction points between the human and the robot. Solutions of the upper body that are estimated then must satisfy the condition that the hands are equal to the pose obtained through the interaction points. A biomechanical model of the upper limb was also implemented to ensure that all of the upper body estimates reflect humanly feasible upper body poses.

Sensor measurements and approximations were used as targets which were converted to tasks for the upper body kinematic model to achieve. These tasks are integrated into the upper body pose through iterative calculation to resolve the redundancy in the upper body. Using the null space, each task was prioritized such that a lower priority task that conflicts with a higher priority task does not negatively affect the previously calculated upper body estimate.

Experiments were performed to verify the accuracy of the nullPose method as well as validate the potential use of the nullPose method in a practical pHRC application set in difficult environments. The experiments were performed in both a lab environment where the accuracy of the estimated upper body pose could be measured against a commercial motion capture system as well as a dusty environment where abrasive blasting is performed.

The nullPose method provides a robust method of estimating the human co-worker's upper body pose during pHRC, which is one of the prerequisites for robots being able to appraise the capability of human co-workers and adapt the assistance based on the needs of the human co-worker. Using this method the physical strength of the human could be estimated allowing for assistance provided to the human to be adapted. An awkward or dangerous pose could also be detected which will allow for the safety of the human to be ensured whether by halting the collaboration or through collision avoidance.

6.1.3 Real-Time Appraisal of Human Strength Using the nullPose Method

Conventionally, estimating the capability of a human such as physical strength requires the motion being performed by the human to be recorded using a motion capture system. The recording is then processed through software packages such as the OpenSim software such that various calculations could be performed to obtain information such as the exerted

force during the motion. In a real pHRC application the use of motion capture systems is not always feasible and post processing of recorded motion is likely to not contribute towards the collaboration between the human and the robot.

The conventional method of estimating the strength of a human required the use of recorded motions which was processed using a computationally expensive Inverse Kinematic (IK) analysis such that musculoskeletal model coordinates are able to be obtained. Using the upper body pose estimated by the nullPose method, the IK analysis could be avoided, allowing for the physical strength of the human to be appraised in real-time.

Experiments were conducted to determine the accuracy of the estimated strength using the nullPose method in comparison to the conventional batch processed method. Experiments performed to determine the accuracy of the estimated strength were performed in a motion capture lab which allowed the upper body pose of the human co-worker to be recorded. The recorded pose was then processed using the OpenSim software to obtain the musculoskeletal model coordinates such that the physical strength of the human co-worker is able to be obtained. The comparison of the strength output using the nullPose method and the conventional batch processed method found that the strength profiles were comparable. The real-time appraisal of the human strength using the nullPose method was also tested in a practical environment, an abrasive blasting chamber where a motion capture system was not able to be used.

6.2 Discussion and Limitations

There are several assumptions and limitations that were implemented during the development of the nullPose method and in the case study where the human strength was estimated. Various models were used to estimate the pose of the human body such that the physical strength of the human was able to be appraised in real-time in both ideal and practical environments. This section discusses the limitations surrounding the nullPose method and the real-time appraisal of human strength.

6.2.1 Inferring the Hand Poses in the nullPose Method

The assumption of inferring the hand poses through the pose of the interaction points in the nullPose method is a limitation to the nullPose method. This assumption holds true in cases where the interaction points are designed ergonomically with contours matching the hand such that the hand of the human co-worker always adopts the same pose. If the interaction point between the human and the robot is in the form of a cylindrical handle, the hand of the human co-worker may be able to rotate around the handle. Obtaining the correct pose of the hand is important as all of the upper body pose estimated by the nullPose method utilizes the hand poses as the basis. Incorrect hand poses may lead to certain joints of the upper limb reaching the biomechanical limits resulting in some upper body poses to be unreachable. One method of resolving the assumption of the hand poses being equal to the handle pose is discussed in the future work Section 6.3.1.

Another limitation in the nullPose method with regards to the hand poses is that the left and right hand of the human co-worker is assumed to be able to be differentiated or that interaction points are left or right hand specific. The manner in which certain end effectors are designed may result in the left and right hand of the human co-worker being able to adopt different left and right hand poses based on what is deemed most comfortable to the human co-worker. In the experiments conducted in this thesis the left and right hand of the operator is always defined such as shown in Figure 6.1.

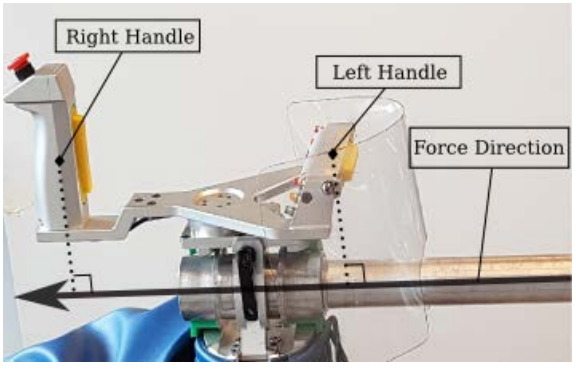

FIGURE 6.1: Defined right and left hand poses on the end effector of the ANBOT.

6.2.2 The Combination of Targets Used by the nullPose Method

To resolve the redundancy in the upper body pose estimate, the nullPose method utilized various tasks based on the available targets. Based on the biomechanical model of the human body, it is unlikely that all tasks are able to be completely achieved. A priority was placed on each task to be used in the redundancy resolution such that calculations of the upper body solution will attempt to accomplish a task with a higher priority before a lower priority task is to be considered. Estimates of the upper body calculated with a lower priority task is performed in the null space of the solution found using the higher priority task. In the different combinations of targets tested in the various experiments the torso pose target is always considered to be the highest priority task. The reason for the torso pose target being placed as the highest priority target is due to the torso pose target being a target that is likely to have the greatest change with respect to the pose of the hand. The torso pose target also places the greatest constraint to the solution space of the upper body pose (6 DOF when the torso position and orientation is used as a target). Placing different priorities to the targets may allow the nullPose method to perform more efficiently or accurately and further testing is required.

During all of the experiments it is assumed that all sensor measurements is available at all times. In a real pHRC application it may not be possible to always rely on specific sets of sensor measurements to be available at all times. The advantage of the nullPose method is that this method does not require specific a target to be available in order to produce an upper body estimate. Currently the tasks to be used and the priority of the tasks are defined at the start of the algorithm. Ideally, the number or priority of tasks to be accommodated by the nullPose method should be adapted based on the integrity of the available sensor measurement. A method of dynamically adapting the task used by the nullPose method is discussed in Section 6.3.2. Additional sensors could be implemented on the handles such that the handedness of the human could be determined such as in [179].

6.2.3 Upper Limb Models Approximating the Human Body

In Chapter 3 it is discussed that when estimating the pose of the human body it is advantageous to individualize models of the human body rather than attempting to generalize the model to fit the general population. In Chapters 4 and 5, a musculoskeletal model of the upper limb and a biomechanical model of the upper limbs used were generic models that were developed to fit a subset of the population.

The kinematic model of the upper limb used by the nullPose method was based on the work done in [174]. This model provided a realistic motion of the shoulder girdle and dynamic limits to each joint based on experimental data. Although each individual's joints may not exactly match up with the limits provided by this model, the estimate provided using the nullPose method utilized both the kinematic model of the upper limb as well as sensor measurements which will take into account some aspects of the individualized nature of the human co-worker. If it is deemed necessary to alter the limits of the biomechanical model joints; these limits can be relaxed or set as a soft limit. An additional task can then be implemented to bring the values of each joint to within the limits.

Similarly a musculoskeletal model of the upper limbs [10] was used to provide a method of estimating the capability of the human co-worker. The musculoskeletal model and the 50 Musculo-Tendon Units (MTU) defined within are able to be used to estimate physical strength. Factors such as the maximum isometric force of each MTU could potentially be adapted such that the estimated strength of the human co-worker provides a better estimate to fit a specific human co-worker.

6.2.4 Human Capability in pHRC

In the case study presented in this thesis, the capability of the human co-worker being addressed is the physical strength. In reality a multitude of factors could determine the outcome of a collaboration between the human and the robot. Physical Strength was chosen as it reflects a value of the human capability that has been previously quantified.

Other factors such as the experience of the human co-worker in the operation being performed, comfort level working with a robot, confidence or physical and mental fatigue are likely to have an effect on the performance of the human and robot collaboration team.

Several limitations also exist in the estimated physical strength of the human co-worker. The physical strength is defined in this thesis as the maximum force that is able to be generated or opposed at the limbs of the human co-worker. It is unlikely that the human co-worker is able to exert the maximum strength at all times; neither is it likely that an operation would require the human to do so. Instead the relative strength at varying poses should be used as a measure of the human capability at a given time and whether more assistance should be given to the human. Another assumption used in the method used to estimate the physical strength of the human is that muscular strength is the only limiting factor. Other factors such as joint stability or muscular fatigue were not taken into account.

The estimated physical strength also assumes that the torso is grounded and that the strength generated by the upper limbs is able to be supported by the lower limbs. This simplification was done such that the physical strength appraisal of the human co-worker could be performed in real-time. For a more accurate estimation of the human physical strength, existing musculoskeletal models of the full human body could be implemented. In this way, the lower body of the human could be taken into account when estimating the strength of the human co-worker. To do so, improvements to the nullPose would be required to provide poses of the lower limbs as well as the upper body, which is discussed in Section 6.3.4.

6.2.5 Benefit of Assistance-as-Needed Paradigm in pHRC

All of the work conducted in this thesis was performed with the motivation of adapting the assistance provided to the human such that a better interaction can be achieved. Whereas an Assistance-as-Needed (AAN) paradigm is able to benefit a patient performing a rehabilitation exercise and slowly regain their capability, the question of whether an AAN paradigm should be implemented in a real pHRC application has not been addressed. The assistance to be provided to the human may hinder the learning capability of humans in

performing a new operation. One theory states that the difficulty of the operation should be matched to the skill level of the human performing the operation [78]. In a pHRC application, if the assistance being provided is below the need of the novice user, it would likely cause the outcome of the operation to be poor. If too much assistance is being provided to the novice user, it might reduce the rate in which the novice user is able to learn the necessary skills for the operation [79, 82]. Additional investigations are required to explore the benefit of an AAN in practical industrial applications.

6.3 Future Work

6.3.1 Accommodating the Rotation of the Human Co-Worker's Hands Around a Cylindrical Handle

The nullPose method presented in Chapter 4 utilized a biomechanical model of the human upper limbs which was used to provide humanly feasible poses. An assumption was made which is to equate the pose of the human co-worker's hands to the pose of the handles attached to the end effector of the robot. With the current setup, the nullPose method is able to estimate the upper body pose of the human in real-time but the assumption made can be quite limiting. If the interaction point of the human and the robot allowed for the orientation of the hand relative to the handle to be different such as a cylindrical handle (Figure 6.2) the assumption is likely to cause the estimated pose of the upper body to be inaccurate. Joint limits set by the biomechanical limit are likely to restrict the ability of the upper limb to reach certain targets. One method to counteract this is by relaxing the joint limits of the wrist. Another way to solve this issue is through an additional joint to be implemented at the hand of the human operator to allow for the orientation of the hand to rotate around the axis of the handle. A method of estimating the hand orientation such as [179] could then be implemented to provide an estimate of the hand orientation to be used by the nullPose method as a means of obtaining the pose of the human co-worker's hands.

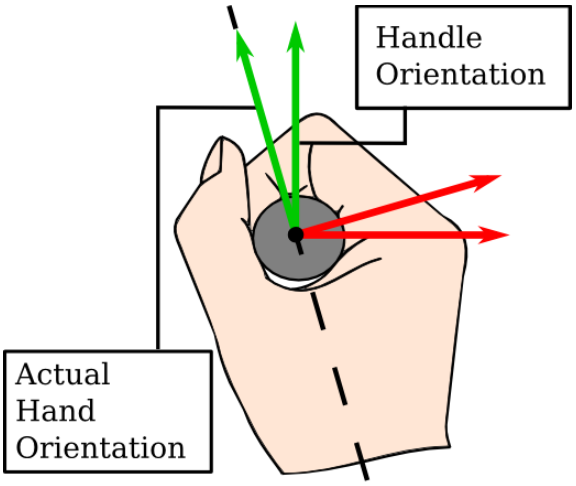

FIGURE 6.2: The actual hand orientation in comparison to the cylindrical handle orientation.

6.3.2 Dynamic Task Allocation Based on Available Sensor Measurements for the nullPose Method

Robustness and performance of the nullPose method may be able to be improved by implementing a method of dynamic task allocation. Tasks developed from sensor measurement targets may have different output rate or certain targets may become unavailable due to occlusion of the human or difficult environment. Resolving the redundancy of the upper body can be performed with what is deemed to be the best set of currently available tasks. The priority of each task may need to be set by the nullPose method itself rather than set by the user. Certain factors may result in some targets becoming less accurate and thus a lower priority should be given to tasks based on these targets. The type of targets may also affect the priority of the tasks. Certain type of targets, such as the full pose of the torso, is likely to be of higher importance than other types of targets, such as the position of the elbow.

6.3.3 Determining the Minimum Combination of Tasks for the nullPose Method

Similarly to the dynamic task allocation, setting the tasks to the minimum number required will improve the performance of the nullPose method. Currently the upper body pose is

calculated iteratively through each task being incorporated into the solution. Whereas too few targets are likely to cause the accuracy of the estimate to be poor, too many targets may result in a lower output rate. If a dynamic task allocation is to be implemented which organizes the task array based on the priority of tasks, the computation can be costly if more targets are to be incorporated into the upper body solution. Different targets may also result in the same outcome being achieved. Appendix B shows a preliminary work in which the different combination of targets were used to constrain the pose of the upper body. An algorithm could be developed to select the minimum number of task to be implemented such that the accuracy of the estimated upper body pose is within an acceptable range.

6.3.4 Extending the nullPose Method for a Full Body Pose Estimation

In the case study for real-time strength appraisal, it is assumed that the lower body of the human is able to support the physical strength being exerted by the upper limbs. In reality if a force being exerted by the upper limb is too great, it is likely going to destabilize the human. If the lower body of the human is to be incorporated in the estimation of the human physical strength, the pose of the lower body may need to be estimated as well. Similarly to the way the torso is divided into two parts at the start of the pose estimation procedure, it is hypothesized that the hip or pelvis could be divided into two with a lower limb attached to each section. The pose of the legs of the human co-worker may be able to be obtained through the addition of a sensor such as a laser scan placed close to the ground. An assumption may also be used such that the poses of the feet matches that of the shoulders of the human in the event that no targets are able to be obtained with respect to the pose of the lower limbs.

6.3.5 Implementing Assistance-as-Needed in pHRC

In an AAN paradigm, the amount of assistance to be provided by the robot is adapted based on the capability of the human. The capability of the human being considered in this thesis is the maximum strength of the human co-worker at the left and right hand. In reality operations are not likely to require the maximum strength of the human. An

operation may be completed by either hand when measuring only the maximum strength of the human co-worker. Therefore a future work is required to determine the contribution of each upper limb towards the operation as the operational load may not be shared evenly between the two upper limbs. Overuse of one of the limbs may result in a higher risk of injury which could be stopped if the contribution of each limb is able to be determined as the collaboration occurs.

AAN paradigms have seen use in rehabilitative applications. The benefit of an AAN paradigm in a real pHRC application needs to be examined. Experiments would need to be conducted to determine the amount of exertion experienced by the human co-worker during physically demanding operations with both adaptive assistance being provided as well as full assistance being provided to the human. Although the AAN paradigm will require more effort from the human co-worker, it is likely to have benefit in other aspects of the operation such as engagement.

Appendix A

Additional Results From Experiments in Chapter 3

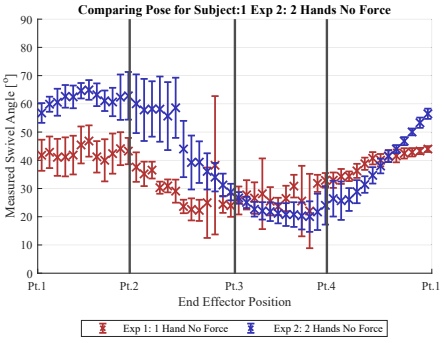

(A)

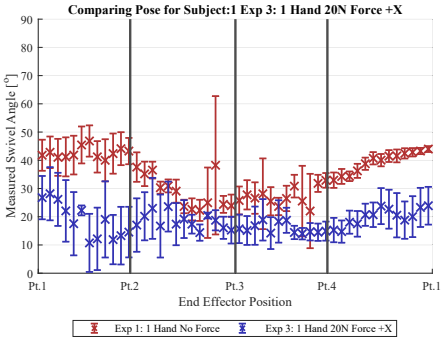

(B)

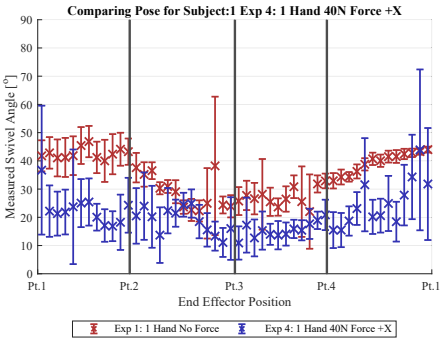

(C)

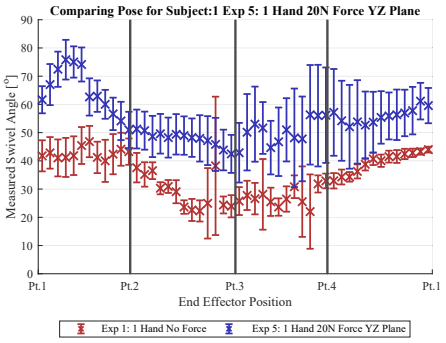

(D)

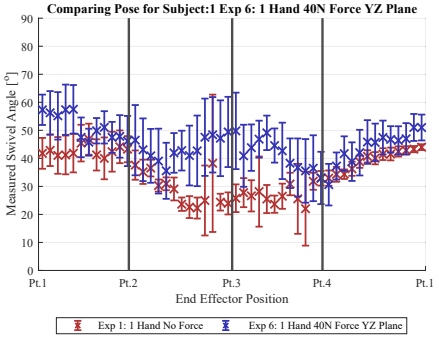

(E)

FIGURE A.1: Comparison of the mean and standard deviation of the swivel angles of subject 1 in (A) Experiment 2, (B) Experiment 3, (C) Experiment 4, (D) Experiment 5 and (E) Experiment 6 to Experiment 1.

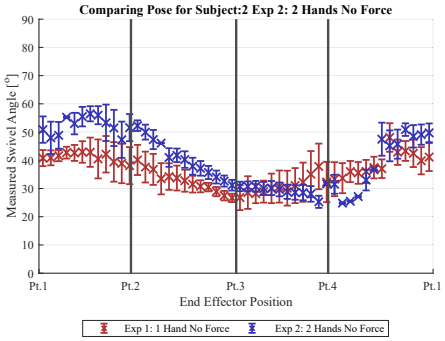

(A)

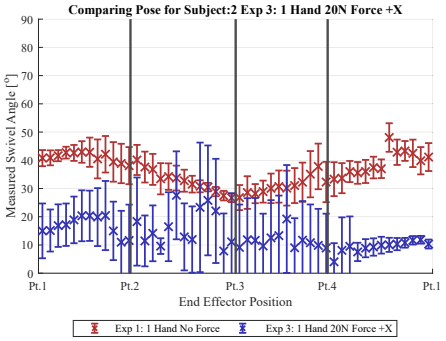

(B)

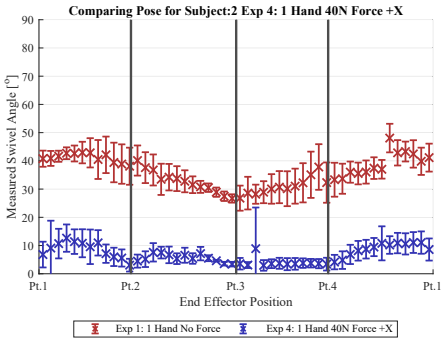

(C)

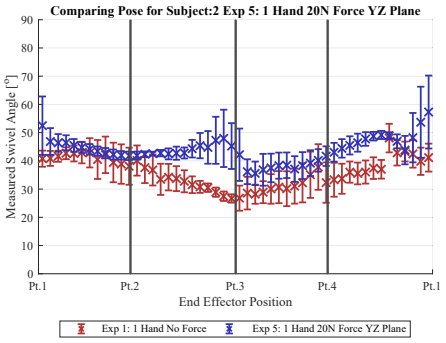

(D)

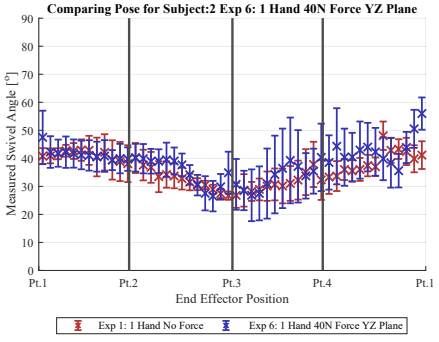

(E)

FIGURE A.2: Comparison of the mean and standard deviation of the swivel angles of subject 2 in (A) Experiment 2, (B) Experiment 3, (C) Experiment 4, (D) Experiment 5 and (E) Experiment 6 to Experiment 1.

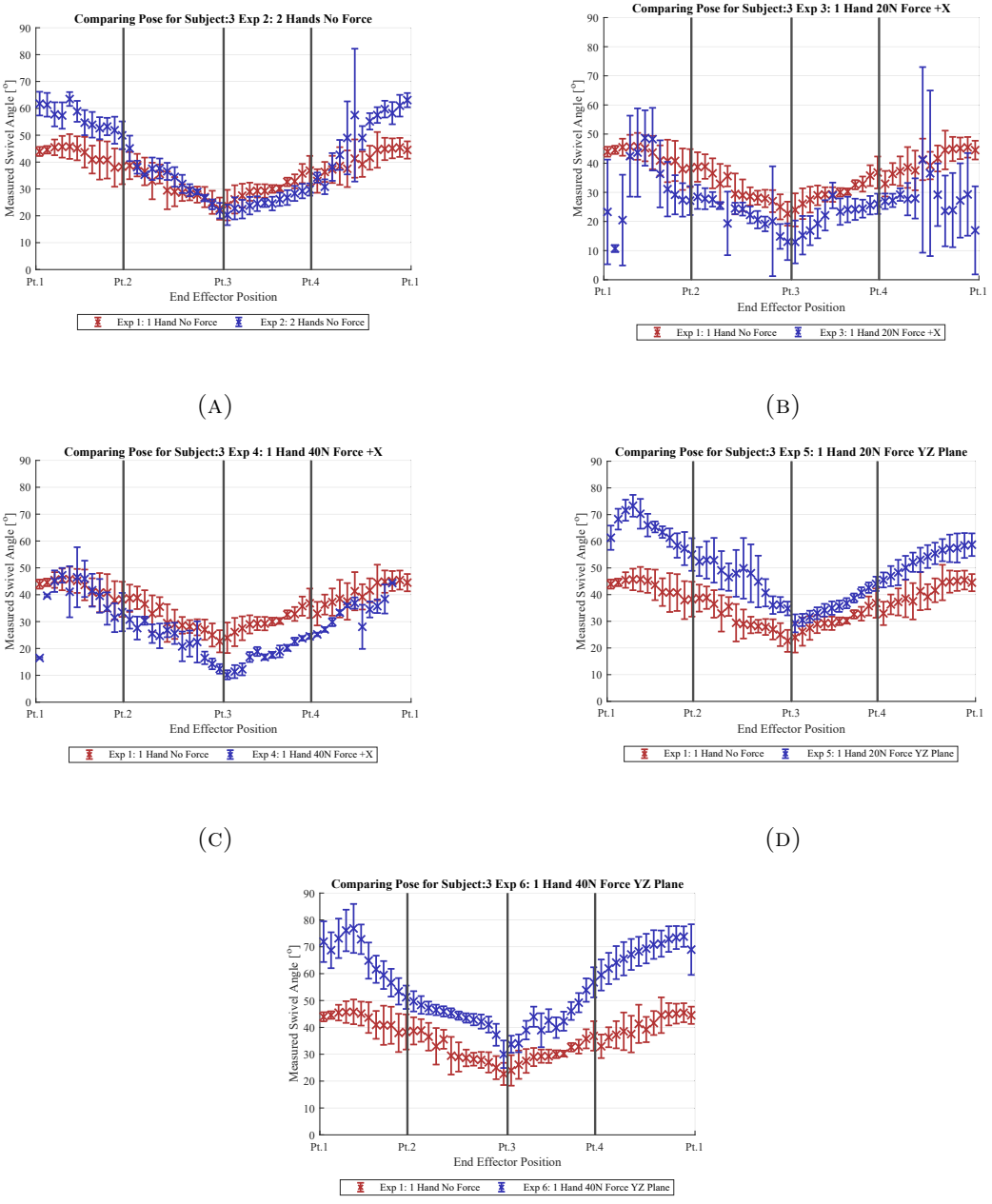

FIGURE A.3: Comparison of the mean and standard deviation of the swivel angles of subject 3 in (A) Experiment 2, (B) Experiment 3, (C) Experiment 4, (D) Experiment 5 and (E) Experiment 6 to Experiment 1.

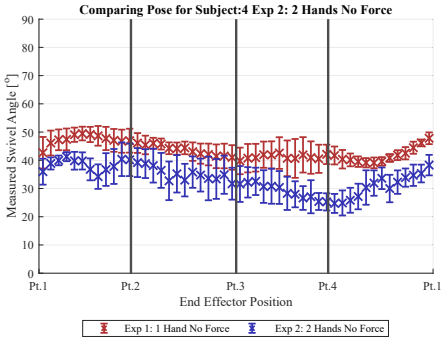

(A)

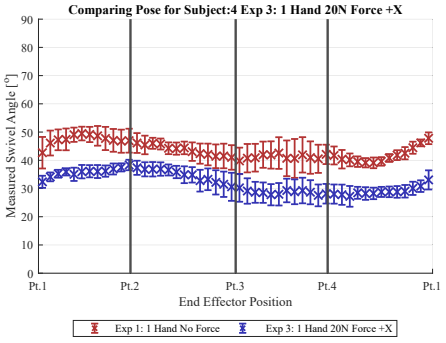

(B)

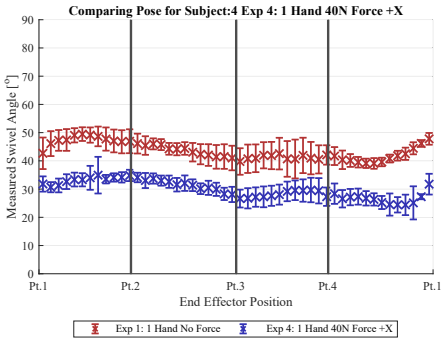

(C)

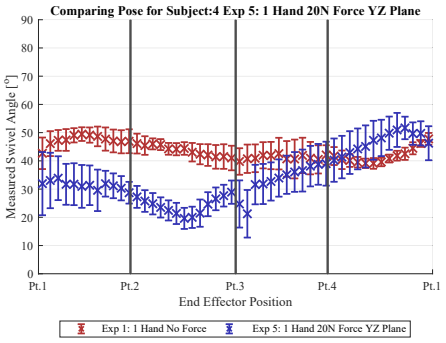

(D)

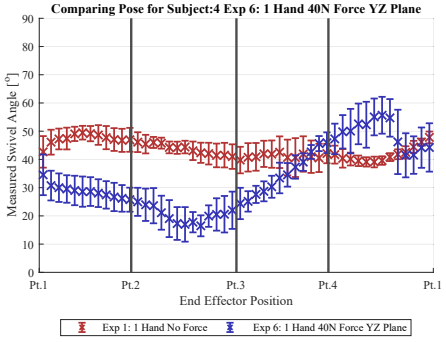

(E)

FIGURE A.4: Comparison of the mean and standard deviation of the swivel angles of subject 4 in (A) Experiment 2, (B) Experiment 3, (C) Experiment 4, (D) Experiment 5 and (E) Experiment 6 to Experiment 1.

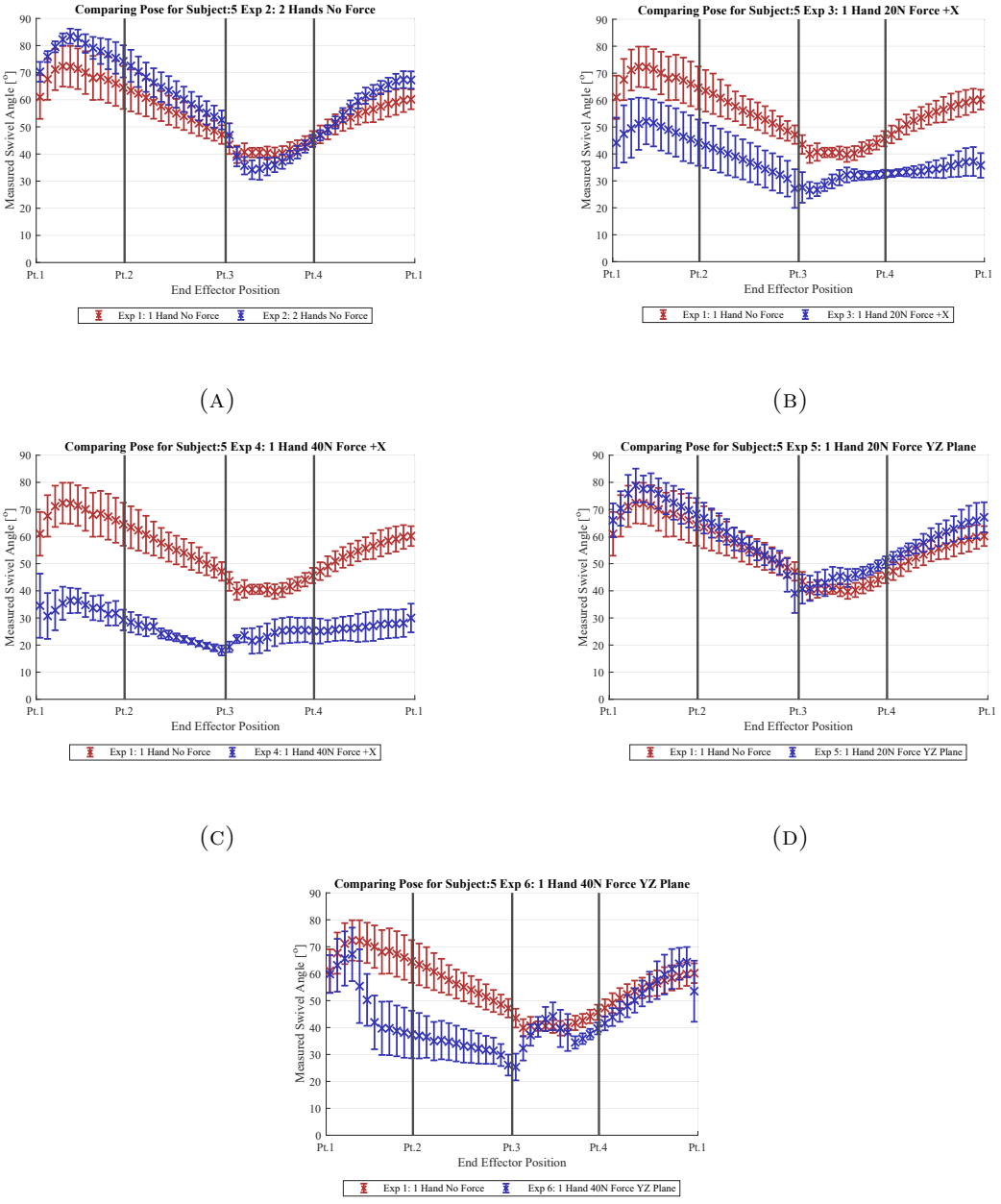

FIGURE A.5: Comparison of the mean and standard deviation of the swivel angles of subject 5 in (A) Experiment 2, (B) Experiment 3, (C) Experiment 4, (D) Experiment 5 and (E) Experiment 6 to Experiment 1.

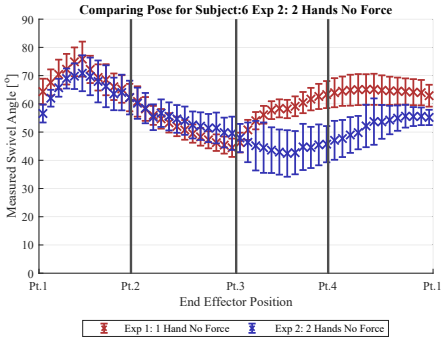

(A)

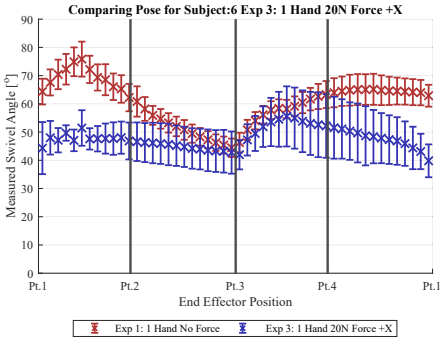

(B)

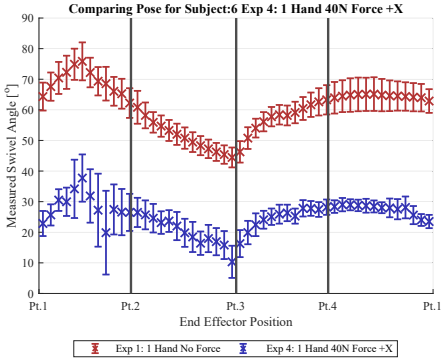

(C)

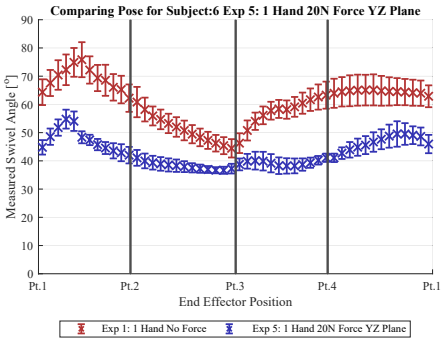

(D)

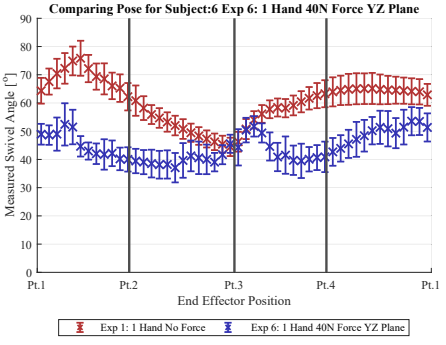

(E)

FIGURE A.6: Comparison of the mean and standard deviation of the swivel angles of subject 6 in (A) Experiment 2, (B) Experiment 3, (C) Experiment 4, (D) Experiment 5 and (E) Experiment 6 to Experiment 1.

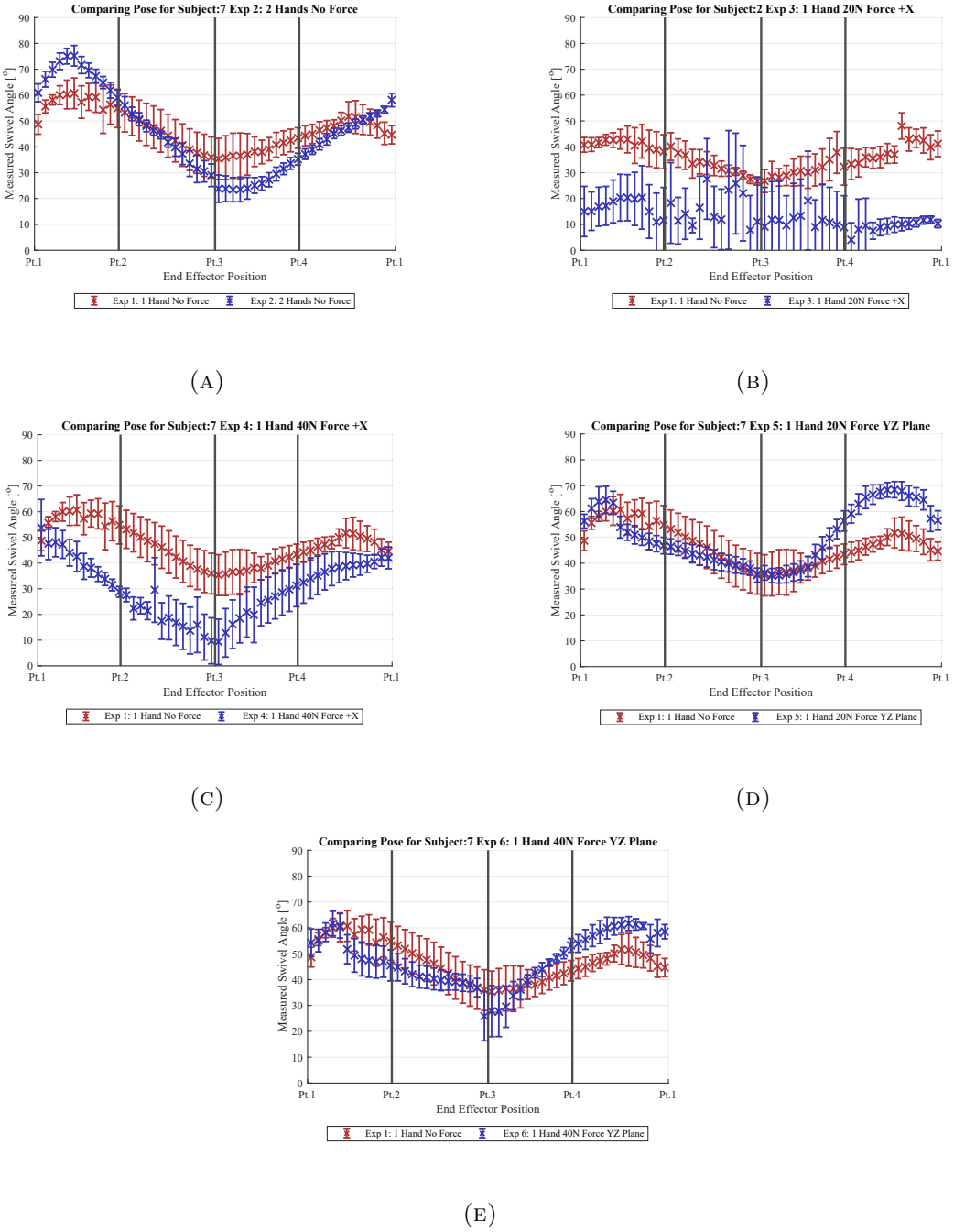

FIGURE A.7: Comparison of the mean and standard deviation of the swivel angles of subject 7 in (A) Experiment 2, (B) Experiment 3, (C) Experiment 4, (D) Experiment 5 and (E) Experiment 6 to Experiment 1.

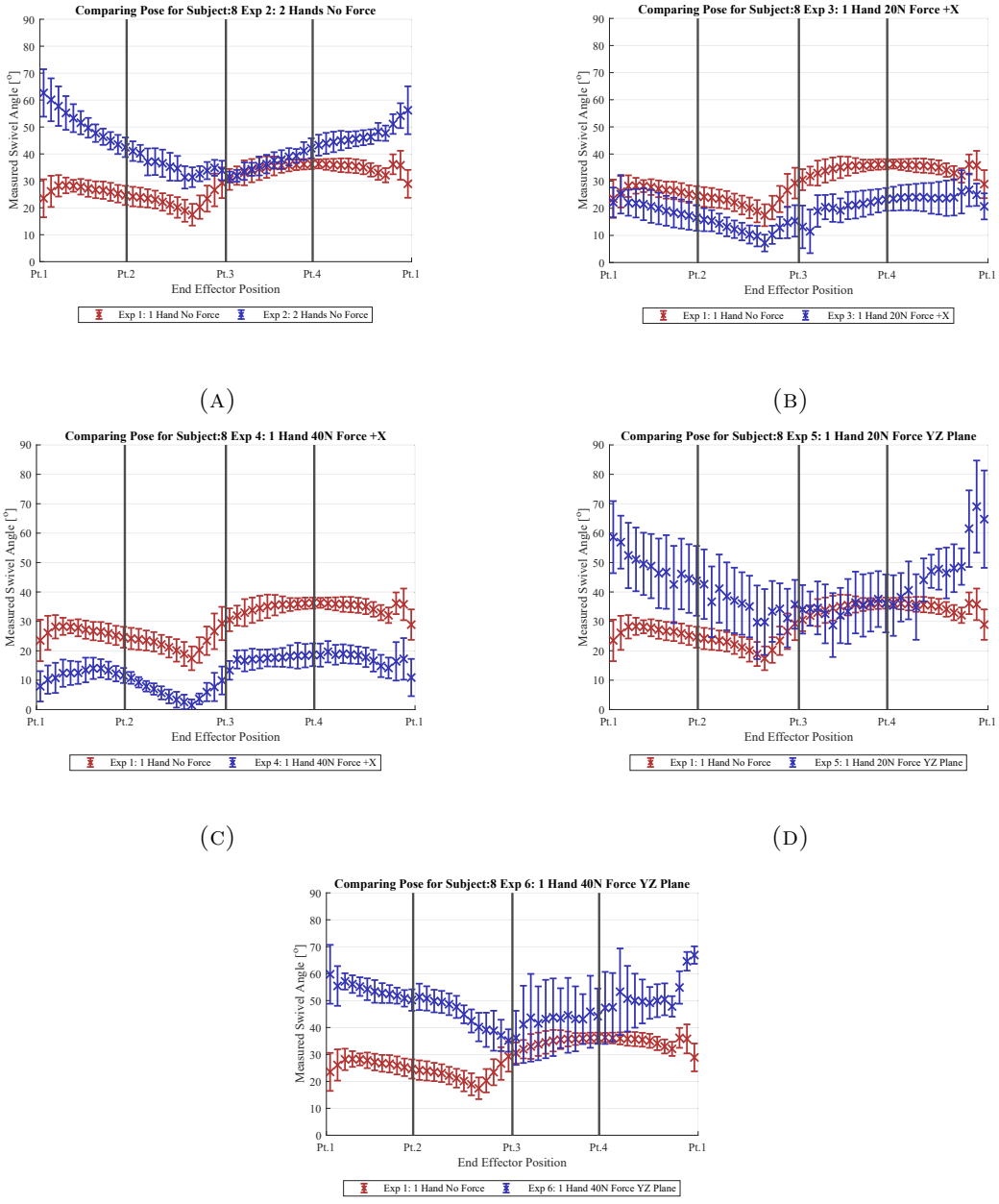

FIGURE A.8: Comparison of the mean and standard deviation of the swivel angles of subject 8 in (A) Experiment 2, (B) Experiment 3, (C) Experiment 4, (D) Experiment 5 and (E) Experiment 6 to Experiment 1.

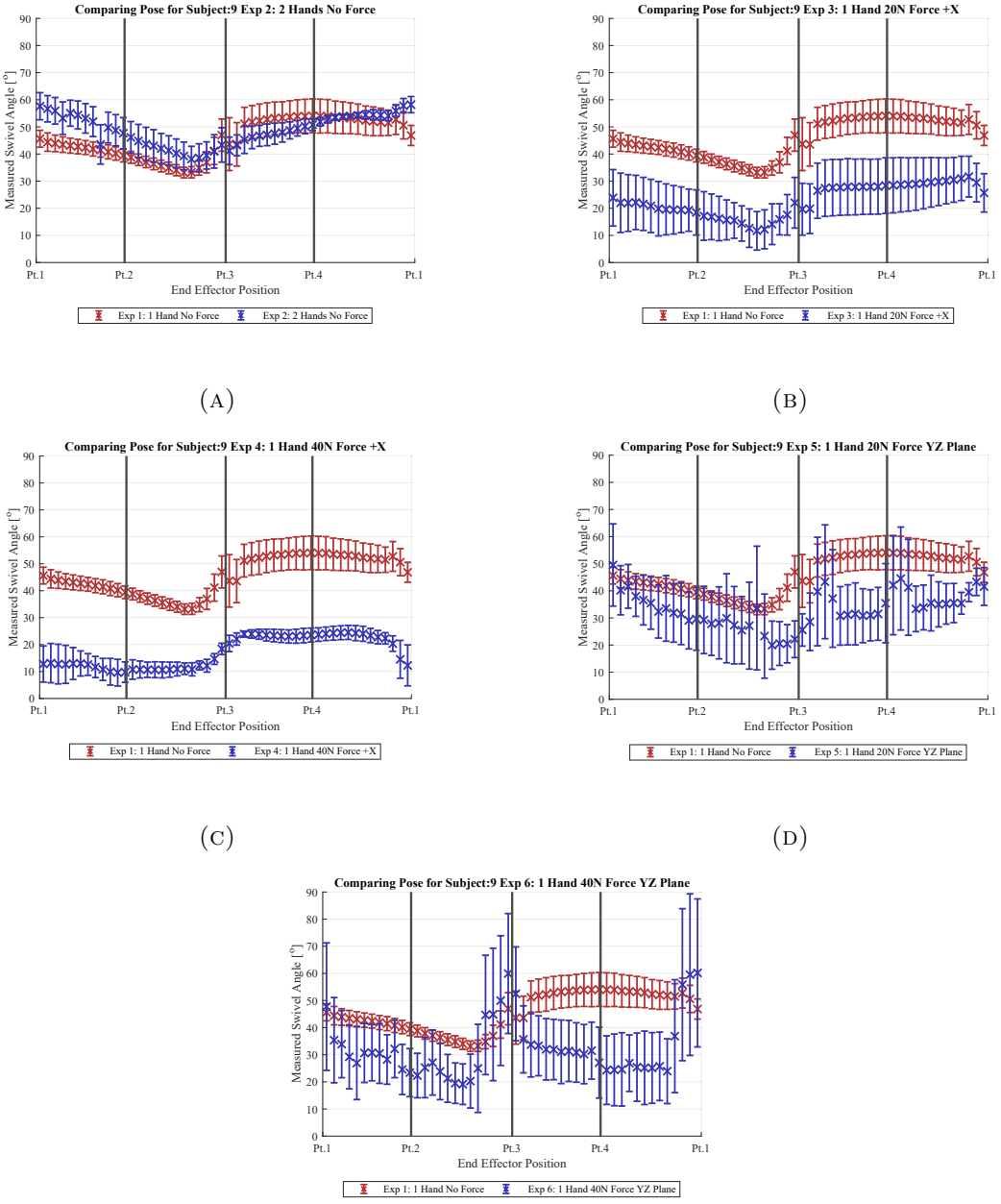

FIGURE A.9: Comparison of the mean and standard deviation of the swivel angles of subject 9 in (A) Experiment 2, (B) Experiment 3, (C) Experiment 4, (D) Experiment 5 and (E) Experiment 6 to Experiment 1.

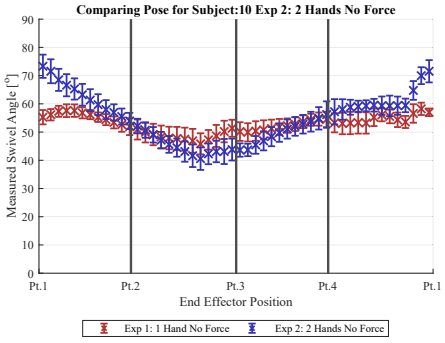

(A)

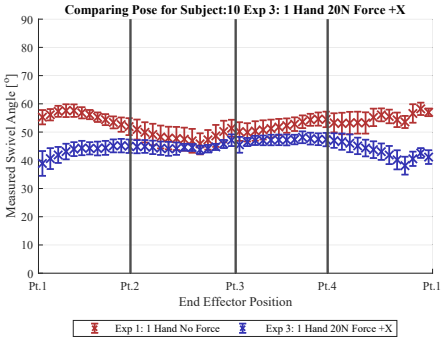

(B)

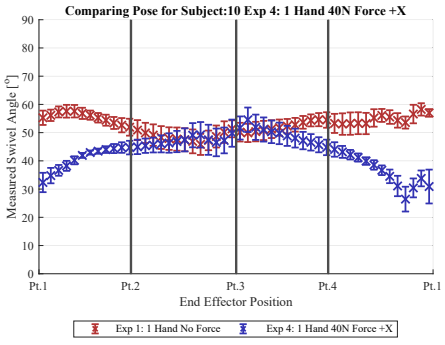

(C)

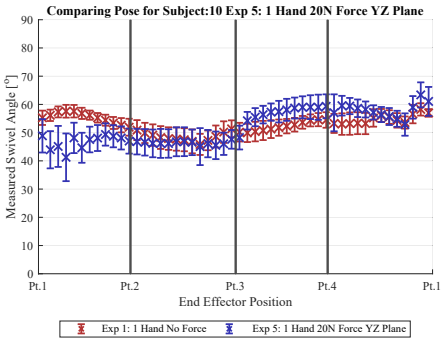

(D)

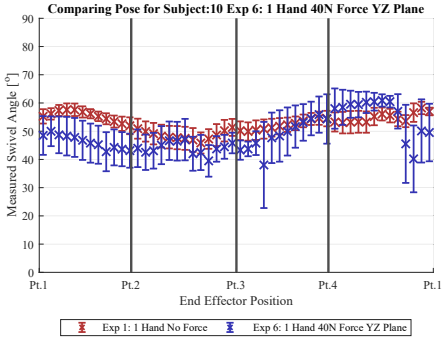

(E)

FIGURE A.10: Comparison of the mean and standard deviation of the swivel angles of subject 10 in (A) Experiment 2, (B) Experiment 3, (C) Experiment 4, (D) Experiment 5 and (E) Experiment 6 to Experiment 1.

Appendix B

nullPose method: Combinations of Targets

Each task being used in the redundancy resolution acts as a constraint for the upper body pose. For example an available elbow position target should constrain the pose of the upper body such that the output of the nullPose matches the obtained target of the elbow. As more and more targets are incorporated into the solution, the more constrained the upper body pose becomes. The minimum number of targets that can be used to fully constrain the upper body pose ranges based on the type of targets being used. Ideally a fully constrained solution means that the output of the nullPose method reflects the true pose of the human. Errors in the sensory measurements means that even with a fully constrained solution, the estimated upper body pose may not be the same as the true pose.

Figure B.1 shows a chart of the different combination that could be used to constrain the pose of the human upper body. In this figure, the Hilbert-Schmidt norm is used to calculate the redundancy in the upper body pose. The lower the norm means the more constrained the upper body, with a zero Hilbert-Schmidt norm corresponding to a fully constrained solution. The Hilbert-Schmidt norm N_{HS} (Equation B.1 was calculated using the projection into the null space matrix $\boldsymbol{P}$ (Equation 4.4).

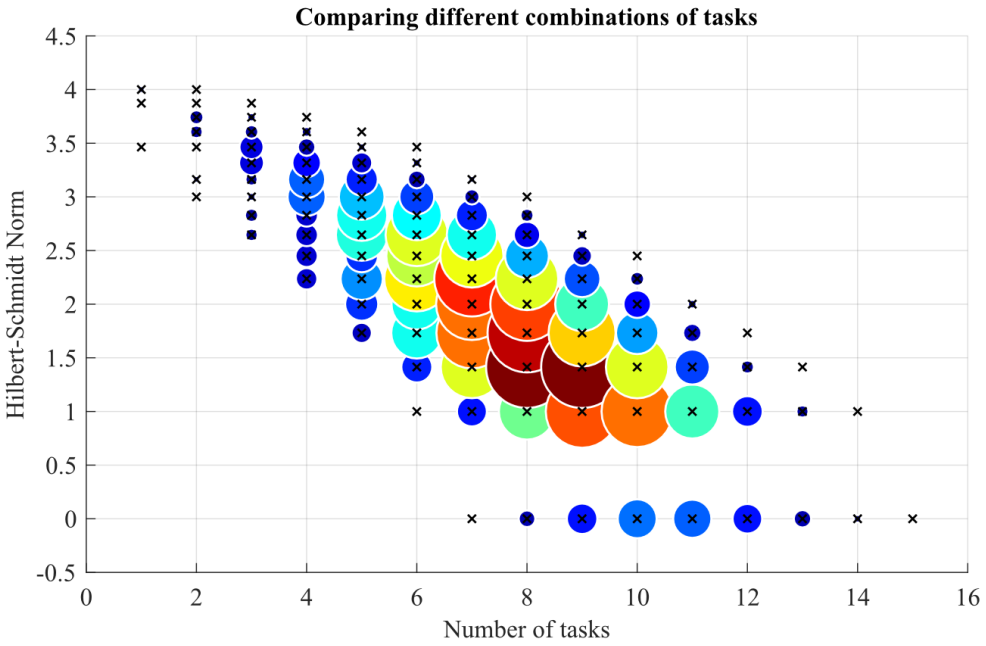

FIGURE B.1: The Hilbert-Schmidt Norm of the null space based on the different combination of tasks that can be implemented.

$$N_{HS} = \sqrt{Tr(\boldsymbol{P} * \boldsymbol{P})} \qquad where \quad Tr(\boldsymbol{A}) = \sum_{i=1}^{n} a_{ii} \tag{B.1}$$

There are a wide variety of targets that could be used to assist the redundancy resolution of the upper body pose. Table B.1 represent but a subset of targets that could be used to assist in the resolution. Depending on the sensors that are available during the collaboration with the robot, the upper body pose were found to be fully constrained with a minimum of seven targets.

Target #	Information Name
1	Maintaining a closed kinematic chain
2	Left torso half position
3	Right torso half position
4	Left torso half cross section from sensor such as a laser scan
5	Right torso half cross section from sensor such as a laser scan
6	Left torso position based on the height of the human co-worker
7	Right torso position based on the height of the human co-worker
8	Maintaining an upright left torso half orientation
9	Maintaining an upright right torso half orientation
10	Left elbow position
11	Right elbow position
12	Left shoulder position
13	Right shoulder position
14	Prescribing left inner shoulder motion
15	Prescribing right inner shoulder motion

TABLE B.1: A list of potential targets being used to resolve the redundancy of the upper body pose.

	Target #														
Combination #	1	2	3	4	5	6	7	8	9	10	11	12	13	14	15
1	1	0	0	0	0	0	0	0	1	1	1	0	1	1	1
2	1	0	0	0	0	0	0	1	0	1	1	1	0	1	1
3	1	0	1	0	0	0	0	0	1	1	1	0	0	1	1
4	1	1	0	0	0	0	0	0	1	1	1	0	0	1	1

TABLE B.2: The combination of seven sets of information being used to obtain a fully constrained upper body pose where a 1 symbolize a target being used and a 0 symbolizes an information that is not used. Target # corresponds to the information shown in Table B.1

Appendix C

Additional Simulation Results of the nullPose Method

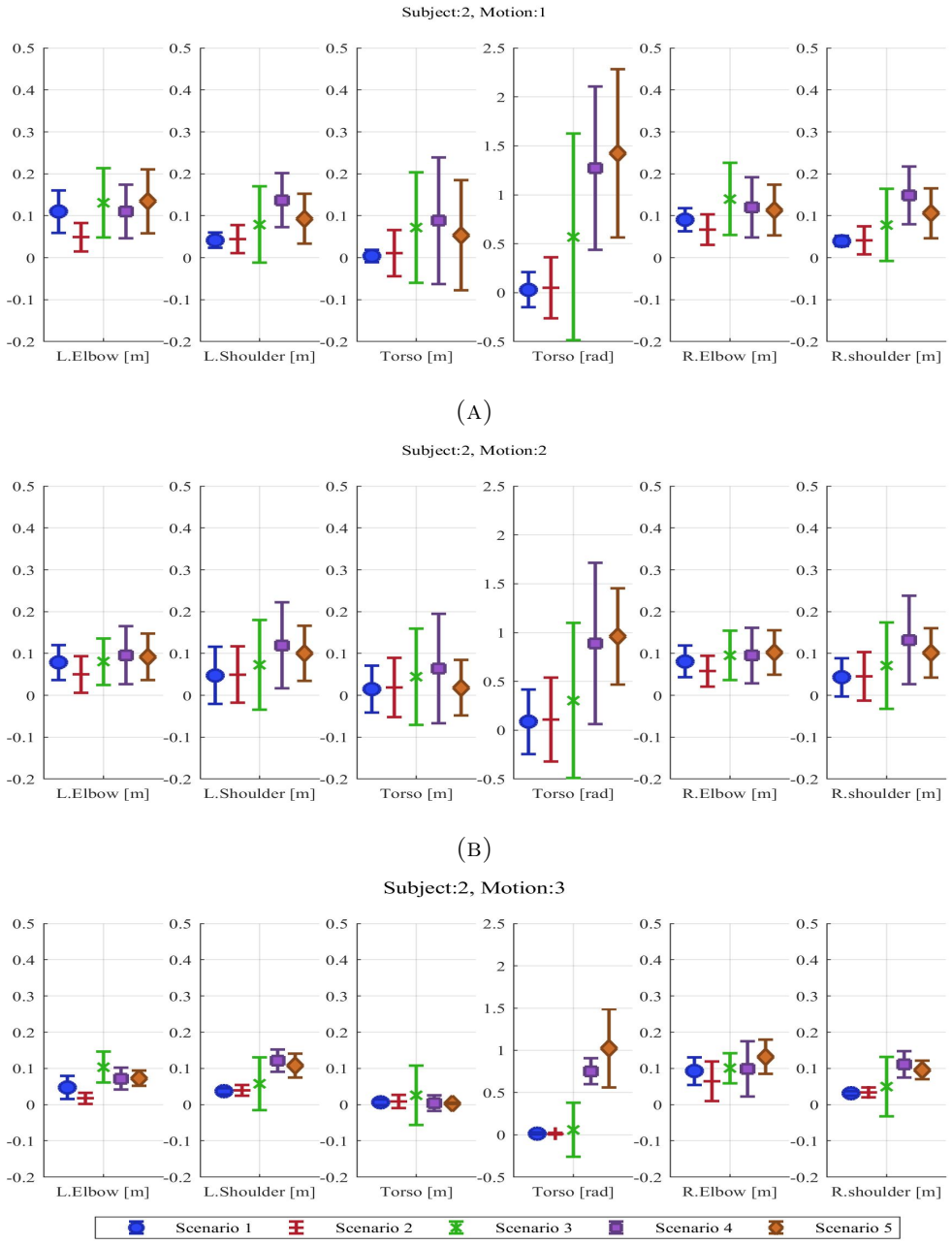

FIGURE C.1: Graphed result of the mean error with standard deviations of the upper body segments for Subject 2 in (A) Motion 1, (B) Motion 2 and (C) Motion 3. Errors are shown in meters for position and radians for rotation.

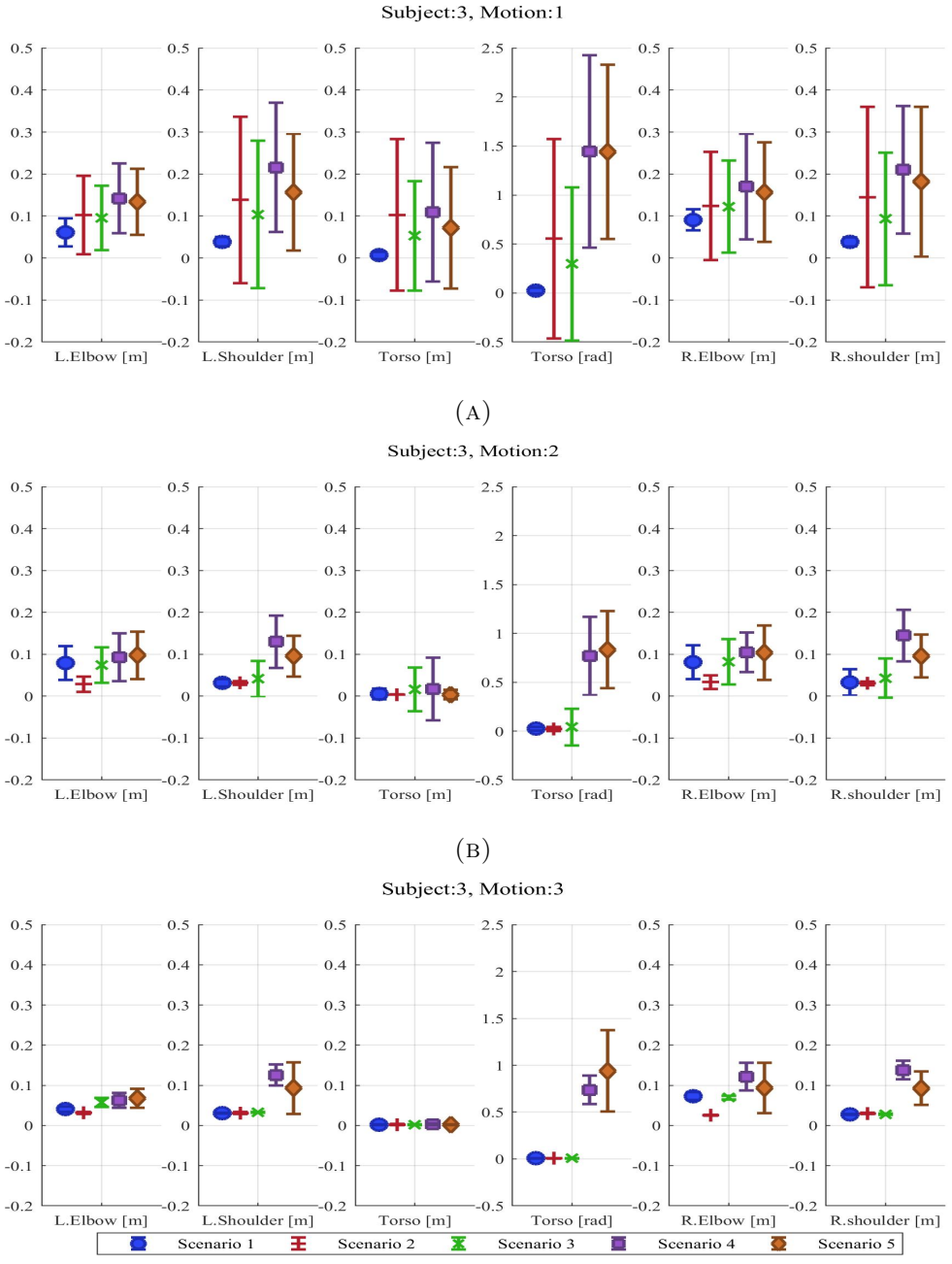

FIGURE C.2: Graphed result of the mean error with standard deviations of the upper body segments for Subject 3 in (A) Motion 1, (B) Motion 2 and (C) Motion 3. Errors are shown in meters for position and radians for rotation.

Appendix D

Shoulder Rotational Matrix Conversion

D.1 Rotational matrix between the scapula frame to the humerus frame of the right upper limb musculoskeletal model

$$\boldsymbol{R} = \begin{bmatrix} C * cos(shl\_rot) + A * sin(shl\_rot) & sin(elv\_ang)sin(shl\_elv) & C * sin(shl\_rot) - A * cos(shl\_rot) \\ cos(elv\_ang)sin(shl\_elv)sin(shl\_rot) & cos(shl\_elv) & -sin(elv\_ang)sin(shl\_elv)sin(shl\_rot) \\ -cos(shl\_rot)sin(elv\_ang)sin(shl\_elv) & & -cos(elv\_ang)cos(shl\_rot)sin(shl\_elv) \\ -B * sin(shl\_rot) - A * cos(shl\_rot) & cos(elv\_ang)sin(shl\_elv) & B * cos(shl\_rot) - A * sin(shl\_rot) \end{bmatrix} \quad \text{(D.1)}$$

where

$$A = cos(elv\_ang)sin(elv\_ang) - cos(elv\_ang)cos(shl\_elv)sin(elv\_ang)$$

$$B = cos(shl\_elv)cos(elv\_ang)^2 + sin(elv\_ang)^2$$

$$C = cos(elv\_ang)^2 + cos(shl\_elv)sin(elv\_ang)^2$$

D.2 Rotational matrix between the scapula frame to the humerus frame of the left upper limb musculoskeletal model

$$\boldsymbol{R} = \begin{bmatrix} C * cos(shl\_rot) + A * sin(shl\_rot) & -sin(elv\_ang)sin(shl\_elv) & -C * sin(shl\_rot) + A * cos(shl\_rot) \\ -cos(elv\_ang)sin(shl\_elv)sin(shl\_rot) & cos(shl\_elv) & -sin(elv\_ang)sin(shl\_elv)sin(shl\_rot) \\ +cos(shl\_rot)sin(elv\_ang)sin(shl\_elv) & & -cos(elv\_ang)cos(shl\_rot)sin(shl\_elv) \\ B * sin(shl\_rot) + A * cos(shl\_rot) & cos(elv\_ang)sin(shl\_elv) & B * cos(shl\_rot) - A * sin(shl\_rot) \end{bmatrix} \quad \text{(D.2)}$$

where

$$A = cos(elv\_ang)sin(elv\_ang) - cos(elv\_ang)cos(shl\_elv)sin(elv\_ang)$$

$$B = cos(shl\_elv)cos(elv\_ang)^2 + sin(elv\_ang)^2$$

$$C = cos(elv\_ang)^2 + cos(shl\_elv)sin(elv\_ang)^2$$

Appendix E

Distribution of Muscle Activation of the Musculoskeletal Models

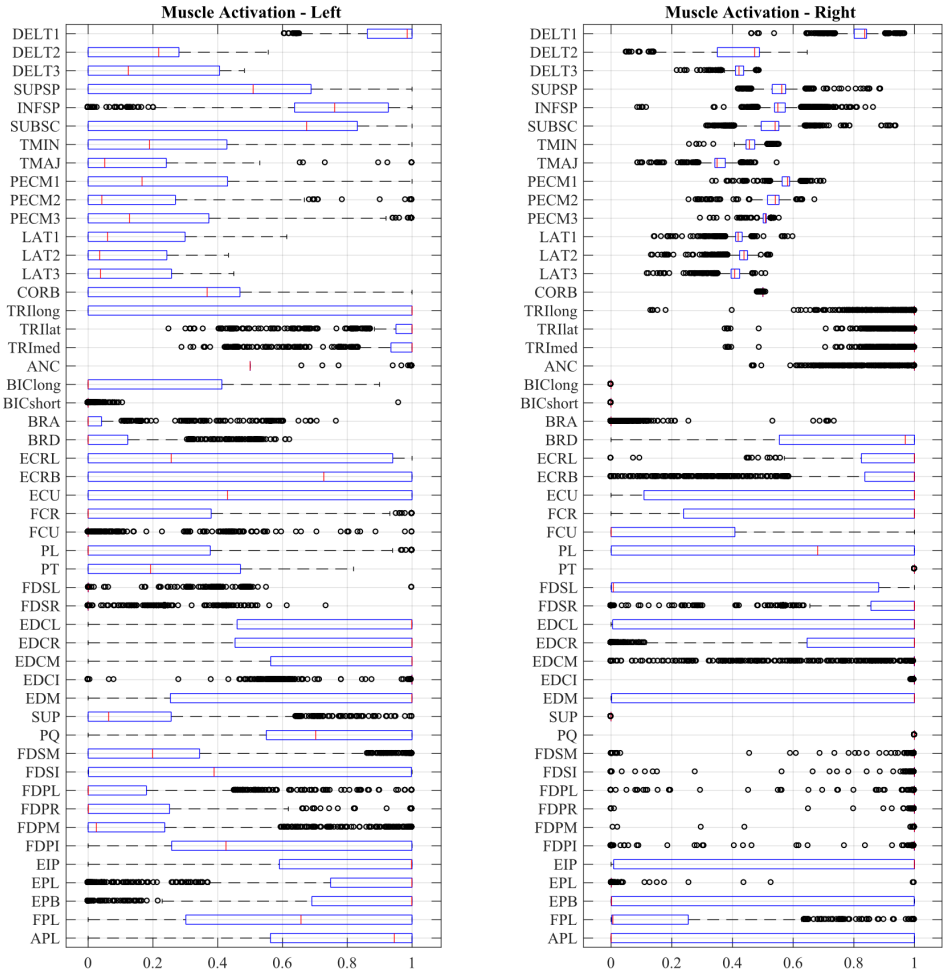

FIGURE E.1: Estimated muscle activation of the right and left musculoskeletal model in Experiment 2.

TABLE E.1: List of muscles in the musculoskeletal model and their abbreviations [10] pt.1.

Abbreviation	Muscle
Shoulder	
Deltoid	
Anterior	DELT1
Middle	DELT2
Posterior	DELT3
Supraspinatus	SUPRA
Infraspinatus	INFRA
Subscapularis	SUBSCAP
Teres minor	TMIN
Teres Major	TMAJ
Pectoralis major	
Clavicular	PMAJ1
Sternal	PMAJ2
Ribs	PMAJ3
Latissimus dorsi	
Thoracic	LAT1
Lumbar	LAT2
Iliac	LAT3
Coracobrachialis	CORB
Elbow	
Triceps	
Long	TRIlong
Lateral	TRIlat
Medial	TRIlmed
Anconeus	ANC
Supinator	SUP
Biceps	
Long	BIClong
Short	BICshort
Brachialis	BRA
Brachioradialis	BRD
Major wrist or forearm	
Extensor carpi radialis longus	ECRL
Extensor carpi radialis brevis	ECRB
Extensor carpi ulnaris	ECU
Flexor carpi radialis	FCR
Flexor carpi ulnaris	FCU
Palmaris longus	PL
Pronator teres	PT
Pronator quadratus	PQ

TABLE E.2: List of muscles in the musculoskeletal model and their abbreviations [10] pt.2.

Abbreviation	Muscle
Wrist/hand muscles	
Flexor digitorum superficialis	
Digit 5	FDSL
Digit 4	FDSR
Digit 3	FDSM
Digit 2	FDSI
Flexor digitorum profundus	
Digit 5	FDPL
Digit 4	FDPR
Digit 3	FDPM
Digit 2	FDPI
Extensor digitorum communis	
Digit 5	EDCL
Digit 4	EDCR
Digit 3	EDCM
Digit 2	EDCI
Extensor digiti minimi	EDM
Extensor indicis propius	EIP
Extensor pollicis longus	EPL
Extensor pollicis brevis	EPB
Flexor pollicis longus	FPL
Abductor pollicis longus	APL

Bibliography

[1] Steve Moody. Two Born Every Minute Inside Nissans Sunderland Factory. URL https://www.carmagazine.co.uk/features/car-culture/two-born-every-minute-inside-nissans-sunderland-factory-car-february-2016/.

[2] Universal Robot. UR10. URL https://www.universal-robots.com/products/ur10-robot/.

[3] Kuka. LBR iiwa. URL https://www.kuka.com/en-au/products/robotics-systems/industrial-robots/lbr-iiwa.

[4] Rethink Robotics. Sawyer. URL https://www.rethinkrobotics.com/sawyer/.

[5] H Kazerooni. Exoskeletons for Human Power Augmentation. In *2005 IEEE/RSJ International Conference on Intelligent Robots and Systems*, pages 3459–3464, Edmonton, Alta, 2005. IEEE. doi: 10.1109/IROS.2005.1545451.

[6] Marc G. Carmichael, Bryan Moutrie, and Dikai Liu. A framework for task-based evaluation of robotic coworkers. In *2014 13th International Conference on Control Automation Robotics and Vision, ICARCV 2014*, pages 1362–1367. IEEE, 2014. ISBN 9781479951994. doi: 10.1109/ICARCV.2014.7064514.

[7] Natural Point Inc. OptiTrack Motion Capture System. URL http://optitrack.com/.

[8] Hyunchul Kim, Levi Makaio Miller, Nancy Byl, Gary M. Abrams, and Jacob Rosen. Redundancy resolution of the human arm and an upper limb exoskeleton. *IEEE Transactions on Biomedical Engineering*, 59(6):1770–1779, 2012. ISSN 00189294. doi: 10.1109/TBME.2012.2194489.

[9] Richardo Khonasty, Marc G Carmichael, Dikai Liu, and Stefano Aldini. Effect of External Force and Bimanual Operation on Upper Limb Pose during Human-Robot Collaboration. *The proceedings of the Australasian Conference on Robotics and Automation (ACRA)*, 2017.

[10] Katherine R S Holzbaur, Wendy M. Murray, and Scott L. Delp. A model of the upper extremity for simulating musculoskeletal surgery and analyzing neuromuscular control. *Annals of Biomedical Engineering*, 33(6):829–840, 2005. ISSN 00906964. doi: 10.1007/s10439-005-3320-7.

[11] Sabre Autonomous Solutions. Alpha 1. URL https://www.sabreautonomous.com.au/.

[12] J. Scholtz. Theory and evaluation of human robot interactions. *Proceedings of the 36th Annual Hawaii International Conference on System Sciences, HICSS 2003*, 2003. ISSN 1098-4275. doi: 10.1109/HICSS.2003.1174284.

[13] Sami Haddadin and Elizabeth Croft. *Physical Human–Robot Interaction*, pages 1835–1874. Springer International Publishing, 2016. ISBN 978-3-319-32550-7. doi: 10.1007/978-3-319-32552-1-69.

[14] Agostino De Santis, Bruno Siciliano, Alessandro De Luca, and Antonio Bicchi. An atlas of physical human-robot interaction. *Mechanism and Machine Theory*, 43(3): 253–270, 2008. ISSN 0094114X. doi: 10.1016/j.mechmachtheory.2007.03.003.

[15] Andrea Cherubini, Robin Passama, André Crosnier, Antoine Lasnier, and Philippe Fraisse. Collaborative manufacturing with physical human-robot interaction. *Robotics and Computer-Integrated Manufacturing*, 40:1 – 13, 2016. ISSN 07365845. doi: 10.1016/j.rcim.2015.12.007.

[16] Mustafa Suphi Erden and Bobby Marić. Assisting manual welding with robot. *Robotics and Computer-Integrated Manufacturing*, 27(4):818–828, 2011. ISSN 07365845. doi: 10.1016/j.rcim.2011.01.003.

[17] Inc. Intuitive Surgical. The da Vinci® Surgical System. URL http://www.davincisurgery.com/da-vinci-surgery/da-vinci-surgical-system/.

[18] Juan Fasola and Maja J. Matarić. Robot motivator: Increasing user enjoyment and performance on a physical/cognitive task. *2010 IEEE 9th International Conference on Development and Learning, ICDL-2010*, pages 274–279, 2010. ISSN 2161-9476. doi: 10.1109/DEVLRN.2010.5578830.

[19] DJ Reinkensmeyer, ET Wolbrecht, V Chan, C Chou, SC Cramer, and JE Bobrow. Comparison of 3D, Assist-as-Needed Robotic Arm/Hand Movement Training Provided with Pneu-WREX to Conventional Table Top Therapy Following Chronic Stroke. *American journal of physical medicine & rehabilitation / Association of Academic Physiatrists*, 91(11):232–41, 2012. doi: 10.1097/PHM.0b013e31826bce79.

[20] Mingming Zhang, Claire T. Davies, Anoop Nandakumar, and Shane Xie. An Assistance-as-Needed Control Paradigm for Robot-Assisted Ankle Rehabilitation. *Rehabilitation Process and Outcome*, 3:15–17, 2014. doi: 10.4137/RPO.S12340.

[21] Marc G. Carmichael and Dikai Liu. Towards using musculoskeletal models for intelligent control of physically assistive robots. In *Proceedings of the Annual International Conference of the IEEE Engineering in Medicine and Biology Society, EMBS*, pages 8162–8165, 2011. ISBN 9781424441211. doi: 10.1109/IEMBS.2011.6092013.

[22] Vincent Hernandez, Nasser Rezzoug, and Philippe Gorce. Toward isometric force capabilities evaluation by using a musculoskeletal model: Comparison with direct force measurement. *Journal of Biomechanics*, 48(12):3178–3184, 2015. ISSN 18732380. doi: 10.1016/j.jbiomech.2015.07.003.

[23] Jia Hua Lin, Raymond W. McGorry, and Chien Chi Chang. Effects of handle orientation and between-handle distance on bi-manual isometric push strength. *Applied Ergonomics*, 43(4):664–670, 2012. ISSN 00036870. doi: 10.1016/j.apergo.2011.10.004.

[24] Tao Kang, Jiping He, and Stephen I Helms Tillery. Determining natural arm configuration along a reaching trajectory. *Experimental Brain Research*, 167(3):352–361, 2005. ISSN 1094-687X. doi: 10.1109/IEMBS.2003.1279599.

[25] Hyunchul Kim and Jacob Rosen. Predicting Redundancy of a 7 DOF Upper Limb Exoskeleton Toward Improved Transparency between Human and Robot. *Journal of Intelligent & Robotic Systems*, 80(S1):99–119, 2015. doi: 10.1007/s10846-015-0212-4.

[26] J. Y.S. Luh. An Anatomy of Industrial Robots and Their Controls. *IEEE Transactions on Automatic Control*, 28(2):133–153, 1983. ISSN 15582523. doi: 10.1109/TAC.1983.1103216.

[27] Woosub Lee, Sungehul Kang, Munsang Kim, and Mignon Park. ROBHAZ-DT3: teleoperated mobile platform with passively adaptive double-track for hazardous environment applications. In *2004 IEEE/RSJ International Conference on Intelligent Robots and Systems (IROS)*, volume 1, pages 33–38, 2004. ISBN 0-7803-8463-6. doi: 10.1109/IROS.2004.1389325.

[28] Sungchul Kang, Changhyun Cho, Changwoo Park, Jonghwa Lee, Dongseok Ryu, and Munsang Kim. ROBHAZ-DT2: Passive double-tracked mobile manipulator for explosive ordinance disposal. In *International Conference on Intelligent Robots and Systems (IROS)*, pages 355–364, 2003. ISBN 3540328017. doi: 10.1007/10991459.34.

[29] Benjamin Johnen, Carsten Scheele, and Bernd Kuhlenkötter. Measurement of Industrial Robot Trajectories With Reorientations. *Mechanical Engineering Research*, 4(1):43, 2014. ISSN 1927-0615. doi: 10.5539/mer.v4n1p43.

[30] Zengxi Pan, Joseph Polden, Nathan Larkin, Stephen Van Duin, and John Norrish. Recent progress on programming methods for industrial robots. *Robotics and Computer-Integrated Manufacturing*, 28(2):87–94, 2012. ISSN 07365845. doi: 10.1016/j.rcim.2011.08.004.

[31] Jean Scholtz, Mary Theofanos, and Brian Antonishek. Development of a Test Bed for Evaluating Human-Robot Performance for Explosive Ordnance Disposal Robots. In *Human-Robot Interaction*, pages 10–17, Salt Lake City, Utah, USA, 2006.

[32] G. R. Ward and S. R G Went. Robot safety. *Industrial Robot*, 22(1):10–13, 1995. ISSN 0143991X. doi: 10.1108/EUM0000000004173.

[33] Chia Han John Yang, Gavin Paul, Peter Ward, and Dikai Liu. A path planning approach via task-objective pose selection with application to an inchworm-inspired climbing robot. *IEEE/ASME International Conference on Advanced Intelligent Mechatronics, AIM*, pages 401–406, 2016. doi: 10.1109/AIM.2016.7576800.

[34] Peter Ward, Palitha Manamperi, Philip Brooks, Peter Mann, Waruna Kaluarachchi, Laurent Matkovic, Gavin Paul, Chia-Han Yang, Phillip Quin, David Pagano, Dikai Liu, Ken Waldron, and Gamini Dissanayake. Climbing Robot for Steel Bridge Inspection: Design Challenges. In *Proceedings for the Austroads Publications Online*, pages 1–13, 2014.

[35] D K Liu, G Dissayanake, P B Manamperi, P A Brooks, G Fang, G Paul, S Webb, N Kirchner, P Chotiprayanakul, N M Kwok, and T R Ren. A Robotic System for Steel Bridge Maintenance: Research Challenges and System Design. In *Australasian Conference on Robotics and Automation*, Canberra, Australia, 2008.

[36] Gavin Paul, Stephen Webb, Dikai Liu, and Gamini Dissanayake. Autonomous robot manipulator-based exploration and mapping system for bridge maintenance. *Robotics and Autonomous Systems*, 59(7-8):543–554, 2011. ISSN 09218890. doi: 10.1016/j.robot.2011.04.001.

[37] Mohamed Walid Ben Ghezala, Amel Bouzeghoub, and Christophe Leroux. RSAW: A situation awareness system for autonomous robots. In *2014 13th International Conference on Control Automation Robotics and Vision, ICARCV 2014*, pages 450–455. IEEE, 2014. ISBN 9781479951994. doi: 10.1109/ICARCV.2014.7064347.

[38] Panagiota Tsarouchi, Sotiris Makris, George Michalos, Alexandros Stereos Matthaiakis, Xenofon Chatzigeorgiou, Athanasios Athanasatos, Michael Stefos, Panagiotis Aivaliotis, and George Chryssolouris. ROS based coordination of human robot cooperative assembly tasks-An industrial case study. *Procedia CIRP*, 37:254–259, 2015. ISSN 22128271. doi: 10.1016/j.procir.2015.08.045.

[39] Luigi Gammieri, Marco Schumann, Luigi Pelliccia, Giuseppe Di Gironimo, and Philipp Klimant. Coupling of a Redundant Manipulator with a Virtual Reality Environment to Enhance Human-robot Cooperation. *Procedia CIRP*, 62:618–623, 2017. ISSN 22128271. doi: 10.1016/j.procir.2016.06.056.

[40] Fan Liu and Ajit Narayanan. A human-inspired collision avoidance method for multi-robot and mobile autonomous robots. In *International Conference on Principles and*

Practice of Multi-Agent Systems, pages 181–196, 2013. ISBN 9783642449260. doi: 10.1007/978-3-642-44927-7.13.

[41] Sang Duck Lee, Min Cheol Kim, and Jae Bok Song. Sensorless collision detection for safe human-robot collaboration. In *IEEE International Conference on Intelligent Robots and Systems*, pages 2392 – 2397, 2015. ISBN 9781479999941. doi: 10.1109/IROS.2015.7353701.

[42] Zhijun Li, Jun Luo, Hing Xi, and Aiguo Ming. Development and control of compliant hybrid joints for human-symbiotic mobile manipulators. *International Journal of Advanced Robotic Systems*, 4(1):3, 2007. ISSN 17298806. doi: 10.5772/5714.

[43] Antonio Bicchi and Giovanni Tonietti. Fast and "soft-arm" tactics. *IEEE Robotics and Automation Magazine*, 11(2):22 – 33, 2004. ISSN 10709932. doi: 10.1109/MRA.2004.1310939.

[44] Giovanni Tonietti and Antonio Bicchi. Adaptive Simultaneous Position and Stiffness Control for a Soft Robot Arm. *IEEE/RSJ International Conference on Intelligent Robots and Systems*, 2:1992 – 1997, 2002.

[45] R Alami, A Bicchi, R Bischoff, R Chatila, and A De Luca. Safe and Dependable Physical Human-Robot Interaction in Anthropic Domains: State of the Art and Challenges. In *IEEE/RSJ International Conference on Intelligent Robots and Systems*, pages 1–16, 2006. doi: 10.1109/IROS.2006.6936985.

[46] George Michalos, Sotiris Makris, Panagiota Tsarouchi, Toni Guasch, Dimitris Kontovrakis, and George Chryssolouris. Design considerations for safe human-robot collaborative workplaces. *Procedia CIRP*, 37:248–253, 2015. ISSN 22128271. doi: 10.1016/j.procir.2015.08.014.

[47] George Michalos, Sotiris Makris, Jason Spiliotopoulos, Ioannis Misios, Panagiota Tsarouchi, and George Chryssolouris. ROBO-PARTNER: Seamless human-robot cooperation for intelligent, flexible and safe operations in the assembly factories of the future. *Procedia CIRP*, 23:71 – 76, 2014. ISSN 22128271. doi: 10.1016/j.procir.2014.10.079.

[48] ISO/TC 299 Robotics. ISO 10218-1:2011 Robots and robotic devices – Safety requirements for industrial robots, 2011.

[49] ISO/TC 299 Robotics. ISO 10218-2:2011 Robots and robotic devices – Safety requirements for industrial robots – Part 2: Robot systems and integration, 2011.

[50] ISO/TC 299 Robotics. ISO 13482:2014 Robots and robotic devices – Safety requirements for personal care robots, 2014.

[51] ISO/TC 299 Robotics. ISO/TS 15066:2016 Robots and robotic devices – Collaborative robots, 2016.

[52] Ken Young and Craig G. Pickin. Accuracy assessment of the modern industrial robot. *Industrial Robot: An International Journal*, 27(6):427–436, 2000. ISSN 0143-991X. doi: 10.1108/01439910010378851.

[53] Rok Goljat, Jan Babic, Tadej Petric, Luka Peternel, and Jun Morimoto. Power-augmentation control approach for arm exoskeleton based on human muscular manipulability. In *Proceedings - IEEE International Conference on Robotics and Automation*, pages 5929 – 5934, 2017. ISBN 9781509046331. doi: 10.1109/ICRA.2017.7989698.

[54] J. Krüger, T.K. Lien, and A. Verl. Cooperation of human and machines in assembly lines. *CIRP Annals - Manufacturing Technology*, 58(2):628–646, 2009. ISSN 00078506. doi: 10.1016/j.cirp.2009.09.009.

[55] Xi Vincent Wang, Zsolt Kemény, József Váncza, and Lihui Wang. Human-Robot collaborative assembly in cyber-physical production: Classification framework and implementation. *CIRP Annals - Manufacturing Technology*, 66(1):5 – 8, 2017. ISSN 17260604. doi: 10.1016/j.cirp.2017.04.101.

[56] Safe Work Australia. Statistics on Work-Related Musculoskeletal Disorders. Technical report, 2016. URL http://creativecommons.org/licenses/by/3.0/au/deed.en%5CnIn.

[57] Nahema Sylla, Vincent Bonnet, Frédéric Colledani, and Philippe Fraisse. Ergonomic contribution of ABLE exoskeleton in automotive industry. *International*

Journal of Industrial Ergonomics, 44(4):475–481, 2014. ISSN 18728219. doi: 10.1016/j.ergon.2014.03.008.

[58] Ho Shing Lo and Sheng Quan Xie. Exoskeleton robots for upper-limb rehabilitation: State of the art and future prospects. *Medical Engineering and Physics*, 34(3):261 –268, 2012. ISSN 13504533. doi: 10.1016/j.medengphy.2011.10.004.

[59] R Riener, T Nef, and G Colombo. Robot- aided neurorehabilitation of the upper extremities. *Medical and Biological Engineering and Computing*, 43:2–10, 2005.

[60] Rui C.V. Loureiro, William S. Harwin, Kiyoshi Nagai, and Michelle Johnson. Advances in upper limb stroke rehabilitation: A technology push. *Medical and Biological Engineering and Computing*, 49(10):1103–1118, 2011. ISSN 01400118. doi: 10.1007/s11517-011-0797-0.

[61] Roberto Colombo, Fabrizio Pisano, Silvestro Micera, Alessandra Mazzone, Carmen Delconte, M. Chiara Carrozza, Paolo Dario, and Giuseppe Minuco. Robotic techniques for upper limb evaluation and rehabilitation of stroke patients. *IEEE Transactions on Neural Systems and Rehabilitation Engineering*, 13(3):311 – 324, 2005. ISSN 15344320. doi: 10.1109/TNSRE.2005.848352.

[62] Carolynn Patten, Elizabeth G Condliffe, Christine A Dairaghi, and Peter S Lum. Concurrent neuromechanical and functional gains following upper-extremity power training post-stroke. *Journal of NeuroEngineering and Rehabilitation*, 10(1):1, 2013. doi: 10.1186/1743-0003-10-1.

[63] Gerdienke B. Prange, Michiel J. A. Jannink, Catharina G. M. Groothuis-Oudshoorn, Hermie J. Hermens, and Maarten J. IJzerman. Systematic review of the effect of robot-aided therapy on recovery of the hemiparetic arm after stroke. *The Journal of Rehabilitation Research and Development*, 43(2):171, 2006. ISSN 0748-7711. doi: 10.1682/JRRD.2005.04.0076.

[64] Doo Han Yoo and Se Yun Kim. Effects of upper limb robot-assisted therapy in the rehabilitation of stroke patients. *Journal of Physical Therapy Science*, 27(3): 677–679, 2015. ISSN 0915-5287. doi: 10.1589/jpts.27.677.

[65] H I Krebs, B T Volpe, M L Aisen, and N Hogan. Increasing productivity and quality of care: robot-aided neuro-rehabilitation. *Journal of rehabilitation research and development*, 37(6):639–52, 2000. ISSN 0748-7711.

[66] Sunil M. Prasad, Sandip M. Prasad, Hersh S. Maniar, Celeste Chu, Richard B. Schuessler, and Ralph J. Damiano. Surgical robotics: Impact of motion scaling on task performance. *Journal of the American College of Surgeons*, 199(6):863–868, 2004. ISSN 10727515. doi: 10.1016/j.jamcollsurg.2004.08.027.

[67] Paulos Yohannes, Paul Rotariu, Peter Pinto, Arthur D Smith, and Benjamin R Lee. Comparison of robotic versus laparoscopic skills: is there a difference in the learning curve? *Urology*, 60(1):39–45, 2002. ISSN 00904295. doi: 10.1016/S0090-4295(02)01717-X.

[68] Sunil M Prasad, Hersh S Maniar, Nathaniel J Soper, Ralph J Damiano, and Mary E Klingensmith. The effect of robotic assistance on learning curves for basic laparoscopic skills. *The American Journal of Surgery*, 183(6):702–707, 2002. ISSN 00029610. doi: 10.1016/S0002-9610(02)00871-1.

[69] T. Kawamura, K. Takanaka, T. Nakamura, and H. Osumi. Development of an orthosis for walking assistance using pneumatic artificial muscle: A quantitative assessment of the effect of assistance. In *2013 IEEE 13th International Conference on Rehabilitation Robotics (ICORR)*, pages 1–6. IEEE, jun 2013. ISBN 978-1-4673-6024-1. doi: 10.1109/ICORR.2013.6650350.

[70] Raffaele Spinelli, Giovanna Ottaviani Aalmo, and Natascia Magagnotti. The effect of a slack-pulling device in reducing operator physiological workload during log winching operations. *Ergonomics*, 58(5):781–790, may 2015. ISSN 0014-0139. doi: 10.1080/00140139.2014.983184.

[71] Sivakumar Balasubramanian, Julius Klein, and Etienne Burdet. Robot-assisted rehabilitation of hand function. *Current Opinion in Neurology*, 23(6):661–670, 2010. ISSN 13507540. doi: 10.1097/WCO.0b013e32833e99a4.

[72] Leonard E Kahn, Peter S Lum, W Zev Rymer, and David J Reinkensmeyer. Robot-assisted movement training for the stroke-impaired arm: Does it matter what the

robot does? *Journal of Rehabilitation Research and Development*, 43(5):619–630, 2006. doi: 10.2307/1942049.

[73] Amy A. Blank, James A. French, Ali Utku Pehlivan, and Marcia K. O'Malley. Current Trends in Robot-Assisted Upper-Limb Stroke Rehabilitation: Promoting Patient Engagement in Therapy. *Current Physical Medicine and Rehabilitation Reports*, 2(3):184–195, 2014. ISSN 2167-4833. doi: 10.1007/s40141-014-0056-z.

[74] H. Kawamoto and Y. Sankai. Power assist method based on phase sequence driven by interaction between human and robot suit. *RO-MAN 2004. 13th IEEE International Workshop on Robot and Human Interactive Communication*, pages 491–496, 2004. doi: 10.1109/ROMAN.2004.1374809.

[75] S. M.Mizanoor Rahman, Ryojun Ikeura, Masaya Nobe, and Hideki Sawai. Controlling a power assist robot for lifting objects considering human's unimanual, bimanual and cooperative weight perception. In *IEEE International Conference on Robotics and Automation*, pages 2356–2362. IEEE, 2010. ISBN 9781424450381. doi: 10.1109/ROBOT.2010.5509321.

[76] Brian Gleeson, Karon Maclean, Amir Haddadi, Elizabeth Croft, and Javier Alcazar. Gestures for industry: Intuitive human-robot communication from human observation. In *8th ACM/IEEE International Conference on Human-Robot Interaction*, pages 349–356, 2013. ISBN 9781467330558. doi: 10.1109/HRI.2013.6483609.

[77] Vaibhav V Unhelkar, Jorge Perez, James C Boerkoel Jr, Johannes Bix, Stefan Bartscher, and Julie A Shah. Towards control and sensing for an autonomous mobile robotic assistant navigating assembly lines. In *2014 IEEE International Conference on Robotics and Automation (ICRA)*, pages 4161 – 4167, Hong Kong, China, 2014. IEEE. doi: 10.1109/ICRA.2014.6907464.

[78] Mark A. Guadagnoll and Timothy D. Lee. Challenge Point: A Framework for Conceptualizing the Effects of Various Practice Conditions in Motor Learning. *Journal of Motor Behavior*, 36(2):212–224, 2004. ISSN 00222895. doi: 10.3200/JMBR.36.2.212-224.

[79] Matthew Gombolay, Anna Bair, Cindy Huang, and Julie Shah. Computational design of mixed-initiative human–robot teaming that considers human factors: situational awareness, workload, and workflow preferences. *International Journal of Robotics Research*, 36(5 - 7):597 – 617, 2017. ISSN 17413176. doi: 10.1177/0278364916688255.

[80] Michael A Vidulich and Pamela S Tsang. Mental Workload and Situation Awareness. *Handbook of Human Factors and Ergonomics*, 4:243–273, 2012.

[81] Raja Parasuraman, Thomas B. Sheridan, and Christopher D. Wickens. Situation Awareness, Mental Workload, and Trust in Automation: Viable, Empirically Supported Cognitive Engineering Constructs. *Journal of Cognitive Engineering and Decision Making*, 2(2):140–160, 2008. ISSN 1555-3434. doi: 10.1518/155534308X284417.

[82] Valentina Squeri, Angelo Basteris, and Vittorio Sanguineti. Adaptive regulation of assistance 'as needed' in robot-assisted motor skill learning and neuro-rehabilitation. In *IEEE International Conference on Rehabilitation Robotics*, pages 1 – 6, 2011. ISBN 9781424498628. doi: 10.1109/ICORR.2011.5975375.

[83] Kazuo Kiguchi and Yoshiaki Hayashi. An EMG-based control for an upper-limb power-assist exoskeleton robot. *IEEE Transactions on Systems, Man, and Cybernetics, Part B: Cybernetics*, 42(4):1064–1071, 2012. ISSN 10834419. doi: 10.1109/TSMCB.2012.2185843.

[84] Neville Hogan, Hermano I. Krebs, Brandon Rohrer, Jerome J. Palazzolo, Laura Dipietro, Susan E. Fasoli, Joel Stein, Richard Hughs, Walter R. Frontera, Daniel Lynch, and Bruce T. Volpe. Motions or muscles? Some behavioral factors underlying robotic assistance of motor recovery. *The Journal of Rehabilitation Research and Development*, 43(5):605, 2006. ISSN 0748-7711. doi: 10.1682/JRRD.2005.06.0103.

[85] Eric T. Wolbrecht, Vicky Chan, David J. Reinkensmeyer, and James E. Bobrow. Optimizing compliant, model-based robotic assistance to promote neurorehabilitation. *IEEE Transactions on Neural Systems and Rehabilitation Engineering*, 16(3): 286–297, 2008. ISSN 15344320. doi: 10.1109/TNSRE.2008.918389.

[86] David J. Reinkensmeyer, O. Mine Akoner, Daniel P. Ferris, and Keith E. Gordon. Slacking by the human motor system: Computational models and implic implications for robotic orthoses. In *31st Annual International Conference of the IEEE Engineering in Medicine and Biology Society: Engineering the Future of Biomedicine*, pages 2129–2132. IEEE, 2009. ISBN 9781424432967. doi: 10.1109/IEMBS.2009.5333978.

[87] Aodhán L. Coffey and Tomás E. Ward. Slacking in the context of agent-based assessment in virtual rehabilitation systems. In *2014 36th Annual International Conference of the IEEE Engineering in Medicine and Biology Society*, pages 5844–5847, 2014. ISBN 9781424479290. doi: 10.1109/EMBC.2014.6944957.

[88] Laura Marchal-Crespo and David J. Reinkensmeyer. Review of control strategies for robotic movement training after neurologic injury. *Journal of NeuroEngineering and Rehabilitation*, 6(1):20, 2009. ISSN 17430003. doi: 10.1186/1743-0003-6-20.

[89] Ali Utku Pehlivan, Fabrizio Sergi, and Marcia K. OMalley. A Subject-Adaptive Controller for Wrist Robotic Rehabilitation. *IEEE/ASME Transactions on Mechatronics*, 20(3):1338–1350, 2014. ISSN 10834435. doi: 10.1109/TMECH.2014.2340697.

[90] Jeremy L Emken, Raul Benitez, and David J Reinkensmeyer. Human-robot cooperative movement training: learning a novel sensory motor transformation during walking with robotic assistance-as-needed. *Journal of neuroengineering and rehabilitation*, 4:8, 2007. ISSN 17430003. doi: 10.1186/1743-0003-4-8.

[91] Walid Hassani, Samer Mohammed, Hala Rifaï, and Yacine Amirat. Powered orthosis for lower limb movements assistance and rehabilitation. *Control Engineering Practice*, 26(1):245–253, 2014. ISSN 09670661. doi: 10.1016/j.conengprac.2014.02.002.

[92] Eric T. Wolbrecht, Vicky Chan, Vu Le, Steven C. Cramer, David J. Reinkensmeyer, and James E. Bobrow. Real-time computer modeling of weakness following stroke optimizes robotic assistance for movement therapy. In *2007 3rd International IEEE/EMBS Conference on Neural Engineering*, pages 152–158. IEEE, may 2007. ISBN 1-4244-0791-5. doi: 10.1109/CNE.2007.369635.

[93] Marco Guidali, Philippe Schlink, Alexander Duschau-Wicke, and Robert Riener. Online learning and adaptation of patient support during ADL training. *IEEE*

International Conference on Rehabilitation Robotics, 2011. ISSN 19457898. doi: 10.1109/ICORR.2011.5975434.

[94] Marco Guidali, Alexander Duschau-Wicke, Simon Broggi, Verena Klamroth-Marganska, Tobias Nef, and Robert Riener. A robotic system to train activities of daily living in a virtual environment. *Medical and Biological Engineering and Computing*, 49(10):1213–1223, 2011. ISSN 01400118. doi: 10.1007/s11517-011-0809-0.

[95] Peter S. Lum, Charles G. Burgar, Machiel Van der Loos, Peggy C. Shor, Matra Majmundar, and Ruth Yap. MIME robotic device for upper-limb neurorehabilitation in subacute stroke subjects: A follow-up study. *The Journal of Rehabilitation Research and Development*, 43(5):631, 2006. ISSN 0748-7711. doi: 10.1682/JRRD.2005.02.0044.

[96] D Gijbels, I Lamers, and L Kerkhofs. The Armeo Spring as training tool to improve upper limb functionality in multiple sclerosis: a pilot study. *Journal of NeuroEngineering and Rehabilitation*, (2008):1–8, 2011.

[97] Sai K. Banala, Suni K. Agrawal, and John P. Scholz. Active Leg Exoskeleton (ALEX) for gait rehabilitation of motor-impaired patients. In *2007 IEEE 10th International Conference on Rehabilitation Robotics, ICORR'07*, pages 401–407, 2007. ISBN 1424413206. doi: 10.1109/ICORR.2007.4428456.

[98] Monica A. Perez, Bjarke K.S. Lungholt, Kathinka Nyborg, and Jens B. Nielsen. Motor skill training induces changes in the excitability of the leg cortical area in healthy humans. *Experimental Brain Research*, 159(2):197–205, 2004. ISSN 00144819. doi: 10.1007/s00221-004-1947-5.

[99] Marc G. Carmichael and Dikai Liu. Admittance control scheme for implementing model-based assistance-as-needed on a robot. *Proceedings of the Annual International Conference of the IEEE Engineering in Medicine and Biology Society, EMBS*, pages 870–873, 2013. ISSN 1557170X. doi: 10.1109/EMBC.2013.6609639.

[100] Virginia Ruiz Garate, Andrea Parri, Tingfang Yan, Marko Munih, Raffaele Molino Lova, Nicola Vitiello, and Renaud Ronsse. Walking Assistance Using Artificial Primitives: A Novel Bioinspired Framework Using Motor Primitives for Locomotion Assistance Through a Wearable Cooperative Exoskeleton. *IEEE Robotics and Automation Magazine*, 23(1):83–95, 2016. ISSN 10709932. doi: 10.1109/MRA.2015.2510778.

[101] Weiguang Huo, Samer Mohammed, Yacine Amirat, and Kyoungchul Kong. Active Impedance Control of a lower limb exoskeleton to assist sit-to-stand movement. In *IEEE International Conference on Robotics and Automation*, pages 3530–3536, 2016. ISBN 9781467380263. doi: 10.1109/ICRA.2016.7487534.

[102] Vincent Hernandez, Nasser Rezzoug, and Philippe Gorce. Toward isometric force capabilities evaluation by using a musculoskeletal model: Comparison with direct force measurement. *Journal of Biomechanics*, 48:3178–3184, 2015. ISSN 18732380. doi: 10.1016/j.jbiomech.2015.07.003.

[103] Marc G. Carmichael and Dikai Liu. Estimating physical assistance need using a musculoskeletal model. *IEEE Transactions on Biomedical Engineering*, 60(7):1912–1919, 2013. ISSN 00189294. doi: 10.1109/TBME.2013.2244889.

[104] Walid Hassani, Samer Mohammed, and Yacine Amirat. Real-Time EMG driven Lower Limb Actuated Orthosis for Assistance As Needed Movement Strategy. In *Robotics: Science and Systems*, Berlin, Germany, 2013. doi: 10.15607/RSS.2013.IX.054.

[105] Marc G. Carmichael and Dikai Liu. Upper limb strength estimation of physically impaired persons using a musculoskeletal model: A sensitivity analysis. In *Annual International Conference of the IEEE Engineering in Medicine and Biology Society, EMBS*, pages 2438–2441, 2015. ISBN 9781424492718. doi: 10.1109/EMBC.2015.7318886.

[106] Mustafa Suphi Erden and Aude Billard. Robotic Assistance by Impedance Compensation for Hand Movements while Manual Welding. *IEEE Transactions on Cybernetics*, 46(11):2459–2472, 2016. ISSN 21682267. doi: 10.1109/TCYB.2015.2478656.

[107] T. Tsumugiwa, R. Yokogawa, and K. Hara. Variable impedance control based on estimation of human arm stiffness for human-robot cooperative calligraphic task. *Proceedings 2002 IEEE International Conference on Robotics and Automation (Cat. No. 02CH37292)*, 1:644–650, 2002. ISSN 10504729. doi: 10.1109/ROBOT.2002.1013431.

[108] Mustafa Suphi Erden and Aude Billard. End-point impedance measurements at human hand during interactive manual welding with robot. In *IEEE International Conference on Robotics and Automation*, pages 126–133, 2014. ISBN 978-1-4799-3685-4. doi: 10.1109/ICRA.2014.6906599.

[109] Samuele M. Marcora, Walter Staiano, and Victoria Manning. Mental fatigue impairs physical performance in humans. *Journal of Applied Physiology*, 106(3):857–864, 2009. doi: 10.1152/japplphysiol.91324.2008.

[110] Jeroen Van Cutsem, Samuele Marcora, Kevin De Pauw, Stephen Bailey, Romain Meeusen, and Bart Roelands. The Effects of Mental Fatigue on Physical Performance: A Systematic Review. *Sports Medicine*, 47(8):1569–1588, 2017. ISSN 11792035. doi: 10.1007/s40279-016-0672-0.

[111] Masaaki Tanaka, Akira Ishii, and Yasuyoshi Watanabe. Neural effect of mental fatigue on physical fatigue: A magnetoencephalography study. *Brain Research*, 1542:49–55, 2014. ISSN 18726240. doi: 10.1016/j.brainres.2013.10.018.

[112] Asako Honda. Active rest promoting both performance and recovery from subjective fatigue during mental work sessions. *International Journal of Psychophysiology*, 94 (2):229, 2014. ISSN 01678760. doi: 10.1016/j.ijpsycho.2014.08.896.

[113] M Takahara, R Nakamura, Y Ono, and F Oki. Effect of a 20-minute nap after sleep restriction on physical performance. *International Journal of Psychophysiology*, 94(2):228–229, 2014. ISSN 01678760. doi: http://dx.doi.org/10.1016/j.ijpsycho.2014.08.895.

[114] Nicholas J. La Delfa and Jim R. Potvin. A musculoskeletal model to estimate the relative changes in wrist strength due to interacting wrist and forearm postures. *Computer Methods in Biomechanics and Biomedical Engineering*, 20(13):1403 – 1411, 2017. ISSN 14768259. doi: 10.1080/10255842.2017.1366994.

[115] Lihui Wang, Bernard Schmidt, and Andrew Y C Nee. Vision-guided active collision avoidance for human-robot collaborations. *Manufacturing Letters*, 1(1):5–8, 2013. ISSN 22138463. doi: 10.1016/j.mfglet.2013.08.001.

[116] Photchsra Ratsamee, Yasushi Mae, Kenichi Ohara, Tomohito Takubo, and Tatsuo Arai. Human - Robot Collision Avoidance Using a Modified Social Force Model With Body Pose and Face Orientation. *International Journal of Humanoid Robotics*, 10 (01):1350008, 2013. doi: 10.1142/S0219843613500084.

[117] Daniel Roetenberg, Henk Luinge, and Per Slycke. Xsens MVN : Full 6DOF Human Motion Tracking Using Miniature Inertial Sensors. *Xsens Motion Technologies BV, Tech. Rep*, 1, 2009.

[118] Ståle A. Skogstad, Kristian Nymoen, and Mats Hovin. Comparing Inertial and Optical Mocap Technologies for Synthesis Control. *Creative Commoncs*, 2011.

[119] Alexander M. Aurand, Jonathan S. Dufour, and William S. Marras. Accuracy map of an optical motion capture system with 42 or 21 cameras in a large measurement volume. *Journal of Biomechanics*, 58:237 – 240, 2017. ISSN 18732380. doi: 10.1016/j.jbiomech.2017.05.006.

[120] Microsoft. Kinect. URL https://developer.microsoft.com/en-us/windows/kinect.

[121] Intel. RealSense. URL https://www.intel.com.au/content/www/au/en/architecture-and-technology/realsense-overview.html.

[122] Rune Havnung Bakken and Lars Moland Eliassen. Real-time three-dimensional skeletonisation using general-purpose computing on graphics processing units applied to computer vision-based human pose estimation. *The International Journal of High Performance Computing Applications*, 31(4):1–15, 2015. doi: 10.1177/1094342014566289.

[123] Loren Arthur Schwarz, Artashes Mkhitaryan, Diana Mateus, and Nassir Navab. Human skeleton tracking from depth data using geodesic distances and optical flow. *Image and Vision Computing*, 30(3):217–226, 2012. ISSN 02628856. doi: 10.1016/j.imavis.2011.12.001.

[124] Alexander Toshev and Google Christian Szegedy. DeepPose: Human Pose Estimation via Deep Neural Networks. In *IEEE Conference on Computer Vision and Pattern Recognition*, pages 1653–1660, 2014. doi: 10.1109/CVPR.2014.214.

[125] Jonathan Tompson, Arjun Jain, Yann Lecun, and Christoph Bregler. Joint Training of a Convolutional Network and a Graphical Model for Human Pose Estimation. In *28th Annual Conference on Neural Information Processing Systems*, pages 1799–1807, Montreal, Canada, 2014.

[126] Zhao Liu, Jianke Zhu, Jiajun Bu, and Chun Chen. A survey of human pose estimation: The body parts parsing based methods. *Journal of Visual Communication and Image Representation*, 32:10 – 19, 2015. ISSN 10959076. doi: 10.1016/j.jvcir.2015.06.013.

[127] Zhi Li, Jay R yan Roldan, Dejan Milutinović, and Jacob Rosen. The rotational axis approach for resolving the kinematic redundancy of the human arm in reaching movements. In *Annual International Conference of the IEEE Engineering in Medicine and Biology Society.*, pages 2507–2510, 2013. ISBN 9781457702167. doi: 10.1109/EMBC.2013.6610049.

[128] J F Soechting, C A Buneo, U Herrmann, and M Flanders. Moving effortlessly in three dimensions: does Donders' law apply to arm movement? *The Journal of neuroscience : the official journal of the Society for Neuroscience*, 15(9):6271–80, 1995. ISSN 0270-6474.

[129] Marjan A. Admiraal, Martijn J.M.A.M. Kusters, and Stan C.A.M. Gielen. Modeling Kinematics and Dynamics of Human Arm Movements. *Motor Control*, 8(3):312–327, 2004.

[130] Vincent De Sapio, James Warren, and Oussama Khatib. Predicting reaching postures using a kinematically constrained shoulder model. *Advances in Robot Kinematics*, pages 209–218, 2006. doi: 10.1007/978-1-4020-4941-5-23.

[131] Liliana Lo Presti and Marco La Cascia. 3D skeleton-based human action classification: A survey. *Pattern Recognition*, 53:130–147, 2016. ISSN 00313203. doi: 10.1016/j.patcog.2015.11.019.

[132] K. H.E. Kroemer, W. S. Marras, J. D. McGlothlin, D. R. McIntyre, and M. Nordin. On the measurement of human strength. *International Journal of Industrial Ergonomics*, 6(3):199–210, 1990. ISSN 01698141. doi: 10.1016/0169-8141(90)90034-Y.

[133] P. Schantz, E. Randall-Fox, W. Hutchison, A. Tyden, and P. -O Åstrand. Muscle fibre type distribution, muscle cross-sectional area and maximal voluntary strength in humans. *Acta Physiologica Scandinavica*, 117(2):219–226, 1983. ISSN 1365201X. doi: 10.1111/j.1748-1716.1983.tb07200.x.

[134] Karen D. Gordon, Richard D. Pardo, James A. Johnson, Graham J.W. King, and Thomas A. Miller. Electromyographic activity and strength during maximum isometric pronation and supination efforts in healthy adults. *Journal of Orthopaedic Research*, 22(1):208–213, 2004. ISSN 07360266. doi: 10.1016/S0736-0266(03)00115-3.

[135] Tomohiro Hayashi, Hiroaki Kawamoto, and Yoshiyuki Sankai. Control method of robot suit HAL working as operator's muscle using biological and dynamical information. In *2005 IEEE/RSJ International Conference on Intelligent Robots and Systems, IROS*, pages 3063 – 3068, 2005. ISBN 0780389123. doi: 10.1109/IROS.2005.1545505.

[136] Panagiotis K. Artemiadis and Kostas J. Kyriakopoulos. A switching regime model for the emg-based control of a robot arm. *IEEE Transactions on Systems, Man, and Cybernetics, Part B: Cybernetics*, 41(1):53 – 63, 2011. ISSN 10834419. doi: 10.1109/TSMCB.2010.2045120.

[137] Meghan E. Vidt, Melissa Daly, Michael E. Miller, Cralen C. Davis, Anthony P. Marsh, and Katherine R. Saul. Characterizing upper limb muscle volume and strength in older adults: A comparison with young adults. *Journal of Biomechanics*, 45(2):334–341, 2012. ISSN 00219290. doi: 10.1016/j.jbiomech.2011.10.007.

[138] Aaron Sell, Leda Cosmides, John Tooby, Daniel Sznycer, Christopher Von Rueden, and Michael Gurven. Human adaptations for the visual assessment of strength and fighting ability from the body and face. *Proceedings of the Royal Society B: Biological Sciences*, 276(1656):575–584, 2009. ISSN 14712970. doi: 10.1098/rspb.2008.1177.

[139] Chao Yuan, Weijun Wang, Changsoo Han, and Hyeunseok Choi. A three degree of freedom force/torque sensor to measure foot forces. In *12th International Conference on Control, Automation and Systems (ICCAS)*, pages 2028–2032, 2012. ISBN VO -.

[140] Gab-soon Kim, Hyun-min Kim, Hoe-in Kim, Ming-guo Pio, Hee-suk Shin, and Jung-won Yoon. Development of 6-axis force / moment sensor for measuring the fingers ' muscular strength of human. In *IEEE International Symposium on Industrial Electronics*, pages 428–433, 2010. ISBN 9781424463916.

[141] Antony Tran, Dikai Liu, Ravindra Ranasinghe, Marc Carmichael, and Chuanbo Liu. Analysis of Human Grip Strength in Physical Human Robot Interaction. *Procedia Manufacturing*, 3:1442–1449, 2015. ISSN 23519789. doi: 10.1016/j.promfg.2015.07.320.

[142] Christopher Thomas, Paul A. Jones, James Rothwell, Chieh Y. Chiang, and Paul Comfort. An Investigation into the Relationship between Maximum Isometric Strength and Vertical Jump Performance. *Journal of Strength and Conditioning Research*, 29(8):2176–2185, 2015. ISSN 15334295. doi: 10.1519/JSC.0000000000000866.

[143] Scott L. Delp, Frank C. Anderson, Allison S. Arnold, Peter Loan, Ayman Habib, Chand T. John, Eran Guendelman, and Darryl G. Thelen. OpenSim: Open-Source Software to Create and Analyze Dynamic Simulations of Movement. *IEEE Transactions on Biomedical Engineering*, 54(11):1940–1950, 2007. ISSN 0018-9294. doi: 10.1109/TBME.2007.901024.

[144] Kurt Manal, Karin Gravare-Silbernagel, and Thomas S. Buchanan. A real-time EMG-driven musculoskeletal model of the ankle. *Multibody System Dynamics*, 2012. ISSN 13845640. doi: 10.1007/s11044-011-9285-4.

[145] Antonie J. van den Bogert, Thomas Geijtenbeek, Oshri Even-Zohar, Frans Steenbrink, and Elizabeth C. Hardin. A real-time system for biomechanical analysis of human movement and muscle function. *Medical & Biological Engineering & Computing*, 51(10):1069–1077, 2013. ISSN 0140-0118. doi: 10.1007/s11517-013-1076-z.

[146] Yoann Blache, Mickaël Begon, Benjamin Michaud, Landry Desmoulins, Paul Allard, and Fabien Dal Maso. Muscle function in glenohumeral joint stability during

lifting task. *PLoS ONE*, 12(12):e0189406, 2017. ISSN 19326203. doi: 10.1371/journal.pone.0189406.

[147] Edward K Chadwick, Dimitra Blana, Antonie J (Ton,) Van Den Bogert, and Robert F Kirsch. A Real-Time, 3-D Musculoskeletal Model for Dynamic Simulation of Arm Movements. *IEEE Transactions on Biomedical Engineering*, 56(4):941 – 948, 2009. doi: 10.1109/TBME.2008.2005946.

[148] C. Pizzolato, M. Reggiani, L. Modenese, and D. G. Lloyd. Real-time inverse kinematics and inverse dynamics for lower limb applications using OpenSim. *Computer Methods in Biomechanics and Biomedical Engineering*, 20(4):436 – 445, 2017. ISSN 14768259. doi: 10.1080/10255842.2016.1240789.

[149] Bence J Borbély and Péter Szolgay. Real - time inverse kinematics for the upper limb: a model - based algorithm using segment orientations. *BioMedical Engineering OnLine*, 16(1):21, 2017. doi: 10.1186/s12938-016-0291-x.

[150] Victor Grosu, Svetlana Grosu, Bram Vanderborght, Dirk Lefeber, and Carlos Rodriguez-Guerrero. Multi-axis force sensor for human-robot interaction sensing in a rehabilitation robotic device. *Sensors*, 17(6):1294, 2017. ISSN 14248220. doi: 10.3390/s17061294.

[151] Massimo Sartori, Monica Reggiani, Dario Farina, and David G. Lloyd. EMG-Driven Forward-Dynamic Estimation of Muscle Force and Joint Moment about Multiple Degrees of Freedom in the Human Lower Extremity. *PLoS ONE*, 7(12):e52618, 2012. ISSN 19326203. doi: 10.1371/journal.pone.0052618.

[152] Angela DiDomenico and Maury A. Nussbaum. Estimation of forces exerted by the fingers using standardised surface electromyography from the forearm. *Ergonomics*, 51(6):858–871, 2008. ISSN 00140139. doi: 10.1080/00140130801915980.

[153] Usama J. Naeem, Asaad A. Abdullah, and Caihua Xiong. Estimating human arm's muscle force using Artificial Neural Network. In *2012 IEEE International Symposium on Medical Measurements and Applications Proceedings*, pages 1–6, 2012. ISBN 978-1-4673-0882-3. doi: 10.1109/MeMeA.2012.6226662.

[154] X. Hu, W. M. Murray, and E. J. Perreault. Muscle short-range stiffness can be used to estimate the endpoint stiffness of the human arm. *Journal of Neurophysiology*, 105(4):1633–1641, 2011. ISSN 0022-3077. doi: 10.1152/jn.00537.2010.

[155] M. Voinescu, D. P. Soares, R. M. Natal Jorge, A. Davidescu, and L. J. Machado. Estimation of the forces generated by the thigh muscles for transtibial amputee gait. *Journal of Biomechanics*, 45(6):972–977, 2012. ISSN 00219290. doi: 10.1016/j.jbiomech.2012.01.010.

[156] Christina Wiktorin, Kristina Selin, Lena Ekenvall, Åsa Kilbom, and Lars Alfredsson. Evaluation of perceived and self-reported manual forces exerted in occupational materials handling. *Applied Ergonomics*, 27(4):231–239, 1996. ISSN 00036870. doi: 10.1016/0003-6870(96)00006-3.

[157] Stephen Bao and Barbara Silverstein. Estimation of hand force in ergonomic job evaluations. *Ergonomics*, 48(3):288–301, 2005. ISSN 00140139. doi: 10.1080/0014013042000327724.

[158] Rupesh Kumar and Shrawan Kumar. Musculoskeletal risk factors in cleaning occupation-A literature review. *International Journal of Industrial Ergonomics*, 38 (2):158–170, 2008. ISSN 01698141. doi: 10.1016/j.ergon.2006.04.004.

[159] S.C. Gandevia. Spinal and Supraspinal Factors in Human Muscle Fatigue. *Physiological Reviews*, 81(4):1725–1789, 2001. doi: https://doi.org/10.1152/physrev.2001.81.4.1725.

[160] Florian Monjo and Nicolas Forestier. Muscle fatigue effects can be anticipated to reproduce a movement kinematics learned without fatigue. *Neuroscience*, 339:100–108, 2016. ISSN 18737544. doi: 10.1016/j.neuroscience.2016.09.042.

[161] M. Gorelick, J. M.M. Brown, and H. Groeller. Short-duration fatigue alters neuromuscular coordination of trunk musculature: Implications for injury. *Applied Ergonomics*, 34(4):317–325, 2003. ISSN 00036870. doi: 10.1016/S0003-6870(03)00039-5.

[162] Jeffrey C. Cowley, Jonathan B. Dingwell, and Deanna H. Gates. Effects of local and widespread muscle fatigue on movement timing. *Experimental Brain Research*, 232 (12):3939–3948, 2014. ISSN 14321106. doi: 10.1007/s00221-014-4020-z.

[163] M. A. Huysmans, M. J.M. Hoozemans, A. J. van der Beek, M. P. de Looze, and J. H. van Dieën. Fatigue effects on tracking performance and muscle activity. *Journal of Electromyography and Kinesiology*, 18(3):410–419, 2008. ISSN 10506411. doi: 10.1016/j.jelekin.2006.11.003.

[164] Foster B. Stulen and Carlo J. De Luca. Muscle Fatigue Monitor: A Noninvasive Device for Observing Localized Muscular Fatigue. *IEEE Transactions on Biomedical Engineering*, 12:760–768, 1982. ISSN 15582531. doi: 10.1109/TBME.1982.324871.

[165] Xianlian Zhou, Phillip Whitley, and Andrzej Przekwas. A musculoskeletal fatigue model for prediction of aviator neck manoeuvring loadings. *International Journal of Human Factors Modelling and Simulation*, 4:1–29, 2014.

[166] Ruina Ma, Damien Chablat, Fouad Bennis, and Liang Ma. Human Muscle Fatigue Model in Dynamic Motions. In *Advances in Robot Kinematics*, pages 1–8, Innsbruck, Austria, 2012.

[167] Miguel T. Silva, André F. Pereira, and Jorge M. Martins. An efficient muscle fatigue model for forward and inverse dynamic analysis of human movements. In *Procedia IUTAM*, 2011. ISBN 3512184170. doi: 10.1016/j.piutam.2011.04.024.

[168] Marc G. Carmichael and Dikai Liu. Experimental evaluation of a model-based assistance-as-needed paradigm using an assistive robot. *Proceedings of the Annual International Conference of the IEEE Engineering in Medicine and Biology Society, EMBS*, pages 866–869, 2013. ISSN 1557170X. doi: 10.1109/EMBC.2013.6609638.

[169] D Tolani and N I Badler. Real-time inverse kinematics of the human arm. *Presence: Teleoperators & Virtual Environments*, 5(4):393–401, 1996. ISSN 1054-7460.

[170] Australian Standards. Safety of machinery - Electrical equipment of machines. *Australian Standards IED 60204-1*, 2016.

[171] Nathan Kirchner, Gavin Paul, and Dikai Liu. Bridge maintenance robotic arm: mechanical technique to reduce the nozzle force of a sandblasting rig. In *1st International Symposium on Digital Manufacturing*, number ISSN: 1671-4431, pages 12–18, 2006.

[172] Shu Zon Lou, Chii Jeng Lin, Pei Hsi Chou, You Li Chou, and Fong Chin Su. Elbow load during pushup at various forearm rotations. *Clinical Biomechanics*, 16(5):408–414, 2001. ISSN 02680033. doi: 10.1016/S0268-0033(01)00008-0.

[173] Biman Das and Yanqing Wang. Isometric pull-push strengths in workspace: 1. strength profiles. *International Journal of Occupational Safety and Ergonomics*, 10 (1):43–58, 2004. ISSN 10803548. doi: 10.1080/10803548.2004.11076594.

[174] Nives Klopčar and Jadran Lenarčič. Kinematic model for determination of human arm reachable workspace. *Meccanica*, 40(2):203–219, 2005. ISSN 00256455. doi: 10.1007/s11012-005-3067-0.

[175] Fabrizio Flacco, Alessandro De Luca, and Oussama Khatib. Control of Redundant Robots under Hard Joint Constraints: Saturation in the Null Space. *IEEE Transactions on Robotics*, 31(3):637–654, 2015. ISSN 15523098. doi: 10.1109/TRO.2015.2418582.

[176] Shay Ohayon and Ehud Rivlin. Robust 3D Head Tracking Using Camera Pose Estimation. In *ICPR 2006, 18th International Conference on Pattern Recognition*, volume 1, pages 1063–1066, 2006.

[177] Hyun Kyung Kim and Yanxin Zhang. Estimation of lumbar spinal loading and trunk muscle forces during asymmetric lifting tasks: application of whole-body musculoskeletal modelling in OpenSim. *Ergonomics*, 60(4):563–576, 2017. ISSN 13665847. doi: 10.1080/00140139.2016.1191679.

[178] Luka Peternel, Nikos Tsagarakis, Darwin Caldwell, and Arash Ajoudani. Robot adaptation to human physical fatigue in human–robot co-manipulation. *Autonomous Robots*, 42(5):1011–1021, 2018. ISSN 15737527. doi: 10.1007/s10514-017-9678-1.

[179] Antony Tran, Dikai Liu, Ravindra Ranasinghe, and Marc Carmichael. Identifying Human Hand Orientation around a Cylindrical Handle- bar for physical Human-Robot Interaction Experiment Design and Data Collection. In *ISR 2018; 50th International Symposium on Robotics*, pages 1–8, Munich, Germany, 2018.